Dynamics of Weather Regimes:
Quasi-stationary Waves and Blocking

by

Brian Bennett Reinhold

B.A. Brandeis University

(1976)

SUBMITTED IN PARTIAL FULFILLMENT
OF THE REQUIREMENTS OF THE
DEGREE OF

DOCTOR OF PHILOSOPHY

at the

MASSACHUSETTS INSTITUTE OF TECHNOLOGY

December, 1981

Signature of Author _____

Department of Meteorology and Physical Oceanography
December 31, 1981

Certified by _____

Raymond T. Pierrehumbert
Thesis Supervisor

Accepted by _____

Peter Stone
Department Chairman

TABLE OF CONTENTS

Dynamics of Weather Regimes:
Quasi-stationary Waves and Blocking

by

Brian Bennett Reinhold

Submitted to the Department of Meteorology and Physical Oceanography on December 31, 1981 in partial fulfillment of the requirements for the degree of Doctor of Philosophy in Meteorology

ABSTRACT

We hypothesize that periods of quasi-stationary behavior in the large scales is integrally associated with an organized behavior of the synoptic scales, thus the terminology "weather regimes". To investigate our hypothesis, we extend the model of Charney and Straus (1980) to include an additional wave in the zonal direction which is highly baroclinically unstable and can interact directly with the externally forced large-scale wave. We find that such a model aperiodically vacillates between two distinct weather regime states which are not located near any of the stationary equilibria of the large-scale state. The state of the model flow may remain in either one of these two states for several synoptic periods. During each of the two regimes, the net transports by the transient disturbances are found to have consistent, zonally inhomogeneous structure, the form of which depends upon the regime. This result implies that the transports appear as a net additional external forcing mechanism to the large-scale wave, accounting for the differences between the time mean regime state and the stationary equilibria.

Following the analysis proceedure of Frederiksen (1979), we show that the observed structure of these net transports can be accounted for by the spatial modulation of the baroclinically most unstable eigenmodes by the large-scale wave. We then consider only the tendency equations of the large-scale variables where the effects of the transients are parameterized by solving the stability problem at each time step. We find that such a dynamical system possesses two absolutely stable "regime-equilibria" which are very close in phase space to the time mean states of the regimes appearing in the full model. We then demonstrate that the instantaneous component of the transients are also capable of transfering the state of the model flow from the attractor basin of one of the stable regime-equilibria to the attractor basin of the other. Our experiments thus indicate that the transients are important in determining the qualitative behavior of both the instantaneous and time mean components of the large-scale flow in our system, and suggest that the very different short range climates in the atmosphere can result from entirely internal processes.

Thesis Supervisor: Raymond T. Pierrehumbert
Title: Professor of Meteorology

BACKGROUND

One of the most interesting, but poorly understood, phenomena in synoptic meteorology is the occurrence of large-amplitude, planetary scale waves, which often persist for periods long compared to the passing of a transient synoptic-scale wave. On a day to day basis, these phenomena appear as persistent, large-scale undulations or meanderings of the circumpolar westerly jet on middle and upper level tropospheric weather maps.

The impact of these events on regional weather can be quite significant, since migratory cyclones have a tendency to be "steered" by the upper level flow pattern. The maintenance of a quasi-stationary wave, or persistence in the upper level flow patterns, is then experienced at the surface as either persistent or repetitive weather, depending upon ones relative position with respect to the tracks of the migratory cyclones. Surface regions sufficiently equatorward or poleward of the storm track would experience an extended period of dry warm or cold weather, respectively, while regions within the storm track may experience excessive precipitation or highly variable weather on a day to day basis, as a result of the passing disturbances.

Occasionally, the quasi-stationary wave possesses such

remarkable persistence and obtains such large amplitude that the migratory cyclones are diverted far from their climatologically determined paths for an anomalously extended period of time. These events are so strikingly prominent on the daily weather maps that synoptic meteorologists have come to refer to the extreme example of a quasi-stationary wave as a "block" or an "omega block" since the undulation in the jet stream often resembles the shape of the Greek letter Ω .

The persistence of a planetary-scale quasi-stationary wave and its associated pattern of migratory cyclones will be referred to as a "weather regime" in recognition of its influence over a considerable fraction of the globe's surface weather. Blocking, from this viewpoint, is simply a special case of the more general weather regime phenomenon.

Weather regimes are perhaps more common than generally recognized, although some rather striking examples which have occurred over the North American sector during the period from 1976 to 1981 have substantially increased interest in this phenomenon. At least two reasons may account for the lack of recognition of many regimes. One is that most regimes do not appear as striking as the relatively rare Eastern Atlantic block, for which the quasi-stationary component of the flow strongly dominates the fluctuating synoptic component of the flow. Another reason seems to be that unless the nature of

the weather induced by a given regime is sufficiently extreme to arouse public interest, i.e., drought, heatwaves, excessive precipitation, etc., it will often exist unnoticed.

The concept of regimes has not always been so absent from the jargon of the meteorologist; in fact, at one time, the concept was actively pursued. In the early to mid nineteen forties several meteorologists, most notably Baur, Elliot, Krick, and Namias, studied a phenomenon which they referred to as "weather-types" or "grosswetterlage". In the interests of extended-range forecasting, the studies catologued the shapes of the upper-level quasi- stationary waves and the associated tracks of cyclone events as well as the general flows of surface warm and cold air. But for some reason, by the early nineteen fifties, the concept of weather-typing phased itself out of analytic meteorology and has since never gotten re-established into the field.

In order to clarify and establish more concretely the phenomenon of weather regimes, we now present a few examples of atmospheric cases. The occurrence of weather regimes (or quasi-stationary waves) is most easily demonstrated by considering the limited-contour analyses of Sanders (personal communication). Since 1976, Professor Sanders at MIT has maintained what he has called Northern-Hemispheric Continuity Charts. These charts are generated by tracing and superposing

for periods of one week the daily 552 dam height contour of the 00Z 500 mb NMC final analysis (transmitted over NAFAX). The quasi-stationary waves are defined by the envelope or "eyeball average" of the daily contours. Regions over which the flow is steady will generally be marked by a narrow, fairly constant meridional width envelope while regions where the flow is unsteady will generally be marked by a wide and bulging envelope. From the presently accumulated 4.5 year sample (which excludes the months June through August) there are several cases which can serve to illustrate the occurrence of atmospheric weather regimes.

The first example to be considered is the 18 day period from January 26, 1980 to February 15, 1980, shown in Figure A. This was the year that brought record breaking drought to the Olympic Winter Games in the Northeastern United States and record snowfalls to the Southeast States. The most prominent steady features which appear on the map are the large-scale trough which occurs just downstream of the highly disorganized flow over the Eastern Pacific and Western North America, and the near zonal flow from Central Asia to the mid-Pacific. In addition, there appears to be a somewhat more disorganized, smaller scale, ridge-trough-ridge pattern over Europe and Western Asia. However, it is not possible to ascertain from the analysis whether the "disorganization" is real or an artifact of the lack of two- dimensional information. (For

example, if the height gradients of the quasi- stationary pattern over Europe happen to be markedly weaker than other regions about the globe, a given synoptic-scale transient disturbance will produce a higher amplitude "wiggle" in that location, introducing a spuriously erratic appearance to the otherwise steady regime). Over the Eastern Pacific and Western North America, on the other hand, the erratic behavior is much more evidently a consequence of unsteady flow, for the fluctuations are primarily larger scale.

The Eastern North America-Atlantic trough case is an excellent example of the dramatic influence a regime can have upon the behavior of the transient disturbances. The asterisks, eight of which are concentrated in the Western Atlantic, correspond to the occurrence of surface "bombs" (explosively intensifying cyclones) as defined by Sanders and Gyakum (1980). According to Sanders and Gyakum, this frequency of bombs is excessive, suggesting the presence of a regionally highly active baroclinic zone. Many of these bombs initiated in the Gulf States (a process which, combined with the southward extent of the cold trough, brought the Southeast States anomalous snowfall amounts) and exploded out over the Gulf Stream, but the deepening cyclones repetitively were "steered" too far to the east to bring precipitation to the dessicating, anomalously cold, Northeast States. Though we generally regard the synoptic events as a "consequence" of the

large-scale configuration, we do not mean to imply that such is the case here. (Indeed, we intend to show that it is equally likely that the repetitive bomb events were necessary to maintain the large-scale pattern).

The second example, plotted in Figure B, is the period from February 5, 1977 to February 20, 1977, which is the last 16 days of the now infamous winter regime of 1976-1977. Outside of the very prominent ridge-trough pattern over North America, the flows are basically zonal across Europe followed by a low amplitude Central Asian ridge and Western Pacific trough. A significant difference between this 16 day period and the February, 1980 case in Figure A is that the flow appears quite steady everywhere about the globe.

The feature of interest, however, is the high amplitude ridge-trough pattern over North America. This pattern was established well before the first day included in the figure, being recognizable as early as the previous October, making this particular regime the longest lasting regime of the data set. The weather associated with this regime had economically disastrous consequences across much of the United States: the west coast suffered severe drought and anomalous warmth, while the east coast, especially the Central East States, was engaged in a record deep freeze.

One of the most spectacular features of the 1976-1977 ridge-trough regime was its sudden collapse. Figure C is a plot of the 15 day period from February 22, 1977 to March 8, 1977, which directly follows the period shown in Fig. B, save February 21. The ridge-trough pattern, which had persisted for longer than four months, was completely obliterated in less than two days. In contrast, the rest of the globe, except for Europe, remained essentially unchanged.

The third example, shown in Figure D, is another high amplitude ridge- trough regime over North America, similar to the 1976-1977 case. This plot encompasses the 16 day period from December 31, 1980 to January 15, 1981 (which marked the end of the 4.5 year data set). The 1981 regime, similar to the 16 day period selected in the 1977 case, is accompanied by steady behavior about the globe, again with a low amplitude mid-Asian ridge and Western Pacific trough. However, the flow over the Eastern Atlantic and Europe is markedly different. In the 1981 case, a large-amplitude ridge-trough pattern extends from the Central Atlantic across Europe, in contrast to the zonal flow observed in the 1977 case (Fig. B).

The weather associated with the 1981 North American ridge-trough regime is subtly different from the 1977 case. First, the regime did not become established until the last days of December 1980, and persisted only about 18 days or so.

Second, the feature has a somewhat greater amplitude with a trough axis further east than the 1977 case. The subtle eastward shift has brought polar blasts down on New England instead of the Central East States. These outbreaks result in substantially colder weather in New England and the East Coast States since the cold air is not modified by the eastward travel across the Appalacians as in 1977. In addition, warmer temperatures have crept further eastward across the Great Plain States.

The paths taken by cyclones during this regime were remarkably repetitive. Weak Alberta cyclones traveled southeastward into the Great Lakes Regions and turned northeastward, perhaps associated with weak coastal secondary cyclogenesis. As the primary or secondary storm moved northeastward, it rapidly intensified, too far to the north and east to bring substantial precipitation amounts west of Newfoundland, but not sufficiently far north and east for the Northeast States to avoid the cold arctic blasts on the leeward sides of the intensifying storms.

The last two cases, shown in Figures E and F, are examples of a regime which has not been too common during the winters since 1976; ridging in the Eastern Pacific and troughing on the West Coast followed by a disorganized attempt at East-coast ridging. This pattern, in a gross sense, is the

reverse of the 1976-1977 and 1981 cases. Figures E and F consist of the 20 day period from March 14, 1977 to April 2, 1977 and the eleven day period from March 26, 1979 to April 5, 1979. The flows in both examples have considerable synoptic signal over North America and, in the 1977 case, part of Western Asia. The remainder of the global flow patterns (except over the Eastern Pacific) are, on the other hand, considerably different in the two cases. The weather associated with these North American regimes seems to have two possibilities for the East Coast. The tendency for East-Coast ridging brings anomalous warmth, but the highly variable synoptic waves often develop into cutoff circulations which linger painfully over the Western Atlantic, bringing extended periods of drizzle, rain, cloudiness, and otherwise general misery, to the Northeast Coast. In the March 26-April 5 case of 1979, it rained 8 out of the 11 days at Logan airport in Boston, Mass., while in the March 14- April 2, 1977 case, a drizzly, rainy period was followed by a heat wave.

There are several other examples of persistent atmospheric states which have not been displayed. Two of noterity were the ridge-trough regimes over North America during the 1977-1978 and 1978-1979 winters, both of which persisted on the order of 30 days. Each brought heavy precipitation amounts to the eastern United States but a subtle shift in the position of the large- scale trough

between the two cases resulted in heavy snows one year on the East Coast followed by heavy rains in the succeeding year. Another event of note was the intense heat wave of the 1980 summer. Though the summer months were not analyzed, one can be reasonably confident that the heatwave is undoubtedly associated with an anomalous weather regime.

SUMMARY

The limited number of examples above are presented primarily to familiarize the reader with the phenomenon of interest and enable him or her to visualze this otherwise difficult-to-describe feature. Though there is insufficient data to provide conclusive evidence about the behavior and properties of the weather regimes, there are a few statistics of note which can be surmised from this limited sample. First and foremost, there is an extreme diversity in the observed regime persistence, with (subjectively determined) durations ranging from as short as 11 days to as long as 130 days, with no clear evidence of a preferred time scale. Second, regimes appear to be rather strongly localized. This property was evident in the February 1980 case (Figure A), where one sector of the globe varied erratically while other sectors remained essentially unchanged, and in the transition of the 1976-1977 regime (Figures B and C), where the North American sector underwent a radical transition while the ridge-trough over

Asia and the Western Pacific persisted with no change. Third, a few regimes were noted to establish and or collapse at rates approaching a synoptic time scale.

In spite of the presentation of some fairly well defined "textbook" cases, it remains an extremely difficult task to precisely quantify the weather regime (a problem discussed by Dole, 1982). For this reason it is necessary to explicitely point out the distinction between the weather regime and the "stationary" and "transient" wave decomposition frequently used in general circulation studies, with which it may be confused. The stationary wave is computed as the residual non-zonal component of the atmospheric flow field averaged over some (arbitrarily) chosen time period, i.e., a month, season, year, etc. Though a regime may persist for as long as a season, such instances appear to be exceptional, and it is generally unlikely that the stationary wave decomposition will adequately represent the weather regime phenomenon. Since the majority of observational studies consider several months, seasons, or even years in their analyses to generate the stationary and transient components, we may reasonably assume that several regimes, fractions of regimes, as well as periods of "unsteady" flow, are included in the data, and thus a single regime will be partitioned in an unknown manner between the stationary and transient components. It is evident from the qualitative description provided in this section and the

techniques used to compute the stationary and transient waves, that the three features represent distinctly different entities. The stationary waves, in this case, may simply represent an "unoccupied average", e.g., the weighted average of the various regime states.

The purpose of this dissertation is to investigate the weather regime phenomenon. Based on what we have described in this section, a potentially very important aspect of the regimes so far neglected in theoretical studies is the influence of the organized behavior of the synoptic-scale disturbances. The investigation of the role of the transients and their feedbacks upon the planetary scales during periods of weather regimes as well as periods of regime transition is the primary new contribution of this work.

1. INTRODUCTION

The occasional persistence of certain large-amplitude planetary-scale atmospheric features and their influence upon the behavior of the transient synoptic-scale disturbances has long been noted by forecasters and synoptic meteorologists. Among such persistent events, the group of phenomena known as blocking is perhaps the most striking. Although blocking has been the subject of much research, the dynamical processes which establish and maintain these quasi-stationary features and couple them to the baroclinic disturbances are not yet well understood.

A promising approach toward explaining blocking is provided by the concept of multiple flow equilibria introduced by Charney and DeVore(1979). The multiple flow equilbrium results suggest that the atmospheric flow system in the presence of zonally inhomogeneous external forcing mechanisms (e.g., topography, land-sea contrasts, heat sources and sinks, etc.) can possess not one, but several equilibrium flow configurations. The hypothesis, as stated by Charney and DeVore, is that the general behavior of the atmosphere can be understood as a flow which is driven by smaller scale instabilities from one quasi-stable equilibrium point to another. In this theory, the particular event of blocking occurs when the atmospheric trajectory approaches a quasi-

stable equilibrium solution which possesses both a high wave amplitude and low zonal index configuration.

One of the more important assumptions of the multiple flow equilibria theory (MFET) is that some of the equilibrium flow configurations in the atmosphere are quasi-stable in the sense that a solution starting from an initial condition not too far from the equilibrium point remains close to that point for a long period of time. However, we are interested in the time dependent behavior of the solution after long periods of time, far from the initialization, i.e. once the solution has settled down into its attractor. It is not always clear that the equilibria form part of the attractor, unless they are absolutely stable. If the equilibria are stable, we know that once the trajectory enters a finite region about the equilibria, it will remain confined to that region and approach the equilibrium state. In that case, the time dependent problem becomes trivial. However, if the equilibria are all unstable, there are no mathematical grounds upon which we can make the assumption that the equilbria and the time dependent behavior are related.

Several authors have studied the stability properties of equilibrium states in various highly simplified models. Most of these studies considered barotropic atmospheres. The barotropic equilibria were generally found to be stable or

weakly unstable to all perturbations (see Charney and DeVore(1979) and Charney et. al. (1981)). These observations provided the primary motivation for explaining the quasi-stationary disturbances of the atmosphere as manifestations of these equilibria. The analysis of the baroclinic equilibria, on the other hand, results in substantially different conclusions. For realistically large values of the driving, Charney and Straus (1980) and Roads (1980a,1980b) found that the baroclinic equilibria were highly unstable to smaller scale perturbations. However, it was generally assumed that the effects of the synoptic scale instabilities were minimal and thus it was concluded that "realizable" equilibria, i.e. those which would be part of the time dependent attractor, were solutions which were found to be stable or weakly unstable to perturbations restricted to the scale of the equilibria. These assumptions, however, have not been validated and clearly require further investigation.

We do know that the real atmosphere is highly baroclinically unstable to perturbations on the synoptic scale, in the sense that we frequently observe rapidly growing disturbances on such a scale. A priori, it does not seem possible to predict the manner in which the vigorous synoptic-scale baroclinic disturbances of the atmosphere will interact with the theoretical stationary solutions. It is entirely possible that the instabilities may destroy the

equilibria, as they will most-likely extract energy from the large scale. Indeed, it is not clear whether the stability of the analytically- derived stationary solution with respect to perturbations restricted to the scale of those solutions will have any relevance to the phase space behavior of a system including the synoptic scales. Thus we must study the manner in which the highly active synoptic-scale waves interact with the externally forced stationary waves.

Theoretical and observational studies indicate that the interactions may be significant for both the synoptic and large scales. A modeling study by Frederiksen (1979) demonstrated that the presence of a prescribed planetary-scale wave modulated the baroclinic disturbances in such a manner that the spatial configuration of the net transports by the instabilities had distinct maxima relative to the phase of the large scale wave. In a similar modeling study, Niehaus (1980) showed that a prescribed basic state with wavy structure could also account for the occurrence of storm tracks in terms of certain regions of the basic state wave which were more active baroclinically. In both cases, it is apparent that the presence of a large- scale wave acts in some manner to organize the transients. On the other hand, Gall et. al. (1979), using a general circulation model, demonstrated that the small-scale transient disturbances are capable of forcing planetary scale circulations without the presence of any

zonally inhomogeneous forcing or initial planetary scale perturbations. In addition, Sanders and Gyakum (1980) in their observational analysis have noted the sudden amplification of planetary scale ridges just downstream of a region in which several successive explosively deepening cyclones have occurred. In these studies, it is apparent that the synoptic scales are capable of forcing and altering the large scales.

The combination of the organization of the transients by the planetary scale, and the forcing of the planetary scale by the organized transients suggests a potentially significant feedback process. It is reasonable to expect that these interactions could establish some type of balance. This possibility provides a mechanism through which the highly unstable externally forced planetary scale wave considered in the MFET can equilibrate with its own instabilities. The basic hypothesis in this paper is that exactly such a feedback process is responsible for the occurrence of quasi-stationary behavior in the atmosphere.

Our hypothesis implies that quasi-stationary behavior in the planetary scales is integrally associated with an organized behavior of the synoptic- scale events. In recognition of the fact that the synoptic scales are generally responsible for what is considered "weather", these

quasi-stationary periods will be referred to as weather regimes. The event of blocking, then, which is an unusually steady, high amplitude quasi-steady state, is simply a subset of the more general weather regime phenomenon.

We shall investigate the weather regime phenomenon in the simplest possible model that has the necessary physics to incorporate the feedback process alluded to above. This will be accomplished by extending the model of Charney and Straus to include an additional wave in the zonal direction in such a manner that it can directly interact with the externally forced planetary scale wave. The first aspect of the analysis will be to consider the properties and characteristics of the model theoretical equilibria. We then examine the time-dependent behavior of the model and investigate the appearance of regime-type phenomena. We can then consider the qualitative properties of the regimes as a function of the parameters and their relation to the corresponding theoretically calculated equilibria. The final aspect of the theoretical analysis will be to consider the behavior of the synoptic scales and their roles during both persistent periods and times of transition. In conclusion we will attempt to ascertain in what manner the theory developed in this paper can help us to understand the complex weather regime behavior in the atmosphere.

2. THE MODEL

Our model is essentially the same as the highly truncated two-layer spectral channel model of Charney and Straus (1980). The important difference between the two models is that we retain two waves in the zonal direction so we can represent a baroclinically unstable synoptic scale wave that interacts directly with the large scale wave. As in Charney and Straus, we will use the notation devised by Lorenz (1960b) where $\Psi = \frac{1}{2}(\Psi_1 + \Psi_3)$ is the mean streamfunction, $\tau = \frac{1}{2}(\Psi_1 - \Psi_3)$ is the mean shear streamfunction, $\Theta = \frac{1}{2}(\Theta_1 + \Theta_3)$ is the mean potential temperature, $\sigma = \frac{1}{2}(\Theta_1 - \Theta_3)$ is the static stability, which is assumed constant, and $\chi_1 = -\chi_3$ is the velocity potential. The subscripts 1 and 3 refer to the middle of the upper and lower layers, respectively. The system of equations becomes:

$$\begin{aligned}
&\partial\nabla^2\Psi/\partial t + J(\Psi,\nabla^2\Psi) + J(\tau,\nabla^2\tau) + \beta\partial\Psi/\partial x = \\
&\qquad -.5\,J(\Psi, f h_0/H) + .5\,J(\tau, f h_0/H) + k''\nabla^2(\tau-\Psi) \\
&\partial\nabla^2\tau/\partial t + J(\Psi,\nabla^2\tau) + J(\tau,\nabla^2\Psi) + \beta\partial\tau/\partial x - f\nabla^2\chi = \\
&\qquad +.5\,J(\Psi, f h_0/H) - .5\,J(\tau, f h_0/H) - k''\nabla^2\Psi - 2k'''\nabla^2\tau \\
&\partial\Theta/\partial t + J(\Psi,\Theta) - \sigma\nabla^2\chi = h''(\Theta^* - \Theta)
\end{aligned} \tag{2.1}$$

where the Jacobian $J(A,B)$ is defined as $\partial A/\partial x\,\partial B/\partial y - \partial B/\partial x\,\partial A/\partial y$, f is the coriolis parameter $2\Omega\sin\phi_0$, where ϕ_0 is some specified latitude and Ω is the angular velocity of the earth, β is the gradient of f, $1/a_0(df/d\phi)$,

where a_o is the radius of the earth, $\nabla^2\chi$ is the horizontal divergence given by the continuity equation $\nabla^2\chi = -\partial w/\partial p$ where w is the pressure velocity, k'' is the Ekman damping coefficient at the surface, k''' is the Ekman damping coefficient between the layers, H is the thickness of each layer, h_o is the topographic height, where $h_o/H << 1$, h is the Newtionian cooling coefficient, and Θ^* is a prescribed radiative equilibrium temperature field. The system of equations is closed by the thermal wind relation

$$\nabla^2\gamma = -(c_p b^*/2f)\nabla^2\Theta \qquad (2.2)$$

where c_p is the heat capacity of air at constant pressure, and b^* equals $(p_1/p_{oo})^\kappa - (p_3/p_{oo})^\kappa$ where p_1 and p_3 are the pressure levels at the center of the two layers (400 and 800 mb, respectively), p_{oo} is the surface pressure, 1000 mb., and κ is the ratio $R/c_p = 2/7$, where R is the gas constant. This form of the thermal wind relation for a two layer model is derived by Young (1966). For details of the model, see Appendix I.

Following Lorenz (1960a), we will maximally simplify the two layer quasi-geostrophic system by expanding the dependent variables in orthonormal eigenfunctions of the Laplace operator ∇^2 and retaining the fewest number of modes possible that still possess the necessary physics to simulate the phenomenon of interest. In order to be useful for testing our

hypothesis, the model must contain the interaction between an externally forced planetary scale wave and a baroclinically unstable synoptic scale wave. We must choose our truncation such that this minimum requirement is met.

The decomposition of the equations into spectral form is given by Lorenz (1962, 1963), Young (1966), Yau (1977,1980), Charney and DeVore (1979), and Charney and Straus (1980) and will not be repeated in detail here. In essence, we write the equations in dimensionless form and expand the dependent variables in terms of the orthonormal eigenfunctions F_j. The expansions and the relations between the nondimensional(RHS) and dimensional(LHS) forms of the parameters and the dependent variables (where the nondimensional dependent variables are denoted by subscripts) are given by:

$$L^2\nabla^2 F_j = -a_j^2 F_j$$

$$\Psi = L^2 f \sum \Psi_j F_j \qquad \nabla^2\chi = f\sum w_j F_j \qquad k'' = fk$$

$$\zeta = L^2 f \sum \zeta_j F_j \qquad \Theta^* = AL^2 f \sum \Theta_j^* F_j \qquad k''' = fk'$$

$$\Theta = AL^2 f \sum \Theta_j F_j \qquad t_o = t/f \qquad h'' = fh$$

$$h_o = H\sum h_j F_j \qquad \beta = (L/a_o)\cot\phi \qquad \sigma = AL^2 f \sigma_o$$

$$x_o = xL \qquad y_o = yL \qquad \zeta = \Theta \quad \text{(Thermal wind)}$$

(2.3)

where L is some horizontal scale factor, $A=-(2f/c_p b^*)$, and t_o, x_o, and y_o are the dimensional forms of the time and eastward and northward coordinates, respectively. The spectral form of the equations is obtained by substituting the above expansions

into the original equations. We obtain:

$$\dot{\Theta}_i = \sum_j \sum_{j>k} c_{ijk}(\Theta_j\Psi_k - \Psi_j\Theta_k) + \sigma_0 w_i + h(\Theta_i^* - \Theta_i)$$

$$\dot{\Psi}_i = \sum_j \sum_{j>k} c_{ijk}[(a_j^2 - a_k^2)(\Psi_j\Psi_k + \Theta_j\Theta_k) + \hbar_j(\Theta_k - \Psi_k) + \hbar_k(\Psi_j - \Theta_j)]/a_i^2$$
$$+\beta \sum_j b_{ij}\Psi_j/a_i^2 - k(\Psi_i - \Theta_i)$$

$$\dot{\Theta}_i = \sum_j \sum_{j>k} c_{ijk}[(a_j^2 - a_k^2)(\Psi_j\Theta_k + \Psi_k\Theta_j) - \hbar_j(\Theta_k - \Psi_k) - \hbar_k(\Psi_j - \Theta_j)]/a_i^2$$
$$+ \beta\sum_j b_{ij}\Theta_j/a - w_i/a_i^2 + k\Psi_i - (k + 2k')\Theta_i$$

(2.4)

where $c_{ijk} = L^2/2\pi^2 \iint F_i J(F_j, F_k)\,dx\,dy$ are the interaction coefficients, and $b_{ij} = L/2\pi \iint F_i \partial F_j/\partial x \; dx\,dy$. This system can be further simplified by eliminating w_i between the two Θ equations.

Our model, like that of Charney and Straus, is a channel model with zonal walls at nondimensional $y=0$ and $y=\pi$ and is subject to the boundary conditions of no flow through the wall and no net torque or momentum drag on the wall. The rectangular geometry and these boundary conditions determine the final form of the allowable orthonormal eigenfunctions F_i.

We will choose to truncate the model at two waves in x and two waves in y. This is the fewest number of components possible that provides a planetary scale and a synoptic scale and a nonzero wave-wave interaction coefficient. This wave-wave interaction coefficient is the main new feature of this model and is the dynamic mechanism through which the planetary scale and the synoptic scale are directly coupled.

We will label these eigenfunctions as F_i where $i = 1,2,3,\ldots,10$. They are:

Mode 11	Mode 21
$F_1 = \sqrt{2}\cos(y)$	$F_4 = \sqrt{2}\cos(2y)$
$F_2 = 2\sin(y)\cos(nx)$	$F_5 = 2\sin(2y)\cos(nx)$
$F_3 = 2\sin(y)\sin(nx)$	$F_6 = 2\sin(2y)\sin(nx)$
Mode 12	**Mode 22**
$F_7 = 2\sin(y)\cos(2nx)$	$F_9 = 2\sin(2y)\cos(2nx)$
$F_8 = 2\sin(y)\sin(2nx)$	$F_{10} = 2\sin(2y)\sin(2nx)$

(2.5)

where n is one half the ratio of the meridional wavelength to the zonal wavelength and is related to the global wavenumber m by $m = na_6\cos\phi/L$. In addition, we have classified each set of eigenfunctions into "modes" which represent the scale of the particular two dimensional wave and zonal flow (both the Mode 11 and Mode 21 variables contain eigenfunctions which have only zonal structure, i.e. F_1 and F_4). For example, Mode 12 corresponds to one wave in y and two waves in x, Ψ_7 and Ψ_8. In this manner we can categorize what scales of motion influence a given variable. From the form of the equations, we note that only topography and the nonlinear advective terms provide coupling mechanisms between the modes. The remaining linear terms are effective only within a given mode.

The spectral form of the model then consists of 20

ordinary differential equations for the amplitude coefficients of the ten eigenfunctions of the streamfunction Ψ and the potential temperature Θ. Before the equations can be written down, we must decide upon the form of the heating Θ^* and the topography h_c. To best-simulate the equator to pole differential heating, the model will be driven by applying only a zonally symmetric south to north temperature difference, thus all components of Θ^*_j are zero except Θ^*_1. The nondimensional heating profile is then given by $\Theta^*(y)=\sqrt{2}\,\Theta^*_1\cos y$, which is a fairly good first approximation of the earth's equator to pole radiative equilibrium temperature field. Topography, then, will provide the only zonally inhomogeneous forcing in the model. For consistency with our hypothesis, we require that the flow be forced at the largest possible scale, which is designated by the eigenfunctions F_2 and F_3. For simplicity, only the amplitude of the F_2 topographic component will be chosen different from zero. The final model equations become:

(See following pages) (2.6)

where the non-zero interaction coefficients (the calculation of the interaction coefficients is given in Appendix II) are:

$$-8\sqrt{2}\, n/15\pi = c_1/5 = c_2/4 = c_3/10 = c_4/8 = c_5/16 \qquad 3n/2 = c_6$$

(2.7)

and the eigennumbers $a_1^2, a_2^2, a_3^2, \ldots, a_{10}^2$ are:

$$a_1^2 = 1 \qquad a_3^2 = (n^2+1) \qquad a_5^2 = (n^2+4)$$

$$a_2^2 = (n^2+1) \qquad a_4^2 = 4 \qquad a_6^2 = (n^2+4)$$

$$a_7^2 = (4n^2+1) \qquad a_9^2 = (4n^2+4)$$

$$a_8^2 = (4n^2+1) \qquad a_{10}^2 = (4n^2+4)$$

(2.8)

From the form of the equations we note that there are certain independent subsystems. For example, if all the variables except the Mode 11 variables are set to zero, they will remain zero. The remaining tendency equations for the Mode 11 variables then form an independent subsystem. Other independent subsystems are:

$$\Psi_1\ \Psi_2\ \Psi_3\ \Psi_9\ \Psi_{10}\ \ \Theta_1\ \Theta_2\ \Theta_3\ \Theta_9\ \Theta_{10}$$

i.e., Modes 11 and 22.

3. MODEL SCALING

One of the most important aspects of any model study is the degree to which the model under consideration simulates the atmosphere. Even this particular very simple highly truncated model contains parameters representing the magnitude of various physical effects, such as Ekman friction. Though we can always set these parameters to values we consider appropriate to the atmosphere, this does not guarantee that the model will behave in a manner that we would consider as realistic. The severe truncation and lack of smaller scales undoubtedly enhances the sensitivity of the few remaining scales of motion to the parameters. In fact, it may not be possible to simultaneously have both the dimensional values of all the parameters and the qualitative aspects of the time dependent flow "earthlike". It is reasonable to assume that at least some of the parameters will have to be adjusted to compensate for the effect of spatial scales and physical processes left out of the model.

The relation between the dimensional and nondimensional variables and external parameters is given by (2.3). All we need do then, is to select appropriate values for L, H, f, and the dissipative time scales and all the nondimensional parameters are determined. However, of these scale factors and time scales, only f is known precisely. There are a range

of acceptable values for L, H, and the dissipative time scales which lead to a large range of nondimensional parameters for our model which are arguably earthlike. The problem, however, is not so much the scaling, but the sensitivity of the model to the external parameters. For example, estimates of the atmospheric dissipative time scale easily vary by a factor of three; however, in our model, a factor of three difference in the nondimensional parameter k results in qualitatively very different flows. We shall therefore consider a range of nondimensional parameters and scale factors which arguably correspond to atmospheric values, and then subjectively determine whether or not the qualitative behavior of the model flow is atmospheric. Each category of parameters will be considered individually.

1). The dissipative parameters

Appropriate values for the atmospheric dissipative time scales $(k'')^{-1}$ and $(h'')^{-1}$ are generally ascertained to range from about 6 to 20 days. If we select f to be 10^{-4}/s, its approximate value at 45° north, then the corresponding nondimensional parameters k and h range from .02 to .005. The internal dissipative time scale, $(k''')^{-1}$, which is not well known (but should be very long), will be taken to be about an order of magnitude longer, which gives a nondimensional range of values for k' of .002 to .0005.

2). The beta effect.

Beta is scaled by $L\cot\phi/a_0$ where a_0 is the radius of the earth, about 6400 km. An approximate range for L will be taken to be 1200 to 2000 km., or a channel width πL=4000 to 7000 km., which gives a nondimensional beta of .18 to .33 at 45°N. However, a change of only 5 degrees latitude in where we choose to center our channel (which also changes f slightly), say from 45° to 50°N with L=1600 km., changes nondimensional beta from .25 to .21. Consequently, even for fixed L there is considerable flexibility in our selection of beta.

3). The temperature parameters.

The temperature scales depend upon the parameter A which is determined by the thermal wind relation (2.2). If we choose our model top to be at 200 mb, and the surface to be at 1000 mb., $A=1.1886\times10^{-10}$ s°K/cm^2 (see Young, 1966), which for our previous range of L, gives a range in the quantity AL^2f of 170 to 475. Typical values of the north south radiative equilibrium temperature difference are given by 70 to 200 °K (Stone, personal communication). In our model, since the heating is given by $\Theta^*(y)=\sqrt{2}\,\Theta_1^*AL^2f\cos y$, appropriate nondimensional values of Θ_1^* then range from .05 to .25.

The static stability measures the temperature difference between the middle layer and the upper or lower layer, which in our model is separated by 200 mb. Appropriate values for the lapse rate of potential temperature over the depth of the atmosphere range from perhaps as low as $5^{\circ}K/200$ mb to $15^{\circ}K/200$ mb. For the US standard atmosphere, the lapse rate is approximately $11^{\circ}K/200$ mb. These values correspond to a nondimensional range of σ_0 from about .02 to .06 for the previously mentioned range of L.

4) Topography

The topography is scaled by the thickness H of each model layer. Since we have chosen the model top to be at 200 mb., the thickness of each layer is about 400 mb. which corresponds to an H of about 4 to 5 km. The dimensional mountain height is then given by $\hat{h}_0 = 2H\hat{h}_2 \sin y \cos nx$. The nondimensional value of $\hat{h}_2$ is then restricted by the condition that $\hat{h}_2 << .5$.

5) Wavenumber

The parameter n corresponds to the global wavenumber m through the relation $m = na_e \cos\phi / L$. The selection of n then determines the scale of the longest wave in our model. To be consistent with our hypothesis, we must select n such that the

largest scale in our model corresponds to a planetary scale disturbance, i.e., m<5, but more importantly, n must be chosen such that the 2n wave (Mode 12) is more unstable baroclinically than the n (Mode 11) wave. To meet both of these criteria, we find that n generally must be less than 1.5.

In summary, "arguably" earthlike ranges for our 8 nondimensional parameters are then given by:

$$k=.005 \text{ to } .02,\ k'=.0005 \text{ to } .002,\ \beta=.15 \text{ to } .35,$$
$$\hat{h}_1<.35,\ h=.005 \text{ to } .02,\ \sigma_0=.02 \text{ to } .06,$$
$$\Theta_1^*=.05 \text{ to } .25, \text{ and } n<1.5. \qquad (3.1)$$

Though we cannot justify completely independent variation of certain parameters, we see that there is still considerable flexibility in the range of nondimensional parameters that correspond to earthlike conditions.

However, time dependent calculations with the above nondimensional parameters indicate that the qualitative behavior of the flow does not become "earthlike" until we substantially increase the dissipative parameters and slightly increase the static stability. With the values of the dissipative parameters as they stand, the model has a tendency to develop absurd easterly surface flows (>40 m/s) with an associated near zero zonal flow aloft, a configuration far

from an earthlike situation. The reason for this behavior is not entirely clear, but the fact that the problem can be eliminated by sufficiently increasing the nondimensional dissipative parameters suggests that excessive dissipation is necessary to compensate for the lack of eddy damping that would normally be present in an untruncated model. (The lack of eddy damping in highly truncated models is also discussed by Young (1966)). We have found that increasing the dissipative parameters to values where k and h are greater than .03 is generally sufficient to limit the surface easterlies to reasonable speeds for most ranges of the other parameters.

With the values of the static stability as they stand the time integrations lead to flows in which the small scale circulations are too vigorous, i.e., all the energy is contained in these scales. This problem is directly related to ascertaining the scale height H, or the thickness of each layer of the model. Our selection of 200 mb. as the model top has inadvertently given us an H of 4 to 5 km. However, from the dispersion relation for baroclinic instability in a two layer model (see Pedlosky(1979)) it is found that in order to best simulate the baroclinic dispersion relation of the continuous atmosphere, H should be 7 to 8 km., the typical scale height of baroclinically unstable modes in the continuous atmosphere. With such a scale height, the top of

the model atmosphere then appears to extend into the stratosphere. The problem is that we cannot relate the pressure levels and corresponding heights of the observed atmosphere directly to the two layer approximation and simultaneously simulate the baroclinic processes in the continuous atmosphere. Consequently, since it is more important to simulate the physical processes of the continuous atmosphere, we "stretch" the pressure height relationship in the sense that the 600 mb. level centers at 7 to 8 km. instead of 4 to 5 km. as observed. The stretching of the scale height also demands that the nondimensional values of the static stability and mountain heights must also be stretched. The dimensional static stability and mountain heights that correspond to these stretched nondimensional values then appear unrealistically large, but if they are viewed relative to the pressure levels instead of the scale heights, they become much more realistic. With these considerations, the dimensional static stability parameter σ_o ranges from about .08 to .20.

With these alterations, the following ranges of nondimensional parameters will be considered as "atmospheric" and appropriate for experiments:

$k=.03-.06 \quad k'=.001-.02 \quad \beta=.15-.35$

$\hbar_2 < .35 \quad h=.03-.06 \quad \sigma_0=.09-.20$

$\Theta_1^*=.05-.25 \quad n<1.5.$

(3.2)

As mentioned above, it is not entirely correct to select any arbitrary combination of the 8 parameters. Thus we have considered a range of parameters that result in flows which, qualitatively, are earthlike, primarily to de-emphasize the practice of quantitatively associating a given parameter set with a specific set of external conditions on the earth. However, if we fix L=1600 km., we can narrow our choice of parameters somewhat, though we may wish to vary parameters such as Θ_1^*, $\hbar_2$, and n beyond values which we consider as earthlike for academic purposes. In any case, with L fixed as above, acceptable ranges for the nondimensional parameters dependent upon L become:

$\beta=.20$ to $.27 \quad \sigma_0=.09$ to $.18 \quad \Theta_1^*=.05$ to $.25 \quad n<1.5$

(3.3)

4. MULTIPLE EQUILIBRIA

There already have been a host of studies concerned with the multiple flow equilibrium problem, therefore we will not consider the properties of the equilibria in any great detail. We are primarily interested in obtaining the model equilibria to study their relation to the time dependent behavior of the model when the effects of synoptic-scale instabilties are included.

To obtain the equilibria we could set the tendency terms to zero and solve the twenty simultaneous nonlinear equations for the twenty variables. This would be an arduous if not impossible task. However, obtaining all the equilibria for the twenty variable system is most likely unnecessary. As we have pointed out in the Introduction, any equilibrium state is highly baroclinically unstable to synoptic-scale perturbations (this claim will be explicitly demonstrated shortly through the examination of the stability problem). Though there are undoubtedly model equilibrium solutions with synoptic-scale components, rapidly growing instabilities at the synoptic scale are likely to destroy any degree of organization of the time mean state at this scale. This suggests that we concentrate our efforts upon obtaining only the large-scale equilibria. In our model, the planetary scale corresponds to the directly externally forced Mode 11 variables, which form

an independent subsystem. Thus the equilibria for the Mode 11 prognostic equations are also solutions to the entire twenty variable model.

The implication that only the Mode 11 equilibria are important to the time-dependent behavior of the model is an assumption which can only be truly justified in hindsight. If the synoptic-scale components of the equilibria were important, we would expect to see some signal from them in the time mean, but as will be seen shortly, the only non-zero components in the time-average state of the model flow are the Mode 11 variables.

The Mode 11 system of equations, from which our equilibria will be calculated, is identical to the system from which Charney and Straus obtained their equilibria. To solve the system we reduced the 6 equations in 6 variables to one algebraic equation in Ψ_1 which is solved numerically by a one dimensional binomial chop, (for details, see Appendix III). Consequently, we can always obtain all the roots for any set of external parameters, limited only by the resolution of the computer. The Mode 11 equations are:

$$0= c_1 \hbar_2 (\Theta_3 - \Psi_3) - k (\Psi_1 - \Theta_1)$$

$$0= c_1 n^2 (\Psi_1 \Psi_3 + \Theta_1 \Theta_3) + \beta n \Psi_3 - k (n^2 + 1) (\Psi_2 - \Theta_2)$$

$$0= -c_1 n^2 (\Psi_1 \Psi_2 + \Theta_1 \Theta_2) - \beta n \Psi_2 - k (n^2 + 1) (\Psi_3 - \Theta_3) + c_1 \hbar_2 (\Psi_1 - \Theta_1)$$

$$0= c_1 (\Theta_2 \Psi_3 - \Psi_2 \Theta_3) + c_1 \sigma_0 \hbar_2 (\Psi_3 - \Theta_3) + h (\Theta_1^* - \Theta_1) + k \sigma_0 \Psi_1 - (k + 2k') \sigma_0 \Theta_1$$

$$0= -c_1 [(1 - \sigma_0 n^2) \Theta_1 \Psi_3 - (1 + \sigma_0 n^2) \Psi_1 \Theta_3] + \beta \sigma_0 n \Theta_3 - h \Theta_2 + k \sigma_0 (n^2 + 1) \Psi_2$$
$$- (n^2 + 1) \sigma_0 (k + 2k') \Theta_2$$

$$0= c_1 [(1 - \sigma_0 n^2) \Theta_1 \Psi_2 - (1 + \sigma_0 n^2) \Psi_1 \Theta_2] - \beta \sigma_0 n \Theta_2 - h \Theta_3 + k \sigma_0 (n^2 + 1) \Psi_3$$
$$- (n^2 + 1) \sigma_0 (k + 2k') \Theta_3 + c_1 \hbar_2 \sigma_0 (\Theta_1 - \Psi_1)$$

(4.1)

One solution, which can be obtained immediately by setting all the wave variables equal to zero, is the purely zonal equilbrium state referred to as the Hadley Solution by Lorenz (1962, 1963). From the Ψ_1 tendency equation we see $\Psi_1 = \Theta_1$ which implies that there is no surface flow and thus no interaction with topography. From the Θ_1 tendency equation we obtain

$$\Theta_1 = h \Theta_1^* / (2k' \sigma_0 + h).$$

All the remaining equilibria have nonzero wave components and can only be obtained numerically.

It is not possible to investigate the complete behavior of the wavy equilibria as a function of the eight parameters, but some qualitative aspects of the solutions can be ascertained by varying a given parameter and holding the

others fixed. There are two qualitative aspects of the equilibiria that are of interest to this study. First, we find that the phase and amplitude of the equilibria are very sensitive to small changes in the external parameters, especially k, β, $\hat{n}_2$, Θ_1^* and n (for example, see Figure 1). As mentioned previously, the extreme sensitivity of the equilibria is probably an artifact of the severe truncation. Second, the wavy equilibria occur in pairs; thus the total number of solutions, including the Hadley state, is either one, three or five. At least one of these pairs of wavy equilibria consist of a trough near the mountain ridge while the other solution consists of a ridge (though by no means related by a simple 180 degree phase shift), suggesting the super and subresonant locking phenomena discussed by Charney and DeVore (1979) and Roads (1980a, 1980b).

One property of the equilibria that is of interest to this study is the stability of the equilibria to the various modes. This property can be ascertained in the standard manner by linearizing the model equations about the various equilibrium states and solving an eigenvalue problem for the growth rates γ. The form of the equations is such that the eigenmodes separate into either pure Mode 11, Mode 22, and coupled Mode 21 and Mode 12 structure (the perturbation matrices are given in Appendix IV). The eigenvalues γ of the pure Mode 11 and Mode 22 eigenmodes then determine the

stability of the equilibria to Mode 11 and Mode 22 perturbations respectively. To determine the stability of the equilibria to Mode 12 and Mode 21 disturbances we must consider the detailed structure of the unstable coupled eigenmodes to ascertain which perturbation scale dominates. Through these methods, we can obtain the e-folding times of the instability of each equilibrium state to each of the four classes of modes in the model.

For an example we consider the equilibria and their stability properties as a function of for the parameter set k=.04, k'=.005, β =.22, $\hbar_2$=.3, h=.045, σ_0 =.15, n=1.22 for Θ_1^* ranging from .06 to .18. (This is a case which we consider in Chapter 5, in which we discuss the time dependent behavior of the model). In Figure 1, we plot the amplitude of the Ψ_2 component of the equilibria as a function of Θ_1^*. For low values of Θ_1^* only the Hadley Solution exists, which is purely zonal and has no wave amplitude. For Θ_1^*>.075, two wavy equilibria appear and for Θ_1^*>.105 two more wavy equilibria appear. The upper branch of the first two solutions shall be called the 90° Ridge, since the phase of the Mode 11 wave is generally about 90° west of the orographic ridge for the bulk of the values of Θ_1^* considered, while the lower branch will be referred to as the 45° Trough for similar reasons. The upper branch of the second pair of solutions shall likewise be called the 30° Ridge while the lower branch will be referred to

as the Near Hadley solution since it has very low wave amplitude and a high zonal index. (For plots of the equilibrium flow patterns as they appear in the model, see Chapter 6, on model synoptics).

In Figures 2a and b, we plot the e-folding times of the instabilities of the various equilibria to the four modes of the model. (For this particular case, all the solutions are stable to Mode 22 perturbations, so we need only to consider the other three modes). The 90° Ridge and the 45° Trough are considered in Fig. 2a and the remaining three equilibria in Fig. 2b.

We see that on the whole the stability of the equilibria decreases as θ_1^* increases. The primary exceptions to this tendency are the Mode 11 disturbances labeled "orographic". These orographic or form drag instabilities, discussed in detail by Charney and Straus, are characterized by the lack of an imaginary component in the eigenvalues; thus they are disturbances which grow in place. All the other instabilities are topographically modified baroclinic disturbances. We note that the Mode 12 disturbance is the most rapidly growing instability for all the equilibria, with e-folding times generally less than 4 to 5 days. The only exception is the very high growth rates obtained by the Mode 11 orographic instability of the Near Hadley solution at values of

somewhat greater than .14.

It is also interesting to note that the Hadley Solution becomes completely stable to Mode 11 disturbances at $\Theta_1^* = .13$ since the orographic eigenmode becomes stable and the baroclinic eigenmode does not become unstable until $\Theta_1^* = .14$. For some parameter sets, both orographically and baroclinically unstable Mode 11 eigenmodes exist simultaneously, cf. Charney and Straus (1980).

RECAPITULATION

We have extended the simple highly truncated spectral channel model of Charney and Straus to include both a topographically forced planetary scale wave and a synoptic scale wave which can directly interact. The model has eight external parameters k, k', β, $\hbar_2$, h, σ_0, Θ_1^*, and n which must be specified before the system can be integrated. We then considered a range of nondimensional values for each of these eight parameters which could arguably correspond to earthlike values. A technique was developed to compute all the large-scale equilibria and their respective stabilities to perturbations on the scale of each of the four modes. We are now ready to investigate the time dependent behavior of the model for general sets of external parameters.

5. TIME DEPENDENT BEHAVIOR

We approach the majority of our time dependent investigations in a similar manner: First we select a set of appropriate external parameters which then remain fixed throughout the entire process of integration. Once the parameters are chosen, we use the routines discussed previously to calculate all the equilibria and their respective stabilities. The model is then initialized at one of its equilibrium states and perturbed by a small Mode 21 ($\Psi_5 = .002$) and Mode 12 ($\Psi_7 = .001$) disturbance to which all the equilibria are highly unstable. The equations are then numerically integrated in time steps of 1.5 hours using the N-cycle scheme of Lorenz (1971), with N=4.

The aspects of the time dependent behavior we are most interested in are the periods of quasi-stationarity. As discussed previously, quasi-stationary behavior is observed to be confined primarily to the planetary scale, which in our simple model is represented by the Mode 11 wave. Consequently, we can identify the occurrence of a regime or quasi-stationary period simply by observing the behavior of this single wave.

To analyze the time dependent behavior of the Mode 11 wave, we construct phase space plots whose axes are defined by

the streamfunction variables Ψ_3 and Ψ_2, and observe the motions of this two-dimensional projection of the 20 dimensional model trajectory as a function of time. The occurrence of regimes is then noted by the tendency for the trajectory to be contained within a certain region of phase space for an extended period of time.

Before we actually consider any time dependent calculations, we briefly discuss the behavior of the flow as anticipated by the multiple flow equilibria theory (MFET). As stated in the introduction, one of the primary assumptions of the MFET is that the synoptic-scale baroclinic instabilties provide a mechanism through which the state of the atmosphere vacillates from one "realizable" equilibrium state to another, where "realizable" equilibria are defined by Charney and DeVore, Charney and Straus, and Charney et. al. as those equilibria which are quasi-stable to large-scale perturbations. Implicit in this assumption is that the effects of the synoptic scales upon the equilibria themselves are minimal. These assumptions imply that the qualitative time dependent behavior of our model is determined by the phase space positions of the equilibria and their respective stabilities to Mode 11 disturbances. In particular, the MFET assumes that periods of quasi- stationary behavior and blocks are intimately tied to the location of the calculated quasi-stable equilibria, and the trajectory should be observed

to aperiodically vacillate between such states.

The most important result of our time dependent experiments is that, for a wide range of the external parameters, the model atmosphere is observed to aperiodically settle into one of two distinct flow configurations for extended periods of time. These two preferred states are characterized by the confinement of the Mode 11 components of the trajectory to two distinct regions of phase space, behavior which we will define as quasi-stationarity in the large-scale Mode 11 wave. Superposed upon these quasi-stationary large-scale Mode 11 features are erratic eastward propogating synoptic-scale waves with periods on the order of three to five days. This rather remarkable weather regime behavior is best illustrated by the consideration of an example. We select the parameter set

$k=.05$, $k'=.01$, $\beta=.2$, $\hat{n}_2=.2$,

$h=.045$, $\sigma_0=.1$, $\theta_1^*=.1$, and $n=1.3$,

whose five equilibrium states and respective stabilities to the four modes are given in Table 2.

We can see that the purely zonal Hadley solution (#1) and the low wave amplitude Near-Hadley solution (#2) possess high zonal indexes. The other three solutions possess substantial wave amplitude and lower zonal indexes and are named according to the position of the mid-level wave with respect to the

orography. Two of the equilibria, the Near Hadley solution (#2) and the 90 degree Ridge solution (#3), have easterly surface flow, $\Psi_1 - \Theta_1 < 0$. We also note that even though one of the equilibria is stable and one weakly unstable to Mode 11 perturbations, all of the equilibria are highly unstable to Mode 12 synoptic-scale perturbations. From the form of the eigenmode and the eigenvalue (not shown), it can be ascertained that the Mode 12 instabilities are all propagating baroclinic disturbances. The only non-propagating orographic instabilities for this particular set of parameters are Mode 11 perturbations upon the 30 degree Ridge and Near Hadley solutions.

Figure 3a is a plot of the daily position of the $\Psi_3 - \Psi_2$ component of the trajectory for the first 17 years of the integration period, which is taken as representative of the climatological state of the Mode 11 wave. Though the rather limited range of phases in the climatological state is in itself noteworthy, the most interesting behavior is not revealed until we compare the climatological state of the model with Figures 3b and 3c. The latter two figures are again plots of the daily position of the $\Psi_3 - \Psi_2$ component of the trajectory, but for periods that coincide with the duration of the two single weather regime events. Figure 3b consists of the 175 day period from time step 20765 to 23564, during which the trajectory remained exclusively in the lower

right hand quadrant, while Figure 3c consists of the 580 day period from time step 23564 to 32855, during which the trajectory remained primarily in the upper left hand quadrant. The comparision of the three figures clearly demonstrates the extended period of confinement of the large-scale component of the trajectory relative to the significantly more extensive climatological domain, which is exactly the type of behavior we intuitively associate with a weather regime.

It is also evident from the figures that the phase space trajectories are not, most of the time, confined in small neighborhoods about one or another of the equilibrium points. In fact, in both instances, we note that the equilibrium states lie outside the regions defined by the fringe of the scatter. However, a close inspection of the regimes plotted in Figs. 3b and 3c, which we shall refer to as the trough (or negative) and the ridge (or positive) regimes respectively, suggests that there is some relation between the equilibria and the time dependent quasi-steady states; it is just much more complicated than implied by the MFET.

We consider the details of the trough regime first since a correspon- dence to the equilibria appears more evident in this case. In Figs. 3a and b, we note that the points cluster primarily along a line of constant phase which is almost identical to the phase of the Trough equilibrium

solution (#4). The major discrepancy between the actual time dependent behavior of the trough regime and that anticipated by the MFET is that the Mode 11 mean wave amplitude of the regime state is significantly reduced over that of the corresponding equilibrium state, and though there is extensive vacillation of amplitude on an instantaneous basis, the Mode 11 wave never obtains the amplitude of the equilibrium state. However, the agreement between the phases of the waves in the two states strongly suggests that there exists some type of correspondence between the stationary trough solution and the time dependent trough regime states.

The ridge regime, on the other hand, possesses significant scatter in both the phase and amplitude and does not appear to be as clearly related to any of the equilibria as is the trough regime. The reason for the more complicated behavior is that the ridge regime appears to be an altered limit cycle, instead of an altered equilibrium state. (We will discuss the detailed nature of these limit cycles shortly.) The strong suggestion of quasi- circular or looping motions of the trajectory in Figs. 3a and 3c, which become immediately visible in real-time observations, further support this conclusion. The limit cycle, though, is closely related to the 90 degree Ridge equilibrium state (also to be discussed later), and we will see that the time mean structure of the ridge regime is also fairly well represented by the 90 degree

Ridge equilibrium state. Consequently, for both the ridge and trough regimes, there appears to be some relation between the regimes and some of the equilibria. This relation is clearly quite complex, especially in the case of the ridge regime. However, it is also of interest to note that there are still three equilibria which appear to be of no consequence to the time dependent flow, in spite of the fact that one of them, the Hadley solution, is only weakly unstable to Mode 11 perturbations as is the 90° Ridge Solution. In our model then, knowing the large-scale equilibria and their respective stabilities to Mode 11 disturbances is insufficient information for determining the qualitative aspects of the quasi-stationary time dependent flow.

Though it appears that some properties of the time dependent flow may be related to some of the equilibrium points, the influence of synoptic- scale disturbances on the nature of the regimes is clearly of great importance. This role becomes especially apparent when all the wave-wave interaction coefficients c_6 are set to zero, which then eliminates the direct coupling between the externally forced Mode 11 wave and the smaller scale synoptic waves. The immediate effect is a drastic reduction in the instantaneous fluctuations experienced by the large-scale wave, which previously (from Figs. 3b and 3c) was quite large in both regimes, though the aperiodic amplitude vacillation of the

wave in the trough state continues. However, the most important effect is the fact that for this particular set of external parameters, the ridge regime disappears. The trajectory then remains in the trough regime state for all time.

This behavior is demonstrated in Figure 4, which is generated in the same manner as Figure 3a, except that the wave-wave interaction has been eliminated. We can see that the overall behavior is less erratic than in Fig. 3a in the sense that the trajectory is confined to a smaller region of phase space. From our model equations we see that there are still interactions between the various scales but they are coupled through the zonal flows, and apparently this indirect coupling is incapable of inducing transition or maintaining the ridge regime. (By maintain we mean only that the direct wave-wave interactions are necessary for the occurrence of the ridge regime; we do not mean to imply that the synoptic-scale interactions act as, e.g., a forcing rather than a dissipation.) We have also found that the finite amplitude synoptic-scale disturbances (with and without the wave- wave interaction) differ remarkably from that predicted by linear theory. Though the Mode 12 disturbance grows most rapidly initially, the Mode 22 disturbance achieves the greatest amplitude and generally accounts for the bulk of the synoptic-scale amplitude sufficiently long after

initialization. This aspect is observed in all our experiments, even when linear theory predicts the Mode 22 wave is stable to infinitesimal perturbations (as in case #1 and case #2 to be discussed shortly).

To aid in the further analysis of the individual regime states it is adventageous to develop a quantitative scheme that can isolate quasi-steady periods from all other types of behavior. However, the objective identification and analysis of quasi-steady flow patterns in the atmosphere are not trivial problems (see Dole, 1982), and even though our model is considerably simpler than the real atmosphere, we have not been able to develop an objective scheme which is generally applicable, though we can easily subjectively discern the regime events by eye. Thus to isolate the regime events, we use a method analogous to the zero-decameter, 15-day cutoff criterion used by Dole in his objective analysis of atmospheric persistent anomalies (though we do not first remove a climatological state): we require that the state of the large scale Mode 11 wave, as measured by the sign of the advective term in the Ψ_2 tendency equation, $n^2 c_{123} (\Psi_1\Psi_3 + \Theta_1\Theta_3)$, remain the same for longer than 15 days. Though such a criterion appears at first to be quite weak, by coincidence, it happens to be effective for many parameter sets because the phase of the large-scale Mode 11 wave is often confined to a relatively narrow band, as demonstrated in Figure 3a.

Needless to say, the effectiveness of this ad-hoc criterion in isolating regimes has to be verified subjectively for every new set of external parameters considered. However, when this criterion is applicable, we can easily isolate and calculate the statistics of each individual regime by type, regardless of its persistence, as they occur in the time integrations.

We used this criterion in the case discussed previously (with wave- wave interaction) to calculate the type, length, and mean state of the regimes for a period of 205.5 years or 1.2 million time steps. In Table 3a, we present the type, the time step at the start and finish, the length in days of the regimes in their order of occurrence, and the upper ($\varphi_j = \psi_j + \theta_j$) and lower ($\phi_j = \psi_j - \theta_j$) level time mean state streamfunction for the first 28 years of the integration period. (The time mean states will be discussed shortly).

We can see from the table that the duration of the regimes is highly variable, ranging from as short as 25 days to as long as 1100 days. In addition we note that the occurrence of a ridge regime is not necessarily followed by a trough regime and vice-versa; there are several instances where the same type of regimes repeatedly occur. It is also apparent that the regimes are highly persistent (in spite of the fact that the synoptic-scale disturbances have periods in the order of 3 to 5 days), lasting in the order of months and

years instead of in the order of just a few weeks as commonly envisioned in the atmosphere. Furthermore, the ridge regime appears to be significantly more persistent than the trough regime. This distinction is made even more evident in the computation of the 205-year statistics. Over the 75000 day integration period, the ridge state accounted for 50469 days, while the trough state accounted for a considerably smaller 22565 days and periods of unsteady behavior for the remaining mere 1966 days. The flow behavior, then, for this particular parameter set is both ridge regime dominant (where dominant means a particular regime accounts for more than 50% of the steady or regime-type behavior) and persistent. These two properties of regime dominance and persistence are found to be quite sensitive to changes in the external parameters. Some aspects of this sensitivity will be demonstrated shortly when we discuss the behavior of the regimes as a function of Θ_1^*.

The time average of the model flow over the duration of the individual regime events are found to be non-zero only in the Mode 11 variables, which strongly supports our earlier notion that the baroclinic instability processes completely dominate at smaller scales. From the list of sequential cases in Table 3a we note that the mean states of the regimes undergo apparently random, but minor fluctuations, though there is a tendency for the less persistent regimes to possess both a greater zonal wind speed and lower wave amplitude in

the upper levels. To smooth out some of the random nature of the individual regime statistics, we form 205 year composites by type (ridge and trough) and seven categories of persistence (Cat. 2=15.0-18.75 days, cat. 3=18.75-26.0 days, cat. 4=26.0-32.25 days, cat. 5=32.25-43.75 days, cat. 6=43.75-62.5 days, cat. 7=62.5-125.0 days, cat. 8>125.0 days (note that there is no category 1)). In this manner we can ascertain an overall average regime state and note if there exists any substantial difference between the very persistent versus weakly persistent cases. In Table 3b, we list the time mean state upper and lower level streamfunction of the 205 year composites in phase and amplitude (instead of wave components) by type and category as well as the number of individual regime events and the total number of days that went into the calculation of the composite. For comparision, we also list the upper and lower level streamfunction values of the five equilibria in phase and amplitude form.

We note that the ridge regime is characterized by moderate easterly surface flow ($\phi_1 < 0$) while the trough regime possesses weak surface westerlies. This characteristic is also the case for all the individual regimes except for one 24 day ridge event which occurs at time step 1162108, which indicates that the direction of the surface flow rather than the value of the mean zonal flow in relation to resonance determines the phase of the large-scale wave. It is also

apparent that the trough regimes, especially the more persistent instances, possess both a greater time mean upper level wave amplitude and zonal wind speed than the ridge regimes, but one of the most distinctive differences between the two regimes is the significantly greater variability in the phase of the Mode 11 wave of the ridge regime. The trough regime wave, on the other hand, is nearly fixed in space from case to case.

From Table 3b we can also quantify the relation between the composite regime states and the five equilibria. It is clear that the Hadley, Near-Hadley, and 30 degree ridge solutions have nothing in common with any of the time mean regime states, but the phase of the upper and lower level wave as well as the sense of the surface flow correspond reasonably well between the 90 degree Ridge solution and the ridge regime and the Trough solution and the trough regime. The latter correspondence is distinctly better, as discussed previously, but in both cases, the wave amplitudes of the regime states are significantly smaller than the wave amplitudes of the corresponding equilibria. However, in all cases (individual time mean regime states, composite regime states, and all wavy equilibria) we note the distinct westward tilt of the large-scale wave in height, though the bulk of this tilt is confined to the lower layer, in the sense that the two layer model can be thought of as a "continuous" model with constant vertical

shear, which demonstrates the importance of baroclinicity in all these structures. The phase shift indicates that the waves contribute to the poleward heat transports.

In Figure 5, we plot in phase space the five equilibria, a scatter diagram of the time mean Mode 11 upper level wave streamfunction $\varphi = \Psi + \Theta$ for each of the regimes in Table 3a, and the composites, which are designated by a cicle (●), where the subscript n refers to the category. (Some of the equilibria, in particular solutions #3, #4, and #5, if plotted to scale would be off the figure. Consequently, we have plotted these three states at one half their actual amplitude, and have signified this by placing a subscript next to their respective circles.) It is quite apparent from the figure that the two regimes are significantly different from each other and possess relatively little scatter in their respective time mean states and are well represented by the composites. From the structure of these time mean patterns we see that the two regimes correspond to regionally vastly different climatic states, which are completely internally determined.

The final consideration concerns the degree to which the Mode 11 wave fluctuates during an individual regime event. The observations of the model trajectory during a given regime event suggest that the degree of fluctuation varies anywhere from relatively severe vacillations to nearly stationary

behavior. We can see this range of behavior in Figure 6a and 6b which are plots of the trajectory during fractions of the single 112 day trough regime event (the fourth regime in Table 3a). Figure 6a consists of the 18 day period from time step 4996 to 5284 while Figure 6b consists of the 24 day period from time step 5316 to 5700. We note that the region over which the points are scattered in Fig. 6b is extensively larger than the scatter in Fig. 6a. The very small region in which the trajectory remains confined in Fig. 6a signifies that the large-scale Mode 11 wave remained essentially stationary during this 18 day period of the 112 day regime.

We shall refer to these periods of near stationarity as regime type II behavior, though the distinction between flow that is sufficiently steady to qualify as type II and that which is not, is clearly arbitrary. However, the occurrence of regime type II behavior is of interest since at large amplitude it corresponds to the classic interpretation of the atmospheric block; an event generally characterized by near stationarity in the plantary scales and a large ratio of the planetary to synoptic-scale components. In this sense, the period of time plotted in Fig. 6a is an example of a "block" in our model. (Note that its duration is considerably shorter than that of the regime.) We can then investigate whether or not there are any qualitative dynamical dis tinctions between these periods of regime type II behavior and the more erratic

periods which are, nevertheless, part of regimes. However, from the above discussion, it seems most likely that these distinctions are merely quantitative, and the so-called block is simply a more spectacular, visibly striking, example of a weather regime.

We have discussed the occurrence of regimes and some of their properties for one case in our model. This particular case was selected for demonstration purposes because of its highly idealized two regime behavior. It is important to emphasize at this stage, that the qualitative aspects of the two regime behavior observed in this highly idealized case are also observed in the vast majority of our experiments considering numerous other sets of the previously determined acceptable parameters. However, the detailed properties of these regimes, i.e. time mean amplitude, regime dominance, and persistence, like the properties of the multiple equilibria, are found to be highly sensitive quantitatively to changes in the external parameters in a complex manner. Though both the regimes and equilibria are found to be sensitive to changes in the external parameters, the relation between the ridge and trough regimes and the 90° Ridge and 45° Trough equilibria persist in the same qualitative manner as discussed in the demonstration case; specifically the phase of the trough regimes are generally locked very close to the phase of the 45° Trough solutions and the ridge regimes show

characteristics suggestive of a large-scale Mode 11 limit cycle. The continual appearence of the remnants of a looping trajectory in the ridge regimes in all our experiments made it of interest to investigate the properties of this limit cycle and its relation to the 90 degree Ridge Equilibrium Solution and the ridge regime.

We investigate this question by observing the time dependent behavior of just the Mode 11 six-variable system. It turns out that for a limited range of the external parameters there is, in addition to the existence of several equilibria, a stable limit cycle whose trajectory traces out a counterclockwise loop that remains confined primarily to the upper left hand quadrant of the (Ψ_3 , Ψ_2) phase space plane. This ridge limit cycle continues to exist with the addition of a second y mode (Mode 11 and Mode 21) though it is radically destabilized; that is, it exists only for a narrow range of the external parameters. However, the 12-variable Mode 11 and Mode 21 system possesses a second limit cycle not present in the 6-variable system which is confined primarily to the lower right hand quadrant of the (Ψ_3 , Ψ_2) phase space plane. This new limit cycle defines a much tighter counterclockwise loop than the ridge limit cycle and is stable for a wide range of parameter sets. In Figure 7, we plot some of the equilibria, the 6 and 12 variable limit cycles, and some representative time mean states of the composite regimes for case #2 (to be

discussed shortly) with values of Θ_1^*=.12, .13, .14, .15, and some intermediate values.

In Figure 7, we see that the 6-variable ridge limit cycle is stable for values of Θ_1^* slightly greater than .12, but becomes unstable for values of Θ_1^* in excess of .145. We also note that the limit cycle appears to "develop" out of the 90 degree Ridge Solution and more or less encircle it; the finite amplitude response to the 90 degree Ridge becoming unstable. The 12-variable ridge limit cycle, on the other hand, is stable only for Θ_1^*=.12. (Again, whether the limit cycle is stable or unstable to Mode 11 or Mode 21 disturbances appears to be inconsequential to its incorporation into the detailed behavior of the full model ridge regimes. Our experiments show that the "looping" full model ridge regime exists for many more parameter sets than the 6-variable limit cycle is stable.) Figure 7 also demonstrates that the time mean states of the composite ridge regimes, whether an interaction with the 90 degree Ridge or the limit cycle, still possesses wave amplitudes considerably below that of the purely Mode 11 features.

The trough regime composites behave slightly differently. We note that the time mean wave amplitudes of the regimes actually exceed that of the 12-variable trough limit cycle. However, it is not clear that these limit cycles have any

influence upon the behavior of the full model trough regimes; at least there is no suggestion of the looping signal remaining in the full model. It appears then, that the 12-variable trough limit cycle is simply an artifact of the truncation and completely disappears with the addition of the synoptic scales. In any case, these rather complex behaviors and relations that are observed as we vary the truncation only further support the notion that the presence of the smaller scale instabilities are of qualitative significance to the large-scale externally forced disturbance.

We now investigate the functional dependence of the regime properties and the relation between the regimes and the corresponding equilibria to changes in the external parameters by selecting two case studies in which different values of the driving Θ_1^* are considered. For case #1 we select k=.04, k'=.01, β =.22, $\hbar_2$ =.2, h=.045, σ_0 =.12, and n=1.3 with the following five values of Θ_1^*: .07,.08,.09,.10,.11. For case #2 we select k=.04, k'=.005, β =.22, $\hbar_2$ =.3, h=.045, σ_0 =.15, and n=1.22 with the following 11 values of Θ_1^*: .07, .075, .0775, .08, .09, .10, .11, .12, .13, .14, .15. This gives a total of 16 experiments.

In Table 4a,b the infinitesimal stability of the equilibria to small amplitude perturbations of each of the four modes is given as a function of Θ_1^* for each case. (The

case #2 equilibria and their stabilities were discussed (and graphed) earlier in chapter 4). The equilibria are named according to the phase of the upper level wave when $\Theta_1^*=.10$ in case #1 and when $\Theta_1^*=.12$ in case #2 and identified by continuity as Θ_1^* is changed. The tables show that at higher values of Θ_1^* there are four wavy equilibria. At lower values of the driving the 30 degree Ridge and the Near Hadley solution disappear, while at values of Θ_1^* somewhere between .07 and .08, the remaining two equilibria, which we have defined as corresponding to the regime states, also disappear. This leaves only the purely zonal Hadley solution at the lowest values of Θ_1^* considered in our 16 experiments, which is stable to Mode 11 disturbances. However, we note again that all the equilibria are highly unstable to Mode 12 perturbations, except at the lowest values of the driving where the e-folding time is about 10 days. The existence of instability at these low values of Θ_1^* is important because it implies that the model atmosphere will still possess propagating synoptic-scale disturbances. It will then be of interest to investigate the nature of the large-scale time dependent flow and note whether or not the time mean state of the Mode 11 wave amplitude is zero as would be anticipated by the MFET.

Each of the 16 experiments is initialized in the manner discussed earlier and integrated for 17 years or 100000 time steps. To demonstrate the functional dependence of the time

mean regime states and their relation to the corresponding equilibria upon Θ_1^*, we plot the phase and amplitude of the upper level streamfunction of the composite ridge and trough regimes and their corresponding equilibria as a function of

for both cases in Figures 8a,b,c,d and 9a,b,c,d. (The numbers 8 and 9 correspond to case #1 and case #2 respectively, while a,b,c,d indicate plots of the trough amplitude, trough phase, ridge amplitude and ridge phase respectively.) To demonstrate the sensitivity of the regime persistence and dominance properties to Θ_1^*, we tabulate the total number of days accounted for by the ridge regime, the trough regime, both regimes (the sum of the ridge and trough columns which represent "steady" behavior), and periods of unsteady behavior (everything else) as a function of Θ_1^* in Tables 5a,b (a,b refer to case #1 and case #2 respectively). In addition we list the ten most persistent ridge and trough regimes in each of the 16 experiments.

It is clear from the tables and figures that the tendency for the regimes to persist and for a given regime to dominate depend in a rather complex manner upon Θ_1^*. We have likewise considered variations in other parameters and found that the regime properties depend in a complex manner upon these parameters as well. However, if we compare the statistics of the two regimes in case #1 and case #2 we observe two characteristics which appear to be relatively consistent as

is varied; first, since Figs. 8 and 9 are plotted to the same scale, we see that the trough regimes, especially the most persistent (highest) categories, possess a greater time mean wave amplitude than the ridge regimes (though the wave amplitude of both regime states is significantly reduced over that of the corresponding equilibria) at all values of θ_i^* above the point where the Mode 11 equilibria cease to exist. (Note that this relation also holds for the Trough and 90 degree Ridge Solutions). Second, whereas the wave amplitude of the trough composites appear to be more erratic (Figs. 8a, 9a) and their phases highly consistent (Figs. 8b, 9b), the wave amplitudes of the ridge composites are highly consistent (Figs. 8c, 9c) while the phases tend to be more erratic (Figs. 8d, 9d). However, the analysis of the two cases demonstrate other important features which are of significance to the understanding of the qualitative behavior of the regime phenomenon.

First, the eight figures demonstrate that the mean state of the seven composite regime categories vary continuously as a function of θ_i^*, in spite of the fact that the large-scale Mode 11 stability properties (see Figs. 2a and 2b) behave in a complex and discontinous manner. The continuous variation of the regime states while the Mode 11 stability properties switch from orographically unstable to absolutely stable to baroclinically unstable suggests that these detailed stability

properties are inconsequential to the final time dependent behavior of the flow.

A second, and most interesting, observation is that the multiple regime states continue to exist at values of the driving where the stationary Mode 11 equilibria no longer exist. (In case #1 this occurs at $\Theta_1^* = .07$ and in case #2 it occurs at $\Theta_1^* = .07$ and .075). This observation clearly demonstrates the importance of the dynamical influence of the synoptic-scale disturbances in our model. The existence of these regimes also implies that the synoptic- scale disturbances are capable of directly forcing and maintaining the large- scale circulation, further demonstrating the importance of accounting for the synoptic-scale interactions in the understanding of weather regime phenomena.

Third, and last, the one characteristic of the regime behavior that is evident in all 16 experiments involving Θ_1^* (as well as other experiments involving the remaining seven external parameters) is the highly variable duration of a single given regime event, regardless of the tendency for the individual regimes to persist. An excellent example of this indeterminent persistence is given in case #2 for $\Theta_1^* = .15$. In spite of the fact that the general state of the flow for this parameter set is highly unstable, one regime persisted for 102 days, more than twice the length of the second most persistent

event. Though it may be highly improbable, there is no reason not to assume that a 1000 day event may eventually occur. We demonstrate the highly arbitrary nature of the regime persistence by plotting the total number of regime events of a given type for case #2 with Θ_1^*=.12 and .14, which persist for x number of days or longer in Figure 10. (To minimize statistical fluctuations, we ran the model for 1.5 million time steps or 93,750 days or about 257 years.) For comparison, the cumulative distributions obtained by Dole (1982) for both positive and negative 5-dam persistent anomalies are also plotted.

If we had considered only periods longer than 15 days, all the distributions would be straight lines on the log-linear plot (except at the tail ends where a given event is statistically very rare), indicating that the probability a given event will persist for n+1 days, if it persists for n days, is constant. A dynamically preferred time scale, on the other hand, would appear as a bulge, e.g., some type of deviation from a straight line. Clearly, for periods greater than 15 days, our statistics (as well as Dole's) do not imply the existence of a preferred time scale.

However, a very interesting feature in the persistent anomaly distribution was noted by Dole at much shorter time periods which inspired us, in turn, to investigate the shorter

period model transitions. Between 3 to 10 days, depending upon which distribution is considered, there is a distinct kink, e.g., there is a first-order discontinuity, where the slope of the otherwise straight line distribution becomes abruptly steeper for shorter time periods. In addition, we find a pronounced but continuous bulge at about ten days in the model ridge regimes (not duplicated by Dole's statistics) which corresponds to the remnants of the limit cycle alluded to previously. As discussed by Dole (1982), this change in slope suggests the existence of two distinct dynamical processes, one characterized by relatively little persistence and the other characterized by greater persistence. Dole associates the former process with synoptic-scale disturbances and the latter with what he calls persistent anomalies, or in our terminology, regimes. The "kink" is especially apparent in the Θ_1^*=.12 trough distribution, demonstrating first that the persistent phenomenon is a much more dominant process at Θ_1^* = .12 than at Θ_1^*=.14 or in the atmosphere, and second, that the kink, and, thus, the distinction between the two unique dynamical processes (which is subtle in the atmospheric statistics), is a very real characteristic of externally forced multiply scaled baroclinic systems. For further discussion with regard to these distributions and their implications, the reader is referred to Dole.

With the exception of the model ridge regimes, then,

these distributions indicate that there is no favorable time scale for these phenomena. This result does not agree with the observational results of Charney et. al. (1981) who find a peak in their distributions of atmospheric persistent anomalies at 7 days. However, the statistical significance of this peak has not yet been established. Dole's more comprehensive analysis indicates that such peaks are quite sensitive to the method of analysis and he concluded that a statistically significant peak could not be resolved with his 14 year data set. We are also unable to resolve a distinct peak in our 257 year sample of model data. The resolution of this problem in the atmosphere clearly requires further study, but with regard to the model, it appears quite safe to conclude that there is no dynamically preferred time scale for these weather regime phenomena, except perhaps the "peak" at around 10 days associated with the limit cycle behavior in the ridge regime.

RECAPITULATION

We have investigated the time dependent behavior of our model for many sets of external parameters and found that the Mode 11 wave aperiodically vacillates between two distinct, "randomly" persistent, weather regime states. Though the regimes were a generic property of the model, we found that the quantitative characteristics of these regimes, ie. regime persistence, dominance, and structure, are highly sensitive to

the external parameters, as are the multiple equilibria themselves. A detailed analysis of the individual regime states showed that the time average was non-zero only in the Mode 11 variables and that the two regimes were generally characterized by a Mode 11 trough or ridge slightly west of the orographic ridge. We also noted that during a given regime event, the Mode 11 wave was found to undergo a wide range of fluctuations on an instantaneous basis, from highly erratic to nearly stationary. We then defined the nearly stationary periods as Regime type II behavior and recognized that such behavior at high amplitude was analogous to the classic interpretation of the atmospheric block, which, in turn, implied that blocking was simply a special case of the more general weather regime phenomenon.

Finally we noted that the differences between the observed time dependent behavior and that predicted by the MFET indicated that the synoptic scales must have interacted with the forced disturbances in a considerably more complicated manner than that anticipated by the MFET. It is also apparent that the finite amplitude synoptic-scale disturbances are much more crucial in determining the qualitative behavior of the large-scale flow than the Mode 11 stability properties. We see from Figs. 8 and 9 that the two regime behavior occurs for all values of Θ_1^* and varies continuously as a function of Θ_1^*, in spite of the fact that

the Mode 11 stability properties (graphed in Figs. 2a and 2b and discussed in the Multiple Equilibria section) behave in a complex manner as a function of Θ_1^*. None of this complex behavior is reflected in the time dependent behavior of the full model. We also noted that limit cycles, as well as the equilibria, may account for some of the large-scale behavior in our model.

6. MODEL SYNOPTICS

We have discussed the time dependent behavior of the model in considerable detail, but to further clarify some of the aspects of this behavior we create a series of "weather maps" which display the height and temperature fields at the model mid and lower levels for case #2 with $\Theta_1^*=.12$. For scaling purposes we choose L=1600 km. which gives a channel width πL=5027 km. The height field in dimensional units is then given by

$$z=(L^2 f \sum \psi_j F_j +\text{constant})=(2560 \sum \psi_j F_j +\text{constant}) \text{ meters}$$

where the constant (which is arbitrary in our simple model) is taken to be 5460 meters at the midlevel (to correspond to the 500 mb. surface) and 1440 meters at the lower level (to correspond to the 850 mb. level). Actually, the model mid and lower levels should be 600 and 800 mb. respectively, but these levels are not as familiar as the 500 and 850, and since the correspondence between a given model level and an atmospheric pressure level is by no means precise, the differences are rather inconsequential.

The dimensional temperature field is given by

$$\Theta =(AL^2 f \sum \Theta_j F_j +\text{constant})=(304 \sum \Theta_j F_j +\text{constant})^\circ K$$

where the constant is taken to be 253° K, the approximate mean

500 mb. temperature. Since G_0 is constant, the temperature field has the same form at all levels, thus we plot only the 500 mb. temperature but on the 850 mb. level. This practice is reasonable since the temperature field is directly proportional to the thickness field in our simple model. The scaling also gives us the radiative north-south temperature difference which for $\Theta_1^* = .12$ is 110°K.

In Figures 11a,b,c,d we plot the Near Hadley, 90°Ridge, 45° Trough, and the 30°Ridge respectively. In Figures 11 e,f we plot the category 7 trough and ridge regime mean state composites respectively. The height contours are every 6 decameters and the isotherms every 18°K, and the units of distance in the x-direction are given in degrees with respect to the mountain ridge (not to be confused with degrees latitude on earth). We note that the time mean regime states in Figs. 11e and f are represented fairly well by the 90°Ridge and 45°Trough (Figs. 11b and c), though the amplitudes of the time mean states are considerably reduced over that of the equilibria. In addition, we note that the temperature gradients are quite excessive. This again is related to the difficulty of representing the heights of the pressure levels of the continuous atmosphere to the two layer model. (However, if we chose the model top to be at 0 mb. instead of 200 mb., a common practice in two layer models, b^* would change such that each contour represents only 12°K,

which gives a much more reasonable, but still excessive, temperature gradient of 60°K). Since the temperature is determined by the vertical structure, the dimensional temperature field, similar to the static stability and the mountain heights, is likewise "stretched". Otherwise, we see that the phase relation between the temperature and height fields has structure which is characteristic of baroclinic systems. At 850, 500 and 250 mb. (levels 3,2, and 1), the phase of the time mean ridge and trough regime waves are given by -5°, -69°, and -87° degrees and 178°, 143°, and 135° degrees respectively. In spite of the simplicity of our model, we still obtain a reasonable vertical structure, in the sense the two layer model can be related to a continuous model with constant vertical shear, where the bulk of the westward phase shift occurs in the lower layer and the maximum amplitude in the upper layer.

Nevertheless, none of these patterns above are what we would call realistic primarily because they all lack smaller scale components. However, we also plot the instantaneous unfiltered flow configurations during both a trough and ridge regime event in Figures 11 g,h. Both of these examples are taken during a period of high amplitude, regime type II behavior (a model block), though the ridge case happened to be more unsteady and less persistent than the trough. We can see that these two figures are surprisingly realistic, considering

the simplicity of the model, especially at the 500 mb. level, where the lack of smaller scale disturbances is not so apparent. (The weak high over low and "split flow" that appear in the ridge of the trough regime are merely coincidental and are not apparent in the succeeding days). Clearly, the characteristics of the surface weather during these two regime events would be remarkably different, and thus for extended range forecasting purposes for the model atmosphere, it becomes critical to be able to predict the regime states. Furthermore, these very different persistent patterns occur for a fixed external forcing, and thus are entirely internally determined.

7. SYNOPTIC-PLANETARY SCALE INTERACTIONS

Our time dependent experiments have demonstrated two important facts; first, the highly simplified model possesses the necessary physics for the development of weather regimes, and second, the additional physical process which we represent by including a second wave in the x-direction (the direct interaction between an externally forced planetary scale wave and a highly unstable baroclinic wave) is an essential mechanism in the multiple regime phenomenon, and its inclusion is important in determining the final qualitative behavior of the large-scale circulation. In the Introduction, we suggest that the mutual interaction between the planetary and synoptic-scale waves establishes regime type phenomena by the equilibration of a feedback process. This feedback occurs through the process whereby the large-scale disturbance modulates the development of its own instabilities such that the net transports by these instabilities, in turn appear as a zonally inhomogeneous forcing to the large-scale wave. A priori we know that the baroclinic modes will result in time mean correlations that are non-zero since these correlations represent the net heat and momentum transports, but the potentially significant aspect to the feedback mechanism is the possible existence of wave structure in the net transport fields. In this section we investigate the quantitative details of this equilibration mechanism diagnostically by

consideration of the time mean regime budgets.

The budgets are calculated in the standard manner of applying the Reynolds' decomposition to the instantaneous system of model equations and evaluating the individual terms over the lifetime of a given regime event, a proceedure also followed by Dole (1982) in his study of atmospheric anomalies, which we will discuss in more detail later. It is very important to our study that the period over which we compute the budgets be chosen to coincide with the duration of a given regime event. We specifically avoid the common practice of selecting arbitrary periods over which to perform our analysis, e.g., a week, month, or season, since we may then include fractions of the two different regimes as well as periods of unsteady behavior. It is also important for the validity of the Reynolds' decomposition that the regime persist for periods very long compared to the passing of a synoptic-scale disturbance. In our model (and in the atmosphere) many regimes persist only in the order of a few weeks, corresponding to perhaps 3 to 5 synoptic periods. Though we generally consider such periods as persistent, mathematically, such a small number of transient events does not consist of a statistically significant sample. Consequently, we compute the budgets for an ensemble of regimes of a given type, which are, by our previous definition, the regime composites. In this manner, we reduce

spurious fluctuations in the budget terms from sampling problems to a minimum.

The general system of time mean prognostic equations for our model which result from the Reynolds' decomposition, consists of 20 equations, 20 time mean variables, and on the order of 100 correlation or Reynolds' stress terms. However, the equations for the analysis of the time mean regime budgets are considerably simplified by our previous observation that only the Mode 11 variables have a non zero time mean state over the duration of a regime event, and by the fact that the time mean tendency terms are approximately zero. With these simplifications the general system of 20 equations reduces to the 6 time mean Mode 11 prognostic equations. This system of equations is identical in form to the instantaneous system of Mode 11 equations from which we obtained the stationary equilibria, except for the addition of the correlation terms. However, the individual terms in the 6-equation Mode 11 system represent both thermodynamic and hydrodynamic processes, which leads to difficulties in interpreting the various physical mechanisms. To separate these physical processes, we rewrite the equations in terms of the time mean upper and lower level streamfunction φ and ϕ, and do not eliminate w between the thermodynamic and shear equations. This process gives us a 9 equation system; 6 equations for φ_1, φ_2, φ_3, ϕ_1, ϕ_2, and ϕ_3 and 3 equations for Θ_1, Θ_2, and Θ_3. In this system, w can

be written as a result of purely thermal processes, e.g. Newtonian cooling and temperature advection (from the θ equations). Then the w terms in the upper and lower level vorticity equations represent the thermal effects while all the remaining terms represent the various inertial effects. The final set of equations from which we calculate the budgets are as follows:

(See the following page) (7.1)

where we have labeled the individual terms (or groups of individual terms) by the scale and nature of the physical process they represent. All the correlation terms are denoted by adxx (advection xx) where xx represents the scale of the smallest wave present in the interaction, while BETA, TOP2, DISS, and INT refer to the time mean beta, topographic, dissipative (frictional in the vorticity equations and thermal in the w equations), and internally dissipative processes respectively, while AD11 (advection 11) refers to the advection of the time mean quantities by the time mean flow.

The correlation terms (ad11, ad21, ad12, ad22) are of primary interest since they represent the net effects of the transient disturbances. From the form of the correlation or stress terms, we can see that their influence upon the large-scale circulation is then analogous to a specified vorticity

or heat source or sink; thus the concept of synoptic-scale forcing. Clearly, if the time mean states of the correlation terms are zero (no synoptic-scale forcing) the solutions to the above system are the stationary equilibria of Charney and Straus. In this sense, it may be convenient to view the weather regime as one of perhaps several solutions to the time mean prognostic system with the time mean tendency terms set to zero, analogous to the manner in which the stationary equilibria are solutions to the instantaneous system with the instantaneous tendency terms set to zero.

Our budget analysis consists of computing diagnostically the phase and amplitude (instead of wave components) of the time mean of each of the individual terms (or groups of terms) in the 9 equations for the 7 categories of composite ridge and trough regimes. In addition, we also compute various combinations of terms. First we compute the sum of the correlation terms, ad11+ad21+ad12+ad22=sum, which in the vorticity equations give the net advection of perturbation vorticity by the perturbed flow, and in the w equations, give the net advection of perturbed potential temperature by the perturbed flow. Second, we sum AD11 and BETA (denoted by BEAD) in the vorticity equations since they are both very large and generally 180°out of phase. Third we calculate the net effects of the nonlinear or correlation components of w, denoted by "wnln", and the linear components of w, denoted by

WLIN, (which are both purely thermodynamic) upon the vorticity equations. For the final step we combine the thermodynamic and hydrodynamic components resulting from the correlations between the transient motions, wnln+sum=nlns, and the mean field components, WLIN+INT+DISS+TOP2+BEAD=LINS. Over the lifetime of a regime, then, the sum of nlns+LINS should be approximately zero. Numerically this is accomplished by calculating each individual term every time step (1.5 hrs.) and averaging over the duration of a given regime. At the end of the integration, the time mean budgets of the individual trough and ridge regimes are placed into one of the 7 categories from which the final weighted statistics of the composites are obtained.

Despite our primary focus on the nature of the synoptic-scale transport quantities, we consider all the physical processes in our budget analyses for two reasons. First, we need to consider the role of the transient forcing quantities relative to the other physical processes, and second, the budget statistics provide a means of quantitatively comparing the model weather regimes to atmospheric phenomema. In Table 6a we present the budget analysis for the category seven 34-year trough and ridge composites for case #2 with $\Theta_1^* = .12$. (For convenience, each nondimensional term is multiplied by 1000.) To better compare the variation of the transports in the different categories,

we plot the phase and amplitudes of the upper level transport terms ad11, ad21, ad12, and "sum" in Figure 12.

There are two distinct aspects of the nonlinear transport quantities apparent in Figure 12 which demonstrate that the synoptic scale transient forcing has zonally inhomogeneous structure. First, we see that the individual nonlinear transport terms are concentrated into relatively confined areas of the figure as a function of category in a given regime state which indicates that the transports are highly consistent from regime to regime of a given type. Second, the algebraically identical nonlinear transport quantities which are highly consistent within a given regime, are very different between the trough and ridge regime states. The first type of behavior indicates that the transports are distinctly organized during the occurrence of weather regimes, while the second type of behavior implies that the nature of the organization is somehow dependent upon the structure of the large-scale wave.

These two results are also obtained when we consider the budget analysis for the individual (instead of composite) trough and ridge regime states. Though the budget statistics possess considerable fluctuations for the less persistent regimes (as expected), the magnitudes of the fluctuations do not exceed the mean. The statistics of the most persistent

regimes, on the other hand, possess fluctuations in the budget terms of the same order as the composites. Both the individual and composite analyses, then, support the notion that there exists a consistently organized behavior in the transient disturbances whose transports possess a non zero time mean zonally inhomogeneous structure. According to our time mean prognostic equations, then, these transports appear as a zonally inhomogeneous forcing to the large-scale wave.

In order to provide some insight as to the role of the transients in the maintenance of the time mean regime states, we plot two "balance of forces" diagrams for the upper level waves of the 7 categories of composite trough and ridge regimes in Figures 13a and b respectively. Each term, as well as the time mean state wave, is represented by a vector. The projections of the various force vectors perpendicular and along the wave vector then provide a means of ascertaining the role of the various processes in the maintenance of the time mean wave, e.g., components of forces along and opposite the wave vector are directly enhancing and dissipating the wave respectively, while components 90° to the left and right of the wave vector are attempting to propogate the wave westward and eastward respectively. The two largest terms BETA and AD11, which are purely barotropic processes, exceed all the remaining terms by nearly an order of magnitude, but since they act in opposing manners and are always constrained to lie

perpendicular to the wave vector, we plot only their sum BEAD, which is of the same order as the remaining terms in the budgets. This near balance between the BETA and AD11 effects indicate that the time mean state of the upper level wave is near barotropic resonance. However, the condition for resonance of the upper level wave alone does not imply that the full model is near its resonant state.

The first aspect of the two figures which is of note is that all the force vectors of a given type are constrained to a narrow region in space. The lack of variability in the budgets of both regimes indicates that the behavior during the periods we have composited for analysis is remarkably similar. The second point of note is that the manner in which the forces establish a balance in the two regime states is considerably different (a behavior we most likely would not have noted had we selected arbitrary periods of time over which to compute our budgets). In the trough composites (Fig. 13a), the two largest magnitude forces, WLIN and BEAD, are oriented primarily perpendicular to the wave vector while in the ridge composites (Fig. 13b) WLIN BEAD, and nlns are about equal in magnitude with much larger components of WLIN and nlns directed along and opposite the wave vector instead of perpendicular to it. In both cases, however, after cancellation of the perpendicular (propogating) component of the forces, we note that the upper level wave is maintained

primarily by WLIN (advection of mean potential temperature by the mean flow) and dissipated by nlns (the transients), though both of these projections are quite small.

Similar relationships between the budget terms described above are also obtained by Dole (1982) in his study of atmospheric persistent anomalies. Dole's persistent anomalies are defined by carefully tested selection criteria and composited by type similar to our regimes, and thus his study provides (to the best of our knowledge) the only observational work which is consistent with our regime analysis. Dole finds that the dominant processes (in order) tend to be the time mean advection of absolute vorticity (equivalent to our BEAD) and what he refers to as divergence effects, which is essentially temperature advection (equivalent to our WLIN). The remaining processes, including external forcing mechanisms, dissipation, and the effects of transients, are all within the levels of observational noise; thus their magnitudes cannot be ascertained with much confidence. However, the implications are that the transients, as well as the dissipative processes, act to damp the wave, though both mechanisms are relatively weak.

The results of our analysis are then in qualitative agreement with those of Dole, which provides evidence that the model regime phenomenon bears some resemblance to the

atmospheric event. However, perhaps the most interesting aspect of the combined budget analyses is the fact that the effects of the transients and topography are relatively small, and thus to a first approximation, appear negligible. Clearly the assumption that neglecting terms which appear small in the budgets would lead to qualitatively correct solutions would lead to erroneous conclusions in the case of external mechanisms, for no regime-type phenomena are observed in our model in the absence of topography. In an analogous manner, we have shown in Chapter 6 that the presence of interacting baroclinic transients has a major effect upon the nature of the large-scale flow and the occurrence of regimes. It does not appear possible, then, to conclude that a given process is negligible based solely upon the relative magnitudes of the budget terms. In fact, the small contribution to the budgets by the time averaged transient terms which we have obtained diagnostically must account entirely for the relatively large differences between the stationary equilibria and the time mean regime states. We can at least partially demonstrate that the relatively small transports do account for the rather large differences in the time mean state by consideration of an example. In the w equation, the driving is given by the quantity $-h\,\Theta_1^*/\sigma_0 = -.036$ in our nondimensional units, which corresponds to convergence south of the channel center and divergence to the north of the channel center. The net transient term "sum", given by 5.7487/1000 in the category 7

ridge regime (Tab. 6a), then acts to oppose the divergence pattern established by Θ_i^*, which is equivalent to reducing Θ_i^* from .12 to Θ_e^* where Θ_e^* is given by $(\sigma_0/h)(.036-.0057487)=.109$. From Fig. 1 we can see that this small change in Θ_i^* accounts for a rather significant change in the stationary equilibria. Of course this single alteration cannot account for all the observed differences between the stationary equilibria and the time mean regime states; however, if we solved the above system of 6 Mode 11 time mean prognostic equations using our diagnostically determined values for the correlation terms, by definition, the solutions should be very close to the observed time mean regime states.

The purpose of our budget analysis, however, is not to attempt to understand the roles of the various mechanisms in the maintenance of the time mean regimes, but to study the organization of the transient disturbances. In the single case discussed above, the transients are both consistently organized from category to category and very different in the two regime states. It is then of interest to investigate the degree to which this behavior is maintained as the external parameters are changed.

We compute the budgets for all the parameter sets studied in Chapter 5 and find that the transports, analogous to the

time mean regime states, vary continuously as a function of the parameters, and for a majority of the cases considered, behave in a very consistent manner in each of the two different regimes. To demonstrate these aspects of the transient behavior we plot the phase of the transient forcing, the time mean state wave and corresponding equilibrium state as a function of Θ_1^* for the case #1 trough regime composites in Figure 14a, and a similar plot for the case #2 ridge regime composites in Fig. 14b. (The only reason we choose the two different cases for the two regimes is that in the more extensive case #2, the trough regime becomes so rare at low values of the driving most of the categories contain no data, thus we resort to the less extensive case #1).

In both figures we see that the difference between the phase of the transient forcing terms and the time mean Mode 11 waves is very consistent for a given value of Θ_1^*, and that the behavior of the transients vary continuously as a function of Θ_1^*. We also note that at progressively lower values of the driving, a larger component of the transient forcing is directed along the wave vector, and at values of Θ_1^* below which the equilibria cease to exist the transients actually act to maintain the time mean regime state. At more realistic values of the driving, on the other hand, the transients are primarily dissipative, and it appears that the phase difference between the mean wave and the transient forcing

tends toward 180° as Θ_1^* is progressively increased.

The final point of interest is to compare the budgets of the composite regimes in Table 6a with the budgets calculated in two subset periods of Regime type II behavior. The first example is a moderate amplitude 31-day ridge and the second example is a high amplitude 46-day trough (which corresponds to a classic block). The results, which are presented in the same format as Table 6a, are given in Table 6b; in addition, the transient terms are plotted as solid triangles and rectangles in Fig. 12. We can see that there are no significant differences between the two trough regimes but in the ridge regime type II event, the adl1 term has become considerably smaller (which is to be expected since the fluctuations in the Mode 11 wave, by definition, are less). Thus the transient forcing is primarily a result of the adl2 terms. (Note that the magnitudes of the transients in the type II cases are, nevertheless, of the same size as in the regular regimes). Outside of the differences in the adl1 terms, the statistics of both regime types are similar. This result supports the previous claim that such impressively steady periods are simply extreme examples of the more general weather regime phenomenon.

RECAPITULATION

The diagnostic budget analyses have demonstrated several important facts. First, the transients do, in fact, distinctly organize in a consistent manner and act as a zonally inhomogeneous forcing to the large scale during periods of weather regime type behavior. Second, the structure of the organization of the transports is highly dependent upon the regime type, third, the behavior of the transient forcing term varies continuously as a function of the parameters, as do the time mean regime states, and fourth, at low values of the driving Θ_1^*, the transients act to directly maintain the large-scale wave, while at more realistic (higher) values of Θ_1^*, the transients act as a dissipation. Though we found the magnitudes of the transient components to be small relative to some of the other budget terms, we have shown that the transports can account for the differences between the stationary equilibria and the time mean regime state. We have also argued that certain processes cannot be considered negligible just because the budget terms are small, providing as examples the profound influences both topography and the transients have upon the large-scale flow. Finally, comparison of the model regime budgets to those obtained by Dole in his study of atmospheric persistent anomalies strongly indicates that the model phenomenon is a dynamically representative counterpart to the atmospheric phenomenon.

8. SUMMARY

Motivated by the recently developed MFET and the subjective impression that periods of quasi-stationary behavior in the large scales are integrally associated with an organized behavior in the synoptic scales, we proposed the hypothesis that such periods of weather regime type behavior are established through the equilibration of a feedback mechanism whereby the zonally inhomogeneously externally forced planetary-scale wave modulates its own instabilities such that the net transports, in turn, appear as an additional zonally inhomogeneous forcing to the large-scale wave. To test this hypothesis, we developed one of the simplest possible models that contains the interaction between a zonally inhomogeneously externally forced planetary- scale wave and a highly baroclinically unstable synoptic-scale wave, by adding a second wave in the zonal direction to the 12-variable model of Charney and Straus (1980). We then study the time dependent behavior of the model by introducing a small synoptic-scale perturbation about the large-scale Mode 11 stationary equilibria; the equilibria are always highly unstable to such perturbations.

The most important result of our experiments is that when both large- scale topography and wave-wave interaction are included in the model, the flow possesses two weather regime

states, which are characterized by the confinement of the large-scale Mode 11 wave component of the trajectory to two distinct regions of phase space for periods of time which are long compared to the 3 to 5 day vacillations of the smaller scales. A more comprehensive analysis of the individual regimes for numerous parameter sets reveal several important qualitative properties:

1. The time mean state of the regimes is non zero only in the Mode 11 variables, which indicates that any smaller scale components of stationary equilibria, if they exist, are subsequently destroyed by the highly active synoptic-scale baroclinic mechanisms.

2. The time mean states of the two regimes are generally characterized by either a Mode 11 upper level trough about 40° to 50° west of the orographic ridge or a ridge about 70° to 110° west of the topographic ridge. The ridge regime generally possesses surface easterlies while the trough regime possesses surface westerlies, which indicates that the two regime states are not super and subresonant pairs.

3. The degree to which the large-scale wave vacillates on a day to day basis during periods of regime type

behavior is extremely variable, ranging from highly erratic to nearly stationary. Periods of near-stationary behavior are subsequently defined as Regime type II behavior since at large amplitude, Regime type II behavior is reminiscent of the classic interpretation of the block.

4. The regimes appear to have no dynamically preferred time scale in the sense that the probability a given regime will persist n+1 days, given that it persists n days, is constant.

5. Transition from one regime to another, which can occur on a synoptic time scale, as well as the two extraordinarily different regime short-range climates, which correspond to extremely different states of the weather on a local basis, result from purely internal processes, i.e., they occur for a single fixed set of external parameters.

In spite of the simplicity of our model, several of the above properties are consistent with the results of Dole's (1982) study on atmospheric persistent anomalies. Of particular significance is Dole's observation that the anomaly events, which he finds to occur most frequently over the eastern Pacific, eastern Atlantic, and the Urals, are 1) both

positive (ridges) and negative (troughs), 2) occur (independently) with about equal frequency at each of the 3 regions, and 3) do not form ideal antisymmetric pairs. In addition, Dole finds no indication that either type of anomaly event has a preferred time scale, and thus the persistence of an individual anomaly event is, to a certain extent, arbitrary. Furthermore, Dole notes that at any one of the three preferred regions, a given season could be dominated by positive events, negative events, a mixture of both, or an absence of any type of persistent behavior at all. These events are also observed to establish and or dissipate very rapidly; e.g. Dole finds that two days before the anomaly meets his selection criteria, even in the composites, that there is no recognizable sign of their pattern. The similarities between Dole's results and the model regimes then strongly indicate that the model weather regimes bear some resemblance to the atmospheric event.

Another important result of our experiments is the observation that the regions in phase space about which the trajectory remains confined during periods of weather regime type behavior, are not centered on the stationary equilibria as anticipated by the MFET. In fact, the stationary equilibria generally lie outside of the volume defined by the furthest extent of the large-scale trajectory. Nevertheless, there are significant indications that the regimes are

associated with a certain select set of equilibria or limit cycles (which we refer to as the "corresponding" equilibria). This association is indicated primarily by the fact that the phase of the time mean wave and the direction of the surface flow are similar in both the regimes and the corresponding equilibria. However, it is not clear why only two of the stationary equilibria are associated with regimes and the other three stationary equilibria are not.

One possible explanation suggests that "realizable" equilibria in the time dependent problem are those which are either stable or weakly unstable to large-scale (Mode 11) perturbations. This assumption is clearly not valid in our model since we find several parameter sets for which the regimes associate with equilibria that are unstable to Mode 11 perturbations while some of the remaining equilibria, which appear to have no influence upon the flow, are either stable or weakly unstable to Mode 11 perturbations. In fact, we find that the large-scale Mode 11 stability properties of all the stationary equilibria, including the occasional appearence of orographic instability, to vary in a complex manner as a function of the external parameters, yet none of this complex behavior is reflected in the nature of the full model weather regimes. Furthermore, two-regime behavior (both with time mean zonally inhomogeneous wave structure) is observed to exist for parameter sets where the only stationary equilibrium

state is the purely zonal Hadley Solution.

It is quite apparent, then, that we cannot predict the qualitative nature of the large-scale flow in our model knowing only the stationary equilibria and their large-scale stability properties, as is implicitly assumed by the MFET. The presence of the synoptic scales and their mutual interaction with the forced stationary equilibria is of importance in determining both the instantaneous and time mean state of the large scale, and accounts for the differences between the Mode 11 stationary equilibria and the time mean regime states.

The budget analyses of the two regime states demonstrate that the synoptic scales are organized during the regime events such that their net time mean transports have zonally inhomogeneous structure on the scale of the Mode 11 wave, and therefore appear as either a heat or vorticity source, and act as an additional forcing mechanism upon the large-scale wave. Though our budgets show that these transport quantities are small, they are sufficient to account for the differences between the stationary equilibria and the time mean regime states. The inclusion of these transport quantities in the large- scale Mode 11 equations then allows for a self-consistent solution where the effects of the transient feedbacks have been considered.

There are, however, several aspects of the feedback mechanism which are unclear. First, we have not yet established the mechanism by which the large scale organizes the transients. Second, the budgets indicate that the magnitudes of the net transports, though highly consistent from case to case, are quite small relative to some of the other physical processes. This result raises the question of how a small forcing can result in such a profound change in the time mean states. These questions are considered in the succeeding chapters.

9. ESTIMATES OF EDDY TRANSPORTS FROM STABILITY THEORY

We have demonstrated in the previous chapters that during the occurrence of weather regime behavior the time averaged (net) transports by the transient disturbances are spatially organized and act as a zonally inhomogeneous forcing mechanism to the large-scale wave. The next stage of this analysis is to understand the mechanisms through which the transports are organized. The fact that the phase structure of the net transports during the trough and ridge regimes are so different, indicates that the large-scale wave plays an important role in the organization process. Frederiksen (1979) and Niehaus (1980) have both done studies which indicate that the presence of a prescribed large-scale zonally inhomogeneous circulation can organize the transports of the smaller scale disturbances by modulation of the shapes of the baroclinically unstable modes. Frederiksen was able to qualitatively account for the observed high-pass variance distribution of Blackmon et. al. (1977) by computing the time averaged (net) transports of the baroclinic disturbances which develop from a prescribed planetary-scale wavenumber three pattern superposed upon the climatological zonal flow. Without the large-scale wave, the time averaged (net) transports are zonally homogeneous. It is then of interest to investigate whether we can account for the observed structure of the net transports during periods of regime type behavior

in our model by performing an analysis similar to that of Frederiksen. For convenience, we shall refer to this analysis as the "Frederiksen-Niehaus problem" or "Frederiksen problem".

Frederiksen's calculation is based upon the assumption that the baroclinically most unstable eigenmode of his prescribed circulation equilibrates to some finite amplitude while maintaining its spatial structure. The net heat and vorticity transports which result from this propagating disturbance are then obtained by taking the time average of the products of the meridional velocity components of the most unstable eigenmode with the thermal and vorticity structures of the most unstable eigenmode. The product contains terms which involve oscillating components (that may be very large on an instantaneous basis) as well as terms where the oscillating components cancel. In the time average, the oscillating components eventually average to zero over several periods, leaving only the stationary non-propagating cross terms. This calculation will be further illustrated below when we consider its application to our study.

In our model, the prescribed planetary-scale circulation corresponds to the time mean state of the regimes, thus the first aspect of the problem is identical in form to the calculation of the stability of the stationary equilibria except that we replace the equilibria with the time mean

states.

Performing a perturbation analysis about the time mean state may at first appear inconsistent since the time mean states are not solutions to the instantaneous system of equations. Clearly, if we initialized the full model with the time mean state and a small synoptic-scale perturbation, the time- dependent behavior would most likely be catastrophically violent since the large-scale processes alone, regardless of the net effects of the transients, are far from an equilibrium and highly unbalanced; thus the eigenmodes and eigenvalues of the stability calculation of the time mean state would not be representative of the initial model behavior. However, we are interested in ascertaining whether the eigenmodes that develop on the time mean state are, in fact, representative of the finite amplitude disturbances that are present during the said regime, and we hope that the transports due to these eigenmodes balance the large-scale equations. If the calculated eigenmodes are a reasonable facsimile of the actual finite amplitude disturbances, the net transports of these eigenmodes will possess structure similar to those obtained in the budget studies.

Mathematically, the analysis is then identical to the stability calculation of the stationary equilibria if we assume that the eddy transport terms, which represent the

long-term averaged effects of the transients, are constants, and thus drop out of the stability matrix. As discussed in Chapter 4, the form of the equations is such that the 20X20 stability matrix reduces to three submatices; a 6X6 matrix involving only Mode 11 perturbations, a 10X10 matrix involving coupled Mode 21 and Mode 12 perturbations, and a 4X4 matrix involving only Mode 22 perturbations. The baroclinically most unstable mode for all sets of external parameters we have considered is one of the eigenmodes of the 10X10 coupled Mode 21 and Mode 12 matrix, thus we will concentrate on the transports which result from this submatrix. The general form of the coupled Mode 21 and Mode 12 perturbation is given by

$$\underset{\sim}{\Psi}(t) = B[\ \text{Real}\ (\ \underset{\sim}{\psi}\, e^{\gamma t}\ )]$$

where B is an arbitrary amplitude coefficient and $\underset{\sim}{\Psi}$ and $\underset{\sim}{\psi}$ are vectors of the form (ψ_1, ψ_2, ψ_3, θ_4, θ_5, θ_6, ψ_7, ψ_8, θ_7, θ_8) where the components of the eigenvector $\underset{\sim}{\psi}$ and the eigenvalue γ are complex. The behavior of the individual spectral components, say ψ_i' , is then given by[1]

$$\psi_i' = B[\ \text{Real}\ (\ \psi_i\, e^{\gamma t})].$$

The net transports or correlation terms are then obtained by taking the time average of the products of these individual terms, for example, one of the components of the heat transport is given by

$$\psi_i' \theta_j' = B\ \text{Real}\ (\ \psi_i e^{\gamma t}\ )\ B\ \text{Real}\ (\ \theta_j e^{\gamma t}\ ) =$$
$$B^2 (\ \psi_i e^{\gamma t} + \psi_i^* e^{\gamma^* t}\ )(\ \theta_j e^{\gamma t} + \theta_j^* e^{\gamma^* t}\ )/4$$

where the * denotes the complex conjugate. Expanding we

obtain the following:

$$\psi_i'\theta_j' = B^2 (\psi_i\theta_i e^{a\gamma t} + \psi_i^*\theta_j^* e^{a\gamma^* t} + (\psi_i\theta_j^* + \psi_i^*\theta_j) e^{(\gamma+\gamma^*)t}).$$

We now assume, as in Frederiksen, that the perturbation attains a finite amplitude while retaining its structure, so that all the exponential quantities are replaced by their trigonometric parts, which is equivalent to setting the real part of γ to zero. The only non zero components of the expansion remaining in the time average are then the cross terms $\psi_i\theta_j^* + \psi_i^*\theta_j$; $(\gamma + \gamma^* = 0)$, since the oscillating time dependent components cancel. In this manner, we can calculate the various transport quantities ad11, ad21, ad12, ad22 that appear in the time mean Mode 11 prognostic equations (see 7.1 of Chapter 7) and compare them to those obtained diagnostically in our budget study.

However, there are several reasons for discrepancies between the theoretical and diagnostic analyses. The primary cause is that the most rapidly growing perturbation does not necessarily become the most dominant structure at finite amplitude (Pedlosky(1981)). Either nonlinear exchange processes, such as transfer of energy from the most unstable mode to other modes may become significant, or less unstable perturbations and secondary instabilities may simply continue to grow long after the initially most unstable mode equilibrates at finite amplitude. In addition, the use of the time mean state is not necessarily the most appropriate basic

state for the stability analysis as the time mean state already reflects the influence of the eddy fluxes. Though these complications may be quantitatively significant, the fact that Frederiksen is able to account qualitatively for the observed distribution of the time mean atmospheric transports indicates that the modulation of the most unstable baroclinic modes by the large scale is the dominant mechanism.

The first aspect of this analysis is to compute the values of the individual net transport terms ad11, ad21, ad12, ad22 (which are given by 7.1) for the upper and lower level tendency equations and the w equations from the most unstable eigenmodes and to compare them with the corresponding diagnostically ascertained terms in Tables 6a and 6b. Though the linear theory can give us a phase and spatial structure, the amplitude is indeterminate, and at best we can only obtain the relative amplitudes of the net transport terms. Consequently, to obtain a measure of the degree to which the linear calculation reproduces the budget analyses, we calculate the ratios between the amplitudes of each of the theoretically derived values and the corresponding amplitudes obtained from the diagnostically ascertained budgets. If the linear theory then predicts the observed transport structure exactly, the phases of the budget terms and the theoretically derived net transports will be identical and the amplitude ratios of each of the theoretically derived quantities will be

identical.

For our first example we compute the transports from the most unstable eigenmode of the time mean states of the two periods of Regime type II behavior (periods of relatively steady behavior in the large scales on an instantaneous basis) in Table 6b. We consider these periods initially (instead of the composites) since the large-scale wave varies the least about the time mean state. Consequently, these periods are more consistent with the linear analysis which considers the stability of only the time mean state without taking into account the degree to which the large-scale wave fluctuates. The agreement between the linear theory and the diagnostics of Regime type II behavior is then expected, a priori, to be the best.

The stability analysis for the 46-day trough and 31-day ridge in Table 6b each have only one unstable eigenmode: coupled Mode 21 and Mode 12 disturbances, which, when normalized by the largest amplitude component, are as follows:

	REAL	IMAG		REAL	IMAG	
ψ_4	1336	0640		-1333	-2376	
ψ_5	4706	-0339		4630	-0673	
ψ_6	-0258	-4892		0429	-4230	
θ_4	1679	0023		-0239	0849	
θ_5 =	2166	-2382		-0481	-0990	
θ_6	-2152	-2439		-1102	-0064	
ψ_7	7346	-9971		0436	9939	
ψ_8	-10000	-7346		10000	-0187	
θ_7	0524	-4046		3139	3491	
θ_8	-4075	-5222	TROUGH	3527	-3212	RIDGE

In both cases, we can see that the Mode 12 amplitudes $(\Psi_7\Psi_7^* + \Psi_8\Psi_8^*)^{\frac{1}{2}}$ and $(\Theta_7\Theta_7^* + \Theta_8\Theta_8^*)^{\frac{1}{2}}$ have greater relative amplitude than the Mode 21 amplitudes $(\Psi_5\Psi_5^* + \Psi_6\Psi_6^*)^{\frac{1}{2}}$ and $(\Theta_5\Theta_5^* + \Theta_6\Theta_6^*)^{\frac{1}{2}}$ by about a factor of 2 to 4. In Table 7a, we compare the phases and amplitude ratios of the theoretically obtained transports from these eigenmodes to those of Table 6b.

First, we can see that the agreement between the predicted phase and that of the adl2 component of the budgets is excellent. For example, in the trough regime, in the upper level, theory gives 49.1° against the observed (full model) 48.4°, in the lower level theory gives 10.7° against the observed 28.4° (the poorest agreement), while in the w field theory gives 110.0° against the observed 108.8°. Similar quantitative success is also apparent in the ridge regime.

Second, we can see that the theory successfully predicts the relative amplitudes of the adl2 terms, as shown by the fact that the amplitude ratios are nearly constant. For example, in the trough regime, the amplitude ratios for the upper level, lower level, zonal and wave w fields are 1.46, 1.31, 1.31, and 1.26, respectively. (Again, equal success is apparent in the ridge regime.) The fact that the amplitude ratios are nearly constant states that if we multiply each of the theoretically calculated amplitudes of the adl2 terms

(before computing the ratios) by the reciprocal of the average values of the above ratios, we will be able to nearly duplicate the amplitudes of the observed full model ad12 terms.

The ad21 terms, on the other hand, are not predicted quite so successfully by this theory. Though we can see from Table 7a that in many cases the predicted phase of the ad21 component is quite good, except where the amplitude of the observed ad21 component is small, the theoretical technique both underpredicts and poorly replicates the amplitude of the ad21 component. First, we see that the amplitude ratios of the individual predicted terms vary quite considerably, for example, in the ridge regime, the amplitude ratios of the upper level, lower level, zonal and wave w fields are given by .33, .88, .98, and .30, respectively, a variation of about a factor of three. Secondly, if we choose our multiplication factor, discussed above, such that the theoretically predicted ad12 components have the correct amplitudes, the resulting amplitudes of the predicted ad21 terms (which also must be multiplied by this same factor to be consistent) will be too small. The underprediction of the ad21 terms is associated with the fact that in the fully nonlinear model the amplitudes of the Mode 21 variables are comparable to the amplitudes of the Mode 12 variables, whereas the Mode 21 amplitudes of the eigenvectors of the stability problem are considerably smaller

than the Mode 12 amplitudes. Since ad21 involves products of purely Mode 21 terms, we may have anticipated a priori that the magnitudes of the ad21 terms would be underpredicted.

The ad11 and ad22 terms, on the other hand, are predicted to be zero since all perturbations with Mode 11 and Mode 22 components are linearly stable. In the case of Regime type II behavior, ad11 is very small thus the error is minimal. This is not the case for the ad22 term. In Chapter 5 we noted that the Mode 22 wave, though often linearly stable, grew rapidly to substantial amplitude several days after initialization, and maintained a relatively high amplitude state for the duration of most experiments. Clearly either nonlinear exchange processes or a secondary type of instability (perhaps a wave instability of the smaller scale waves of the type discussed by Lorenz (1972)) become important. It is noteworthy, though, that the ad22 component affects the state of the large-scale wave only through their effect on the zonal flow.

In spite of these shortcomings, the linear analysis predicts the spatial structure of the total observed eddy transports during periods of both trough and ridge regime type II behavior quite well. To obtain a more quantitative measure of the success of the linear technique in replicating the observed budgets, we will compare the vector sum of the

components of the eddy transports predicted by theory (ad21 and ad12) to the vector sum of the diagnostically ascertained budget components (ad11, ad21, and ad12) for both the trough and ridge regime type II periods considered in Table 7a. Again, the absolute amplitudes of the theoretically derived transports are indeterminate, thus we shall multiply these transports by some appropriate factor (which is different for the two different regimes) such that the ad12 components given by the theory best simulate the ad12 terms of the budgets. In other words, we wish to find the most appropriate value of the constant B. We choose to best fit the ad12 components (instead of the ad21 components) since the analysis above indicates that the linear theory has a much better potential for predicting the structure of the ad12 components. For the trough regime, we chose $B^2 = .75$ and for the ridge $B^2 = 1.03$. The results of this calculation are presented in Table 7b in a format similar to Table 7a.

From the table, we see that the linear theory generally underpredicts the amplitudes of the observed total eddy transports (though nowhere is it less than 50 percent), while the phases are replicated quite well. The greatest discrepancies between theory and observation, e.g. the upper level vorticity transport in the trough regime (.53 theory to .989 observed) and the w field in the trough regime (1.90 theory to 3.74 observed) occur where the amplitudes of the

ad21 components are comparable or exceed the amplitude of the ad12 components. The fact that the linear theory predicts the spatial structure of the total eddy transports so well without predicting the ad11 component and underpredicting the ad21 component suggests that the ad12 component accounts for the bulk of the eddy transports. In fact, if we look at the amplitudes of the observed eddy transports in Table 7a, we will see that the amplitude of the ad12 term exceeds the amplitudes of all the other terms in every case but one.

For comparison with the Regime type II analysis, we also compute the transports for the category 7 trough and ridge regime composites of Table 6a (the results are listed in Table 7c in the same format as Table 7a). Before we consider the results, a priori we know that the ad11 and ad22 terms will either be zero or vastly underpredicted, since the only information available to the linear calculation is the time mean state of the regimes, which are not very different from the time mean state of the two Regime type II events. (In fact, there are cases where the time mean state of the composites and periods of Regime type II behavior are extremely close). Consequently, the structure of the eigenmodes for the composites will most likely be very similar to those calculated for the periods of Regime type II behavior.

As expected, the results of the theoretical calculation for the composites are very similar to those of Table 7a. Again, both ad11 and ad22 are zero, though ad11 in the diagnostic budgets is no longer a trivial component (especially in the ridge regime), and the magnitudes of the ad21 components are underpredicted. However, the ad12 terms are again excellently represented in both phase and amplitude, and the phase of the ad21 terms, as in the above analysis, are fairly well predicted. Clearly, however, the linear theory will not predict the total eddy transport field in this case as well as it did for the periods of regime type II behavior since the ad11 terms have substantially greater amplitudes. But similar to the periods of regime type II behavior, we see that the amplitudes of the ad12 components still exceed the amplitudes of the ad11 and ad21 components in all cases but two.

The results of these analyses indicate that a substantial percentage of the organization of the transports during periods of weather regime type behavior is, in fact, a consequence of the spatial modulation of the baroclinic transient waves by the large-scale wave. The quantitative agreement between the theoretically computed transports and the diagnostics are excellent in the case of the ad12 components, and the phase of the ad21 components are predicted with reasonable accurracy (some of the reasons for these

differences are discused in Appendix V). The major discrepancies between the theoretical and diagnostic analyses are the underprediction of the magnitude of the ad21 amplitudes and the failure to predict the ad11 and ad22 components, however, since the ad12 component accounts for the bulk of the observed eddy transports, the linear theory is quite successful at replicating the observed eddy transports.

RECAPITULATION

The Frederiksen-Niehaus analysis thus shows that a large percentage of the transport structure can be understood as a result of the modulation of the spatial structure of the baroclinically most unstable eigenmode by the large- scale wave. The analysis is best able to account for the structure of the ad12 eddy transports. Since the ad12 eddy transports also account for the bulk of the observed eddy fluxes, the linear analysis replicates the total observed eddy fluxes reasonably well, especially during periods of regime type II behavior. The analysis does not account for the ad11 and ad22 transports since both the Mode 11 and Mode 22 waves are predicted to be linearly stable.

10. SYNOPTIC SCALE STABILIZATION

We have shown that the qualitative structure of the net synoptic-scale transports as obtained in our diagnostic budget study can, to a certain extent, be accounted for by the modulation of the baroclinic transient disturbances by the large-scale wave. In chapter 7, we demonstrated that these organized transients, in turn, appear as a thermal or vorticity source to the large scale, and that such forcing can account for the observed differences between the stationary equilibria and the time mean regime states. This feedback process then provides a mechanism through which the large-scale wave can equilibrate with its own highly active baroclinic instabilities.

However, there are several aspects of this equilibration process which we have yet to understand. First, in Chapter 7, the results of our budget analysis (as well as Dole's (1982) for atmospheric cases) demonstrate that the magnitude of these transport forcing terms are significantly smaller than other physical processes, such as the advection of time mean relative vorticity by the time mean flow, and appear to be negligible. Thus it is not clear why these small transient terms should have such a profound effect upon the qualitative nature of the large-scale flow. Second, the regimes appear to be "associated" with only two stationary equilibria, in spite

of the fact there are as many as three other stationary equilibria with similar large- scale stability properties. Furthermore, we have noted that two-regime behavior continues to exist for parameter sets where the only stationary equilibrium state is the purely zonal Hadley Solution. It is then not clear what the precise roles of the stationary equilibria and the organized transient disturbances are in the regime dynamics.

We hypothesize that periods of weather regime type behavior occur when the transient disturbances which develop on a given large-scale pattern are organized by the large scale such that the net forcing by the transients acts to stabilize the large-scale wave. In this situation, if the phase or amplitude of the large-scale wave is perturbed by a small amount, the change in the net transports organized by the perturbed large-scale feature act against the sense of the perturbation, forcing the wave back to its original state. From this point of view, then, whether the transients appear to dissipate or directly maintain the large-scale circulation in the budget calculations is only of secondary importance. Their primary importance is in the role they play in the stabilization of the large-scale wave.

In this hypothesis, the final structure of this stable equilibration pattern then depends critically upon the manner

in which the transients are organized by the large-scale flow and the influence the resultant feedbacks have upon the large scale. There is no reason, a priori, to assume that the stationary equilibria, calculated without taking into account the forcing by the synoptic scales, should be near those points in phase space where both the external forcing mechanisms and the synoptic-scale feedbacks stabilize. We can also see that the magnitude of the transients do not have to be large to dramatically alter the state of the large-scale circulation. From our budget calculations of Chapter 7, we note that the time mean regime state is primarily a balance between the time mean advection of the earth's and relative vorticity in the upper level, which indicates that the upper level wave is near resonance. Consequently, a small magnitude force can produce a large change in the state of the wave.

We shall demonstrate that the feedbacks from the organized synoptic- scale baroclinic disturbances act to stabilize the large-scale flow by considering the time dependent behavior of just the Mode 11 model equations given below:

(see following page) (10.1)

In the full model, the effects of the smaller scale disturbances upon the large-scale Mode 11 variables are

incorporated in the terms which we have labeled ad21, ad12, and ad22, which are different from the terms of the same name in the budget studies in that we have not, as of yet, taken any time averages. In Chapter 9, we have shown that the time mean value of the term ad12 and part of the time mean value of ad12 can be obtained by calculating the transports from the most unstable eigenmode of the given large-scale Mode 11 circulation. This result implies, to a certain extent, that the large-scale Mode 11 variables determine the time mean state of ad21 and ad12; or at least a fair percentage of these time mean transports. We shall therefore consider the Mode 11 system of equations in which we parameterize the net effects of the smaller scale disturbances by calculating the corresponding values of the transport terms ad21 and ad12 from the most unstable eigenmode of the given large-scale pattern as we did for the time mean regime states in Chapter 9 above. This parameterization effectively removes the oscillatory components of the transient forcing and retains only the net "Reynolds' stresses" which we expect to be much more slowly varying. We anticipate that the integration of such a dynamical system, where the smaller scale transports are calculated explicitly from the large-scale pattern at each time step, will lead to two absolutely stable "regime-equilibria" whose phase and amplitude should approximate the time mean state of the full model regimes. Unlike the purely Mode 11 stationary equilibria, these regime-equilibria form a

self-consistent solution by directly incorporating the effects of the highly active baroclinic eddies in their dynamics.

The primary difficulty in developing this particular parameterization scheme is the determination of the indeterminate amplitude constant B (see Chapter 9), giving the overall eddy amplitude. This problem is identical to the problem faced by climate modelers when they attempt to predict northward eddy heat transports based upon the zonal temperature profile alone, or other relevant basic state conditions (see Branscome, 1980, who was interested in determining the heat transports that result from the Charney modes). There is, currently, no universally accepted best solution to this problem so we are left with a number of options. Since we are not striving to predict the model regimes, but are more interested in understanding how the feedbacks equilibrate with the large-scale flow, we shall choose a scheme which is most likely overly simplified but, nevertheless, physically reasonable: we shall assume that the total energy (available potential energy and kinetic energy) in the small-scale eddies is some percentage of the total energy in the Mode 11 zonal flow. (We have neglected the contribution to the energy from the large-scale wave since the characteristics of the unstable disturbances are very similar to the classic baroclinic disturbances that develop on zonally symmetric flows.) We reason that such a scheme is perhaps more

realistic than an energy conserving formulation since we know that the stability analysis does not account for all the eddy energy, e.g., the Mode 21 and Mode 22 components. The magnitudes of the individual components of the eigenvector can then be normalized such that its total energy satisfies the above relationship. Since we do not know what the most appropriate value of the energy ratio is, a priori, we will consider the behavior of the model for energy ratios ranging from 0% to 200%. Clearly, these are absurd limits, but by considering such a large range of values, we can investigate the manner in which the purely Mode 11 stationary equilibria are altered by increasing the level of transient energy. We can then work "backwards" and ascertain which energy ratio gives us the best results, and compare this ratio with the actual values obtained from the full model.

A second problem is the parameterization of the term ad22, which is predicted to be zero using the eigenvector analysis, yet in our budgets has substantial amplitude relative to the other transport terms. Fortunately, the ad22 component has only zonally homogeneous structure and thus its influence on the large-scale wave occurs primarly through its effective alteration of the driving Θ_1^* (see Chapter 5), so that we do not expect that it is as important to the stabilization process as the zonally inhomogeneous transports. The inclusion of ad22 will, however, most likely have some

stabilizing effect since the presence of the Mode 22 wave always acts to reduce the effective driving by drawing energy from the zonal flow, and we have shown in the stability calculations that lower values of the driving are generally associated with more stable behavior. To verify the assumption that the effect of ad22 is qualitatively minimal, we will consider experiments in which the effects of the term is either eliminated or retained. When we choose to retain the effect of ad22, we will parameterize the term as being some percentage of the zonal component of the predicted transport terms ad21 and ad12. We select this parameterization scheme since the observed ratio between the ad22 terms and the zonal component of the ad21 and ad12 terms appears to be nearly constant from case to case and category to category in the budgets of a given regime type. This percentage can then be obtained empirically from the budget analyses of Chapter 7 and Tables 6a and 6b.

Both our parameterization schemes are based upon the assumption that the energetics of the flow are essentially the same during both regimes. Such an assumption may introduce further quantitative error, but we do not suspect that it will eliminate the transient-feedback stabilization process. However, the possibility that the energetics of the flow may be significantly different during the two types of regimes has important repercussions in the interpretation of the

partitioning of energy between the "stationary" and "transient" waves in both the model and the real atmospheres. This problem is, however, an object of future study and will not be considered here.

For the first series of experiments, we consider case #2 with $\Theta_1^* = .12$. For those experiments in which we wish to retain the parameterized effects of ad22, we see from Table 6a that in the trough regime, ad22 is about 25% of the zonal component of the transports while in the ridge regime, it is almost 45% of the zonal component of the transports. The absolute magnitude of the zonal transports is also considerably larger in the ridge regime than in the trough regime, which only re-emphasizes the possibility that the energetics of the flow may be significantly different in the two regimes. Since our scheme implicitely assumes that the energetics of the flow are more or less the same, when we wish to retain the parameterized effects of ad22, we shall choose the term to be 33% of the zonal component of the predicted transports. In any case, the results were found to be insensitive to rather large changes in this percentage.

With the above parameterization schemes incorporated into the large- scale equations, we then integrated the model from a number of initial conditions. The most important result of our model integrations is that for a large range of energy

ratios, both with and without the parameterized effects of ad22, there are two absolutely stable solutions. We will refer to these solutions as "regime-equilibria" since they contain the parameterized effects of the baroclinic transient waves. (The purely Mode 11 stationary equilibria are then a special subset of these regime-equilibria where the transient energy is set to zero). In Tables 8a and 9a we list the six Mode 11 midlevel streamfunction and potential temperature variables for the regime-equilibria for selected values of the energy ratio as well as the full model category 7 regimes. Table 8a lists the regime-equilibria for the model in which the parameterized effects of ad22 are excluded, while Table 9a lists the results when such effects are included. In Fig. 15a, we plot the phase space positions of the regime-equilibria in Table 9a. Each solution listed in Table 9a is denoted by a dot which is labeled by its corresponding value of the transient to zonal energy ratio.

The first point of note is that the behavior of the regime-equilibria as a function of the energy ratio, both with and without the parameterized effects of ad22 are qualitatively similar. In fact, the phase space positions of the regime-equilibria for both cases are so close they could not be conveniently plotted on the same diagram, especially the trough solutions, which essentially superposed. However, we can see from Tables 8a and 9a that the two experiments do

show some quantitative differences, but the primary effect of including ad22 appears to be equivalent to simply slightly increasing the transient to zonal energy ratio. The consequences of ad22 does not, then, appear to have a major role in the "phase-fixing" properties of the transient feedbacks. However, we will concentrate on the experiments in which this effect is retained since these regime-equilibria are slightly closer in phase space to the full model regimes than the regime-equilibria calculated without the parameterized effects of ad22.

In Fig. 15a, we can see that the set of solutions as a function of the transient to zonal energy ratio form two branches which more or less "grow" out of the purely Mode 11 stationary equilibria (denoted by triangles) as the ratio is increased. We shall refer to these two solution sets as the ridge and trough branch respectively. As the energy ratio is increased, the wave amplitude significantly decreases, though the phase of the large-scale feature remains relatively constant, except at high energy ratios in the ridge branch where the solution branch curves sharply toward the origin. The phase of the waves in the trough branch, on the other hand, remains essentially constant, but the solution becomes unstable at moderate values (.09) of the energy ratio. In addition, in both Tables 8a and 9a, we note that the zonal flow as a function of increasing energy ratio at first shows a

rather rapid increase in speed for both branches, reaching a maximum near the point where the trough branch becomes unstable, and at a ratio of .09 in the ridge branch. At very high values of the energy ratio, the ridge branch shifts from having surface easterlies to surface westerlies, while at a considerably lower energy ratio, the trough branch appears to go unstable at that point where the sense of the surface flow shifts from west to east. However, one of the most important properties of these two solution branches, both with and without the parameterized effects of ad22, is the fact that the ridge regime-equilibrium definitely becomes more stable as the transient energy levels are increased. We have no quantitative measure of this stability, such as an eigenvalue analysis, but we note that at higher energy ratios, convergence of the trajectory to its final state is much more rapid, in spite of the fact the model is initialized at the stationary 90° Ridge equilibrium for each experiment, which is further away from the final state than the low-energy ratio regime-equilibria. For example, at an energy ratio of .01, after 2880 6 hour time steps (720 days), the ridge regime-equilibrium had converged to five decimal places, whereas at energy ratios of .05, .10, and .50, convergence occurred after 528, 360, and 156 time steps (132, 90, and 39 days) respectively. The trough branch, on the other hand, appears to be uniformly stable until the ratio exceeds .07 whereupon there is a definite increase in the time required

for convergence. For values of the energy ratio greater than .087, the trajectory always moved to the neighborhood of the ridge branch, where it rapidly converged. It is not possible, however, to ascertain whether the trough solution simply disappears or becomes unstable, since the solutions are obtained by straight foward time integration, though it appears that the solution goes unstable since at progressively higher energy ratios the attractor becomes increasingly more difficult to find.

We also ran several experiments starting from initial conditions other than the 5 purely Mode 11 stationary equilbria and found that the trajectory always converged upon one of the two regime-equilibria. However, it is difficult to investigate the boundary between the two attractor basins, though such a map would be of interest, since we are really dealing with a six-dimensional phase space.

To compare these regime-equilibria with the full model regimes, we denote the position of the category 7 trough and ridge regimes with an asterisk. We can see that the two branches pass fairly close to their respective full model regimes. Further inspection of Table 9a shows that the sense of the surface flow, magnitude of the zonal flow, and phase of the large-scale wave of the category 7 regimes are well represented by the regime- equilbria for values of the energy

ratio around .07. It is then of interest to compare this value of the energy ratio with a ratio determined empirically from the full model. However, even if there is a good agreement between what we observe in the full model and that indicated by our parameterized model, it does not imply that the eddy amplitude parameterization is correct, as it does not check the variation of the eddy amplitude with the large-scale wave amplitude.

For the purposes of comparison with the full model, we will consider the energy in just the Mode 21 and Mode 12 components as contributing to the small-scale energy since these components appear in the most unstable eigenmode. We then compute the ratio between this small scale energy and the total energy in the zonal flow at each time step and average over various time periods. For very long periods of time (i.e. several months or years), we find that the transient to zonal energy ratio is about 20%, which is significantly larger than the 7% indicated by our experiments. The reason for this rather substantial discrepancy is that the Mode 12 components of the eigenvector are much greater (by about a factor of four as mentioned in Chapter 9) than the Mode 21 components, though in the full model, these components are of comparable magnitude. Consequently, if we normalize the eigenvector such that it represents 20% of the zonal energy, the amplitude of the Mode 12 components will be more than twice their observed

amplitude while the Mode 21 components will be about half their observed amplitude. However, with .07 as a normalization factor, the Mode 12 components of the eigenvector have the same order as the Mode 12 components of the full model, which indicates that the Mode 12 components are the most important.

Since our parameterization appears to work best when the Mode 12 components of the eigenvector duplicate the Mode 12 components of the full model, it may have been more appropriate to consider just the ratio between the Mode 12 and zonal components of the energy for the normalization factor. This is not an unreasonalble simplification, for as discussed in Chapter 9, the linear analysis works best for the prediction of the ad12 components. The ad21 and ad22 components, on the other hand, appear to result from either secondary instabilities or nonlinear exchange processes, both of which are not reflected in the structure of the eigenvector. In any case, the result of our integrations clearly indicate the organization of the transients and the resultant feedbacks can lead to a stable self-consistent solution, which can dramatically alter the state of the purely stationary Mode 11 equilibria. This result is perhaps the single most important conclusion of our study.

To further demonstrate the role of the transients in

stabilizing the large-scale flow in a manner that is somewhat more convincing, we repeat the above experiment for case #2 with $\Theta_1^*=.15$. For this parameter set, all the purely Mode 11 stationary equilibria and limit cycles are unstable to Mode 11 perturbations except for the 45° Trough Solution. Thus if there is to exist two stable regime-equilibria for some finite value of the transient energy, which we anticipate there must be since there are two full model regimes for this parameter set, the transients must have stabilized at least one of the two solution branches. Then decreasing the transient energy will result in one of the stable regime-equilibria going unstable; an event which is perhaps somewhat contrary to our usual notion of the effects of the baroclinic transients.

In Fig. 15b, we plot the results of our integrations including the parameterized effects of ad22 for $\Theta_1^*=.15$ in a format similar to Fig. 15a. Again we have two solution branches, but in this case, only the trough regime branch appears to "grow" out of a stationary equilibrium state as in Fig. 15a. The ridge regime branch, on the other hand, introduces a new type of behavior for low-energy ratios. For ratios somewhat less than .07, the ridge regime- equilibrium state becomes unstable and develops into a stable, counterclockwise-orbiting limit cycle whose structure is similar to those limit cycles of Figure 7. As the transient energy is further decreased, the limit cycle traces out

progressively larger orbits in phase space and becomes less stable, in the sense that its attractor basin markedly shrinks. At a ratio of .01, the limit cycle is only marginally stable and has to be approached carefully, otherwise the trajectory converges upon the trough regime branch. The purely Mode 11 90° Ridge stationary equilibrium is, of course, unstable, and if there is a stable limit cycle, its attractor is so small we have not yet been able to find it. The individual statistics of the regime-equilibria are listed in Table 9b in a format similar to Table 9a.

The results of our experiments excluding the parameterized effects of ad22 were, again, qualitatively similar. However, the slight role ad22 has in the stabilization of the regime-equilibria can be noted by the behavior of the ridge branch solutions at the lower values of the energy ratio. Unlike the solutions in which ad22 is included, the limit cycles persist at higher values of the energy ratio, and at an energy ratio of .01, the limit cycle is unstable. The statistics of these individual regimes are listed in Table 8b in a format similar to Table 8a.

RECAPITULATION

We have developed a model where the effects of the transients upon the Mode 11 tendency equations are

parameterized by calculating the net transports from the most unstable eigenmode of the large-scale flow. The amplitude of these transports were determined by assuming that the total energy (available potential energy and kinetic energy) in the transients is a certain percentage of the total energy in the zonal flow. We then investigated the time dependent behavior of this model for case #2 with Θ_1^*=.12 and .15 for several values of the transient to zonal energy ratio both with and without the parameterized effects of ad22 and found that for a large range of energy ratios the model trajectory converged upon two absolutely stable regime- equilibria or limit cycles; the final state depending upon the initial conditions. Investigation of the details of these regime-equilibria revealed the following important behaviors:

First, as a function of the energy ratio, the stable regime-equilibria form two branches in phase space, which at certain values of the energy ratio pass very close to the full model trough and ridge regimes. If both the 90 Ridge and 45 Trough stationary equilibria are stable to Mode 11 perturbations, these two branches connect with the stationary equilibria at an energy ratio of zero, and thus we have labled the two solution sets as ridge and trough branches respectively.

Second, as the energy ratio is increased from zero in

both regime- equilibria, the wave amplitude decreases, the zonal flow increases, but the wave phase remains relatively constant. At higher values of the energy ratio, the trough branch becomes unstable while the ridge branch reaches a maximum zonal flow. At very high values of the energy ratio, the surface flow in the ridge branch shifts from easterlies to westerlies and the solution branch curves sharply toward the origin.

Third, increasing the level of transient energy acts to stabilize the ridge regime-equilibria, in the sense that the trajectory converges upon its final state more rapidly. For most parameter sets then, there will be two absolutely stable regime-equilibria whereas there is only one stationary equilibrium that is stable to large-scale disturbances.

Our simple model then shows that the feedbacks induced by the net transports of the organized transient disturbances by the large-scale wave can lead to multiple, absolutely stable solutions. The most important aspect of these solutions is that the highly baroclinically unstable synoptic waves are an integral part of the equilibrium dynamics, and thus demonstrates the mechanism through which the stationary externally forced wave can equilibrate with its own instabilities. The primary role of the organized synoptic-scale disturbances during periods of weather regime

type behavior is, then, to fix the state of the large-scale wave. In such a situation, a perturbation in the state of the large-scale wave induces transients that act against the sense of the perturbation, forcing the large-scale wave back to its original state. There may be more than one such stable fixed point in phase space. The transients can have this important stabilizing kind of effect regardless of whether they appear to directly maintain or dissipate the large-scale wave in the diagnostic budgets, e.g., in the case #1 and case #2 regimes of Chapter 5 at low values of the driving the transients directly maintained the large scale whereas at moderate levels of the driving, the transients acted to dissipate the large scale.

11. SYNOPTIC-SCALE TRANSITION MECHANISM

We have shown that the inclusion of the baroclinic synoptic-scale transient disturbances can interact with the externally forced large-scale wave to establish an absolutely stable regime-equilibrium. However, in both the atmosphere and full model, these regime events do not persist indefinitely, thus either the regimes are "quasi-stable" or some other process which we have omitted in the parameterized model induces "instability" or transition. We shall attempt to show that the detailed behavior of the transients is, in fact, responsible for transition, which is similar to the hypothesis proposed by Charney and DeVore (1979), in the sense they suggested that the transient disturbances were responsible for transfering the state of the atmosphere between the various stationary equilibria.

When we developed the above model, where the effects of the transients were calculated from the net transports of the most unstable eigenmode, we assumed that the oscillatory components of the transports averaged out to zero. On an instantaneous basis, however, these oscillatory components can obtain very large amplitudes and thus, on an instantaneous basis, can exert a powerful influence upon the large scale. Since in the full model these instantaneous transports are not uniform oscillations, but aperiodic with highly erratic

amplitudes, the forcing may become sufficiently intense to transfer the state of the large-scale flow from the attractor basin of one stable regime-equilibrium to the attractor basin of the other stable regime- equilibrium. We hypothesize that exactly such a mechanism alone is responsible for regime transition in the full model.

We shall demonstrate the role of the instantaneous transports in the transition mechanism simply by observing the magnitudes of the various physical processes which contribute to the large-scale tendencies. We select as our example the Ψ_2 tendency equation given below:

$$\begin{array}{lll} & \text{AD11} & \text{BETA} \qquad\qquad \text{FRIC} \\ \dot{\Psi}_2 = c_1 n^2 (\Psi_1\Psi_3 + \Theta_1\Theta_3)/a_2^2 & + \beta n \Psi_3/a_2^2 & - k(\Psi_2 - \Theta_2) \end{array}$$

$$\text{sum}$$

$$+\{c_4 n^2/a_2^2 (\Psi_4\Psi_6 + \Theta_4\Theta_6) +$$

$$3c_6(1-n^2)/a_2^2 (\Psi_5\Psi_8 + \Theta_5\Theta_8 - \Psi_6\Psi_7 - \Theta_6\Theta_7)\}$$

where AD11 represents both large-scale vorticity and temperature advection, BETA is advection of earth's vorticity, FRIC is frictional dissipation, and "sum" is the combined transports of the smaller scale transients. (These terms are related to the terms in the budget study of Chapter 7 with the same name, but they are not identical, since these terms involve both thermal and hydrodynamic processes).

We will plot a time series of the magnitude of the

tendency term $\partial\Psi_1/\partial t$ for a period of time which includes both a regime event and its collapse. We can then compare the contributions of the individual terms labeled AD11, BETA, FRIC, and "sum" over this period and attempt to distinguish the physical process which appears to be most responsible for the breakdown of the regime event.

We present the results for the demonstration case (as defined in Chapter 5) since in this case the regimes are highly persistent and periods of unsteady flow quite rare. Periods of transition or unsteady behavior then show up readily. In Fig. 16a, we plot the time series of AD11, "sum", and the net tendency term $\partial\Psi_1/\partial t$ for a period of 8192 time steps (512 days) starting 1000 time steps after initialization or near the end of the first 75-day regime in Table 3a discussed in Chapter 5. AD11 is denoted by the heavy line at one fourth the scale of "sum" and the tendency term (denoted by light lines). To avoid confusion, "sum" is plotted on the axis beneath that upon which the tendency term and AD11 are plotted. We also split the 512 day period into four sequential 128 day periods.

The most striking aspect of the figure is that the behavior and magnitude of the tendency term at almost all times nearly parallels the contribution from "sum". It is quite clear then that the erratic behavior of the tendency

term $\partial\Psi_2/\partial t$, and thus the erratic nature of the large-scale circulation, is almost entirely a consequence of the transients. AD11, on the other hand, though of much greater amplitude, tends to be balanced primarily by BETA with FRIC taking up some of the small residual (neither BETA or FRIC are plotted), thus the net contribution of the large-scale processes to $\partial\Psi_2/\partial t$ is generally small.

If we now consider the behavior of the various processes during a period of transition (which can be identified in the figure by noting where AD11 crosses the zero axis), we see that the magnitude of both the tendency term and "sum" become very large and undergo rapid fluctuations. This burst of highly active behavior is quite distinct from the almost placid, slow variations of the tendency term which occur during periods of regime type behavior. We also note that during the burst of synoptic transports the contribution to the tendency term from the large-scale processes significantly increases, which, to a certain extent, is to be expected as the transients induce fluctuations in the large scales and the various large-scale processes become unbalanced.

Actually, it is not entirely clear which of the physical mechanisms triggered the initial imbalances, especially since there are five other large- scale tendency terms to investigate. From the rapidly fluctuating nature of the

tendency term (which we do not observe during periods of regime type behavior when the contributions from "sum" are small), it appears that the transient activity was most likely responsible for upsetting the equilibrium.

We also note, however, that there are periods when the transient forcing, and thus the tendency amplitudes, become quite large, yet the regime does not collapse. Apparently, then, either the tendency and current state of the large-scale flow is such that the surge of transient forcing is of insufficient strength to cause collapse, or the transient forcing itself is in the incorrect sense. For example, if the current state of the large-scale flow is fairly distant from its regime-equilibrium state and near the boundary of its attractor basin, the strength of the transient surge would not have to be too intense (if it is in the correct sense) to induce transition. On the other hand, very intense transient surges may not be sufficient to induce transition when the state of the large-scale flow is near its regime- equilibrium. Clearly, we must at least know both the magnitude and sense of the transient forcing as well as the current state and tendency of the large- scale flow to be able to predict transition.

The only conclusion that the previous analysis yields is that the details of the large-scale tendency term can be

primarily accounted for by the detailed behavior of the transient forcing, and consequently, that the degree of erratic behavior in the large scales during periods of regime type behavior is a result of the transient disturbances.

Actually, if we had investigated parameter sets that were more active baroclinically, this correlation between "sum" and the tendency term would not have been so obvious. For example, in Fig. 16b we plot "sum" and the tendency term for a period of 4096 time steps (256 days) for case #2 with Θ_1^*=.12, 4350 time steps after initialization. In this case, "sum" always has substantial amplitude and so does the tendency term, but the rapid vacillations of "sum" induce vacillations in the large-scale variables which are reflected in the vacillations of the tendency term. Consequently, unlike in Fig. 16a, peaks in "sum" do not correspond that well with peaks in the tendency term. However, on the basis that erratic behavior is observed in the tendency term in Fig. 16a only during those periods when the transient forcing becomes active, it seems likely that the instantaneous behavior of the transients should be responsible for the erratic behavior of the large scales in all cases. The only indications we have, then, that the transients initiate the fluctuations for the more active parameter sets are by "induction" from the simpler cases (such as the demonstration case), where there are distinct periods during which the

transient forcing activity nearly ceases and thus the tendencies vary both smoothly and slowly, and by the observation that the variance in the tendency terms and "sum" are nearly equal in Fig. 16a and reasonably similar in Fig. 16b.

The exact details of the processes which lead to transition are undoubtedly complex, most likely involving some triggering mechanism which, under appropriate conditions, leads to a critical imbalance in the large scales. Though the time series does not conclusively indicate that the transients provide the critical triggering mechanism, the fact that the qualitative behavior of the tendency term reflects the qualitative behavior of the synoptic-scale forcing suggests that such is the case. However, there are a couple of experiments and observations which we have considered previously that provide further evidence that the instantaneous forcing by the mobile disturbances initiates regime transition.

One argument is that in our simple model of Chapter 10, where only the uniform, non-oscillatory components of the transports are included in the large-scale dynamics, we obtain two absolutely stable, initial-condition dependent, regime-equilibria or limit cycles. In this model, we have specifically made the effort to remove the instantaneous,

rapidly varying, oscillating component of the transients, and without these components, the model is never observed to switch between its two states or undergo aperiodic and erratic vacillations within a given state. But our strongest argument comes from observing the detailed behavior of the full model regimes themselves.

In Chapter 5, where we discuss the time dependent behavior and the occurrence of multiple regimes, a very important observed aspect of these regimes is their highly variable durations. In spite of this variability, the statistics of the individual regimes of a given type are nearly identical (see Table 3a and 3b), i.e., most properties of the regimes are independent of persistence. In addition, a given regime event is observed to undergo transition at a very rapid rate (in the order of a day or two), regardless of its previous persistence, to either a period of unsteady behavior, another regime, or to re-establish a regime of the same type. This behavior is especially apparent for those parameter sets where the regimes are highly persistent, as in the demonstration case. A given event could last for several years before suddenly, in a single day, undergoing transition to the opposite regime. Since there is no variation of any of the external parameters in our model, the transition process must be internal to the model atmosphere, and such rapid rates are consistent with our hypothesis that the instantaneous

component of the baroclinic synoptic-scale forcing under appropriate conditions transfers the state of the large-scale flow from the attractor basin of one stable regime-equilibrium to the attractor basin of another.

The assumption that regimes undergo transition as a consequence of the surges from the instantaneous component of the transient forcing also would explain the highly arbitrary nature of regime persistence. Without the instantaneous transient forcing, a given regime would persist indefinitely, but as one increases the relative strength of the aperiodic high-amplitude transport surges, the likelihood a regime will be disrupted increases. We can then conclude that a given regime will essentially persist indefinitely or until the occurrence of a transient of sufficient magnitude or sense causes it to collapse. The probability of such a transient-surge event is then reflected in the slope of the cumulative persistence distributions (Fig. 10) discussed in Chapter 5.

RECAPITULATION

We have hypothesized that the instantaneous component of the transient forcing provided the mechanism through which the state of the large-scale flow could be bounced between the attractor basins of the various stable regime- equilibria. To

investigate this hypothesis we first plotted time series of the physical processes that contribute to the $\dot{\psi}_2$ tendency equation during periods of both regime type behavior and transition. In one case we found a distinct correlation between erratic behavior in the tendency terms and increased activity in the transient forcing which occasionally led to transition. In more baroclinically active cases, however, it was not clear which process or processes were actually responsible for the erratic behavior or transition since the flows at all times underwent rapid flutuations. Consequently, to provide further support for the notion that the transients were responsible for both the erratic behavior of the flow on an instantaneous basis and transition, we considered two other arguments.

First, in our simple model, in which the oscillatory components of the transports were eliminated, but the net transports retained, only stable regime-equilibria or limit cycles were possible. No erratic behavior or transition between the two states was observed. Second, and most important, the observed arbitrary persistence of regimes and rates of transition in the full model (which were on a synoptic time scale regardless of the previous duration of the regime) were consistent with the synoptic-surge mechanism. The probability a given regime would persist then appeared to be directly related to the probabilty of sufficiently intense

synoptic-scale surges, which more or less determines the slope of the cumulative distributions discussed in Chapter 5.

These observed properties, as well as the implications from our simplified model and time series plots, then support our hypothesis that the transients are responsible for the process of transition. The aperiodic character of the transient surges then provide an internal mechanism which is responsible for two important observed characteristics of the regimes. First, the rapid variations in the transports appear to be responsible for the degree of fluctuation of the large-scale component of the flow during periods of regime type behavior. (Occasionally, the fluctuations in the large scale become so small, that is the large-scale flow becomes so steady, we defined such periods as examples of Regime type II behavior or "blocks"). Second, the surges in the transports induce the state of the flow to aperiodically vacillate between the two stable regime-equilibria. This event can occur so rarely that regimes will persist for centuries, or so frequently that the state of the flow is almost always "unsteady", making it next to impossible for regimes to get established; but for either extreme, the rate of transition is on a synoptic time scale.

12. ATMOSPHERIC REGIMES

We have shown that weather regimes in our simple model are manifestations of the stable equilibration of the large-scale topographically forced wave with the organized feedbacks from its own structurally modulated baroclinic instabilities. For a given set of external parameters, we find that there are generally two such absolutely stable solutions which we have referred to as regime-equilibria. The state of the flow is then driven by the instantaneous component of the synoptic-scale transients from the attractor basin of one of the stable synoptically forced equilibria to the attractor basin of the other. Our experiments then demonstrate that the synoptic scales provide an internal mechanism which is responsible for both the stabilization and the disruption of the model weather regime events, and thus the inclusion of the synoptic events in our model is essential for determining the qualitative behavior of both the instantaneous and time mean components of the large-scale flow.

We have developed a fairly comprehensive theory of the weather regime phenomenon as it occurs in our simple, highly truncated, two-layer, topographically forced spectral channel model. Clearly, the limited horizontal resolution and vertical truncation of our quasi-geostrophic two- layer model

eliminates several physical processes; in addition to the approximations inherent to a dry, two-layer quasi-geostrophic atmosphere, by maintaining a fixed static stability, we have eliminated the process of static stabilization via the release of baroclinicity (Lorenz (1960b)). By not retaining a sufficient number of degrees of freedom we have also not allowed for the occurrence of "strong" wave-wave interaction, e.g. the interaction of two zonal wavenumber 2n waves with a zonal wavenumber n wave. Consequently, it is entirely possible that we have documented and achieved a partial understanding of an interesting event that is merely an artifact of the highly simplified model. However, comparison of our model results with those of the observed phenomenon suggest that the model regimes qualitatively resemble the atmospheric phenomenon in several respects. To provide a more comprehensive measure of both the successes and shortcomings of the model and the implications of our theory, we will compare, on a point by point basis, the results of our study with the results obtained by Dole (1982) in his observational analysis of atmospheric persistent anomalies.

As discussed in Chapter 5, Dole's persistent anomalies are defined by carefully tested selection criteria and composited by type similar to our regimes. Dole specifically does not obtain his data by considering averages over pre-selected, arbitrary periods of time, e.g., a week, month,

the horizontal length scale π L to be 5000 km.) while the ridge regime possesses an upper level ridge about 70° west of the orographic ridge (about 23° of longitude). These statistics indicate several interesting characteristics about the model flow which can be summarized as follows: First, the antinodes of the two regimes are nearly co-located in space which indicates that certain regions of the model experience a much greater temporal variance in the large scales, associated with the switching between the two regime states, than other regions. Second, the occurrence of a given regime is denoted by one of two wave structures which is always similar in both phase and shape every time that said regime recurs, and third, since the two regimes are not purely antisymmetric pairs in either phase or amplitude, and one regime usually has a tendency to occur more frequently than the other, the climatological state of the model flow is generally non-zonal, and thus possesses what is often referred to as a "stationary" wave. All of these above characteristics are also apparent to some degree in the statistics of Dole's persistent anomalies.

Instead of one "regime", however, Dole finds three regions in the wintertime Northern Hemisphere where the frequency of persistent anomalies is a maximum: the central-eastern Pacific, eastern Atlantic, and the Urals. But on the other hand, in each of these three regions, he finds that the occurrence of an anomaly event is nearly uncorrelated

with the occurrence of an anomaly event at any of the other two regions, which suggests that the anomaly events, though planetary in scale, are regional in character. Since our simple two zonal wave model cannot possibly simulate this regional characteristic, we must consider the model as "representative" of only one of these three regions at any given time.

At any one of these three regions Dole finds that both positive and negative anomalies occur with about equal frequency and magnitude, though they do not form purely antisymmetric pairs. This asymmetry is even further enhanced by recombining the anomaly field with the climatological flow, which, for convenience, we shall refer to as the "net anomaly". This two-state atmospheric flow behavior is highly reminiscent of the behavior exhibited by our full model trough and ridge regimes, though the resulting net anomaly fields in the atmospheric cases do not always possess the distinct trough and ridge patterns apparent in the model. This is especially true in the Atlantic region where the two states are so highly antisymmetric that one state possesses a highly amplified ridge while the other state is nearly zonal. The Pacific region, on the other hand, possesses net anomaly fields which are well represented by the model in the sense that the two atmospheric states are characterized by either a large amplitude ridge or a deep trough over the west coast of

North America. Dole's "Pacific positive" and "Pacific negative" events can then be reasonably well compared to our model trough and ridge regimes, respectively. (The fact that the model qualitatively resembles the Pacific net anomalies much more so than the Atlantic and Urals net anomalies is perhaps a consequence of the fact that the simple model orography represents the North American Corrdilleria much better than it represents either the complex European or Eurasian topography.) In the Pacific and Atlantic regions, then, and perhaps the Urals region as well, similar to our model, the antinodes of the net anomaly fields are located somewhat west of major mountain ridges, which Dole also finds to be the regions of maximum temporal variance.

Perhaps one of the most important results of Dole's analysis of the anomaly characteristics in the three regions is the fact that he finds the horizontal structure of a given type of anomaly event at each region to be remarkably similar from case to case, in the sense that one pattern is highly correlated spatially with the anomaly patterns of most of the cases in that region. The systematic reproducibility of these anomaly structures led Dole to arrive at the important conclusion that the anomalies have both a regional preference and a distinct recurrent structural preference at each of the three preferred regions. The systematic recurrence of these anomaly structures is highly consistent with the recurrent

phase and spatial structure of the model regimes. This behavior suggests that the principal external forcing mechanisms present in the atmosphere may not need to change significantly with time in order for recurrent, persistent anomaly patterns to occur. The atmospheric anomalies, then, consistent with the model regimes, would appear to be multiple flow states for a (roughly) constant external forcing.

Though Dole finds that the anomalies recur with a preferred structure, the actual shape of the atmospheric anomalies, including the Pacific cases, differ significantly from the model regimes in that the atmospheric anomalies possess distinct 2nd y-mode structure, as well as more complicated structures, whereas the model regimes possess purely first y-mode structure. These differences are especially apparent in Dole's empirical orthogonal function (EOF) analysis of the anomalies.

Though one EOF accounts for more than half the variance of the anomaly patterns, four EOFs are required to explain slightly more than 80% of the variance, whereas one EOF in our model (which would have Mode 11 structure centered slightly west of the orographic ridge) would account for almost all of the large-scale variance. It is still significant, however, that Dole finds only a few EOFs are sufficient to account for the bulk of the variance in a system with as many degrees of

freedom as the atmosphere. This observation suggests that the number of regime-equilibria in the actual atmosphere may be quite limited, in spite of the complexity of the external forcing.

In any case, the presence of the second y-mode in the anomaly structure, at sufficient amplitude, gives the net atmospheric anomaly the "split-flow" configuration so often associated with blocking. Such structures in the model are always transient and never observed in the time mean. This model behavior is suspected to be a consequence of our simple, purely Mode 11 topography, although we have not examined the model flows with Mode 21 topography.

We have also mentioned the fact that the model climatology possesses stationary waves, which simply represent the weighted average of the regimes. It then seems plausible that the stationary waves of the atmosphere are also the weighted average of the various types of atmospheric regimes. Thus the amplitude of the stationary waves are, for all practical purposes, a measure of the asymmetries between the regime statistics and frequency of unsteady flow. To a certain extent, then, this view suggests that the so-called stationary waves represent the unoccupied average, except in those regions such as the eastern Asian-western Pacific trough, which Dole finds to be one of the most persistent

features in the Northern Hemisphere. (Perhaps this feature is an example of a regime which is nearly 100% dominant.) The relevence of these stationary waves in budget studies and atmospheric energetics, then, in many regions, is subject to some question, as the properties of the various regimes and periods of unsteady flow may be sufficiently unique to render their net average statistics meaningless.

2. Vertical Structure

The two layer approximation severely limits the types of vertical structure our regimes can possess, and thus we can only discuss these structures in the grossest sense. Though we have only two layers, the two- layer approximation is equivalent to a three dimensional atmosphere with constant shear. We can then define a flow field at any intermediate pressure level as some linear combination of the fields in the two layers. If we do this, we find that the phase shift in the time mean state wave changes very little above 700 mb. or so, and possesses maximum amplitude at the highest defined level. Below 700 mb., on the other hand, the wave shifts rapidly eastward as one approaches the surface. In this sense, the time mean regime states of the two layer model are essentially trying to represent a feature that is equivalent barotropic, with maximum amplitude in the "upper levels" and maximum westward phase shift with height in the "lower

levels". Clearly, however, this construction is extracting a maximum amount of interpretation from a minimum amount of information.

Dole finds qualitatively the same type of structure, equivalent barotropic with maximum amplitude at the tropopause and maximum westward phase shift with height near the surface. However, our model regimes definitely appear to develop a greater westward phase shift with height at "lower levels" than indicated by Dole, and the ridge regimes consistently have greater "lower level" westward phase shifts than the trough regimes, also not indicated in Dole's analysis. Apparently then, the model regimes have a greater role in transporting heat than the corresponding events in the atmosphere. This property may be a consequence of the fact that there are an insufficient number of smaller scale features in our severely truncated model to accomplish these transports.

3. Time Dependent Behavior

Our theory indicates that the general circulation of our model can be understood as a flow which is driven by the instantaneous component of the synoptic-scale forcing from the attractor basin of one stable regime- equilibrium to the attractor basin of another. The erratic, aperiodic nature of

this forcing accounts for the observed highly variable durations of the individual regimes, periods of unsteady "non-regime type" behavior, the degree to which the large-scale component of the flow fluctuates during periods of regime type behavior, as well as the rapid rates at which the state of the model flow can undergo transition between the various types of behavior. Since the external parameters are, at all times, held fixed, the time dependent behavior of the model regimes is then entirely a result of internal processes. Consequently, a very important implication of our theory is the suggestion that the very different short-range atmospheric climates, or anomaly states, occur as a result of processes which are primarily internal to the atmosphere; seasonal cold anomalies, warm anomalies, periods of unsteady flow, as well as the occurrence of abruptly shifting persistent anomalies within a given season, are, then, all possible solutions to the atmospheric dynamic system for a given fixed set of external parameters. There are several aspects of Dole's results which support this concept.

First, he finds that both positive and negative anomaly events can occur within his given 90-day season. For example, in the winter of 74-75, a 14-day Pacific negative event, a 20-day Pacific positive event, and a 11-day Pacific negative event occurred in sequence (though not necessarily immediately following one another), and in the winters of 64-65 and 67-68,

two Pacific positive events were followed by a Pacific negative event. Second, as discussed in Chapter 5, the duration of these individual anomaly events is highly variable, and appears to have no preferred time scale, as shown by the cumulative persistence distribution of Fig. 10. This type of distribution suggests that for durations beyond about 5 days persistence the anomalies can be modeled by a red-noise process, i.e., events which begin and end at random times. Third, three-fourths or more of the total variance of the low-pass (10 days or longer) anomaly fields is accounted for by variations within a given season, and furthermore, much of the season to season variance may simply be a consequence of sampling, since individual anomaly events persist (on the average) for 15 days (though some persist up to a month), and a season is defined as only 90 days. Fourth, and last, the rates at which the individual anomaly events both develop and collapse is very rapid, i.e., on a synoptic time scale, regardless of the previous duration of the anomaly event. This last property is illustrated in Figs. 17a,b (from Dole), which consist of two plots each of the time series of the magnitudes of Dole's composite Pacific positive and Pacific negative anomalies at both the onset (17a) and collapse (17b) of the said events. The composites are constructed such that day zero corresponds to the time when each individual anomaly event first meets (or last meets) Dole's 10 day-10 decameter criteria.

From the figures we can see that the rate of onset (and collapse), especially for the Pacific negative composite event, is strikingly rapid, happening primarily in less than two days. We can also see that the change in amplitude during the periods of transition is remarkably large, going from nearly zero to about 300 meters, or vice-versa. The onset of these events is, then, not only rapid but of substantial amplitude, and since Figs. 17a,b consist of composites, these high-amplitude, abrupt shifts in state represent the average and not a single, perhaps rather unusual, extreme event.

This apparently rapid rate of transition and consequent possibility of abrupt switches from one anomaly state to another, are the two aspects of the anomaly behavior that are the most consistent with the behavior observed in our model. However, we cannot rule out the possibility that some of this erratic behavior, which we attribute to internal processes, occurs in response to changes in the external forcing mechanisms (such as the seasonal cycle, sea surface temperature anomalies, and continental heat sources and sinks), though it appears difficult to account for the rapid rates of transition and abrupt shifts of anomaly states by external processes alone since the external processes appear to vary relatively slowly in time, though radically different behaviors for small changes in the external parameters have been documented in simple forced nonlinear systems (see

Lorenz, 1962, 1963, and Yao, 1980). We hypothesize, on the other hand, that the presence of the changing external forcing mechanisms simply alters the structures of the possible regime- equilibria in some quantitative manner. The atmosphere then aperiodically vacillates between the various regime-equilibria (which may be changing slowly with time) in response to the instantaneous component of the forcing by the transients. Consequently, as in our model, the time dependent characteristics of the anomalies will be "erratic", persisting for highly variable lengths of time and undergoing abrupt, apparently random, transitions.

RECAPITULATION

We have shown that the model weather regimes possess several qualitative characteristics which have been found by Dole (1982) in his study of atmospheric persistent anomalies. The most important of these aspects are as follows:

1. Both the model regimes and the atmospheric persistent anomalies are characterized by large-amplitude positive or negative departures from climatology, which form nearly antisymmetric pairs. We referred to the two model states as the trough and ridge regimes which appeared to best resemble Dole's Pacific positive and negative net anomalies,

respectively.

2. Both the atmospheric and model regimes are observed to systematically recur with similar structure and phase just west of major orographic ridges, which then defined the regions in both the model and atmosphere of maximum large-scale variance.

3. The time mean regime states are nearly "equivalent barotropic", within the limitations of the two-layer model as discussed earlier, with maximum amplitude at the "upper levels" and maximum westward phase shift with height at the surface, though the model regimes appear to be far more baroclinic in structure than the observed anomalies.

4. The persistence of individual weather regime events is highly variable, and there does not appear to be a dynamically preferred time scale.

5. The onset and collapse of regime events is both rapid, e.g., on a synoptic-time scale, and independent of persistence.

6. Regimes of either type are observed to occur in a "random" sequence.

The qualitative agreements between many of the observed features of the model regimes and Dole's persistent anomalies, especially the details of the time dependent behavior, strongly suggest that the state of the atmospheric flow, similar to the model flow, is being driven by the instantaneous component of the synoptic-scale forcing from the attractor of one stable regime-equilibrium to the attractor of another. This behavior suggests the possibility that the extreme variability of the short-range atmospheric climatic states may be determined by processes which are primarily internal to the atmosphere.

13. CONCLUSIONS

We have shown that the externally forced large-scale wave can establish a unique type of equilibrium with the feedbacks from its own structurally modulated highly baroclinically unstable synoptic-scale waves. Unlike the purely stationary equilibria, the net forcing from the transients is an essential component of the equilibrium dynamics and thus the solution implicitly contains mobile synoptic-scale disturbances. We have referred to this unique type of equilibrium situation as a "regime-equilibrium".

To demonstrate the possible existence of this regime-equilibrium, we considered only the Mode 11 externally forced large-scale tendency equations of our full model and parameterized the net effects of the smaller scale transient disturbances by calculating the net transports from the baroclinically most unstable eigenmode that developed upon the given large- scale Mode 11 circulation. The integration of this system, where the organized feedbacks of the transients were implicitly determined from the large-scale flow, then resulted in two absolutely stable regime-equilibria which were very close in phase space to the corresponding full model composite regime states, in spite of the fact the parameterization scheme could not account for all of the eddy transports obtained in our budget study of Chapter 7. A very

significant result of our calculation with the parameterized effects of the transients is that there are two absolutely stable self- consistent solutions, whereas the Mode 11 system alone has generally only one purely stationary equilibrium that is stable to Mode 11 perturbations, and this solution is always unstable to synoptic-scale disturbances.

We could then conclude that the role of the organized transports in the regime dynamics is to stabilize the large-scale circulation, that is when the model flow is in this equilibrium situation, a small perturbation in the state of the large-scale wave will induce net transports which act against the sense of the perturbation and force the wave back to its original state. However, the transient-feedback stabilization process alluded to above considers only the organized net transports of the synoptic disturbances. Our parameterization scheme explicitly excludes the forcing by the rapidly varying, vacillating component of these mobile features which, on an instantaneous basis, can obtain substantial amplitude, and consequently, on an instantaneous basis, could significantly influence the state of the large-scale flow.

Clearly, in both the full model and the atmosphere, the regimes do not persist indefinitely, so something must eventually disrupt the regime- equilibria. In Chapter 11, we

argued that this disruptive mechanism was the instantaneous component of the transient forcing omitted in our "parameterized" model. The aperiodic, occasionally violent surges in these erratic transports then accounted for the sporadic time dependent characteristics of the observed full model and atmospheric weather regimes, e.g., the highly variable durations of the individual regime events, the rapid rates at which regimes establish and or collapse, periods of unsteady behavior when no regime can get established, the random sequencing and abrupt transitions between periods of the various types of regime and unsteady behavior, and the degree to which the large-scale component of the flow fluctuates during periods of regime type behavior. These transient disturbances then provide an internal mechanism which is responsible for both the disruption and stabilization of the weather regime events.

We have shown that not only can the transients act to stabilize the large-scale wave, but the effects of the transients in this process significantly alter the state of the large-scale wave from any type of equilibrium that may exist when the synoptic-scale baroclinic instabilities are artificially excluded. Likewise, the solution of the stability problem upon the zonally asymmetric time mean regime states and work by Niehaus (1980) demonstrates that the presence of the large-scale wave significantly alters the

behavior of the synoptic disturbances from that which would be observed if there were only a zonally symmetric basic state. The mutual coupling between the large scales and the synoptic events then significantly alters the characteristics and behavior of each other from what would be observed if considered "alone", and although it has often been assumed in meteorology that the large scale influences the synoptic scales, a very important implication of our study is that the synoptic events are also of extreme importance in determining the qualitative behavior of both the instantaneous and time mean components of the large-scale flow.

Consequently, we view the quasi-stationary features of the atmosphere as integrally coupled to an organized behavior in the synoptic-scale disturbances, and thus we cannot understand or predict the behavior of the quasi-stationary features without considering the behavior of the associated transients. We then suggest that this mutual coupling between the externally forced large scales and the mobile synoptic events defines a unique dynamical process which we have referred to as a weather regime. We feel that if there is any hope for extended range forcasting by dynamical processes, it relies upon the quantitative understanding of the weather regime phenomenon.

14. REFERENCES

Blackmon, M.L., J.M. Wallace, Ngar-Cheung Lau, and S.L. Mullen, 1977: An observational study of the Northern Hemisphere wintertime circulation. J. Atmos. Sci., 34, 1040-1053.

Branscome, Lee E., 1980: Scales and structures of baroclinic waves and their influence on climatic states. Ph.D. Thesis, Massachussetts Institute of Technology, Cambridge, Mass. 02139. 201 ppg.

Charney, J.G., and J.G. DeVore, 1979: Multiple flow equilibria in the atmosphere and blocking. J. Atmos. Sci., 36, 1205-1216.

Charney, J.G., J. Shukla, and K.C. Mo, 1981: Comparison of a barotropic blocking theory with observation. J. Atmos. Sci., 38,

Charney, J.G., and D.M. Straus, 1980: Form-drag instability, multiple equilibria and propogating planetary waves in baroclinic, orographically forced, planetary wave systems. J. Atmos. Sci., 37, 1157-1176.

Dole, Randall M., 1982: Persistent anomalies of the extratropical Northern Hemispheric wintertime circulation. Ph.D. Thesis, Massachussetts Institute of Technology, Cambridge, Mass. 02139.

Frederiksen, J.S., 1979: The effects of long planetary waves on the regions of cyclogenesis: Linear theory. J. Atmos. Sci., 36, 195-204.

Gall, R., R. Blakeslee, and R.C.J. Somerville, 1979: Cyclone-scale forcing of ultralong waves. J. Atmos. Sci., 34, 1040-1053.

Lorenz, E.N., 1960a: Maximum simplification of the dynamic equations. Tellus, 12, 243-254.

Lorenz, E.N., 1960b: Energy and numerical weather prediction. Tellus, 12, 364-373.

Lorenz, E.N., 1962: Simplified dynamic equations applied to the rotating basin experiments. J. Atmos. Sci., 19, 39-51.

Lorenz, E.N., 1963: The mechanics of vacillation. J. Atmos. Sci., 20, 448-464.

Lorenz, E.N., 1971: N-cycle time-differencing for stepwise numerical integration. Mon. Wea. Rev., 99, 644-648.

Lorenz, E.N., 1972: Barotropic instability of Rossby wave motion. J. Atmos. Sci., 29, 258-264

Niehaus, M.C.W., 1980: Instability of non-zonal baroclinic flows. J. Atmos. Sci., 37, 1447-1463.

Pedlosky, J., 1979: Geophysical Fluid Dynamics. Springer-Verlag, New York.

Pedlosky, J., 1981: The nonlinear dynamics of baroclinic wave ensembles. J. Fluid Mech., 102, 169-209.

Roads, J.O., 1980a: Stable near-resonant states forced by perturbation heating in a simple baroclinic model. J. Atmos. Sci., 37, 1958-1967.

Roads, J.O., 1980b: Stable near-resonant states forced by orography in a simple baroclinic model. J. Atmos. Sci., 37,

2381-2395.

Sanders, F. and J. Gyakum, 1980: Synoptic-dynamic climatology of the "bomb". Mon. Wea. Rev., 108, 1589-1606.

Yao, M.S., 1977: Thermally and topographically forced general circulation regimes in a 2-level quasi-geostrophic atmosphere. Ph.D. Thesis, University of California, Los Angeles, California 90024. 161 pp.

Yao, M.S., 1980: Maintenance of Quasi-stationary waves in a two-level quasi- geostrophic spectral model with topography. J. Atmos. Sci., 37, 29-43.

Young, J.A., 1966: On the relation between zonal heating asymmetries and large-scale atmospheric fluctuations in space and time. Ph.D. Thesis, Massachussets Institute of Technology, Cambridge, Mass. 02139. 260 pp.

FIGS. A-F

Limited contour analyses; 552 decameter contour each day at 500 mb. for selected periods of time. A) 18 days from January 26, 1980 to February 15, 1980. Asterisks (*) refer to surface "bombs" as defined by Sanders and Gyakum (1980). B) 16 day period from February 5, 1977 to February 20, 1977. An example of Pacific Negative associated with Atlantic Negative (see Dole). C) Collapse of regime in Figure B: 15 day period from February 22, 1977 to March 8, 1977. D) 16 day period from December 31, 1980 to January 15, 1981. A second example of Pacific Negative but associated with Atlantic Positive. E and F) 21 day and 11 day Pacific Positive regimes; the "reverse" of the cases plotted in Figs. B and D. Periods are from March 14, 1977 to April 2, 1977 and March 26, 1979 to April 5, 1979, respectively.

FIG. 1

Graph of the Ψ_2 component of the 5 case #2 equilibria as a function of Θ_1^* (heavy lines). The coordinates (ordinate and abscissa) are given by Ψ_2 and Θ_1^* respectively. All units are nondimensional.

FIG. 2a,b

Graph of the nondimensional e-folding times γ for the various modes of the case #2 equilibria as a function of Θ_1^*. a) 45° Trough, (heavy lines), 90° Ridge (light lines) and b) Hadley Solution (heavy lines), Near Hadley Solution (light lines) and 30° Ridge (dashed lines). Negative γ corresponds to a stable solution.

FIG. 3a,b,c

Plots of the $\Psi_3 - \Psi_2$ component of the phase space trajectory each day for varying periods of time for the demonstration case. The coordinates (abscissa and ordinate) in each of the figures are given by Ψ_3 and Ψ_2 respectively and all are plotted to the same nondimensional scale. The five equilibria are denoted by triangles. a) Climatological plot: first 17 years of integration. b) Trough regime: plot each day for 175 day period from time step 20765 to 23564. c) Ridge regime: plot each day for 580 day period from time step 23564 to 32855.

FIG. 4

Identical to Fig. 3a except wave-wave interaction has been removed.

FIG. 5

Scatter diagram in phase space of the time mean Mode 11 upper level (instead of midlevel) wave for each of the regimes listed in Tab. 3a. The coordinates (abscissa and ordinate) are given by φ_3 and φ_2. The five equilibria are denoted by circles (⊙) and those with a subscript 1/2 are plotted at one half their actual amplitude. The time mean 205 year composites are denoted by a line and a number which represents the category. Categories 3 and 4 in the ridge and 3 in the trough contain only 5 regimes or less and are not very representative of the regime statistics.

FIG. 7

Plot in phase space of the case #2 Mode 11 and Mode 21 midlevel stream- function limit cycles for selected values of Θ_1^*. Selected composite regimes (denoted by *) and stationary equilibria (denoted by ▲) are also shown. Mode 11 limit cycles are heavy lines and Mode 21 limit cycles are light lines. At $\Theta_1^* = .15$ the Mode 11 limit cycle is unstable and spirals into the stable 45° Trough Equilibrium state (dashed line). All limit cycles have counterclockwise orbits. The coordinates are given by ψ_3 and ψ_2 (not φ_3 and φ_2).

FIG. 6a,b

Two phase space plots of the midlevel $\psi_3 - \psi_2$ component of the

trajectory each day for selected periods of time during the 4th regime in Tab. 3a. a) Steady 18-day Regime type II behavior, b) More erratic 24-day period starting two days after the last day in Fig. 6a. Notation and units identical to Figs. 3a,b,c, and 4.

FIG. 8a,b,c,d and FIG. 9a,b,c,d

8 plots of the phase and amplitude of the upper level Mode 11 wave stream- function for the various composites and the corresponding equilibria for case #1 and case #2 as a function of Θ_1^*. The abscissa is Θ_1^* and the ordinate either amplitude or degrees (A) with respect to the orographic ridge (not to be confused with degrees longitude on the Earth). "8" refers to case #1 and "9" to case #2. "a" and "c" refer to the amplitude of the trough and ridge regime respectively and "b" and "d" refer to the phase of the trough and ridge regime respectively. The corresponding equilibrium states appear as continuous heavy curves while the 7 regime composites are plotted for every value of Θ_1^* in Tables 5a and b and connected by light lines. In Figs. 9a and c the amplitude of the corresponding equilibrium state becomes so large for increasing Θ_1^* the curves are displaced downward.

FIG. 10

Cumulative persistence distributions for case #2 with $\Theta_1^* = .12$ and .14 and Dole's 5 dm. positive and negative persistent anomalies. The ordinate is the total number of events which persist for n days or longer on a log scale and the abscissa is in days. The model ridge regimes and positive anomalies are denoted by crosses (+) and the trough regimes and negative anomalies by circles (o).

FIG. 11a,b,c,d,e,f,g,h

8 "weather maps" of the midlevel (500 mb.) and lower level (850 mb.) height field and lower level potential temperature (dashed lines) for case #2 with $\Theta_1^* = .12$. The Near Hadley, 90° Ridge, 45° Trough, and 30° Ridge Equilibria are plotted in Figs. a,b,c, and d respectively, while the mean state category 7 trough and ridge regime composites are plotted in e and f respectively. "g" and "h" are two instantaneous weather maps taken during a trough and ridge regime occurrence respectively. The height contours are every 6 decameters and the temperature isotherms (stretched) every 18° C. The units in the x-direction are given in degrees with respect to the orographic ridge (not to be confused with degrees longitude on Earth).

FIG. 12

Plot of the phase and amplitude of the transient forcing terms ad11, ad21, ad12, and "sum" of the upper level vorticity equations for case #2 with $\Theta_1^* = .12$ composite trough and ridge regimes. The ordinate is the φ_2 forcing component and the abscissa is the φ_3 forcing component. "ad11" is denoted by ⊙, and "ad21" by x, "ad12" by ● and "sum" by *. The subscripts next to the symbols refer to the categories, and each group of terms is circled and labled. The subscript "R" refers to the ridge and the subscript "T" to the trough. Also plotted are the forcing terms during periods of Regime type II behavior. The solid triangles (▲) correspond to a 31-day ridge and the solid squares (■) to a 46-day trough. The subscripts 11, 21, 12 and s refer to ad11, ad21, ad12, and "sum" respectively.

FIG. 13a,b

Balance of forces. Plot of the various budget terms and upper level Mode 11 wave in vector form for the 7 categories of a) trough regimes and b) the ridge regimes for case #2 with $\Theta_1^* = .12$. The ordinate and abscissa are the same as in Fig. 12 except multiplied by a factor of 4.

FIG. 14a,b

Plot of the phase of the nonlinear transport terms nlns, time

mean upper level Mode 11 wave, and corresponding equilibrium state upper level wave for the 7 categories of the composite a) trough regimes for case #1 and b) ridge regimes for case #2 as a function of Θ_1^*. Ordinates and abscissa are the same as in Figs. 8b and 9d.

FIG. 15a,b

Phase space plot of the midlevel streamfunction wave of the regime- equilibria for selected values of the transient to zonal energy ratio for case #2 with a) Θ_1^*=.12 and b) Θ_1^*=.15. In both figures the parameterized effects of ad22 have been included. The ordinate and abscissa are given by Ψ_2 and Ψ_3, respectively. The stationary equilibria are denoted by triangles (Δ) and the individual regime-equilibria for those values of the energy ratio listed in Tables 4a and 4b respectively are denoted by enlarged points and labled by their corresponding value of the energy ratio. In Fig. 15a, the category 7 full model trough and ridge regimes are denoted by asterisks (*) (note the close pass of the regime-equilibria to the full model regimes at energy ratios near .07). In Fig. 1b, selected limit cycle trajectories are plotted for those values of the energy ratio where the regime-equilibria are unstable.

FIG. 16a,b

Time series of selected physical processes in the Ψ_2 tendency equation. a) Demonstration case: 512-day period beginning 1000 time steps after initialization; the 512-day period is broken into four 128-day periods. On the upper axis, AD11 (heavy line) and the tendency term $\partial\Psi_2/\partial t$ (light line) are plotted, and on the lower axis "sum" (light line) is plotted. The tendency term and "sum" are plotted on the same scale, but AD11 is first divided by four. b) Case #2 with $\Theta_1^*=.12$: The tendency term (heavy line) and "sum" (light line) are plotted for a total of 256 days beginning 4350 days after initialization. Each axis segment then represents 64 days. Both terms are plotted to the same scale.

FIG. 17a,b

(From Dole (1981)) Time series plots of the amplitude of Dole's composite Pacific positive and Pacific negative anomalies. The ordinate is in meters and the abscissa is in days. Day zero is alligned in a) to correspond to the time when each individual anomaly first meets Dole's 10 day-10 decameter selection criteria, while in b) it corresponds to the time when the individual anomaly last meets the aforementioned criteria. In each figure, the Pacific positive event is denoted by dots and the Pacific negative event by open circles (o). Note the rapid rate of onset and collapse for both anomaly types, in spite of the fact each individual

anomaly event persisted at least 10 days.

TAB. 2

The 5 equilibrium solutions and their respective stabilities to the 4 modes of the model for the demonstration case. The equilibria are given in terms of the midlevel streamfunction Ψ and potential temperature Θ. The asterisk * to the right of the growth rates (in units of hours) indicates that the instability is non-propogating (orographic).

TAB. 3a

The type, length in days, start and finish time step, and the time mean upper and lower level streamfunction of the regimes as they occur in the demonstration case for the first 28 years of integration. A "-1" and "+1" refer to the trough and ridge respectively.

TAB. 3b

The 7 categories of the 205 year composite trough and ridge regimes for the demonstration case. Column 1 is the category, column 2 is the sum total of days of regime of said category that contribute to the composite, and column 3 is the number of regime events that fell into said category. The mean

composite state is given in upper level zonal flow φ_1, amplitude and phase of the upper level wave and ditto for the lower level. For comparison, the upper and lower level streamfunction in phase and amplitude form for the 5 equilibria are also listed.

TAB. 4a,b

Stability of the equilibria as a function of θ_1^* for a) case #1 and b) case #2. Growth rates are given in hours, and an asterisk * indicates a non-propogating instability (orographic). The Mode 22 wave is always stable and thus is not listed. In Table 4b "S" indicates solution is stable.

TAB. 5a,b

Statistics of the regimes for select values of the driving θ_1^* a) case #1 and b) case #2. The total number of days of each experiment (6250) is given in row 1, the total number of days the state of the model flow was in the ridge regime, trough regime, both the ridge and trough regime, and neither the ridge or trough regime (unsteady) are given in rows 2, 3, 4, 5, respectively. The ten most persistent ridge and trough regimes in each experiment are then listed in the next 20 rows. The units are in days. In Table 5b, the dashes indicate that there were less than 10 regimes during the

course of the experiment.

TAB. 6a,b

Budget terms for a) case #2 with Θ_1^*=.12 category 7 composite regimes and b) Regime type II behavior during a single regime event in case #2 with Θ_1^*=.12. The units are the tendencies of the upper and lower level equations (times 1000) in the first 6 columns; the last three columns are the contributions to w. Individual terms explained in text, equations also in text.

TAB. 7a

Comparison of phase and relative amplitudes of the transport terms from the stability calculation with the full model regime budgets for the tendency equations (7.1) in Chapter 7 in phase and amplitude form. φ =amplitude of upper level wave tendency, A=phase of upper level wave tendency, ϕ =amplitude of lower level wave tendency, α =phase of lower level wave tendency, w_1 =zonal w contribution, w_φ =amplitude of wave w contribution, w_α =phase of wave w contribution. The experiments were conducted for case #2 with Θ_1^*=.12 for two periods of Regime type II behavior. Amplitudes from stability calculation (Theory) are divided by the corresponding terms in the regime budgets (Full model).

TAB. 7b

Comparison of the vector sum of the transport components predicted by Theory to that observed in the budgets for periods of trough and ridge regime type II behavior. Amplitudes of the theoretical calculation were obtained by setting $B^2=.75$ in the trough regime and setting $B^2=1.03$ in the ridge regime. Notation otherwise the same as Table 7a.

TAB. 7c

Same as Table 7a for category 7 composite regimes.

TAB. 8a,b and 9a,b

List of regime-equilibria mid-level streamfunction and potential temperature in spectral component form for selected values of the energy ratio for case #2 with a) $\Theta_1^*=.12$ and b) $\Theta_1^*=.15$. In Table 8 the parameterized effects of ad22 are not included whereas in Table 9 they are.

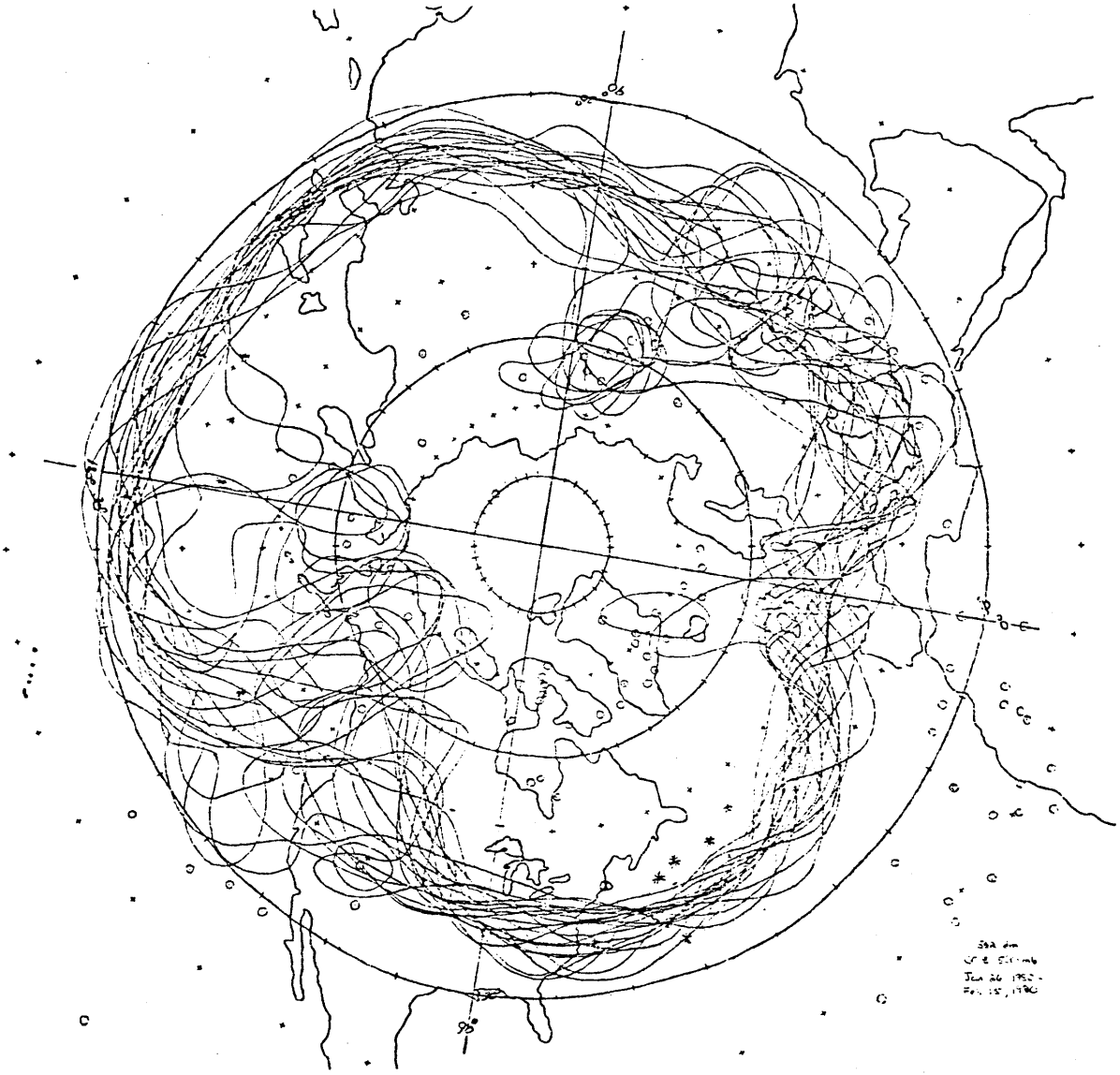

FIGURE A: Limited contour analysis. 552 dm. contour at 500 mb. level. Period consists of 18 days from January 26, 1980 to February 15, 1980. Asterisks refer to surface "bombs" as defined by Sanders and Gyakum (1980). Note steady behavior in Eastern United States and Atlantic as well as East Asia and western Pacific. Note unsteady behavior over the western North American continent.

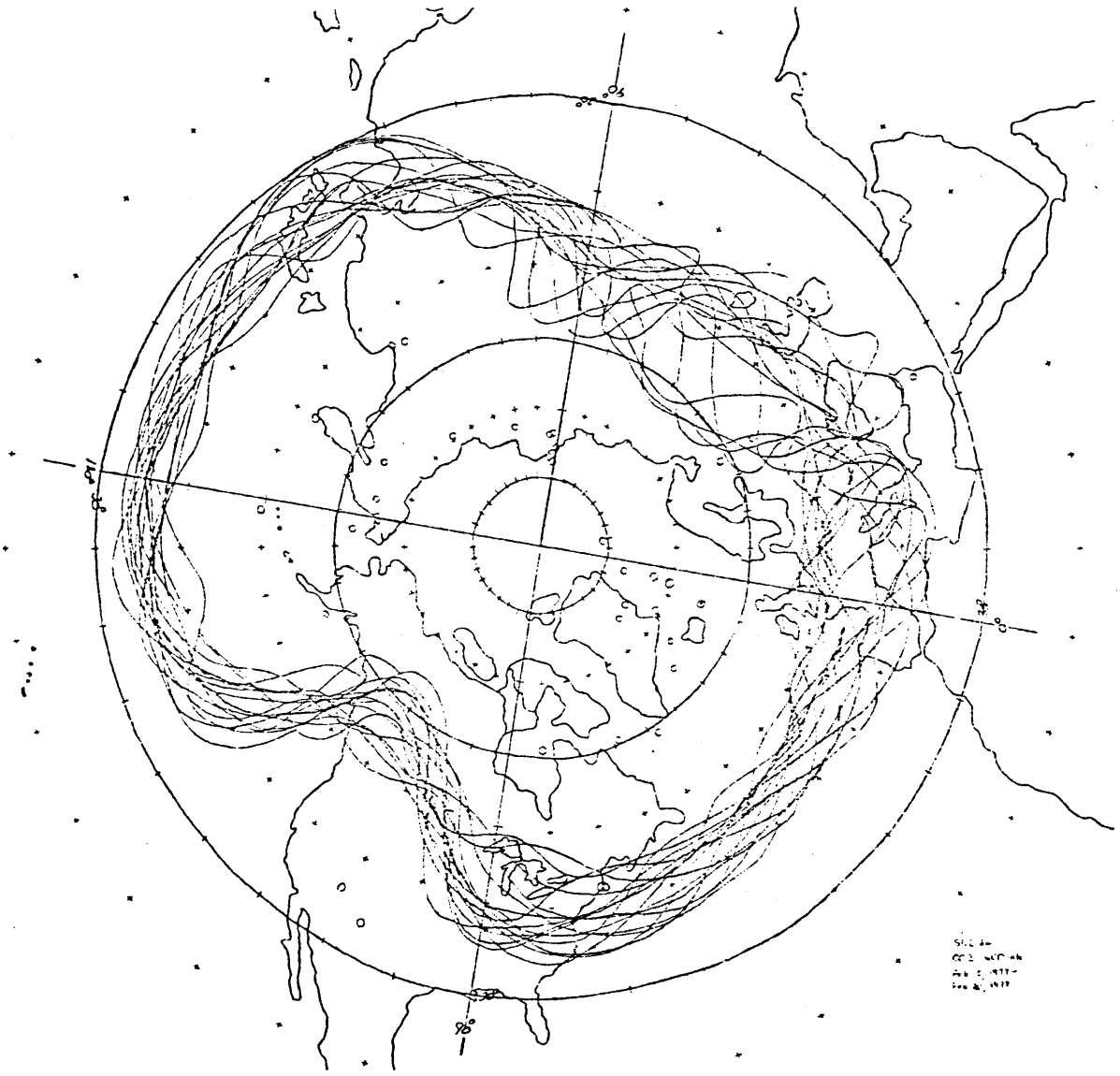

FIGURE B: Same as Figure A except for the 16 day period from February 5, 1977 to February 20, 1977. This is the last 16 days of the now infamous winter regime of 1976-1977. According to Dole (1981), this is an example of Pacific Negative and Atlantic Negative.

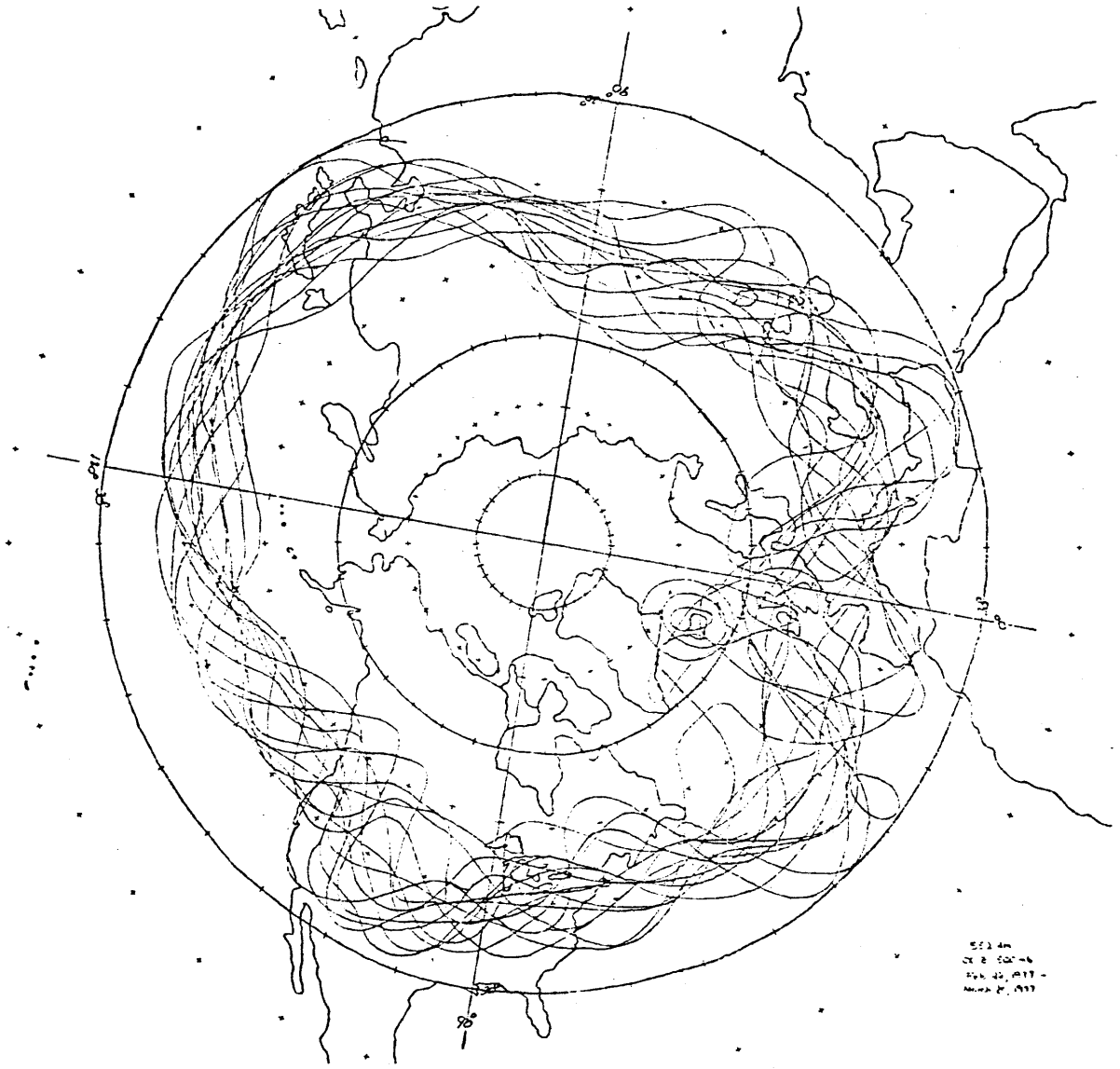

FIGURE C: Sudden collapse of the 1976-1977 regime shown in Figure B. This plot consists of the 15 day period from February 22, 1977 to March 8, 1977. Note complete disappearance of the high amplitude ridge over the Rockies. Notation otherwise the same as in Figures A and B.

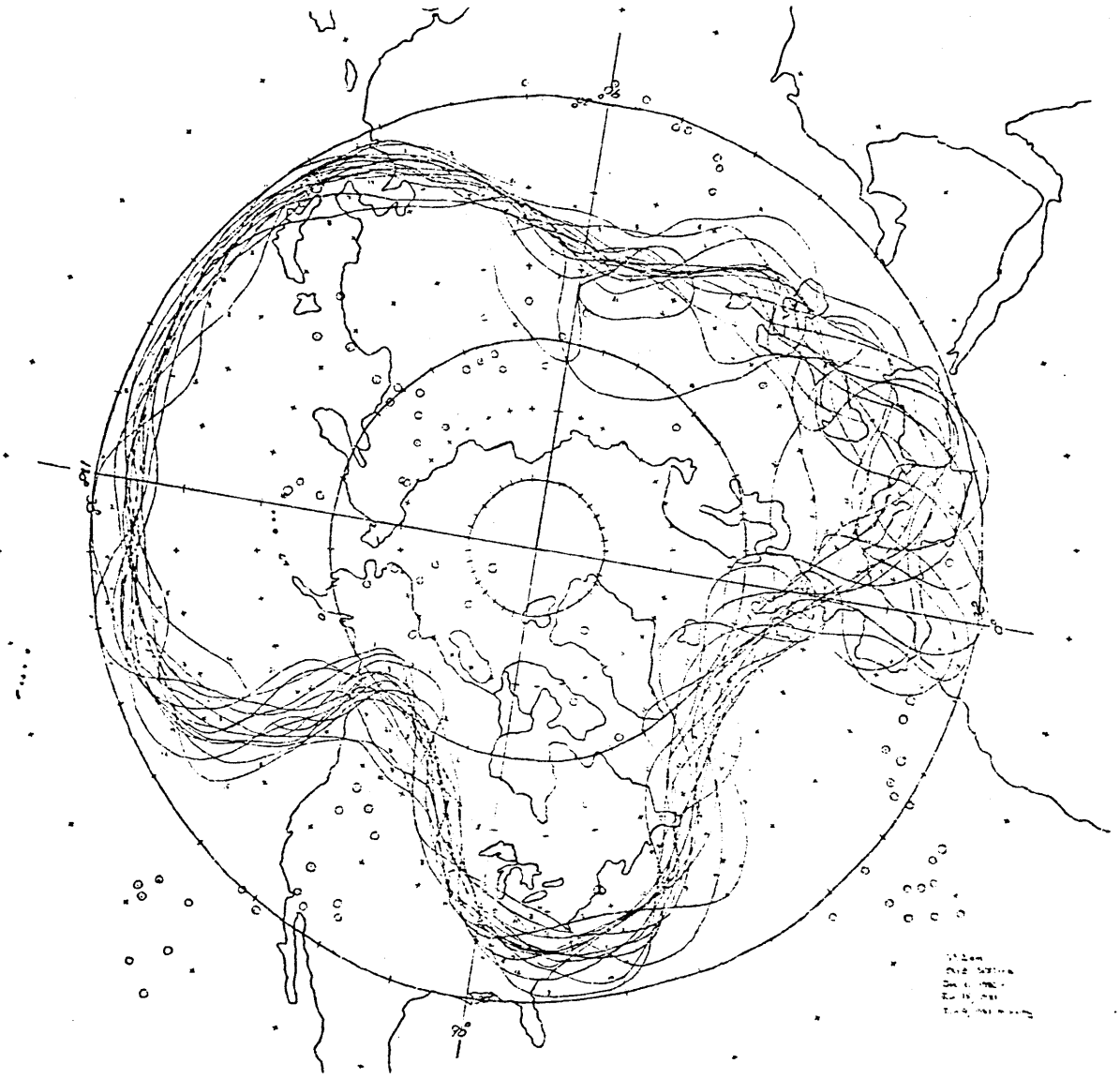

FIGURE D: A second example of Dole's Pacific Negative event but this time associated with Atlantic Positive. The plot consists of the 16 day period from December 31, 1980 to January 15, 1981. Notation the same as in the previous figures.

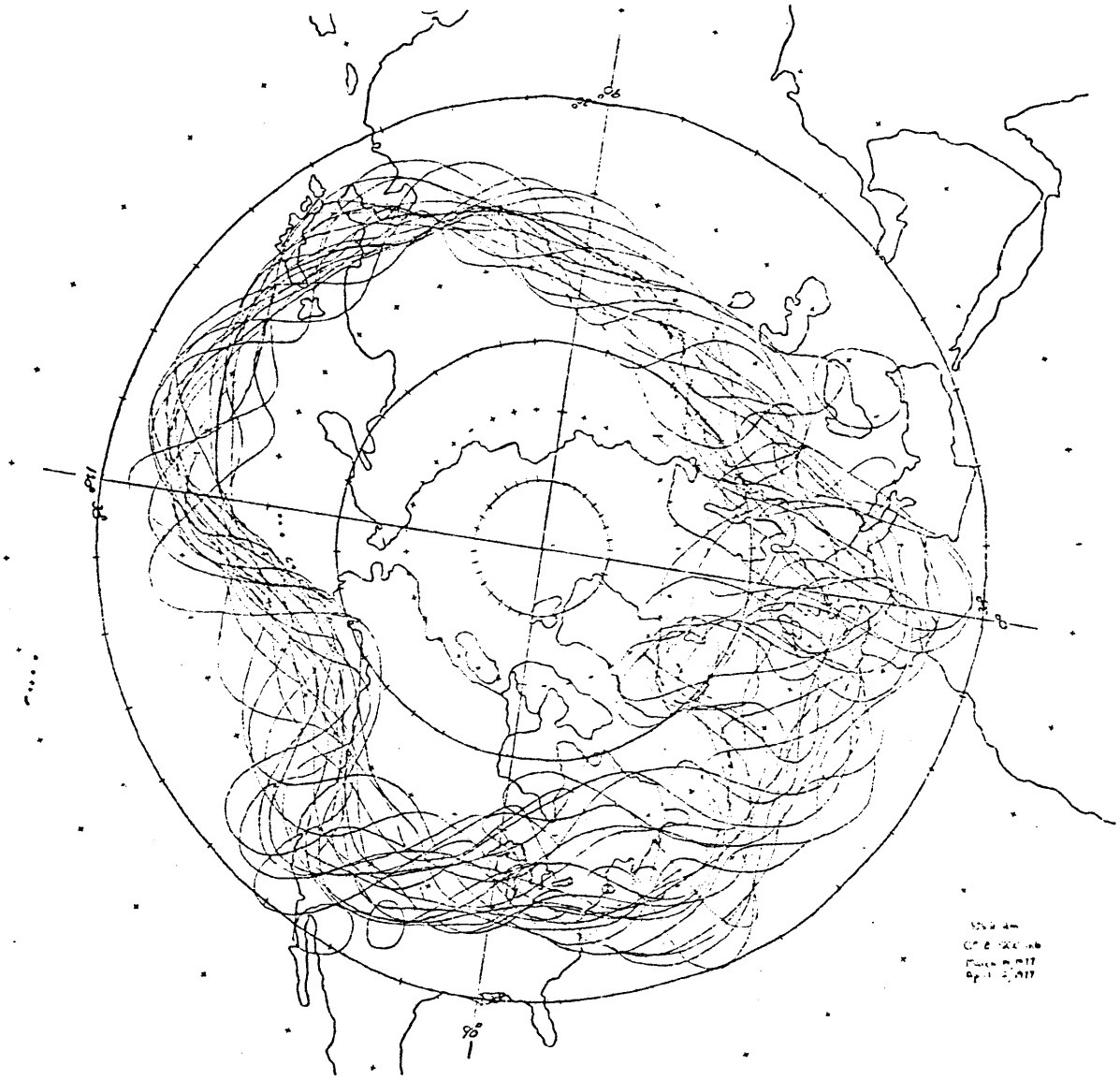

FIGURE E: A regime with the reverse type of flow pattern as shown in Figures B and D, e.g., troughing over the Rockies or Pacific Positive. This plot consists of the 20 day period from March 14, 1977 to April 2, 1977. Notation otherwise the same as in the previous figures.

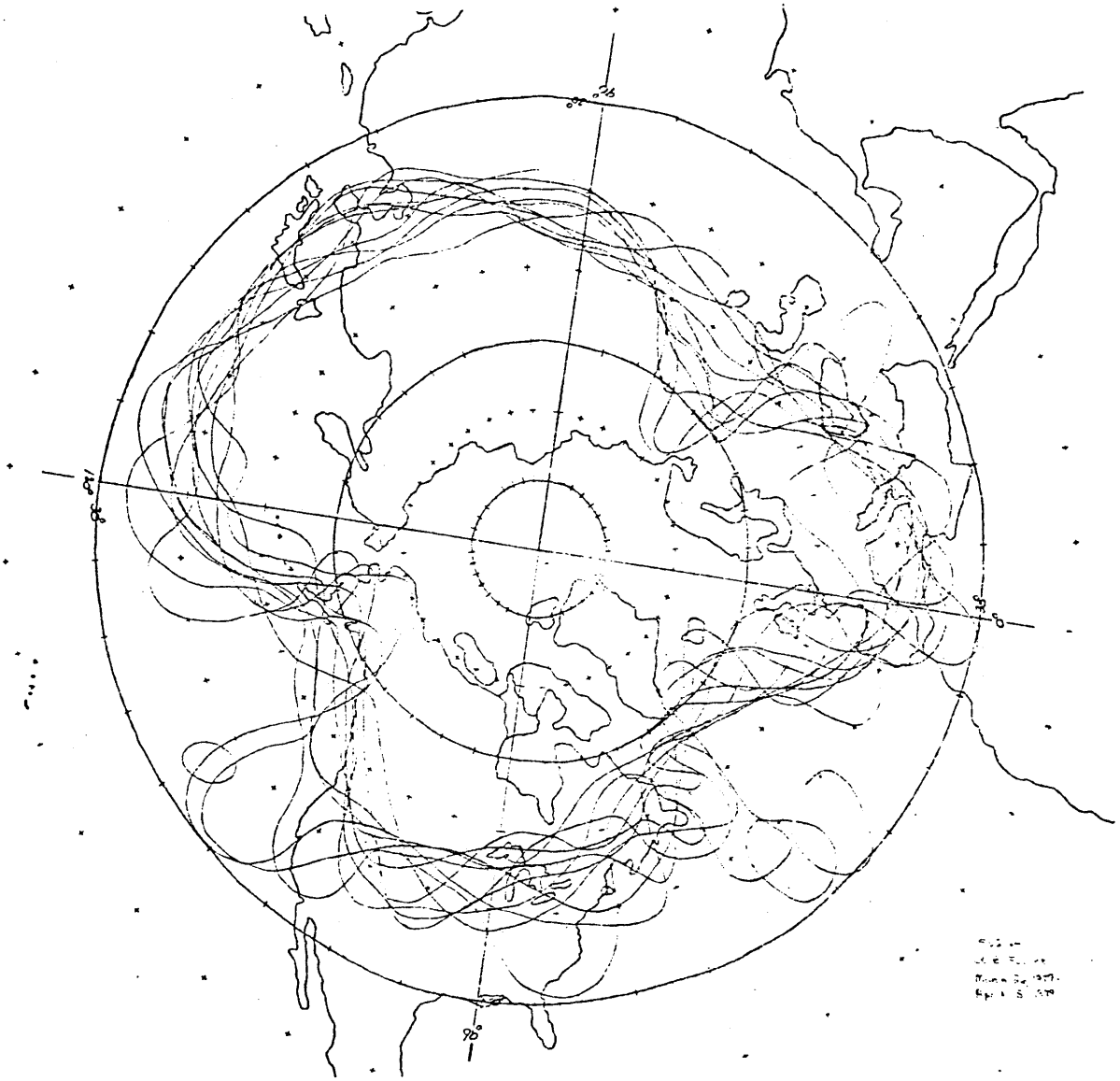

FIGURE F: Another example of a late season Pacific Positive event of rather short duration. Period consists of the 11 days from March 26, 1979 to April 5, 1979. Notation same as previous figures.

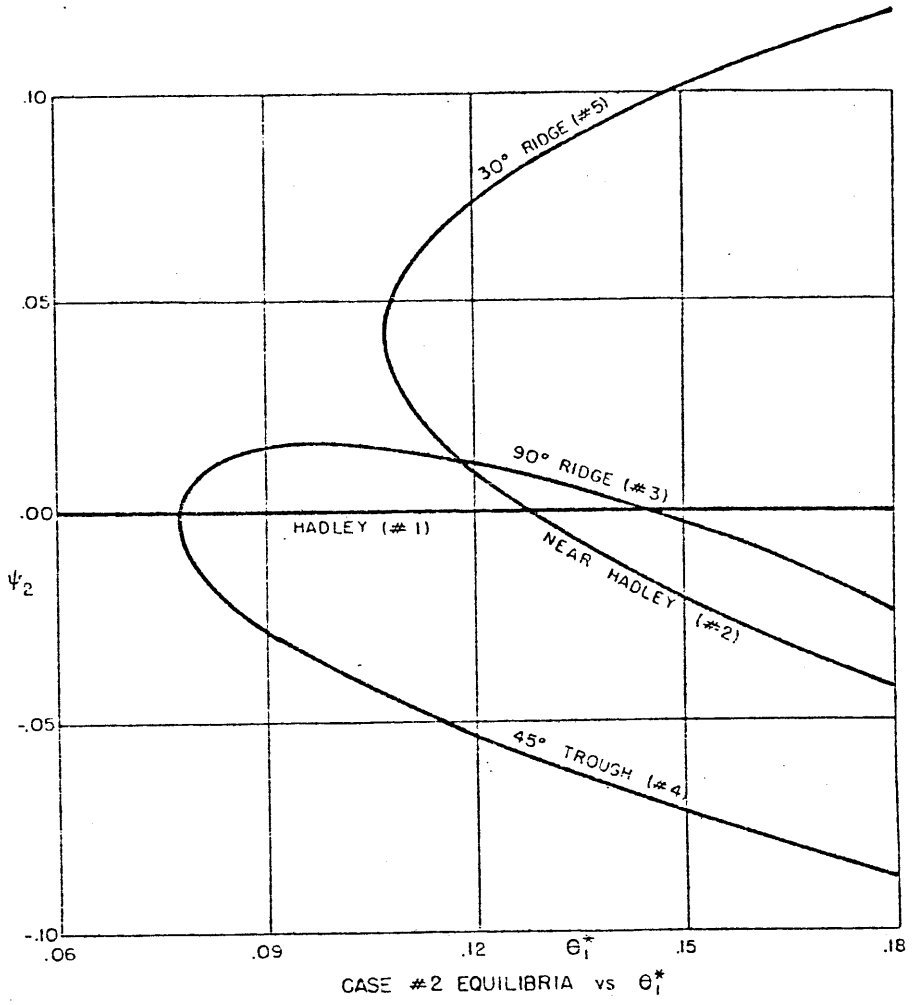

FIGURE 1: Graph of the ψ_2 component of the 5 case #2 equilibria as a function of θ_1^* (heavy lines). The coordinates (ordinate and abcissa) are given by ψ_2 and θ_1^* respectively. All units are nondimensional.

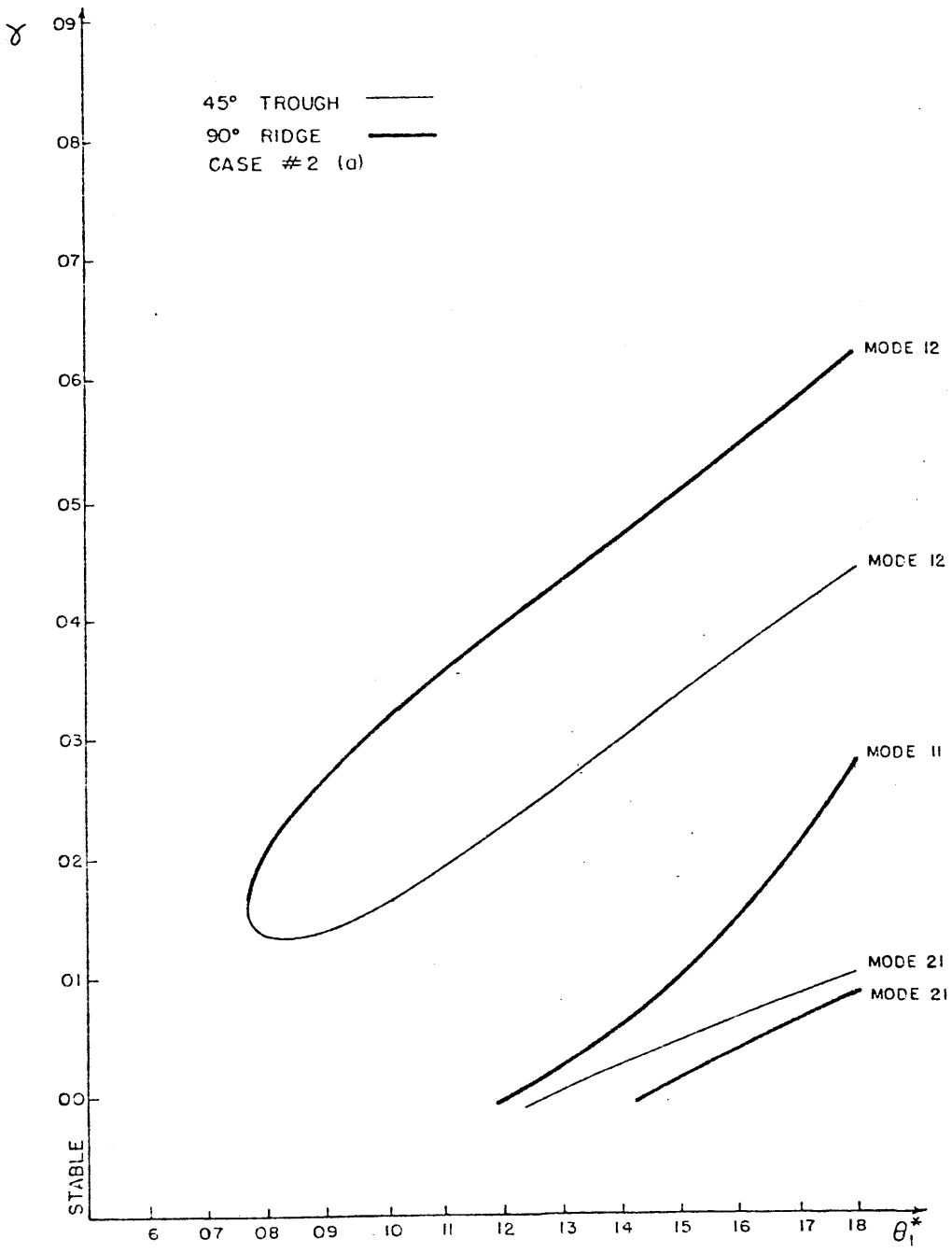

FIGURE 2a: Graph of the nondimensional e-folding times γ for the various modes of the case #2 equilibria as a function of θ_1^*. The heavy lines correspond to the 45° Trough and the light lines to the 90° Ridge. Negative γ corresponds to a stable solution.

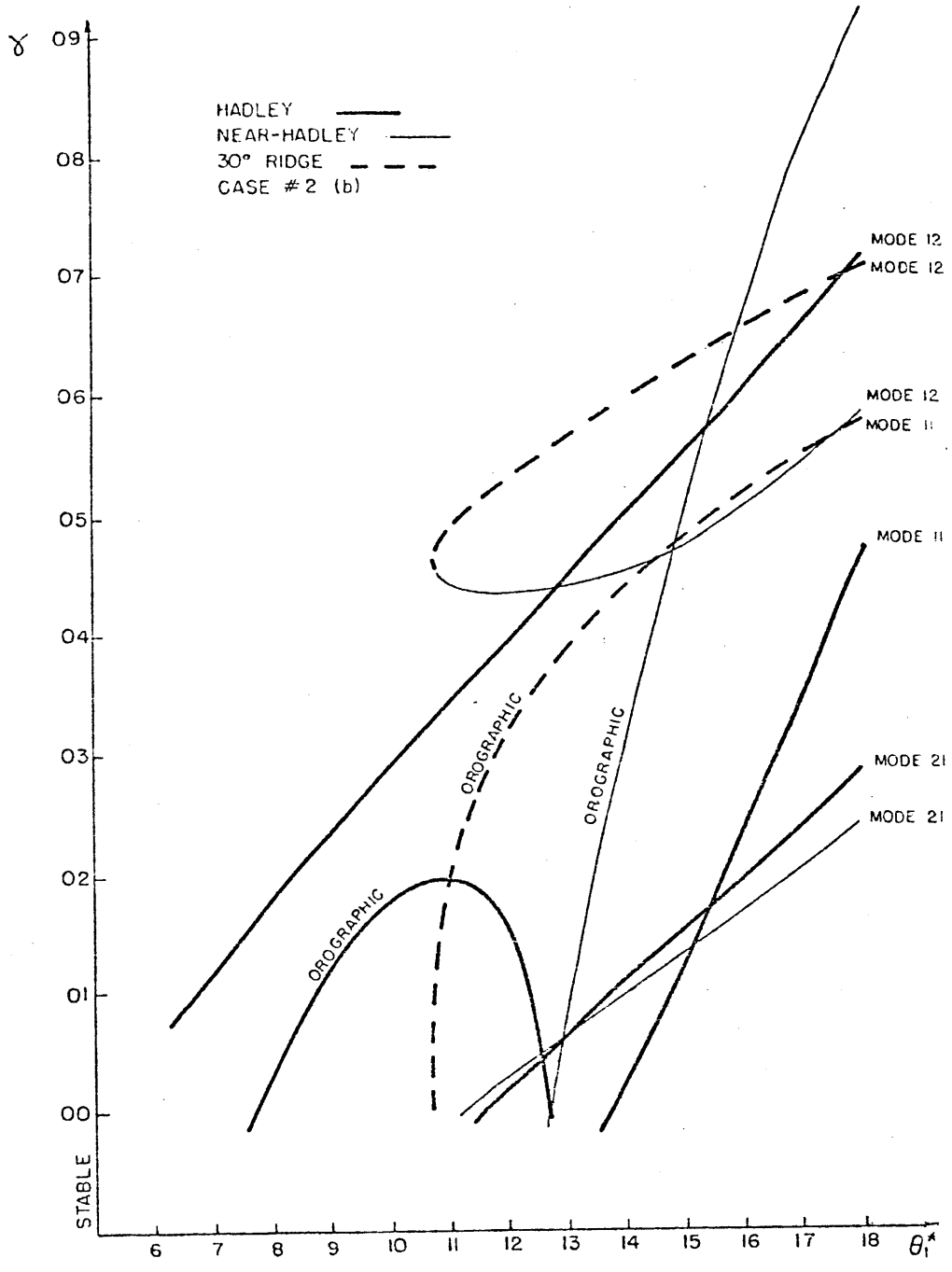

FIGURE 2b: Same as figure 2a except for the Hadley Solution (heavy lines), the Near Hadley Solution (light lines) and the 30° Ridge (dotted lines). The lines labled "orographic" correspond to solutions that grow in place. (See Charney and Straus (1980)).

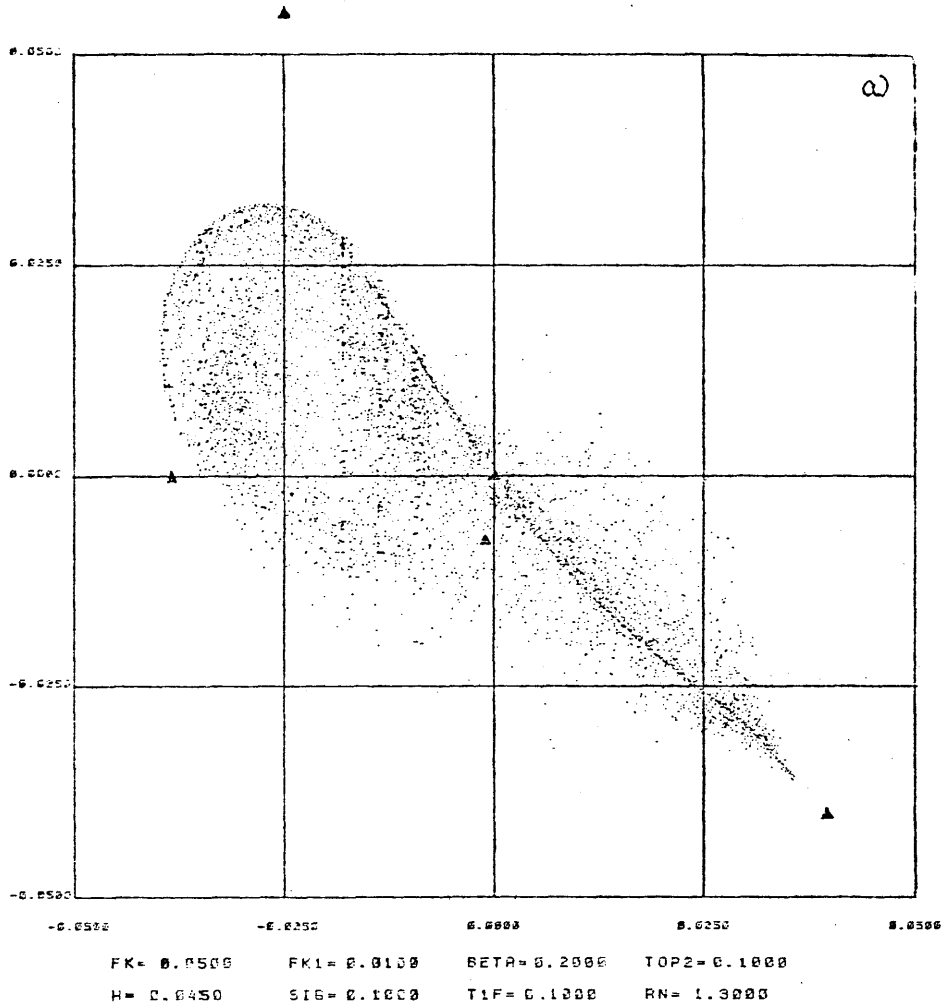

FIGURE 3a: Plot of the $\Psi_3 - \Psi_2$ component of the phase space trajectory each day for 17 years for the demonstration case. The coordinates (abscissa and ordinate) are given by Ψ_3 and Ψ_2 respectively. The 5 purely stationary equilibria are denoted by triangles. The units are nondimensional.

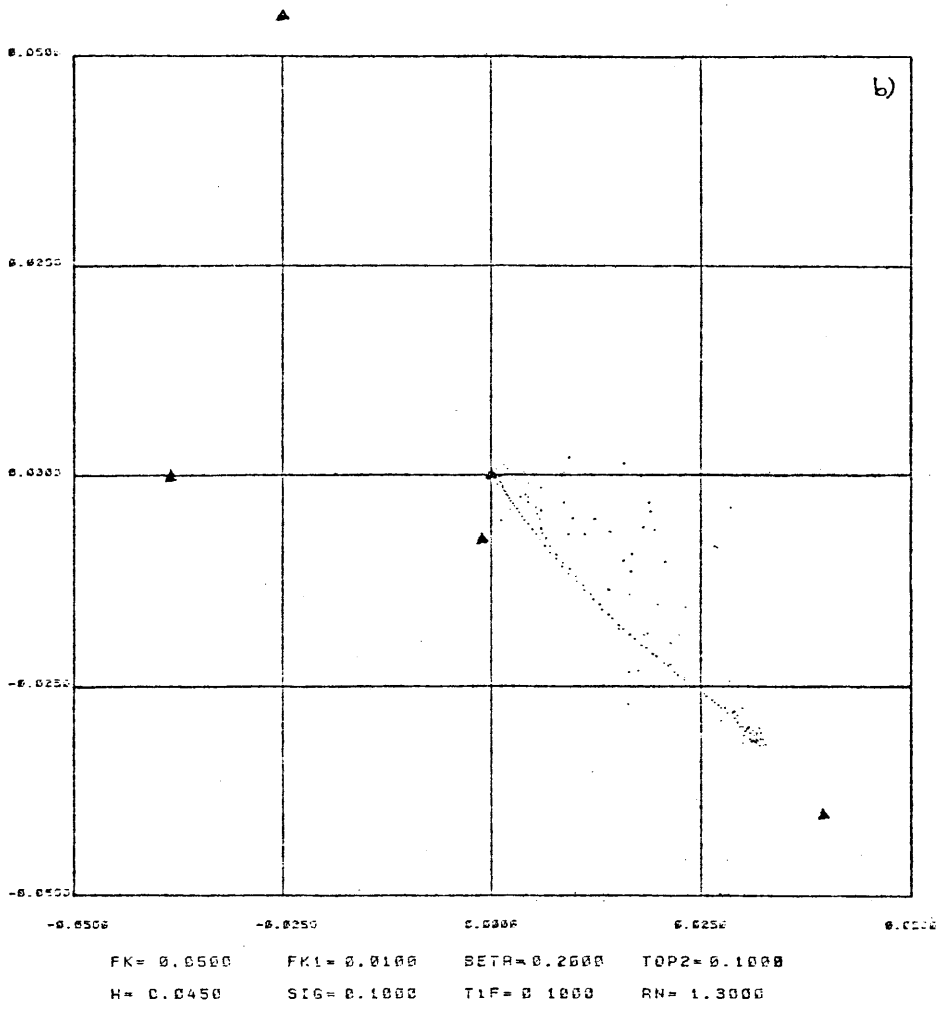

FIGURE 3b: Plot of the "trough" regime, a 175 day period from time step 20765 to 23564. The scale and units are otherwise the same as Figure 3a.

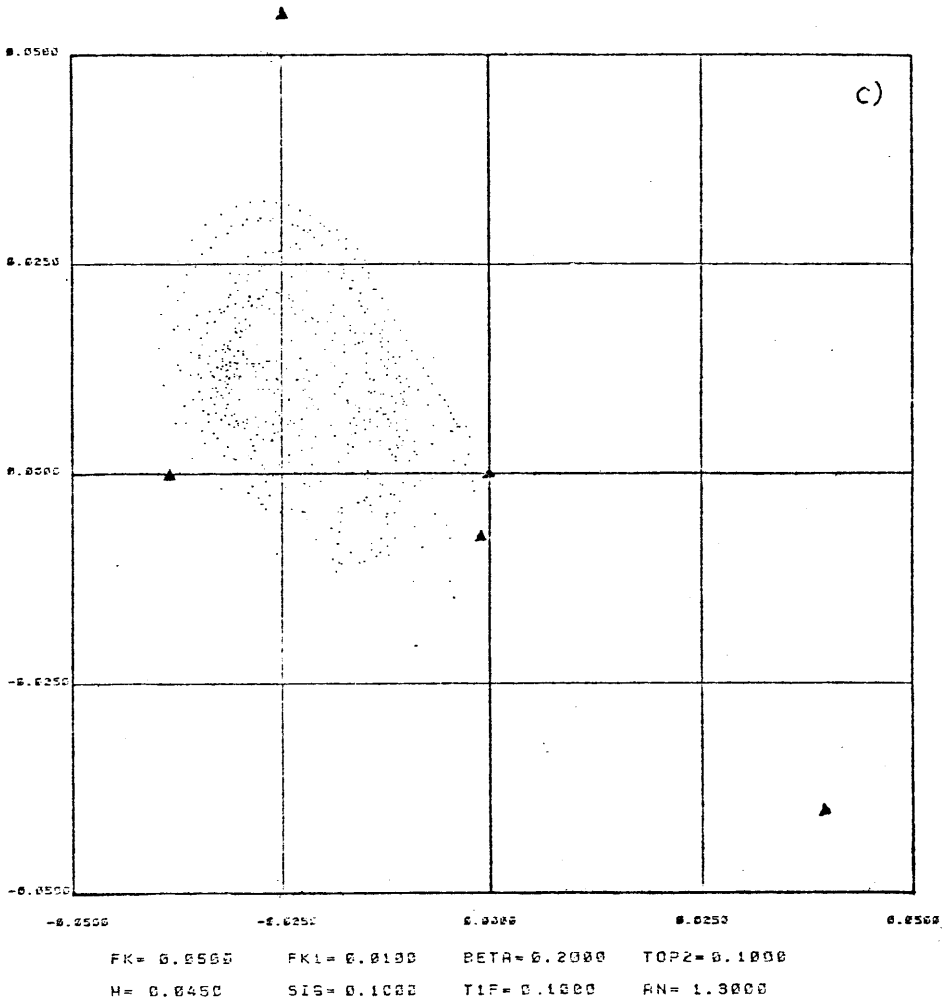

FIGURE 3c: Plot of the "ridge" regime, a 580 day period from time step 23564 to 32855. The scale and units are again the same as Figure 3a.

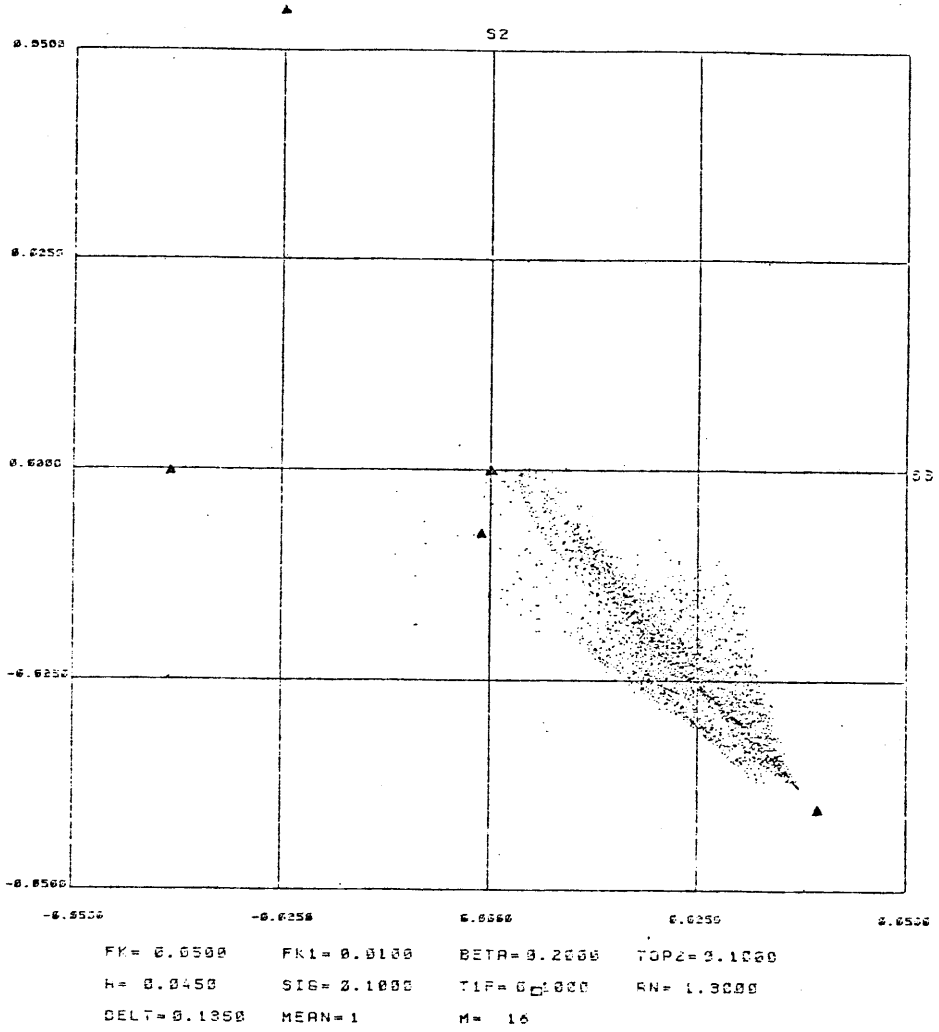

FIGURE 4: Identical to Figure 3a except that the wave-wave interaction has been removed.

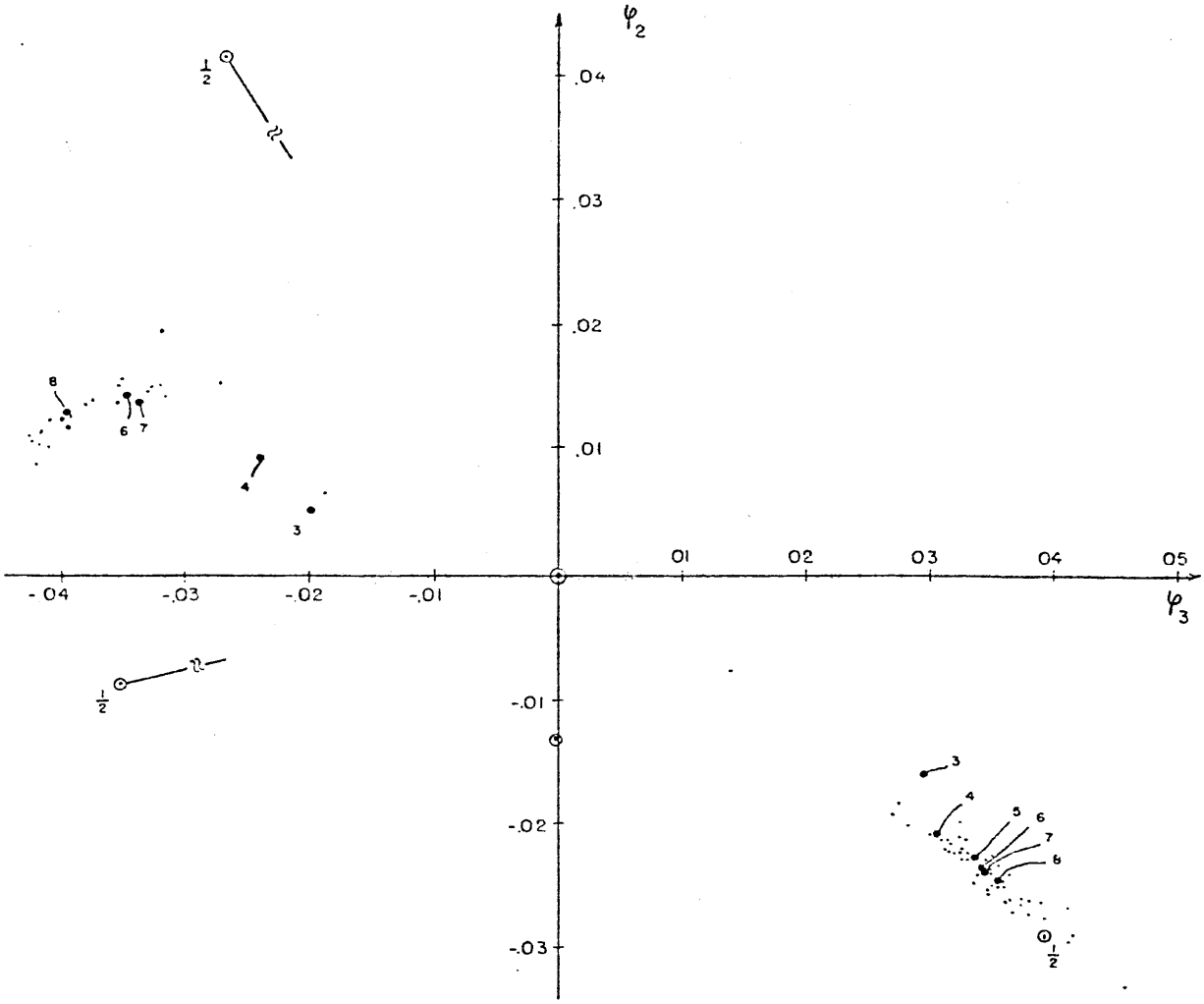

FIGURE 5: Scatter diagram in phase space of the time mean Mode 11 upper level (instead of midlevel) wave for each of the regimes listed in Table 3a. The coordinates (abscissa and ordinate) are given by φ_3 and φ_2 respectively. The five equilibria are denoted by circles (⊙) and those with a subscript 1/2 are plotted at one half their actual amplitude. The time mean 205 year composites are denoted by a line and a number which represents the category. Categories 3 and 4 in the ridge and 3 in the trough contain only 5 regimes or less and are not very representative of the regime statistics.

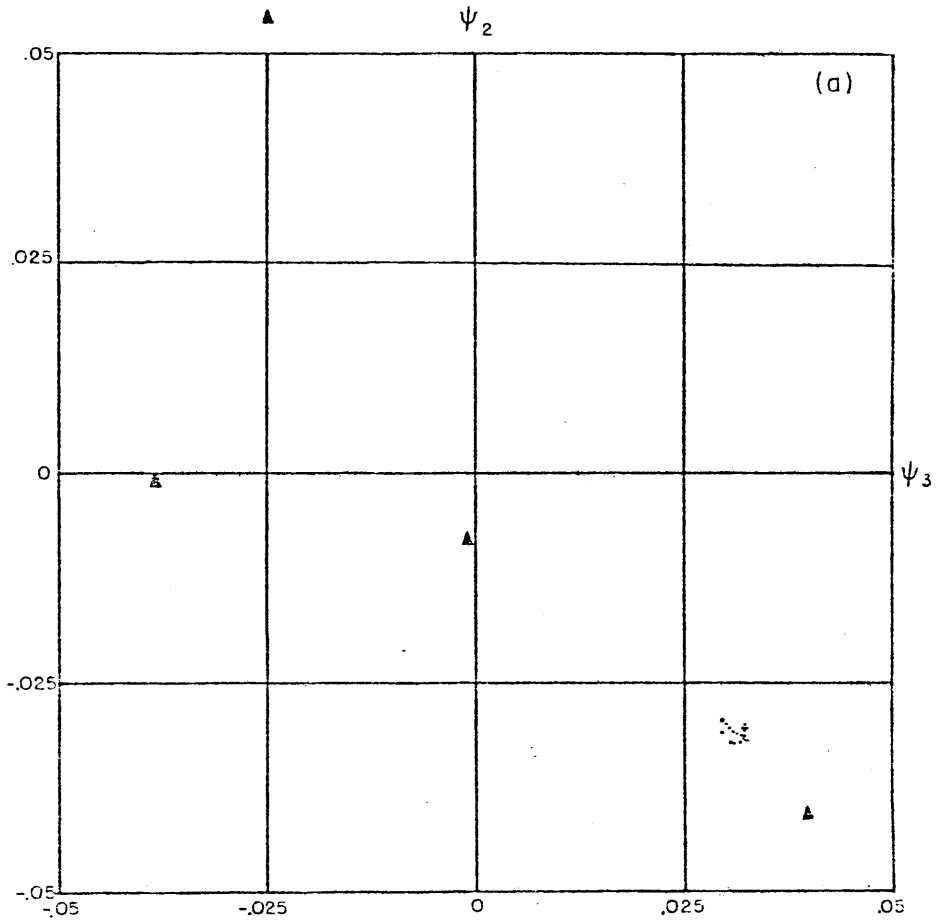

FIGURE 6a: Phase space plot of a period of Regime type II behavior. The plot consists of the Ψ_3 - Ψ_2 component of the trajectory each day for an 18 day period during the 4th regime in Table 3a. Notation and units are the same as in Figures 3a,b,c and 4.

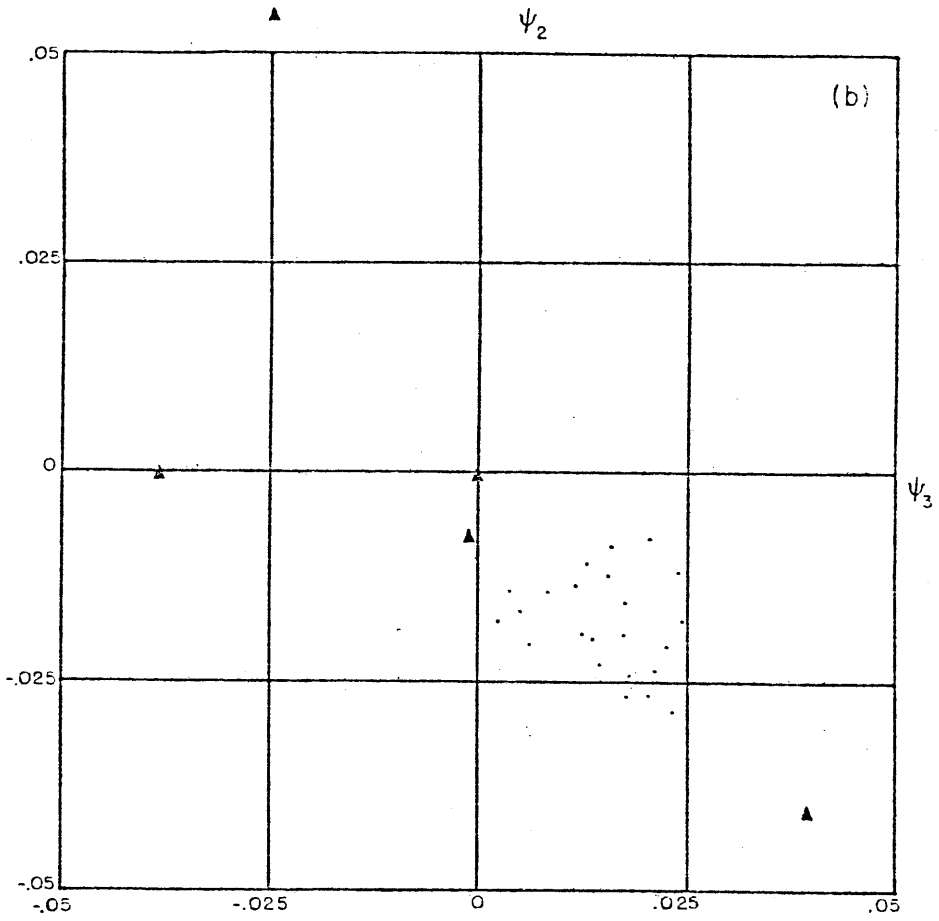

FIGURE 6b: Plot of a more erratic period during the 4th regime in Table 3a. The plot consists of the 24 days starting two days after the last day plotted in Figure 6a. Notation otherwise the same as in Figure 6a.

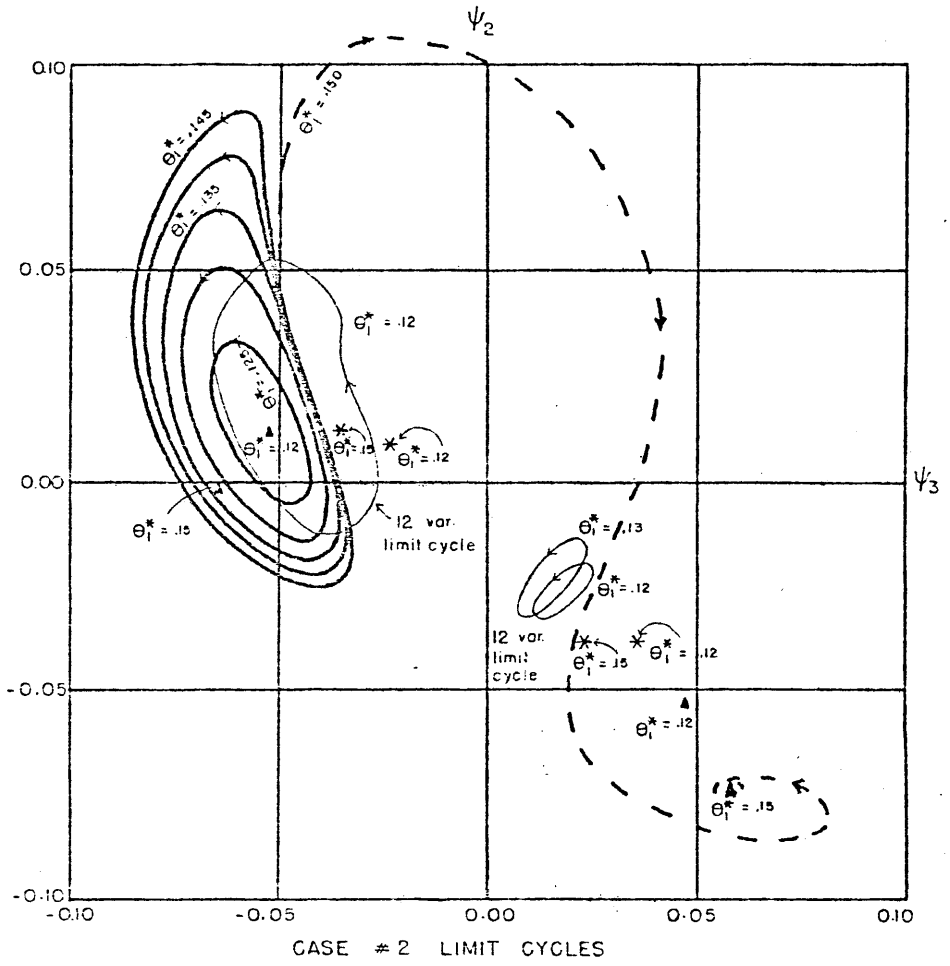

FIGURE 7: Plot in phase space of the case #2 Mode 11 and Mode 21 midlevel streamfunction limit cycles for selected values of θ_1^*. Selected composite regimes (denoted by *) and stationary equilibria (denoted by ▲) are also shown. Mode 11 limit cycles are heavy lines and Mode 21 limit cycles are light lines. At $\theta_1^* = .15$, the Mode 11 limit cycle is unstable and spirals into the 45° Trough Equilibrium state (dashed line). The coordinates are given by ψ_3 and ψ_2 (not ψ_3' and ψ_2').

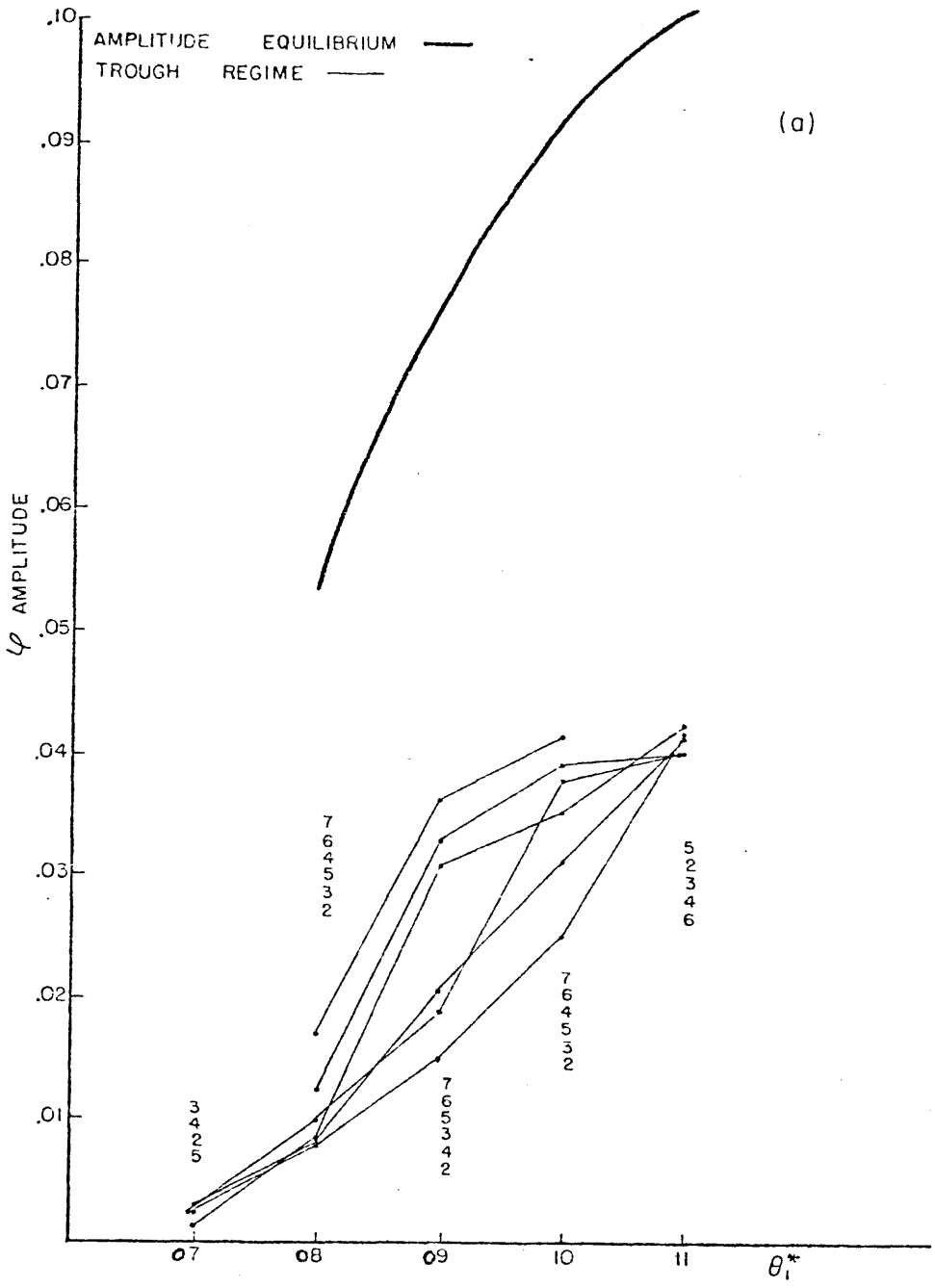

FIGURE 8a: Plot of the amplitude of the upper level Mode 11 wave streamfunction for the various composites and the corresponding equilibria for case #1 as a function of θ_1^*. The abscissa is given by θ_1^* and the ordinate by the amplitude φ. The above plot is for the trough regimes (light lines) and the 45° Trough equilibrium (heavy line). The composites are plotted for every value of θ_1^* listed in Tables 5a and b. The numbers below (or sometimes above) the plotted points are the respective categories. This is true for Figs. 8a-d and 9a-d.

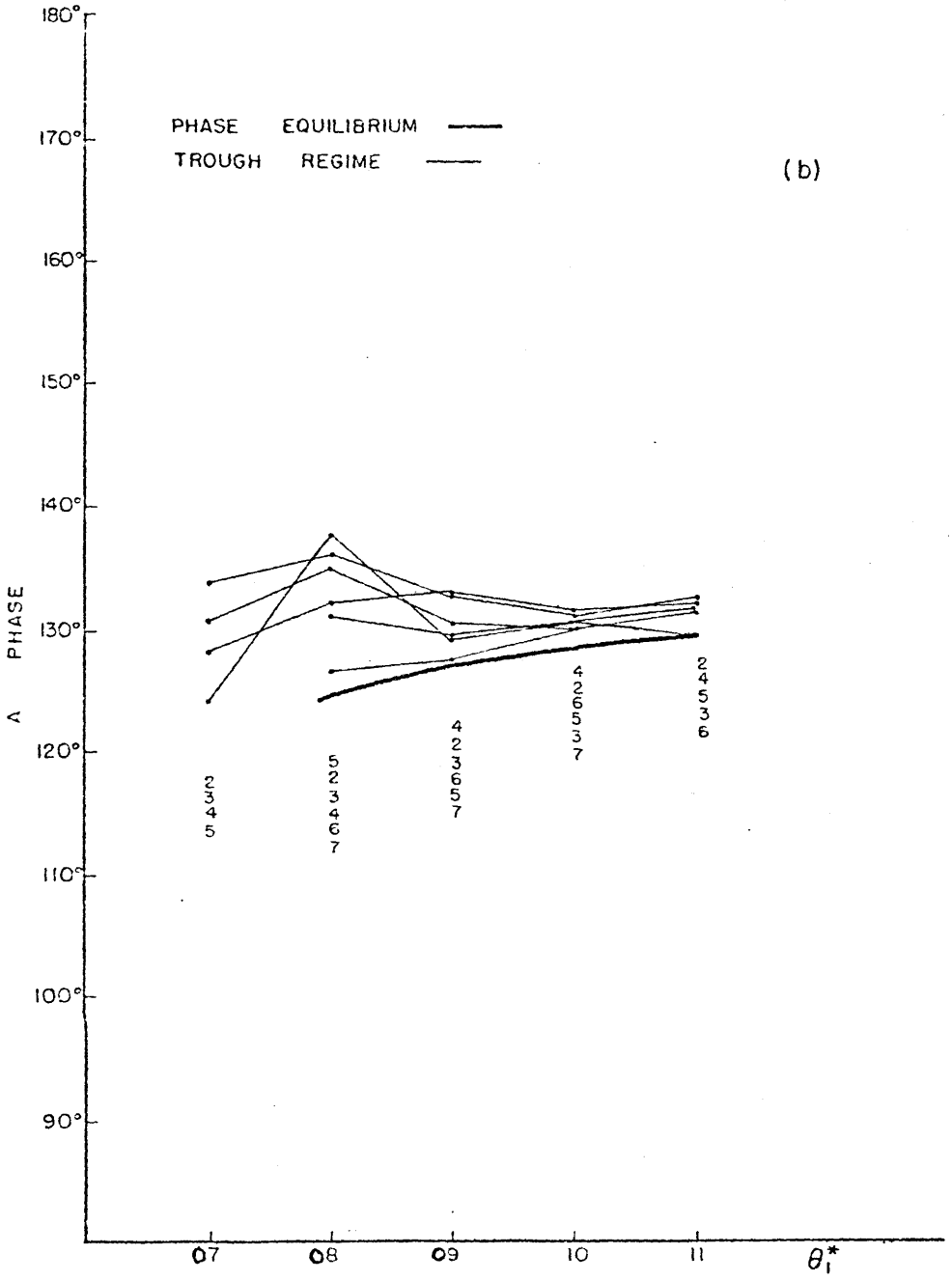

FIGURE 8b: Plot of the phase (A) of the case #1 trough regime composites (light lines) and the 45° Trough Equilibrium (heavy line) as a function of Θ_1^*. The abscissa is given by Θ_1^* and the ordinate by degrees with respect to the orographic ridge (not to be confused with degrees longitude on earth).

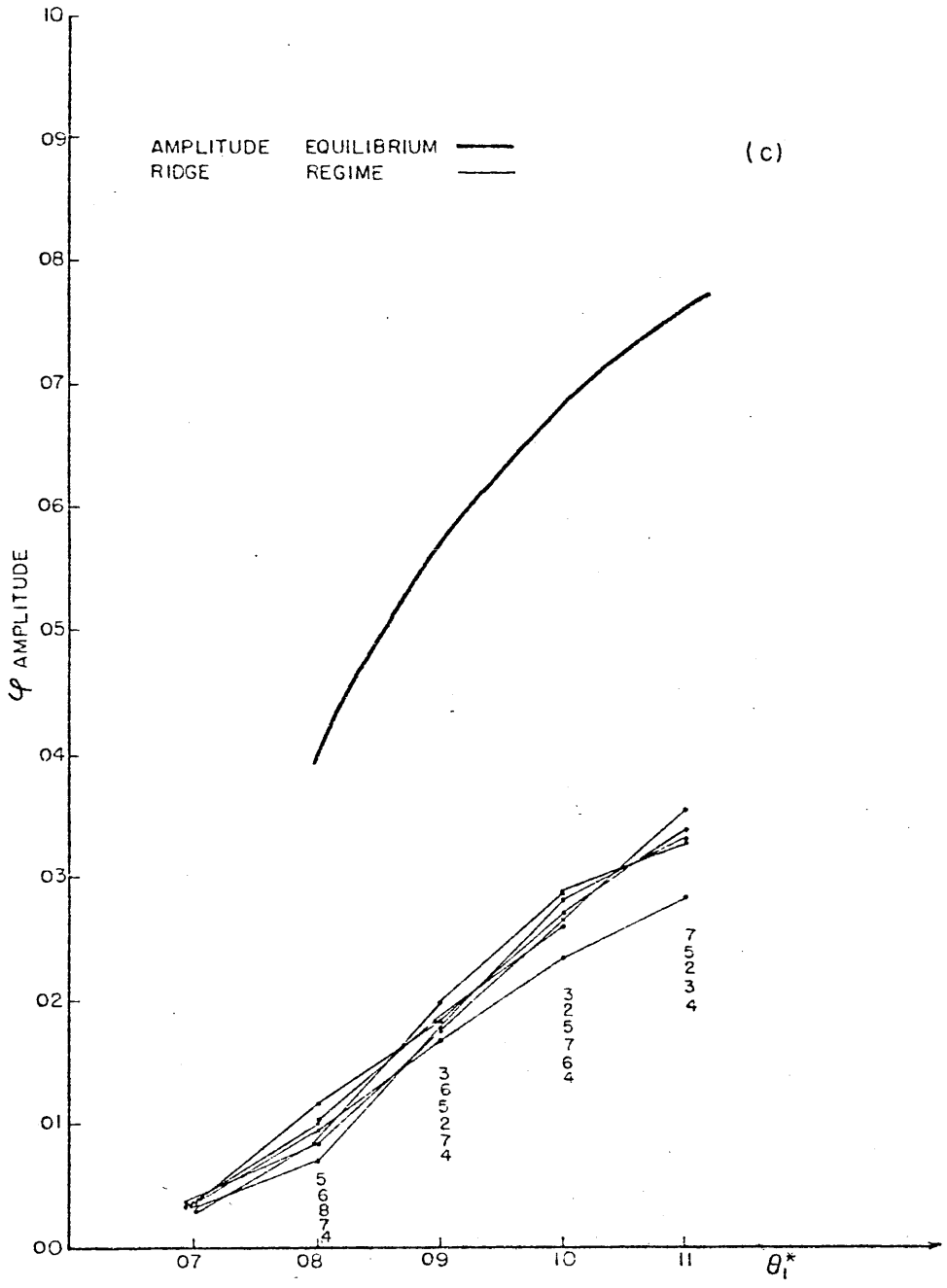

FIGURE 8c: Plot of the amplitude (φ) of the case #1 ridge regime composites (light lines) and the 90° Ridge Equilibrium (heavy line) as a function of θ_1^*. The scale and coordinates are the same as in Figure 8a.

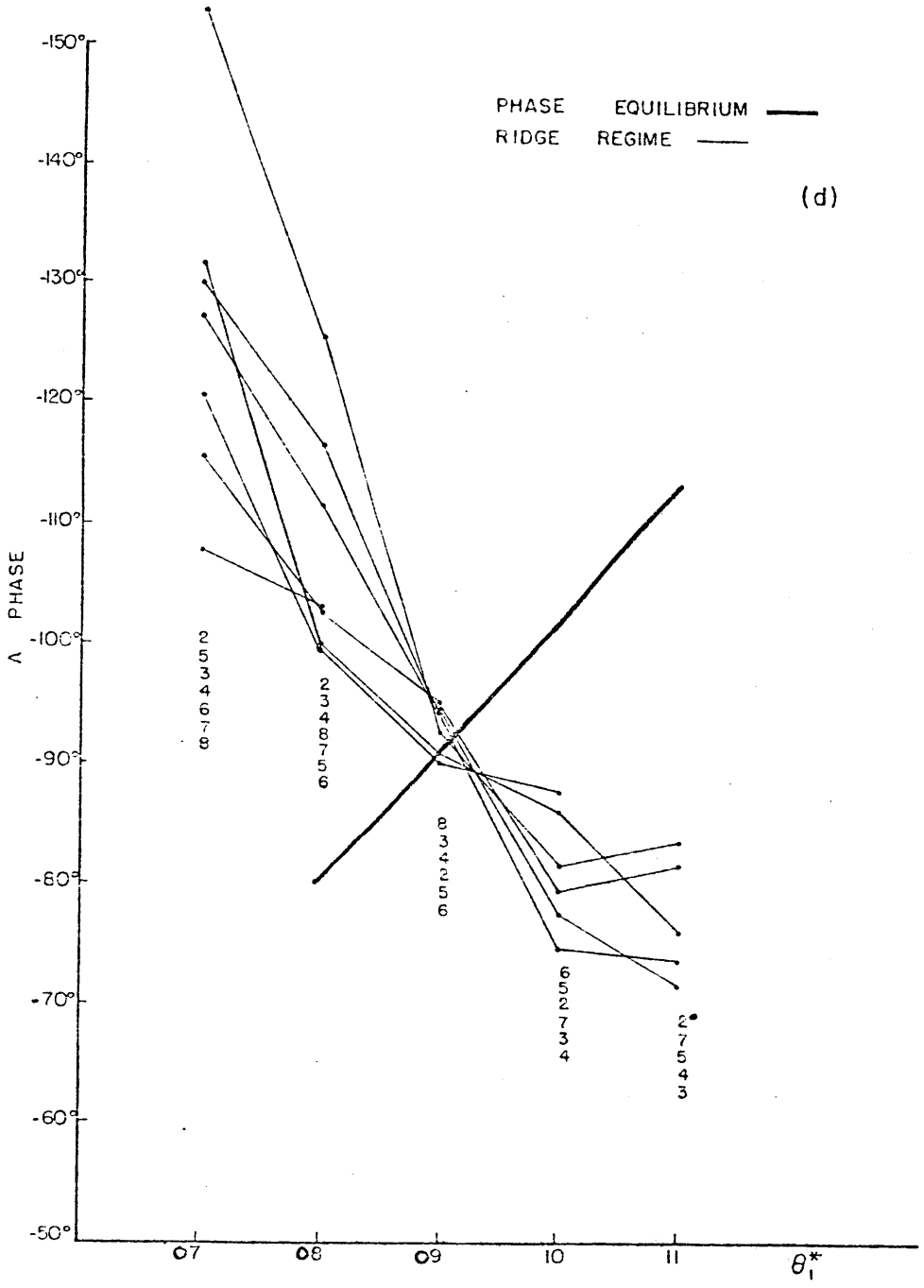

FIGURE 8d: Plot of the phase (A) of the upper level wave streamfunction for the case #1 ridge regime composites (light lines) and the 90° Ridge Equilibrium (heavy line) as a function of Θ_1^*. The ordinate and abscissa are the same as in Figure 8b.

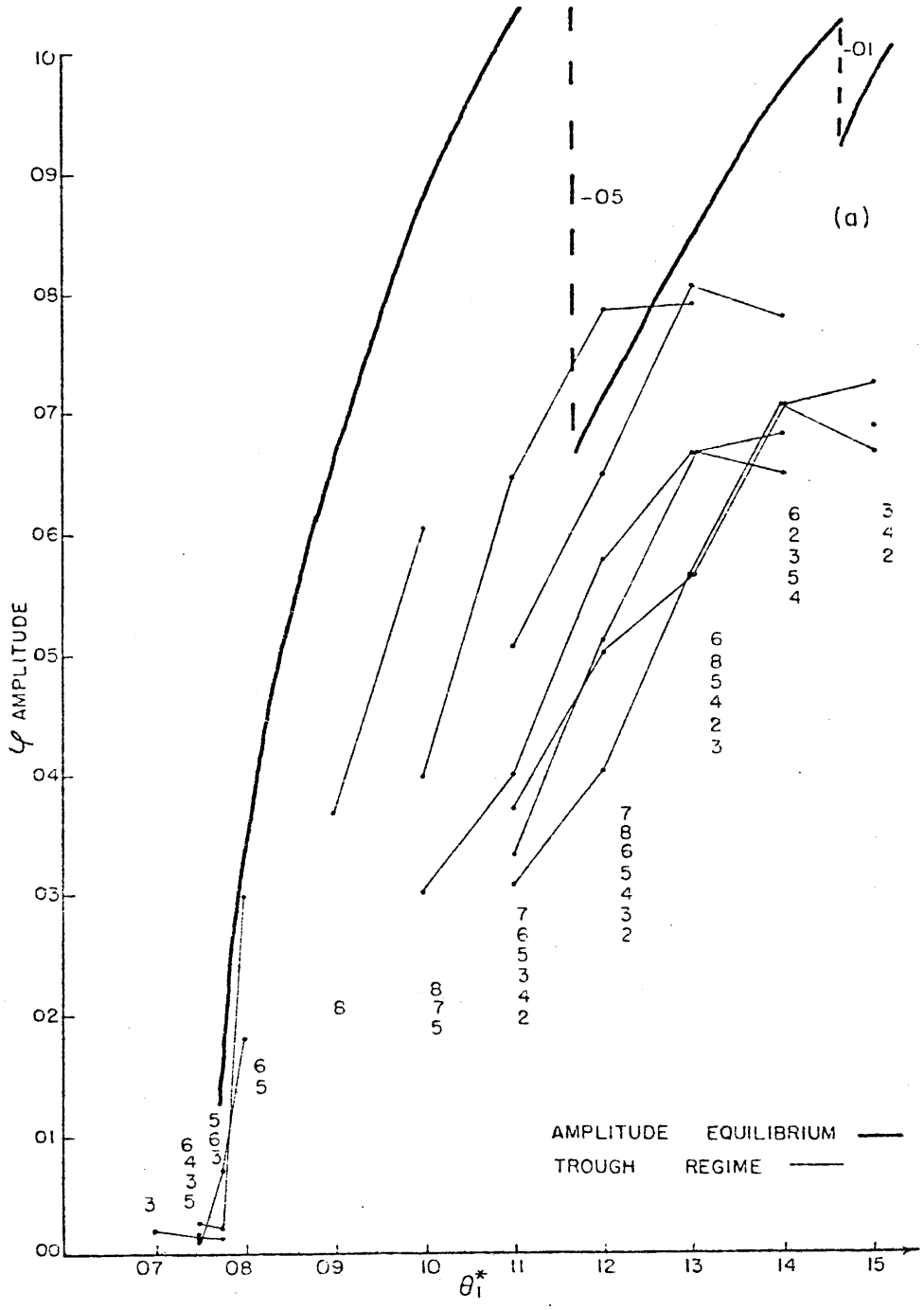

FIGURE 9a: The same as Figure 8a except for the case #2 trough regime composites. At higher values of θ_1^*, the 45° Trough Solution obtains such large amplitude, the curve had to be displaced downward by first -.05 and then by -.01.

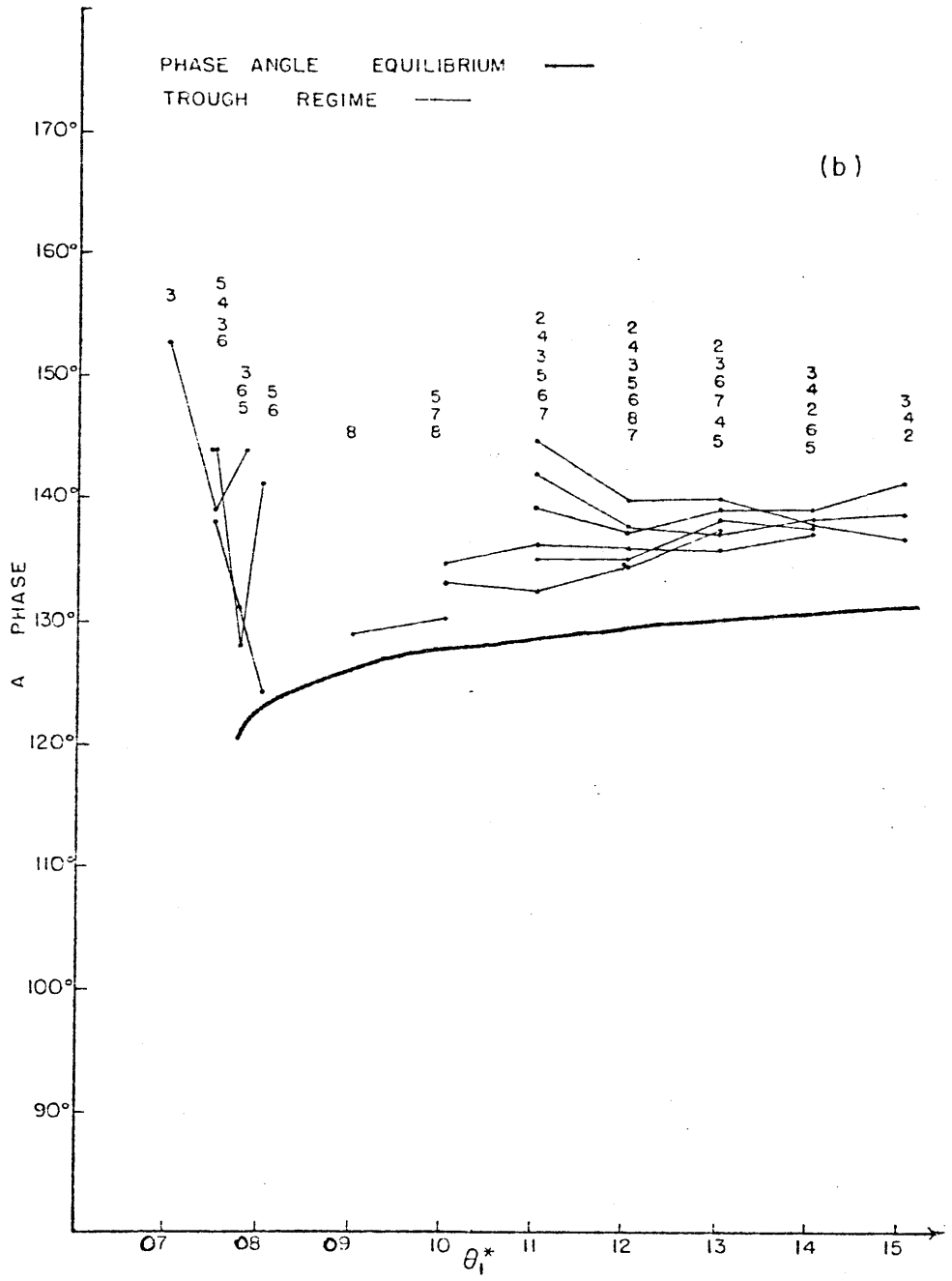

FIGURE 9b: The same as Figure 8b except for the case #2 trough regime composites.

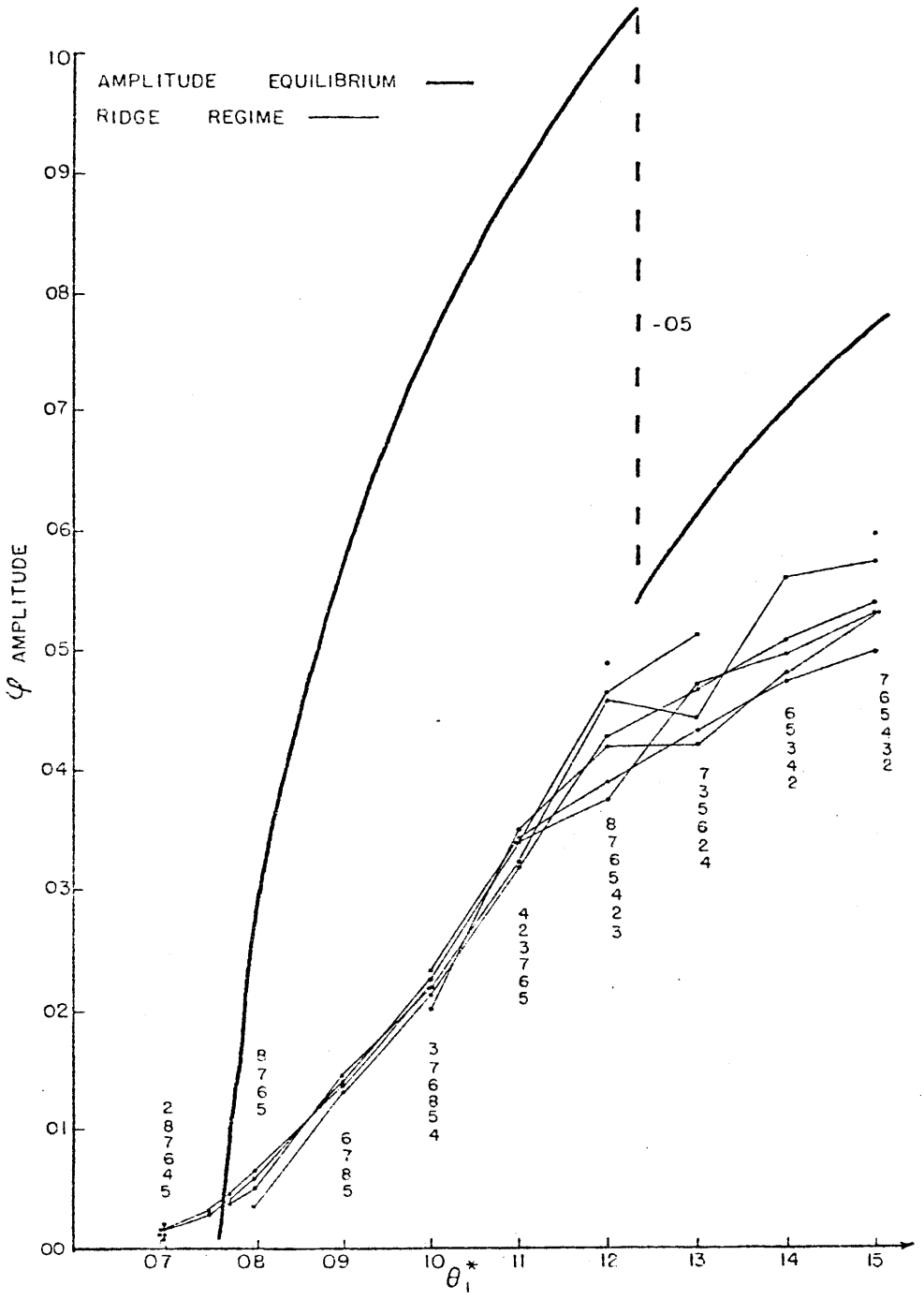

FIGURE 9c: Same as Figure 8c except for the case #2 ridge regime composites. As in Figure 9a, the amplitude of the Equilbrium Solution had to be displaced downward at higher values of θ_1^* to keep it on the figure.

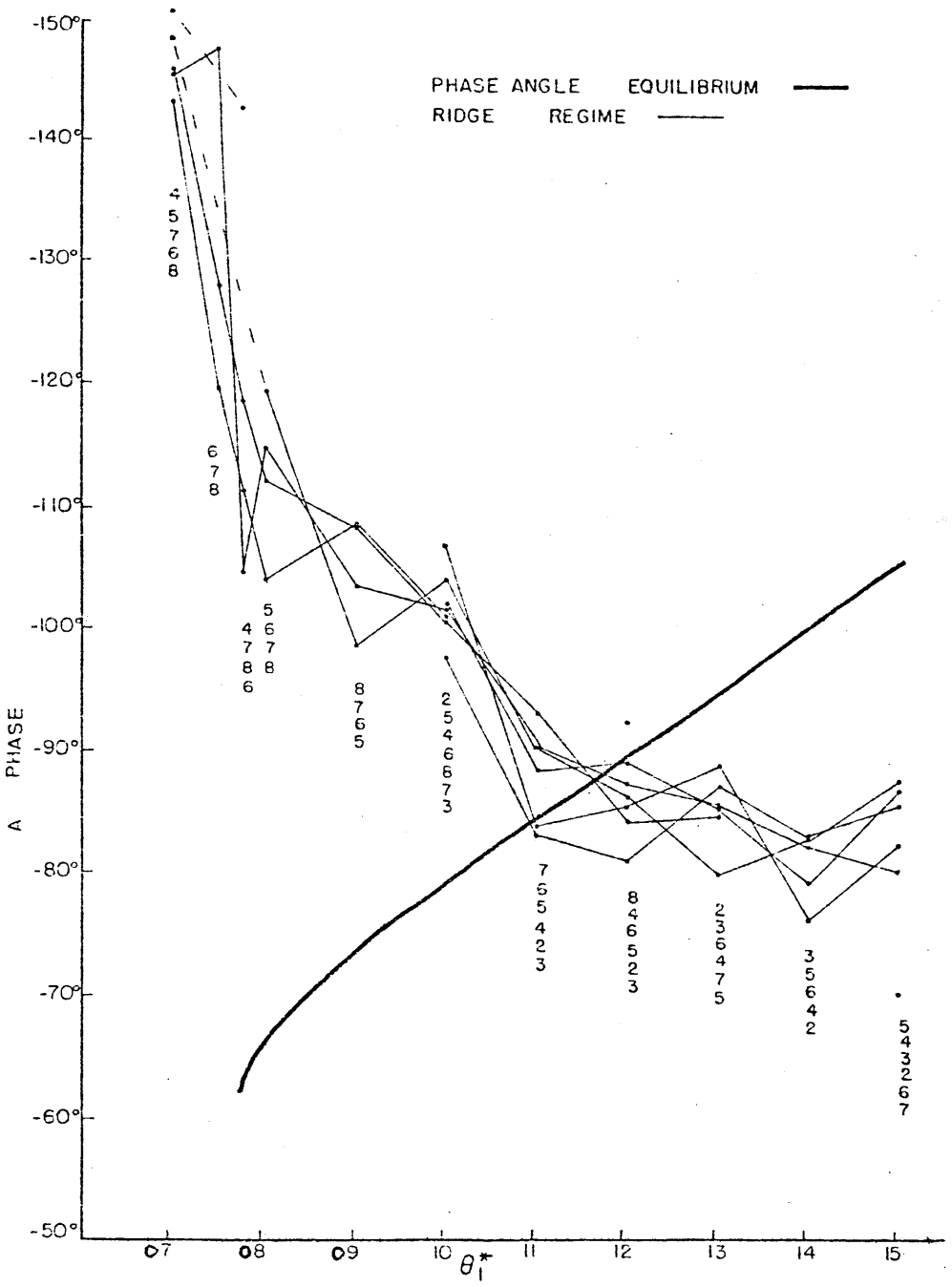

FIGURE 9d: Same as Figure 8d except fot the case #2 ridge regime composites.

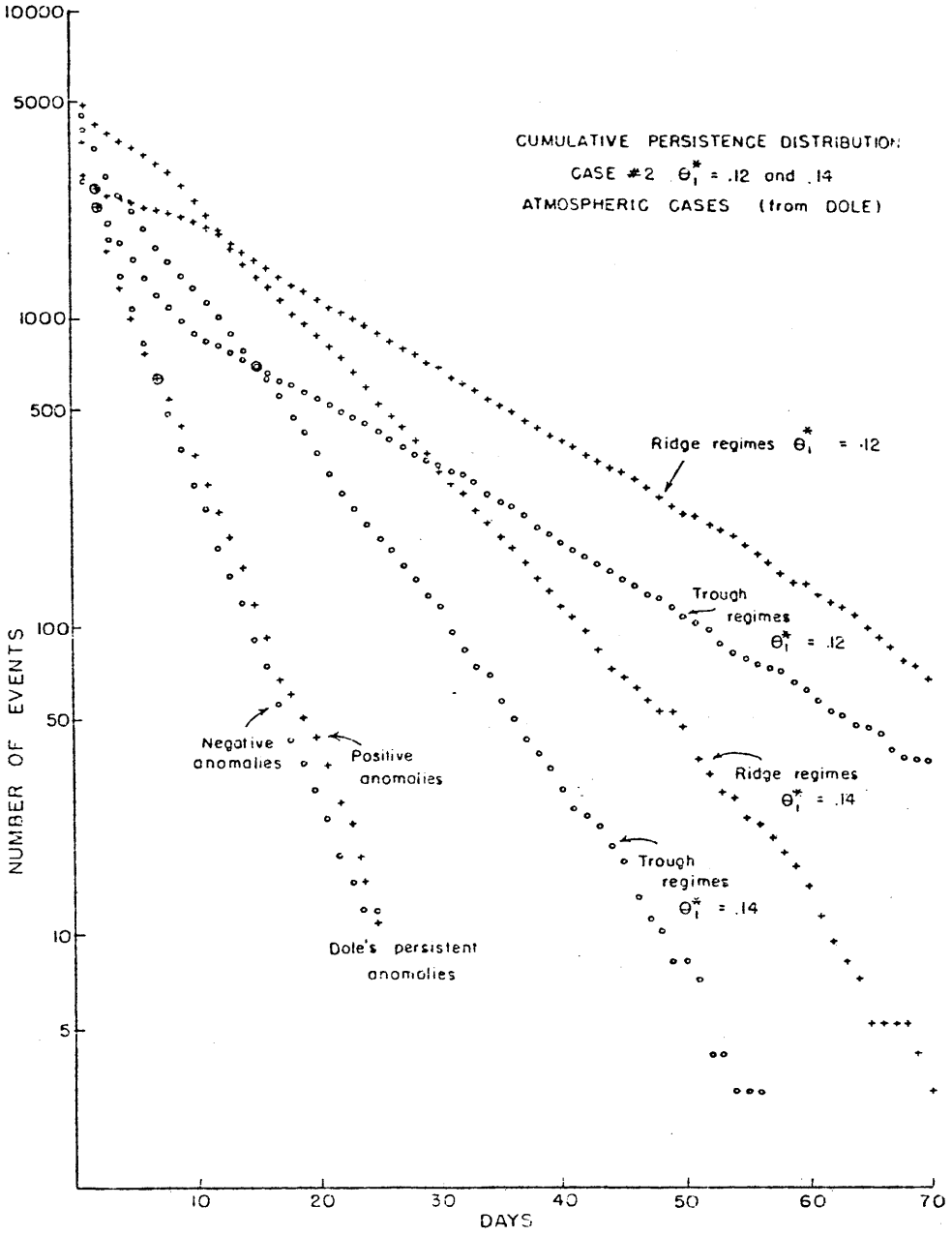

FIGURE 10: Cumulative persistence distributions for case #2 with θ_1^* =.12 and .14 and Dole's 5 dm. positive and negative persistent anomalies. The ordinate is the total number of events which persist n days or longer on a log scale and the abscissa is in days. The model ridge regimes and positive anomalies are denoted by crosses (+) and the negative anomalies and the trough regimes by circles (o).

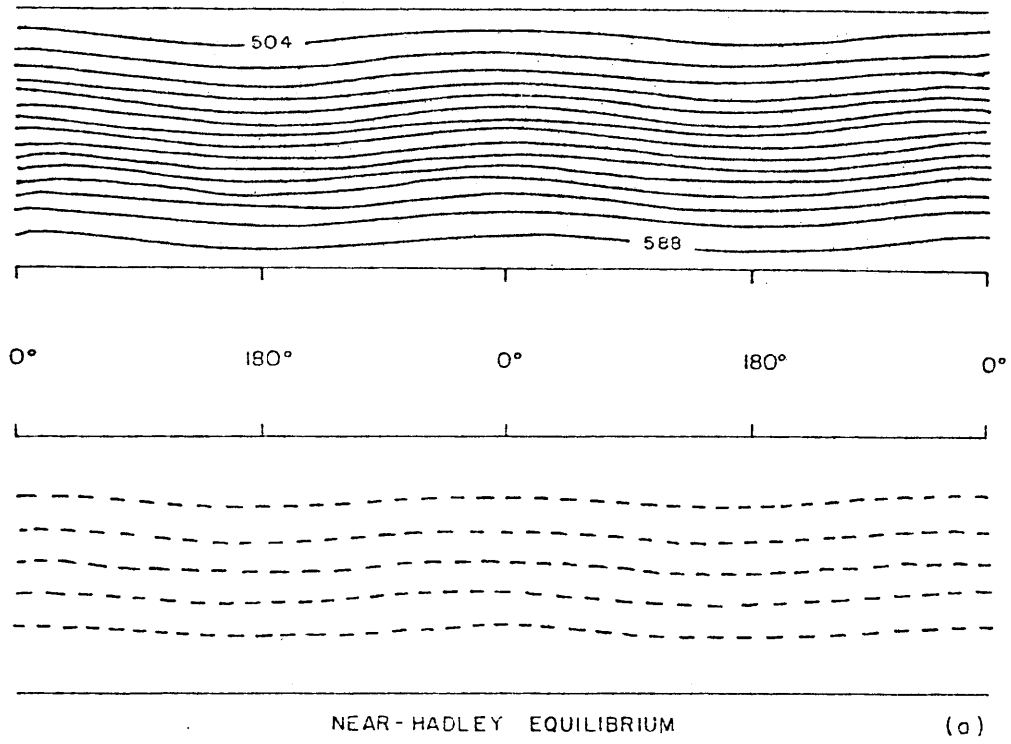

FIGURE 11a: A "weather map" of the midlevel (500 mb) and lower level (850 mb) height field and lower level potential temperature (dashed lines) for case #2 with $\theta_1^* = .12$. The height contours are every 6 decameters and the isotherms every 18° C (stretched). The units in the x-direction are given in degrees with respect to the orogr aphic ridge (0° corresponds to the mountain peak). These units of degrees are not to be confused with degrees longitude on earth.

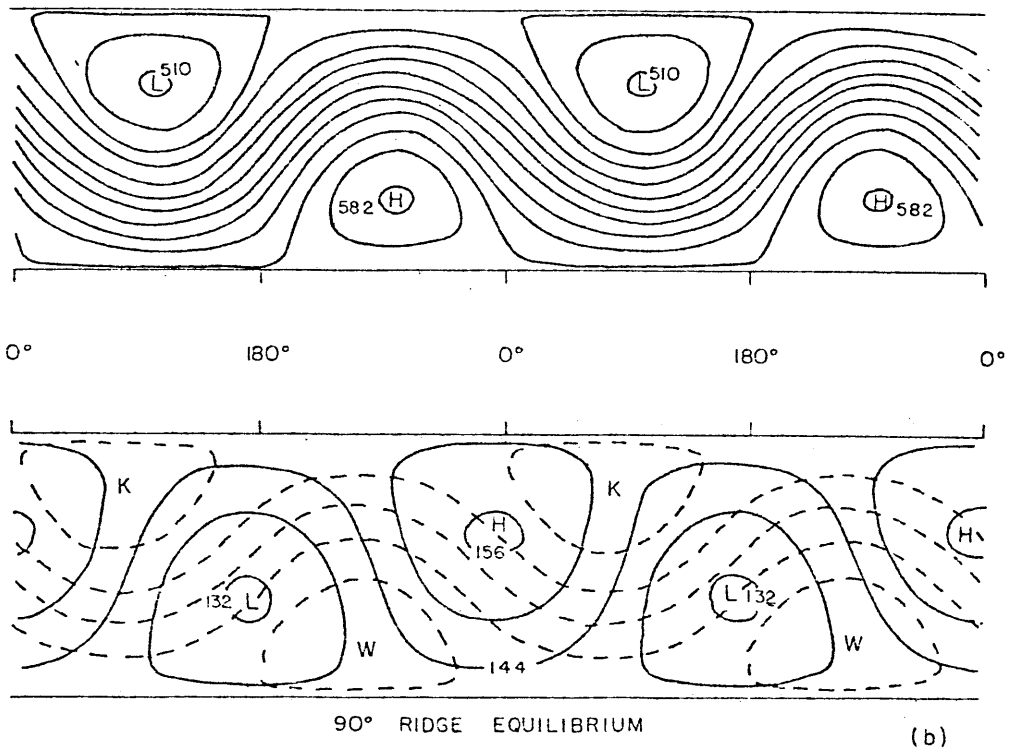

FIGURE 11b: Same as Figure 11 a except for the 90° Ridge Solution.

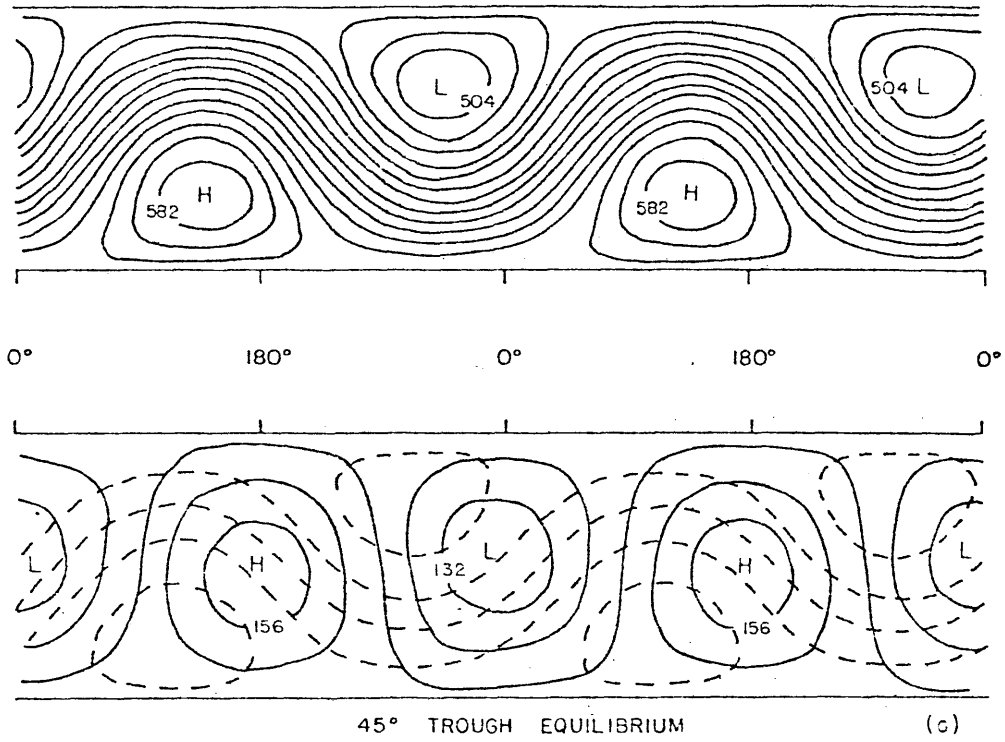

FIGURE 11c: Same as Figure 11a except for the 45° Trough Solution.

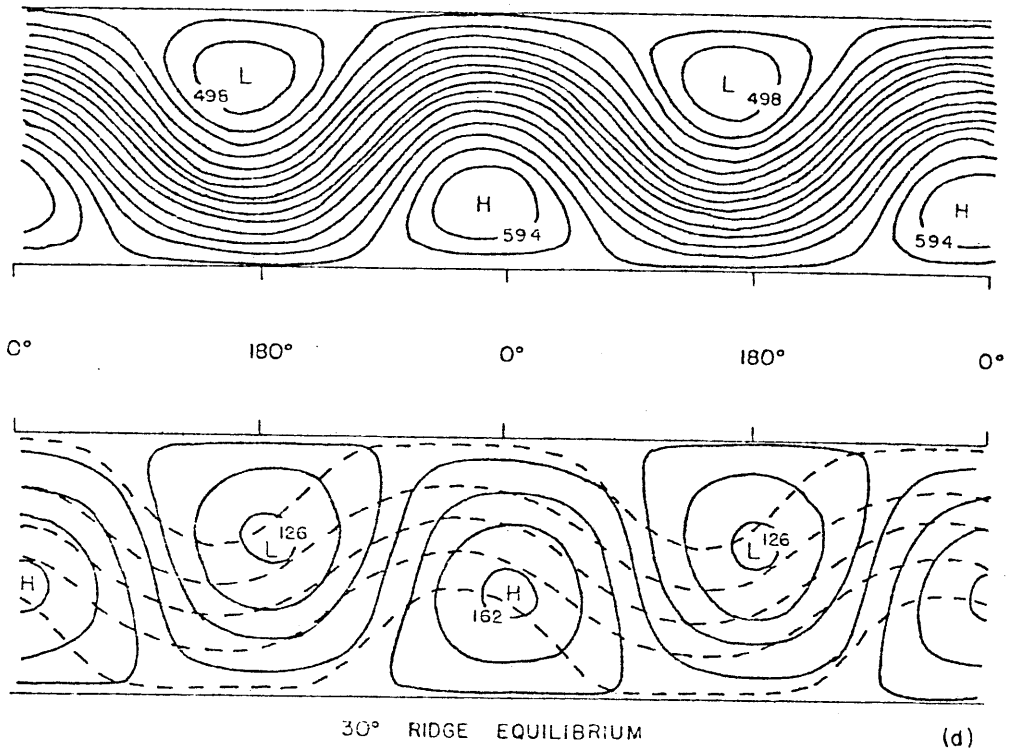

FIGURE 11d: Same as Figure 11a except for the 30° Ridge Solution.

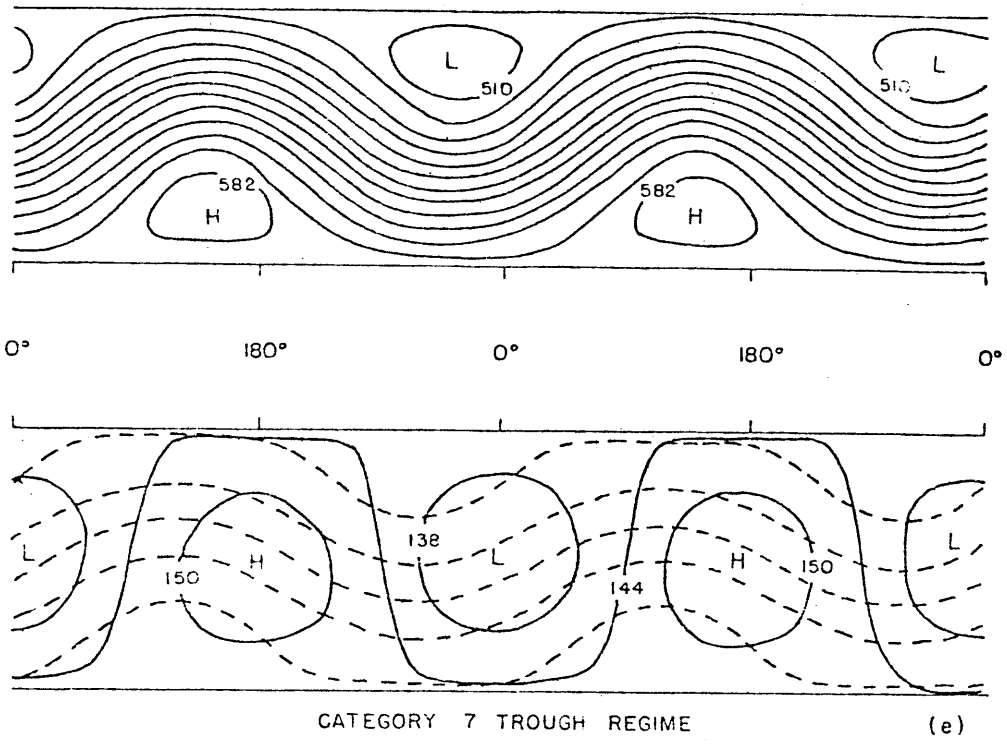

FIGURE 11e: Same as Figure 11a except for the category 7 trough regime.

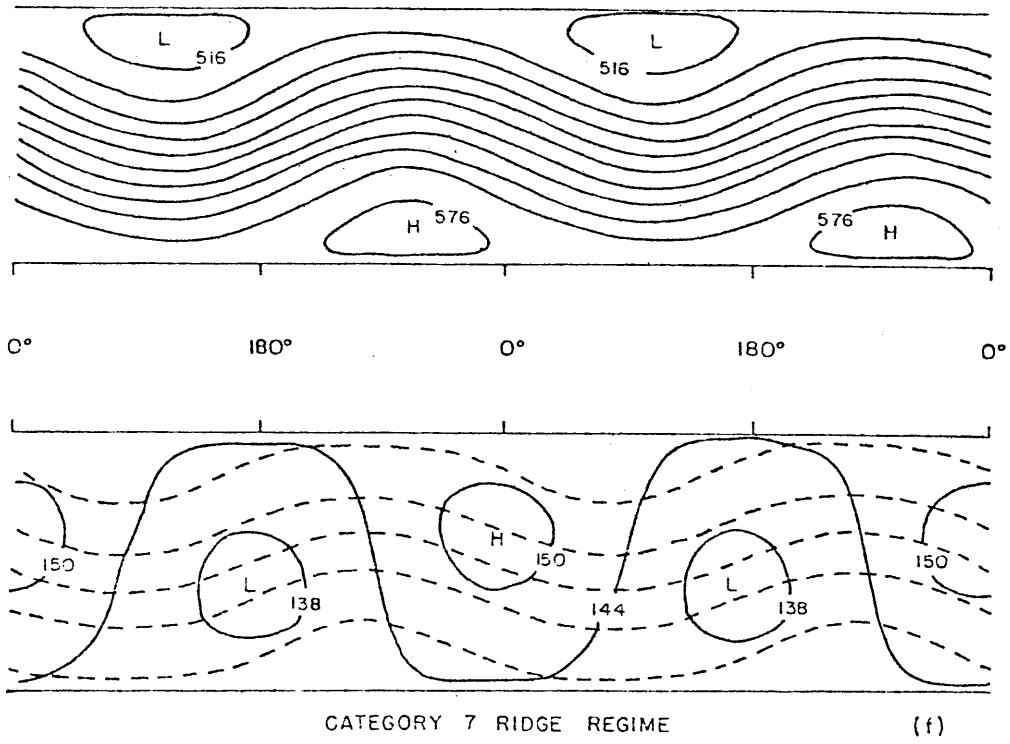

FIGURE 11f: Same as Figure 11a except for the category 7 ridge regime.

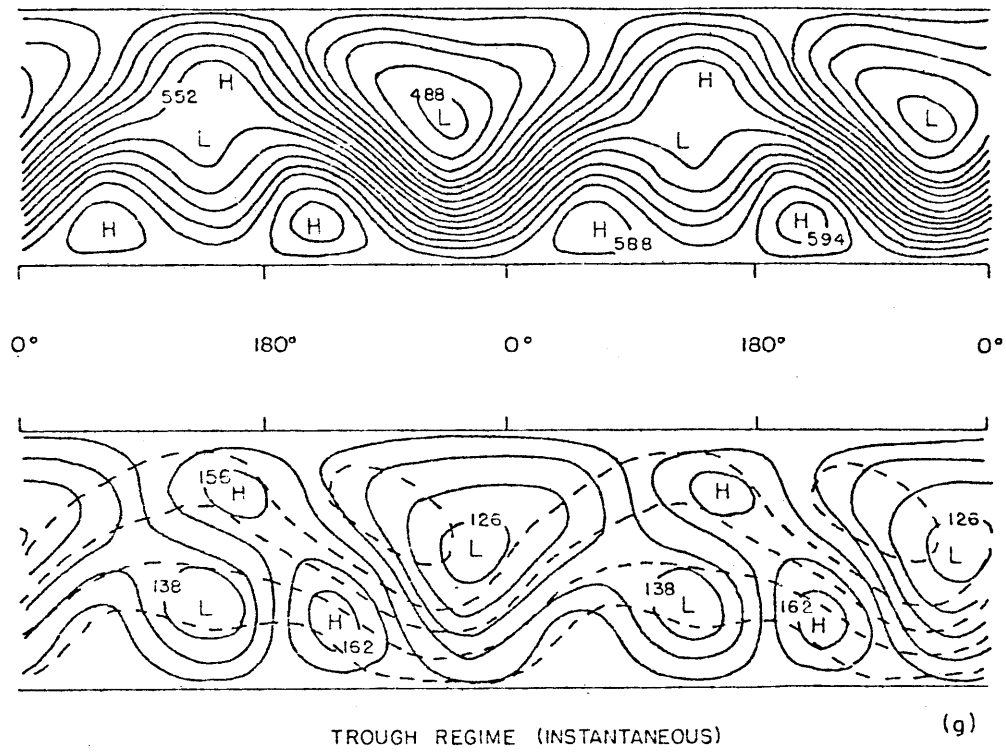

TROUGH REGIME (INSTANTANEOUS) (g)

FIGURE 11g: Same as Figure 11a except for an instantaneous period during a trough regime. All the smaller scale features of the full model are present.

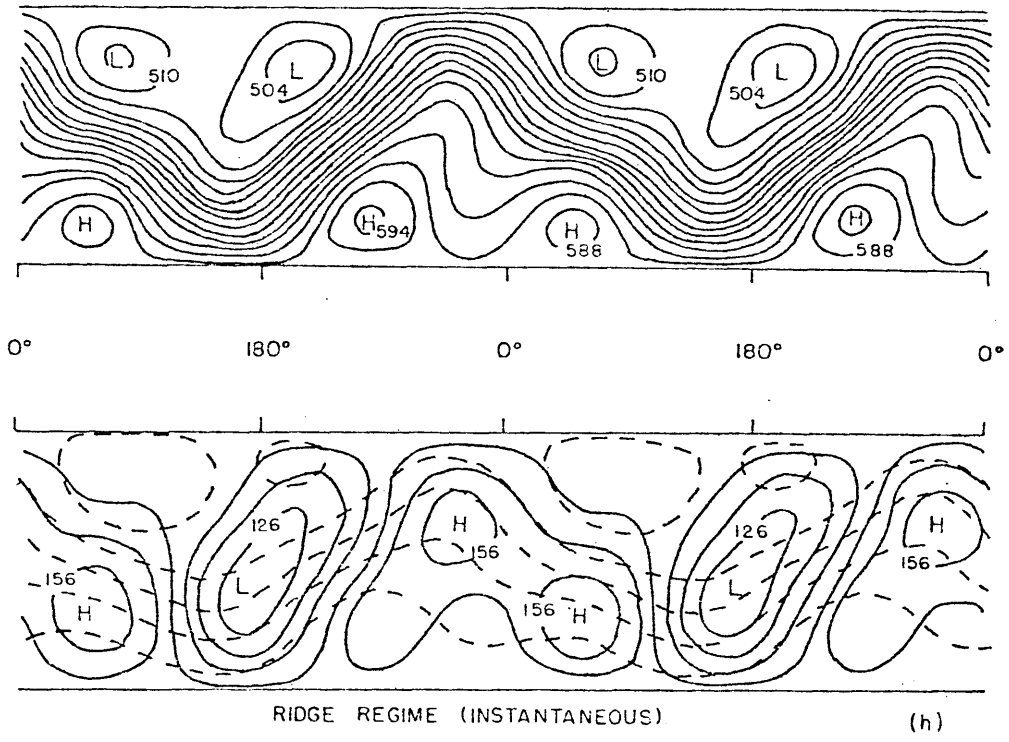

RIDGE REGIME (INSTANTANEOUS) (h)

FIGURE 11h: Same as Figure 11a except for an instantaneous period during a ridge regime. As in Figure 11g, all the smaller scale features of the full model are present.

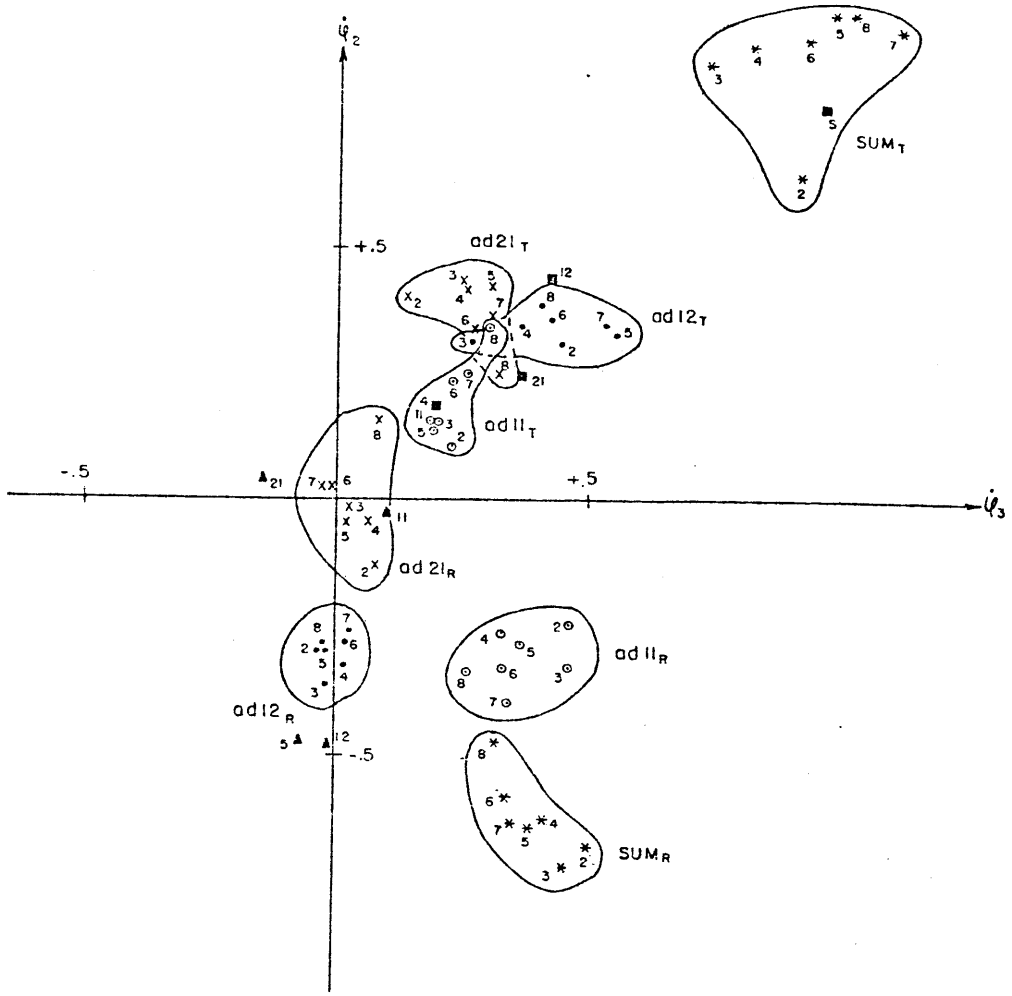

FIGURE 12: Plot of the phase and amplitude of the transient forcing terms ad11, ad21, ad12, and "sum" of the upper level vorticity equations for case #2 with Θ_1^*=.12 composite trough and ridge regimes. The ordinate is the φ_2 forcing component and the abscissa is the φ_3 forcing component. "ad11" is denoted by ⊙, and "ad21" by x, "ad12" by ◦ and "sum" by *. The subscripts next to the symbols refer to the categories, and each group of terms is circled and labled. The subscript "R" refers to the ridge and the subscript "T" to the trough. Also plotted are the forcing terms during periods of Regime type II behavior. The solid triangles (▲) correspond to a 31-day ridge and the solid squares (■) to a 46-day trough. The subscripts 11, 21, 12, and "s" refer to ad11, ad21, ad12, and "sum", respectively.

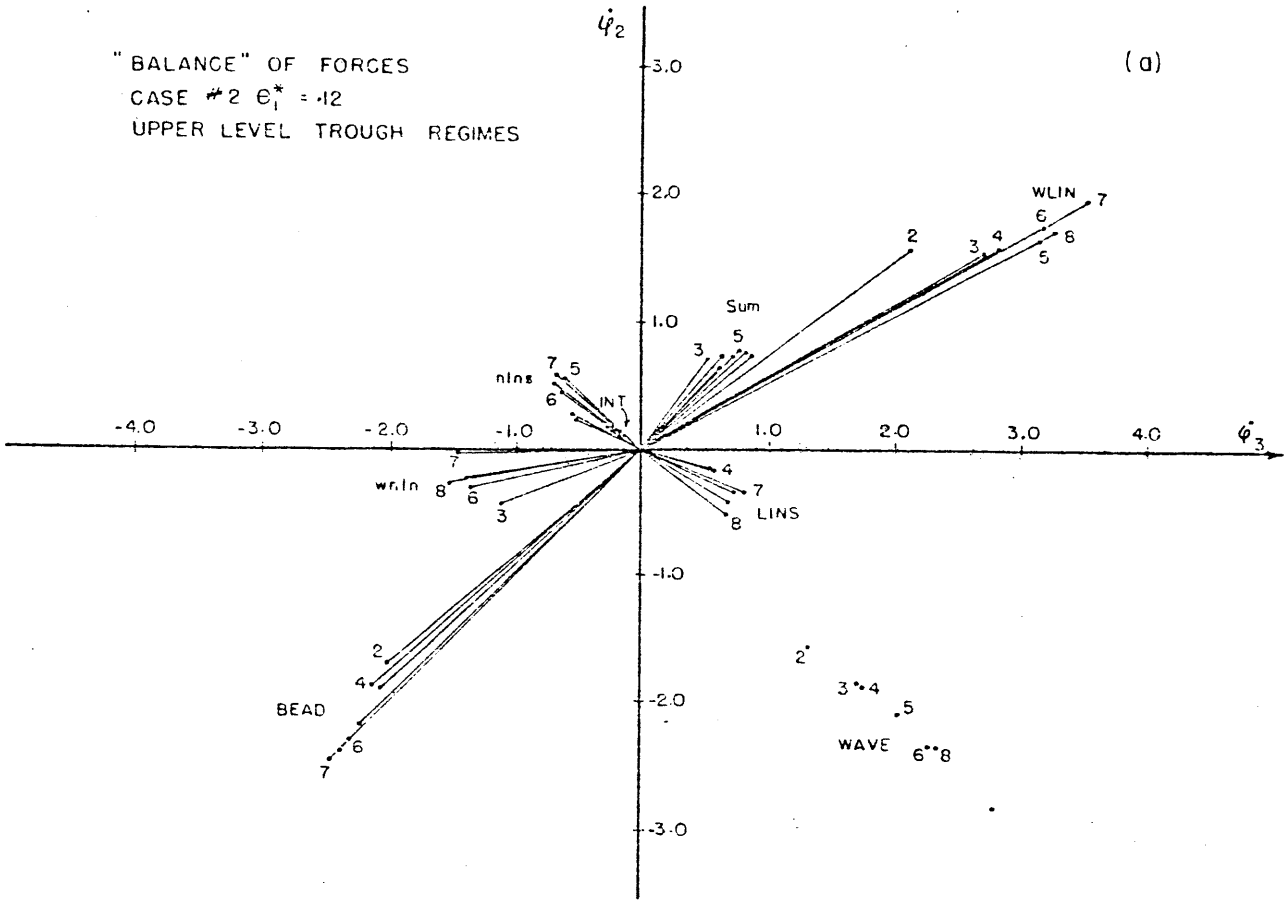

FIGURE 13a: Balance of forces diagram for the trough regime composites for case #2 with Θ_1^*=.12. The various budget terms for the upper level Mode 11 waves are plotted in vector form. The numbers next to the points refer to the respective categories. The ordinate and abscissa are the same as in Figure 12 except that the units are multiplied by a factor of four. For comparison, "sum" is plotted in both figures.

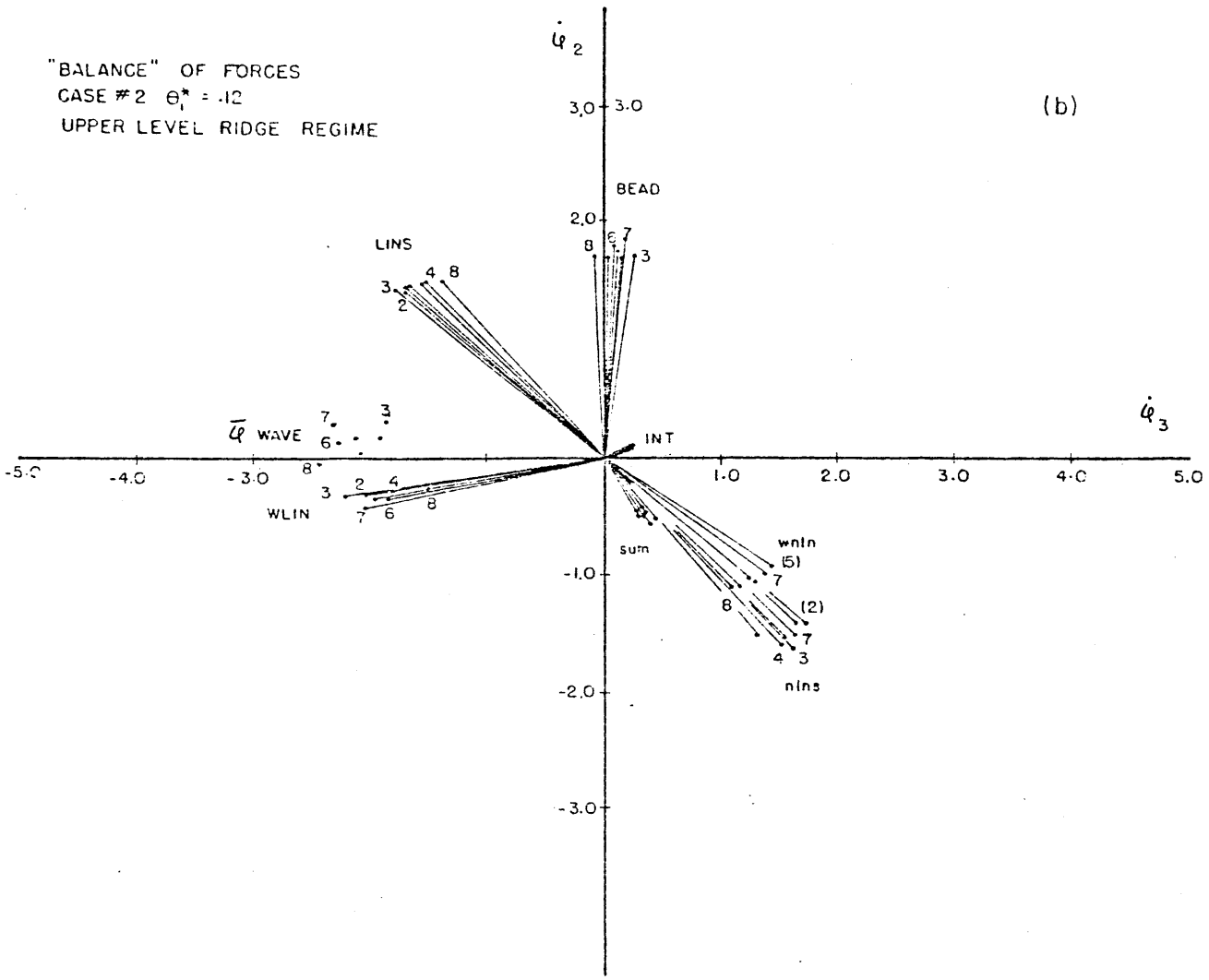

FIGURE 13b: Same as Figure 13a except for the ridge regime composites.

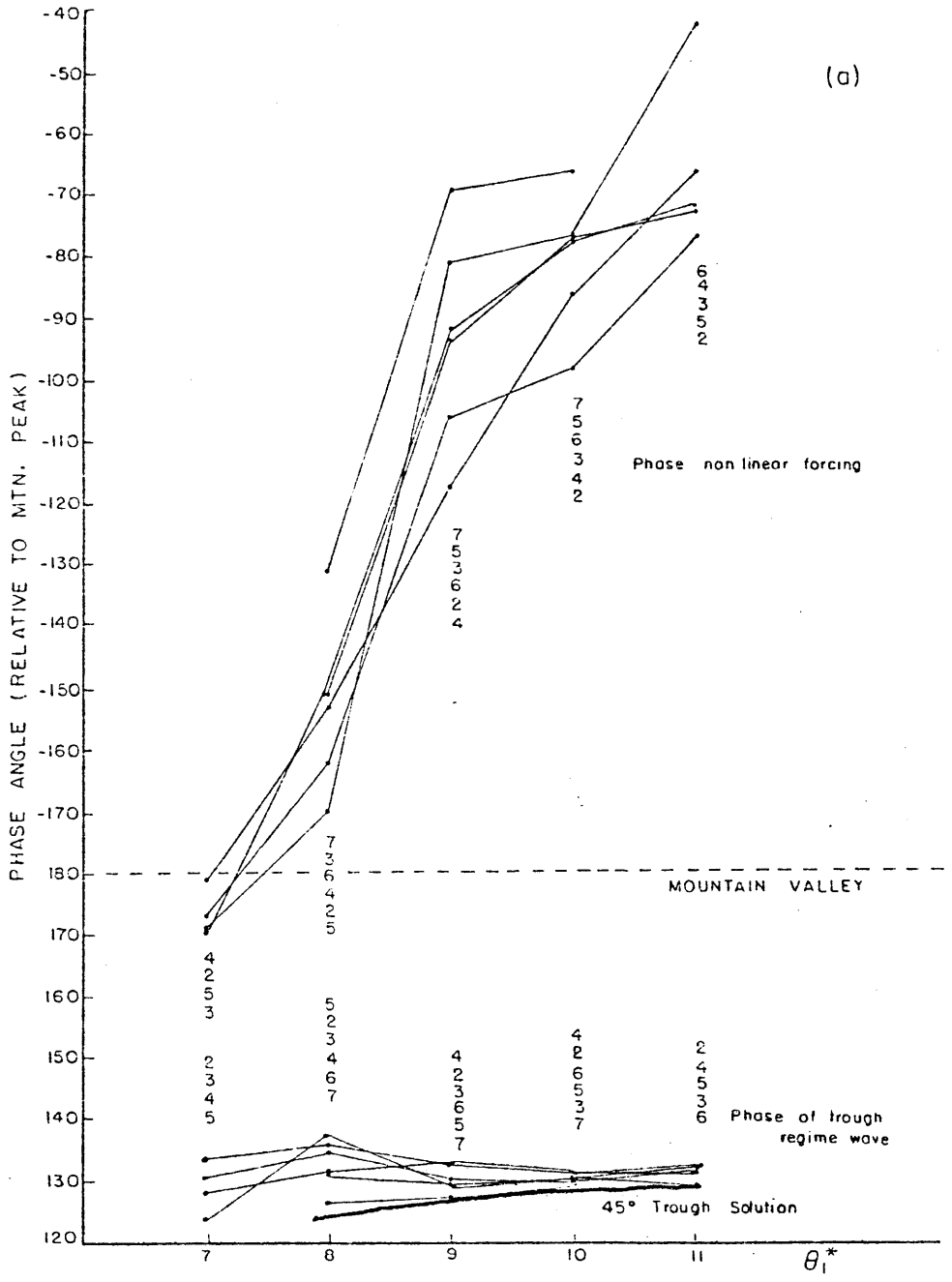

FIGURE 14a: Plot of the phase of the nonlinear transport terms nlns, time mean upper level Mode 11 wave of the trough regime and the corresponding 45° Trough Equilibrium for case #1. The ordinate and abscissa are the same as in Figure 8b. The trough regime composites are denoted by light lines and the 45° Trough Solution by a heavy line. The numbers above and below the dots refer to the categories.

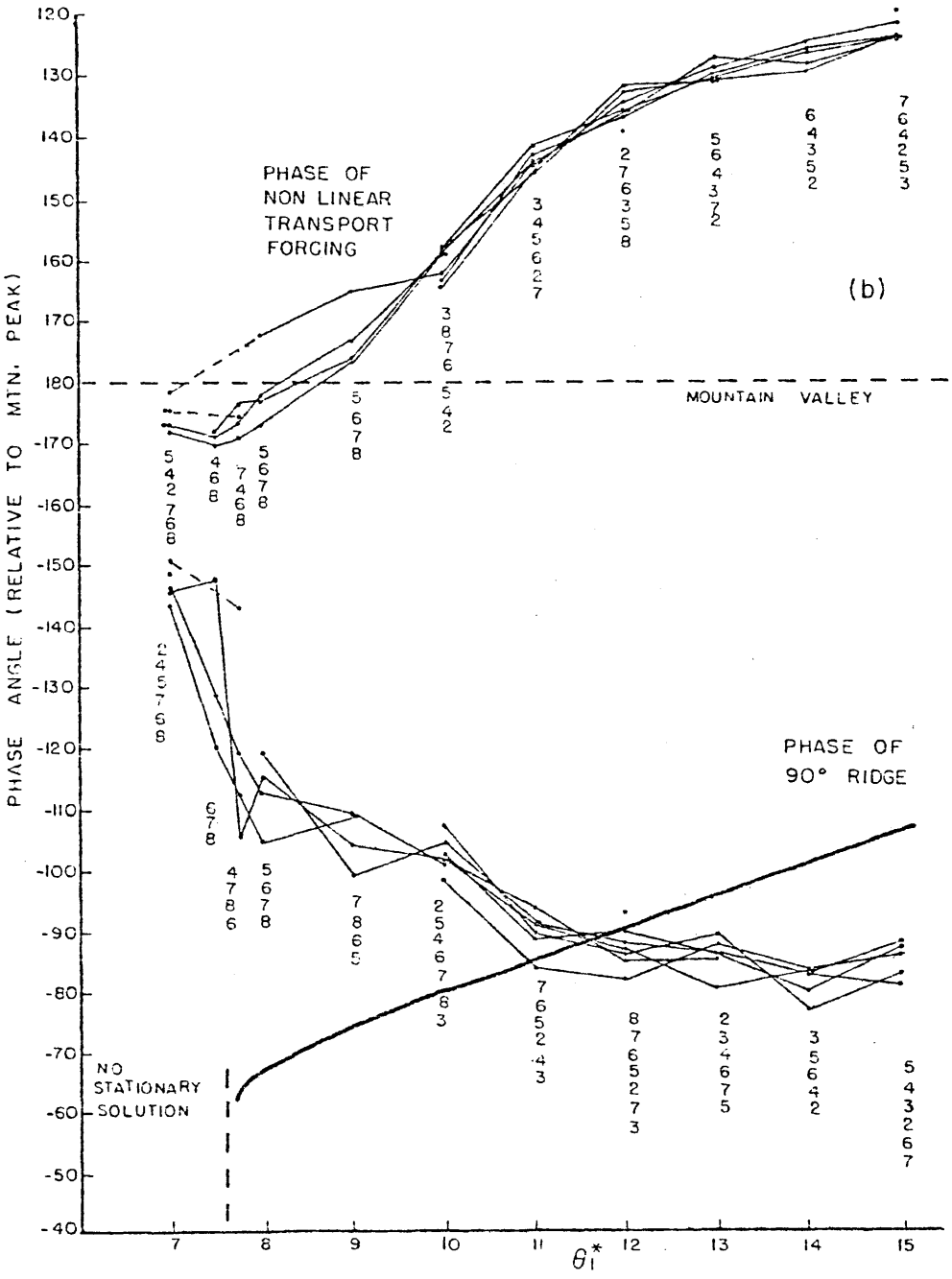

FIGURE 14b: The same as Figure 14a except for the case #2 ridge regimes and the corresponding 90° Ridge Equilibrium. The ordinate and abscissa are the same as Figure 9d.

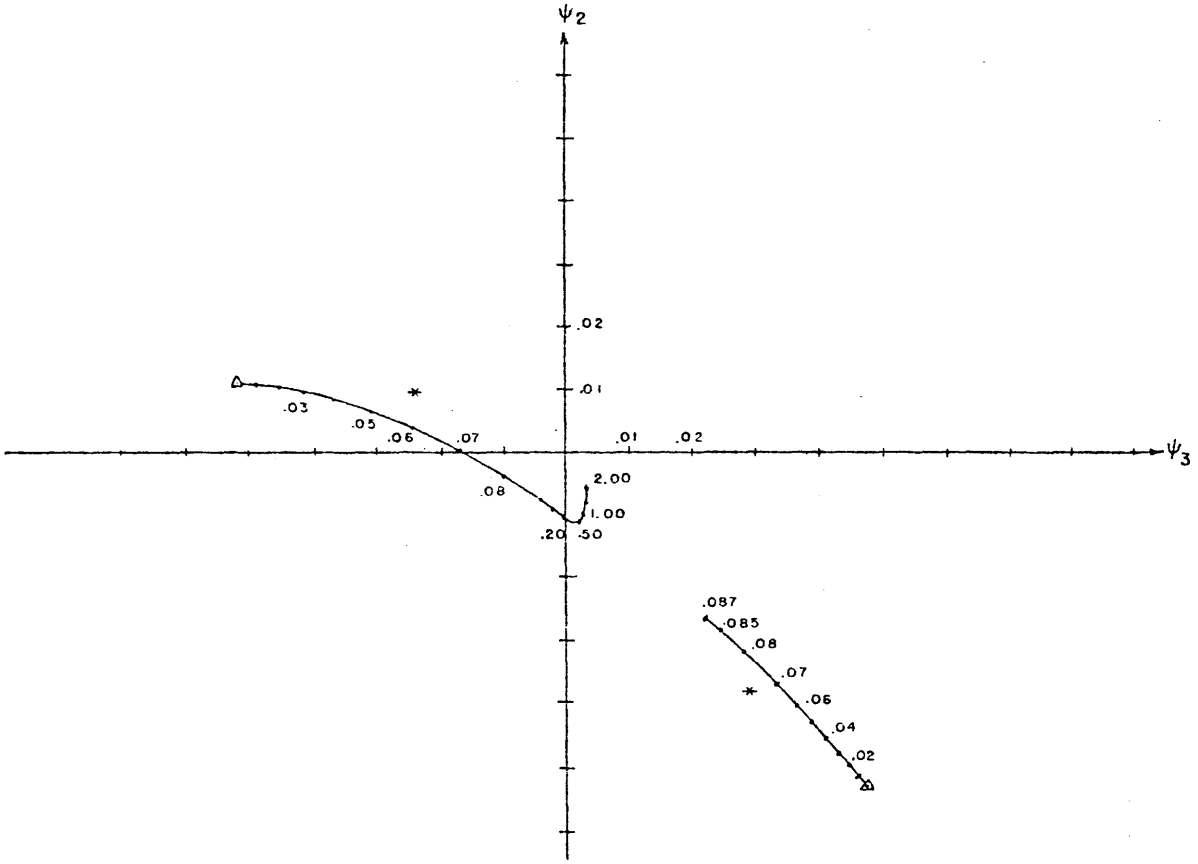

FIGURE 15a: Phase space plot of the midlevel streamfunction wave of the regime-equilibria for selected values of the transient to zonal energy ratio for case #2 with $\theta_1^* = .12$. The parameterized effects of ad22 have been included in these solutions. The ordinate and abscissa are given by Ψ_2 and Ψ_3 respectively. The stationary equilbria are denoted by triangles (Δ) and the individual regime-equilbria for those values of the energy ratio listed in Table 4a are denoted by enlarged points and labled by their corresponding value of the energy ratio. The full model category 7 trough and ridge regimes are denoted by asterisks (*). Note the close pass of the regime-equilibria to the full model regimes at energy ratios near .07.

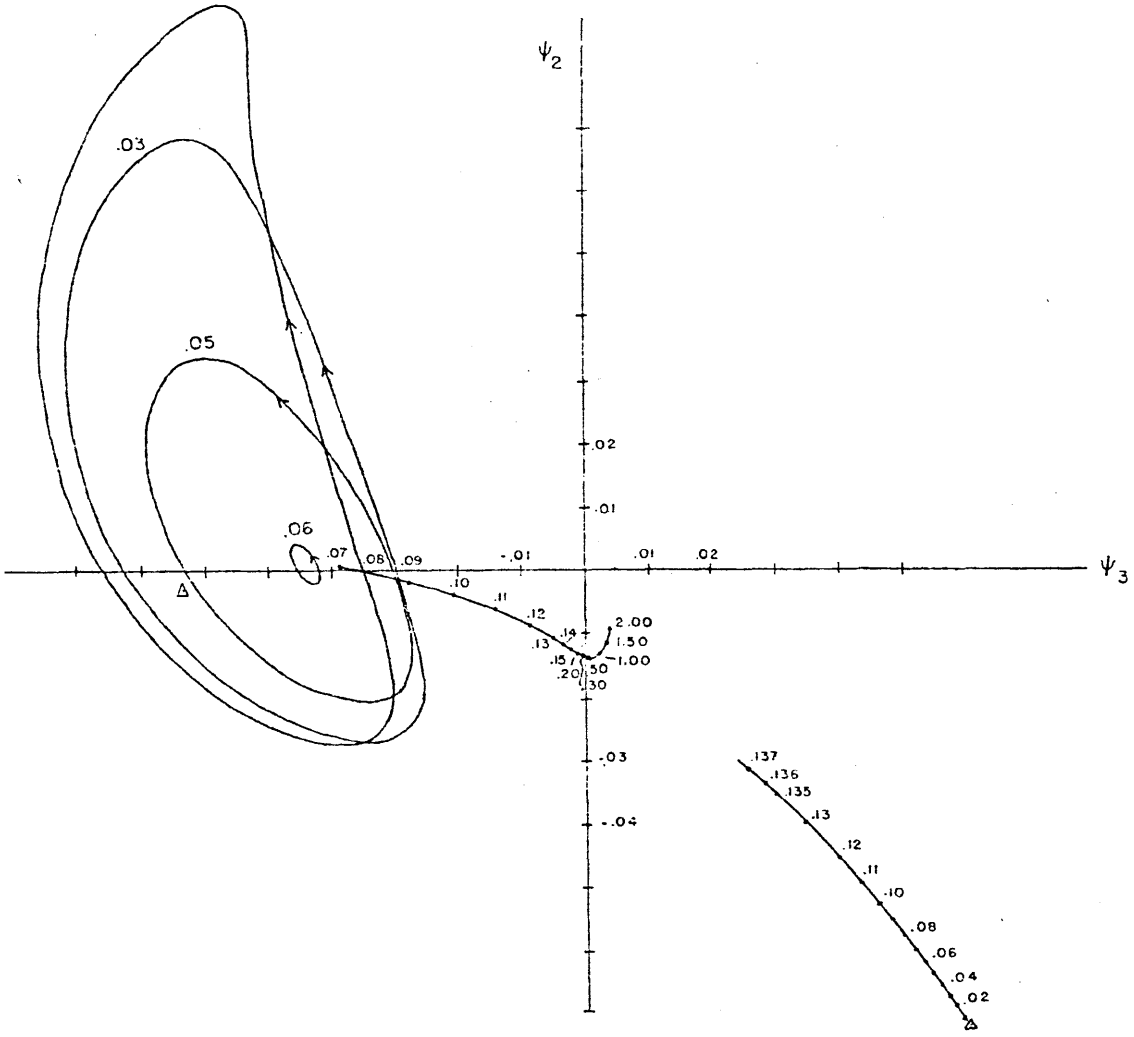

FIGURE 15b: Same as Figure 15a except for case #2 with $\Theta_1^* = .15$. Again, the parameterized effects of ad22 are included, but the full model composite regimes are not. Note that at low values of the energy ratio in the ridge branch the regime-equilibria become unstable and develop into limit cycles.

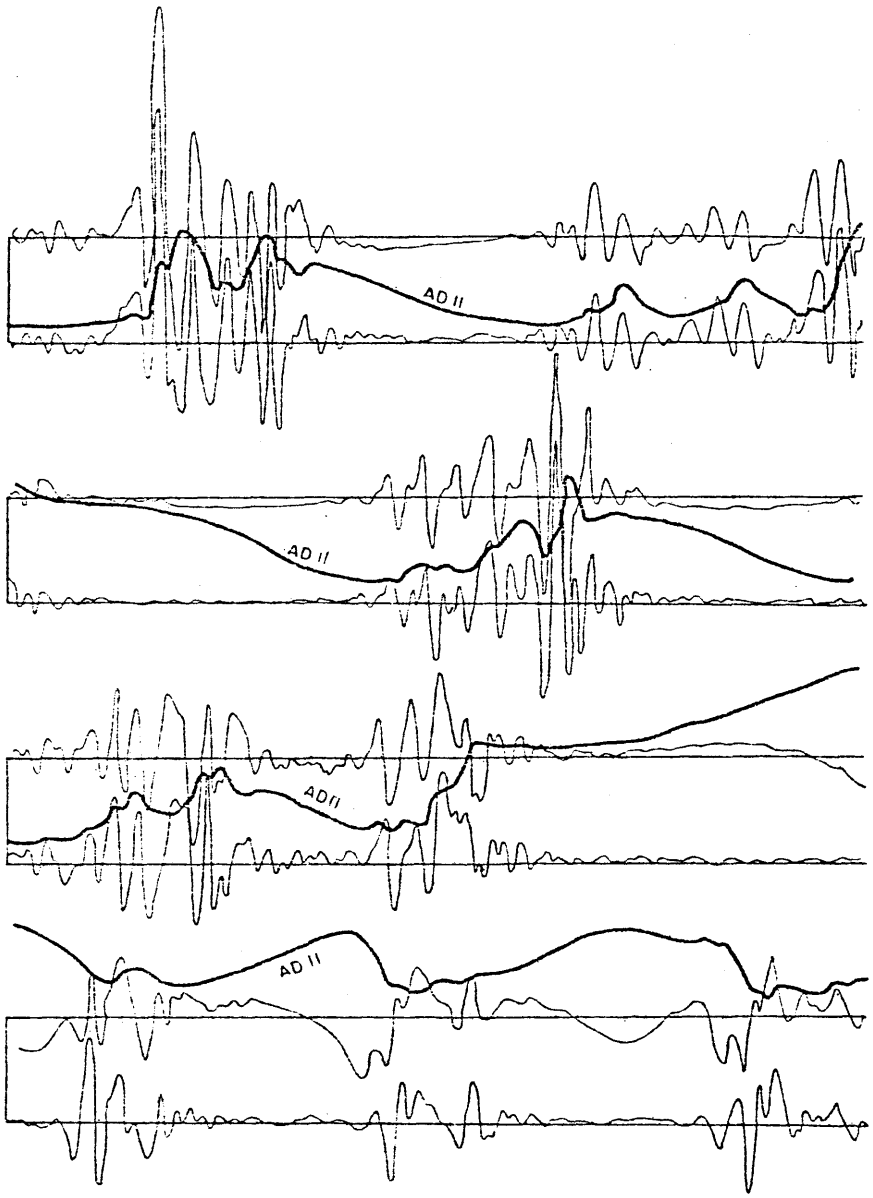

FIGURE 16a: Time series of selected physical processes in the tendency equation for the demonstration case. The time series starts 1000 time steps after initialization and lasts for 512 days. The 512 day period is broken into four 128 day segments. On the upper axis, AD11 (heavy line) and the tendency term $\partial \Psi_2 / \partial t$ (light line) are plotted, and on the lower axis "sum" (light line) is plotted. The tendency term and "sum" are plotted to the same nondimensional scale, but AD11 is first divided by four.

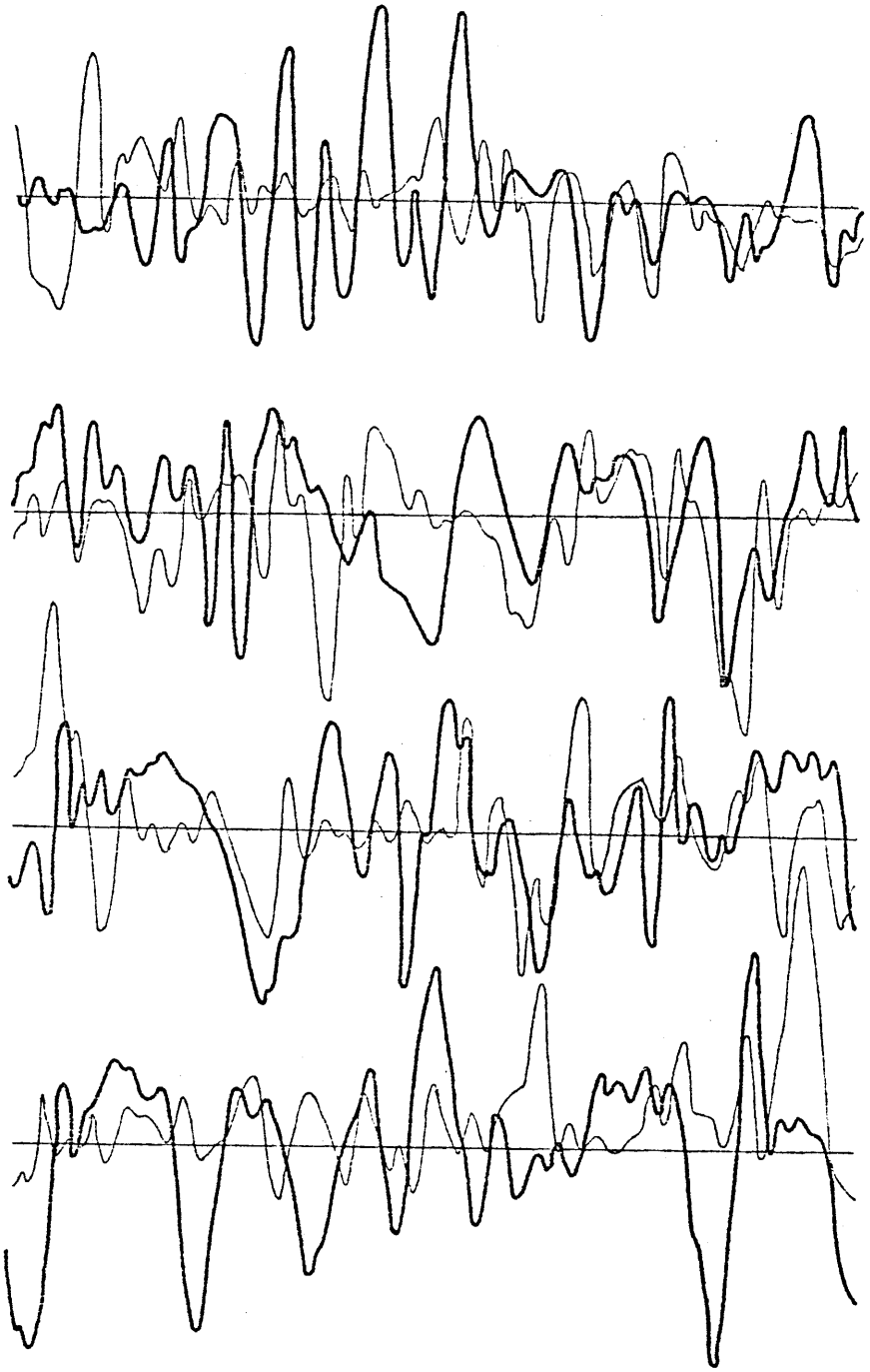

FIGURE 16b: The same as Figure 16a except that AD11 is not plotted, for case #2 with $\Theta_i^* = .12$. In this example, the time series starts 4350 days after initialization and lasts for 256 days. Each axis segment then represents 64 days. The tendency term is denoted by the heavy line and "sum" is denoted by the light line. Both terms are plotted to the same nondimensional scale as "sum" and the tendency term are in Figure 16a.

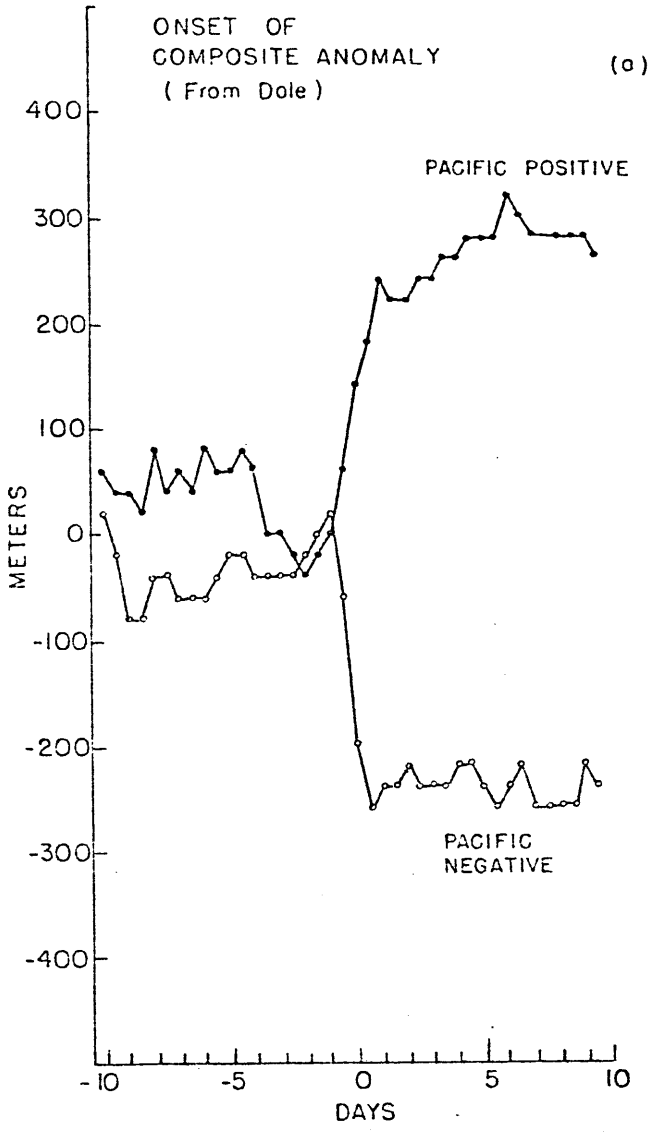

FIGURE 17a: (From Dole) Time series plot of the amplitude of Dole's Pacific Positive and Pacific Negative anomaly composites. The ordinate is in meters and the abscissa is in days. Day zero is alligned to correspond to the time when each individual anomaly first meets Dole's 10 day-10 decameter selection criteria. The Pacific Positive event is denoted by solid circles and the Pacific Negative event by open circles. Note the rapid rate of onset for each of the anomaly events.

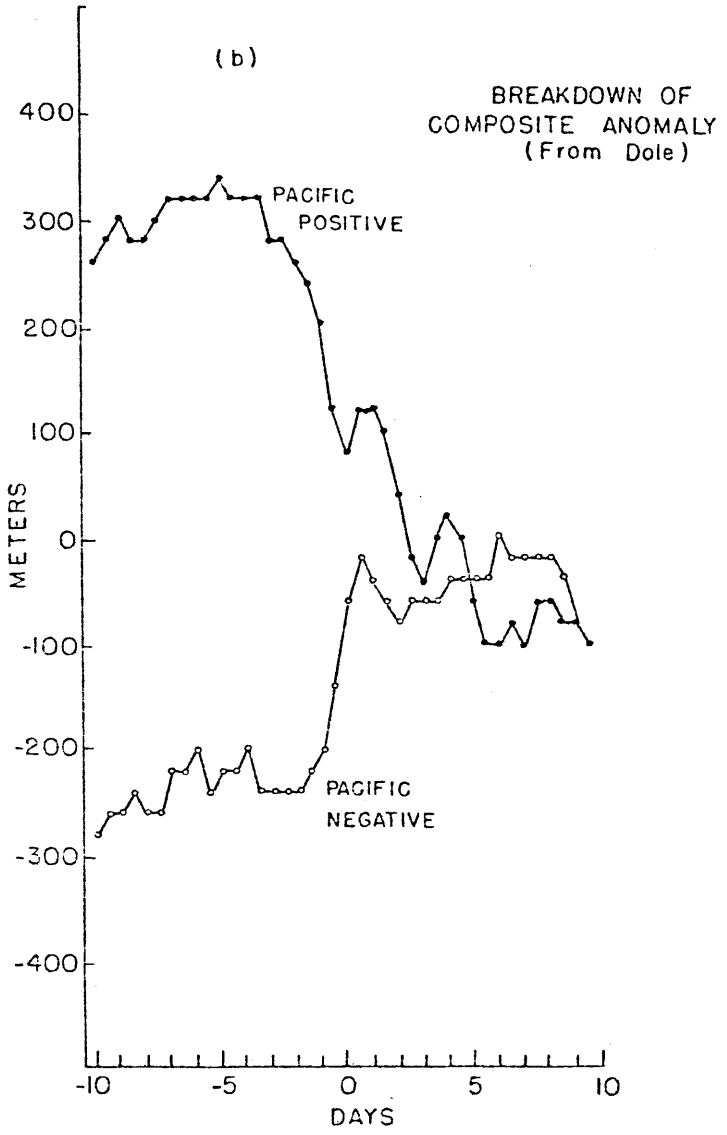

FIGURE 17b: (From Dole) Same as Figure 17a except for the fact that day zero is now alligned to correspond to the day when each individual anomaly event last meets Dole's 10 day-10 decameter selection criteria. Note that as in Figure 17a, the collapse of these events is also very rapid.

EQUILIBRIUM	Ψ_1	Ψ_2	Ψ_3	Θ_1	Θ_2	Θ_3
1) HADLEY	.095745	.000000	.000000	.095745	.000000	.000000
2) NEAR HADLEY	.089248	-.007507	-.000997	.095324	-.005549	.000950
3) 90° RIDGE	.057368	-.000115	-.038418	.074070	-.017091	-.033066
4) 45° TROUGH	.067815	-.040352	.039344	.064646	-.015504	.038329
5) 30° RIDGE	.077456	.054795	-.024950	.067787	.027851	-.028048

STABILITY OF DEMONSTRATION CASE EQUILIBRIA

MODE	HADLEY	NEAR HADLEY	90° RIDGE	45° TROUGH	30° RIDGE
MODE 11	443.13	122.45*	370.83	STABLE	114.07*
MODE 21	334.08	337.84	699.30	STABLE	STABLE
MODE 12	44.64	45.45	54.45	60.61	54.74
MODE 22	495.05	499.17	370.83	STABLE	STABLE

TABLE 2: The 5 equilibrium solutions and their respective stabilities to the 4 modes of the model for the demonstration case. The equilibria are given in terms of the midlevel streamfunction ψ and potential temperature θ. The asterisk (*) to the right of the growth rates (in units of hours) indicates that the instability is non-propogating (orographic).

Type	Length	Start	Finish	φ_1	φ_2	φ_3	ϕ_1	ϕ_2	ϕ_3
-1	75.6	188	1399	.13380	-.02689	.04059	.00225	-.01300	.00088
-1	87.1	1616	3011	.13485	-.03309	.04549	.00200	-.01502	.00083
-1	78.8	3115	4377	.13827	-.02294	.03228	.00138	-.01094	.00039
-1	111.5	4409	6194	.13535	-.02624	.03764	.00197	-.01219	.00090
1	363.4	6194	12009	.13517	.01245	-.03903	-.00416	.01118	-.00138
-1	46.1	12009	12748	.13731	-.02402	.03418	.00149	-.00545	.00069
1	232.8	12797	16522	.13370	.01057	-.04231	-.00545	.01180	-.00174
-1	81.4	16522	17825	.13939	-.02621	.03624	.00125	-.01202	.00038
-1	74.3	18264	19453	.14113	-.02118	.03075	.00191	-.01045	.00053
-1	70.8	19479	20613	.13749	-.02464	.03539	.00155	-.01147	.00067
-1	174.9	20765	23564	.13889	-.02106	.03218	.00206	-.01043	.00068
1	580.6	23564	32855	.13429	.01030	-.04219	-.00549	.01182	-.00177
1	68.0	32883	33972	.14023	.01515	-.02722	-.00106	.00879	-.00040
1	227.4	33997	37637	.13783	.01504	-.03262	-.00227	.01012	-.00077
-1	32.5	37637	38158	.13980	-.02073	.02992	.00166	-.01023	.00081
1	141.9	38158	40429	.13259	.01007	-.04093	-.00521	.01131	-.00171
-1	70.2	40518	41642	.14095	-.02483	.03326	.00131	-.01116	.00063
-1	55.1	41836	42718	.13538	-.01965	.03228	.00258	-.01041	.00115
1	66.7	42807	43857	.13839	.01513	-.03196	-.00194	.00988	-.00077
-1	86.1	44019	45397	.14025	-.02193	.03238	.00163	-.01043	.00058
1	215.8	45397	48851	.13613	.01373	-.03541	-.00307	.01047	-.00104
-1	94.8	48851	50368	.13849	-.02271	.03295	.00157	-.01074	.00053
-1	197.1	50380	53535	.13496	-.02745	.03891	.00210	-.01297	.00070
-1	149.2	53690	56082	.13584	-.02277	.03422	.00241	-.01154	.00086
1	273.4	56082	60458	.13552	.01351	-.03798	-.00379	.01123	-.00124
-1	69.1	60494	61600	.13635	-.02133	.03271	.00178	-.01033	.00089
-1	83.9	61708	63051	.13987	-.02424	.03522	.00152	-.01140	.00047
-1	61.2	63095	64075	.13706	-.02400	.03351	.00150	-.01145	.00050
-1	68.0	64099	65188	.13508	-.02622	.03590	.00103	-.01161	.00067
-1	123.1	65227	67198	.13725	-.02730	.03756	.00147	-.01233	.00048
-1	81.1	67207	68505	.13480	-.02403	.03627	.00296	-.01237	.00109
1	75.3	68505	69710	.13607	.01349	-.03300	-.00243	.00993	-.00112
-1	141.4	69710	71974	.13452	-.02328	.03531	.00223	-.01132	.00079
-1	86.8	71981	73371	.13711	-.02463	.03578	.00196	-.01170	.00074
-1	78.8	73486	74747	.14099	-.02211	.03210	.00117	-.01044	.00044
-1	53.5	74796	75653	.13807	-.02194	.03287	.00180	-.01099	.00080
-1	78.1	75888	77139	.13901	-.02214	.03170	.00146	-.01070	.00039
-1	67.2	77165	78241	.13416	-.02837	.04105	.00203	-.01339	.00096
-1	71.3	78264	79406	.13801	-.02184	.03098	.00137	-.00995	.00050
1	244.1	79406	83313	.13667	.01558	-.03507	-.00267	.01072	-.00084
1	1099.8	83323	100920	.13516	.01215	-.04078	-.00471	.01162	-.00153
-1	56.9	100920	101831	.13503	-.02599	.03721	.00149	-.01220	.00067
-1	272.0	101988	106341	.13567	-.02502	.03578	.00195	-.01187	.00063
1	278.4	106341	110796	.13381	.00887	-.04190	-.00579	.01145	-.00191
1	481.6	111037	118744	.13583	.01195	-.03935	-.00444	.01132	-.00146
-1	61.1	118808	119786	.13468	-.01998	.02821	.00092	-.00948	.00071
1	208.8	119847	123189	.13572	.01258	-.03678	-.01086	.01086	-.00130
-1	65.6	123324	124375	.14213	-.01826	.02738	.00165	-.00925	.00044
1	173.7	124435	127215	.13567	.01229	-.03966	-.00442	.01141	-.00147
-1	108.8	127215	128944	.13450	-.02630	.03877	.00238	-.01277	.00079
-1	81.1	128972	130270	.13590	-.02649	.03705	.00174	-.01234	.00084
-1	66.0	130330	131387	.13686	-.02257	.03472	.00253	-.01164	.00102
-1	67.4	131424	132503	.13952	-.02199	.03131	.00151	-.01047	.00053

Continued

Type	Length	Start	Finish	φ_1	φ_2	φ_3	ϕ_1	ϕ_2	ϕ_3
-1	46.1	132514	133258	.13677	-.02924	.04097	.00101	-.01342	.00059
-1	48.8	133328	134110	.13779	-.02697	.03654	.00079	-.01129	.00032
-1	33.9	134317	134861	.14975	-.00771	.01391	.00023	-.00402	.00021
1	195.7	134861	137993	.13453	.01094	-.04240	-.00537	.01200	-.00179
1	126.6	138036	140062	.13399	.01130	-.04153	-.00499	.01163	-.00164
-1	76.4	140062	141286	.14093	-.02166	.03148	.00109	-.01019	.00049
-1	70.3	141441	142566	.14004	-.02141	.03136	.00173	-.01059	.00054
-1	106.1	142599	144298	.13729	-.02412	.03627	.00204	-.01161	.00073
1	110.2	144298	146062	.13483	.01497	-.03527	-.00269	.01060	-.00088
1	644.9	146080	156399	.13571	.01385	-.03742	-.00359	.01105	-.00117
-1	66.3	156581	157643	.14162	-.01920	.02700	.00107	-.00928	.00021
1	25.3	157755	158161	.14112	.00651	-.01867	-.00237	.00698	-.00100
1	259.9	158422	162582	.13676	.01414	-.03655	-.00325	.01076	-.00105
1	54.5	162597	163468	.13932	.01937	-.03185	-.00100	.01066	-.00060
-1	39.8	163468	164105	.13886	-.01754	.02762	.00194	-.00910	.00079

TABLE 3a continued

TABLE 3a: The type, length in days, start and finish time step, and the time mean upper and lower level streamfunction of the regimes as they occur in the demonstration case for the first 28 years of integration. A "-1" and "+1" refer to the trough and ridge regime respectively.

Composite Ridge Regimes

Cat.	# days	# reg.	φ_1	amp.	phase	ϕ_1	amp.	phase
2	-	-	-	-	-	-	-	-
3	111	5	.14090	.02063	-76.1	-.00243	.00675	-13.3
4	134	5	.14050	.02562	-69.5	-.00259	.00842	-7.9
5	43	1	.14393	.01693	-77.0	-.00219	.00582	-11.8
6	394	7	.13724	.03742	-67.8	-.00305	.01074	-5.9
7	2593	30	.13718	.03585	-67.9	-.00276	.01012	-5.7
8	47688	114	.13531	.04147	-72.4	-.00435	.01148	-7.1

Composite Trough Regimes

Cat.	# days	# reg.	φ_1	amp.	phase	ϕ_1	amp.	phase
2	15	5	.14781	.00095	23.6	.00016	.00022	67.4
3	69	3	.14260	.03354	118.7	.00288	.00916	172.8
4	114	4	.14130	.03684	124.7	.00141	.01023	175.6
5	724	19	.13868	.04047	124.3	.00174	.01118	176.0
6	3869	71	.13704	.04113	124.2	.00189	.01135	176.3
7	10849	127	.13730	.04190	124.6	.00180	.01139	176.6
8	6995	38	.13646	.04348	124.5	.00199	.01180	176.7

EQUILIBRIA	φ_1	amp.	phase	ϕ_1	amp.	phase
#1 Hadley Solution	.19149	.00000	0.0	.00000	.00000	0.0
#2 Near Hadley Solution	.18457	.01306	-179.8	-.00608	.00276	-135.2
#3 90° Ridge	.13144	.07353	-103.5	-.01670	.01780	-17.7
#4 45° Trough	.13246	.09567	125.7	.00317	.02487	177.7
#5 30° Ridge	.14524	.09818	-32.7	.00967	.02712	6.6

TABLE 3b: The 7 categories of the 205 year composite trough and ridge regimes for the demonstration case. Column 1 is the category, column 2 is the sum total of days of regime of said category that contribute to the composite, and column 3 is the number of regime events that fell into said category. The mean composite state is given in upper level zonal flow φ_1, amplitude and phase of the upper level wave and ditto for the lower level. For comparison, the upper an- lower level streamfunction in phase and amplitude form for the 5 equilibria are also listed.

Case #1

DRIVING		.07	.08	.09	.10	.11
	11	STABLE	272.73*	172.41*	205.48*	467.29*
HADLEY	21	STABLE	STABLE	STABLE	613.50	285.71
	12	153.06	108.70	84.27	68.65	57.80
NEAR	11				STABLE	124.48
HADLEY	21				609.72	294.12
	12				66.08	59.88
90°	11		STABLE	874.64	300.00	177.51
RIDGE	21		STABLE	STABLE	STABLE	539.57
	12		104.90	85.71	73.75	63.83
45°	11		STABLE	STABLE	STABLE	STABLE
TROUGH	21		STABLE	STABLE	STABLE	STABLE
	12		133.93	107.91	90.36	78.33
30°	11				106.38*	83.10*
RIDGE	21				STABLE	STABLE
	12				60.73	55.76

TABLE 4a

CASE #2

DRIVING		.07	.075	.0775	.08	.09	.10	.11	.12	.13	.14	.15
	11	S	S	4710*	901*	250*	170*	152*	190*	S	1149	240
HADLEY	21	S	S	S	S	S	S	S	1429	457	273	194
	12	248	199	181	167	127	103	87	75	67	60	54
NEAR	11							S	S	310*	94*	61*
HADLEY	21							S	1136	474	304	224
	12							68	69	68	66	63
90°	11			S	S	S	S	S	S	1200	499	294
RIDGE	21			S	S	S	S	S	S	S	S	2113
	12			169	147	113	96	84	76	69	64	59
45°	11			S	S	S	S	S	S	S	S	S
TROUGH	21			S	S	S	S	S	S	5952	1149	645
	12			205	222	216	184	155	132	114	100	89
30°	11							164*	95*	78*	68*	62*
RIDGE	21							S	S	S	S	S
	12							62	57	53	50	48

TABLE 4b

Stability of the equilibria as a function of θ_1^* for a) case #1 and b) case #2. Growth rates are given in hours, and an asterisk (*) indicates a non-propogating instability (orographic). The Mode 22 wave is always stable and thus not listed. In Table 4b "S" indicates the solution is stable.

CASE #1

DRIVING	.07	.08	.09	.10	.11
# DAYS	6250	6250	6250	6250	6250
# RIDGE	5130	3228	3082	2099	1510
# TROUGH	442	2016	1886	2466	2225
# REGIME	5572	5244	4968	4565	3735
# UNSTEADY	678	1006	1282	1685	2515
TOP TEN RIDGE					
1	379.8	144.9	77.6	77.3	62.9
2	269.7	137.9	76.9	70.2	42.0
3	260.0	94.3	66.8	65.2	40.4
4	209.8	89.4	64.4	62.1	37.1
5	199.4	85.4	62.7	58.9	36.6
6	189.8	83.2	62.6	52.3	33.1
7	179.2	80.6	60.7	50.1	32.7
8	163.1	80.2	60.6	49.4	31.9
9	160.2	78.1	59.0	49.1	30.4
10	143.3	74.2	56.1	46.6	30.3
TOP TEN TROUGH					
1	32.9	116.3	79.8	80.6	52.2
2	32.6	95.6	68.3	66.1	51.9
3	29.8	90.6	67.6	65.3	51.9
4	27.8	89.1	66.8	59.2	42.4
5	26.8	67.3	55.3	53.3	42.2
6	25.3	58.4	54.9	51.6	40.6
7	23.6	51.9	47.5	50.4	35.9
8	23.6	50.9	44.3	49.8	35.6
9	23.4	48.3	44.1	48.6	35.6
10	22.6	47.9	43.6	47.5	35.1

TABLE 5a: Statistics of the case #1 regimes for the 5 select values of the driving θ_1^*. The total number of days of each experiment (6250) is given in row 1, the total number of days the state of the model flow was in the ridge regime, trough regime, both the ridge and trough regime, and neither the ridge or trough regime (unsteady) are given in rows 2,3,4,5, respectively. The top 10 ridges and troughs are then listed in the next 20 rows. The top 10 refer to the 10 most persistent regimes of each experiment. The units are in days.

CASE #2

DRIVING	.07	.075	.0775	.08	.09	.10	.11	.12	.13	.14	.15
# DAYS	6250	6250	6250	6250	6250	6250	6250	6250	6250	6250	6250
# RIDGE	4593	5908	5703	6053	5749	5348	4103	3030	2989	2255	2240
# TROUGH	79	239	221	82	257	595	1460	1708	1217	1086	548
# REGIME	4672	6147	5924	6135	6006	5943	5563	4738	4206	3341	2788
# UNSTEADY	1578	103	326	115	224	307	687	1512	2044	2909	3462
TOP TEN RIDGE											
1	507.0	1131.8	755.8	607.9	410.4	202.9	106.1	116.6	68.6	54.6	102.3
2	243.3	947.8	676.4	602.1	341.1	172.8	91.8	85.5	68.5	52.9	44.9
3	203.3	805.0	602.6	577.1	287.7	256.6	86.3	79.4	65.5	51.6	44.8
4	176.0	509.0	430.6	507.1	263.1	151.8	85.6	77.5	59.6	51.3	43.1
5	174.2	381.4	417.5	493.4	253.7	145.3	81.5	74.0	54.1	47.5	41.4
6	161.3	319.8	346.6	427.2	238.6	141.1	81.1	70.3	50.0	43.9	40.7
7	158.3	289.1	328.9	384.8	208.2	139.4	80.9	66.9	49.6	42.8	39.8
8	152.4	203.1	290.9	380.1	195.7	137.9	80.4	62.4	48.8	42.1	38.9
9	151.6	183.4	275.9	321.1	193.1	132.1	77.4	57.6	48.6	41.8	37.6
10	146.6	167.9	265.9	308.5	187.1	128.5	76.6	51.6	48.0	41.1	37.6
TOP TEN TROUGH											
1	21.1	45.2	45.2	46.6	257.4	142.6	99.5	170.9	84.2	45.8	30.6
2	19.5	39.6	41.6	35.2	-	134.4	92.4	66.5	66.1	40.6	28.4
3	19.4	35.3	35.0	-	-	91.4	81.5	61.5	53.1	39.8	26.4
4	19.4	28.1	34.3	-	-	80.2	79.9	60.5	48.1	35.6	26.1
5	-	26.9	22.0	-	-	73.7	73.7	58.4	42.7	35.1	25.0
6	-	26.3	21.6	-	-	38.1	59.4	56.5	40.1	34.5	24.8
7	-	19.3	21.3	-	-	34.9	58.8	53.4	39.9	34.4	23.0
8	-	19.1	-	-	-	-	54.8	51.6	34.3	32.3	21.6
9	-	-	-	-	-	-	48.1	50.4	33.4	29.6	19.8
10	-	-	-	-	-	-	47.7	49.0	33.4	26.1	19.7

TABLE 5b: Identical to Table 5a except for case #2. The major difference between the two tables is the appearence of the dashes in the listings of the ten most persistent trough regimes. The dash indicates that there were fewer than 10 trough regimes during the entire 6250 day experiment; a clear example of ridge regime dominance in some cases.

CATEGORY 7 RIDGE REGIME

	φ_1	AMP.	PHASE	ϕ_1	amp.	phase	ω_1	AMP.	PHASE
WAVE	0.1685	0.0467	-84.4	-0.0064	0.0144	-5.4			
ad11	-	0.4212	138.9	-	0.0153	-156.3	0.9481	1.1994	-83.3
ad21	-	0.0225	-41.2	-	0.0292	-99.2	0.5975	1.7124	-54.1
ad12	-	0.2099	174.1	-	0.0945	-144.0	2.6667	1.5825	-31.2
ad22	-	-	-	-	-	-	1.5364	-	-
sum	-	0.5830	150.9	-	0.1232	-140.6	5.7487	4.2120	-53.8
AD11	-	6.8937	5.6	-	0.0810	-95.4	3.2271	12.2250	77.9
BETA	-	5.0372	-174.4	-	1.5553	-95.4	-	-	-
BEAD	-	1.8566	5.6	-	1.6363	-95.4	-	-	-
TOP2	-	-	-	-0.5956	1.1327	90.0	-	-	-
DISS	-	-	-	0.5132	1.1535	174.6	-9.7606	6.9266	-102.3
INT	-0.8747	0.2309	77.7	0.8747	0.2309	-102.3	-	-	-
wnln	-5.7487	1.6927	126.2	5.7487	1.6927	-58.3	-	-	-
WLIN	6.5335	2.1293	-102.0	-6.5335	2.1293	78.0	-	-	-
LINS	5.6589	2.2198	-49.0	-5.7413	1.7281	121.8	-6.5335	5.2985	78.0
nlns	-5.7487	2.2356	132.4	5.7487	1.7040	-58.0	5.7487	4.2120	-53.8

CATEGORY 7 TROUGH REGIME

	φ	AMP.	PHASE	ϕ_1	amp.	phase	ω_1	AMP.	PHASE
WAVE	0.1735	0.0788	134.6	0.0029	0.0222	178.2			
ad11	-	0.2873	47.3	-	0.0125	-168.1	0.8666	0.3364	51.5
ad21	-	0.3751	39.9	-	0.0609	26.9	0.9148	1.8192	73.7
ad12	-	0.5033	57.2	-	0.1174	32.1	1.5059	1.6961	108.9
ad22	-	-	-	-	-	-	0.3662	-	-
sum	-	1.1557	49.2	-	0.1663	31.6	3.6535	3.6159	87.3
AD11	-	11.9768	-135.4	-	0.0530	-91.8	5.6142	17.1318	-89.3
BETA	-	8.5003	44.6	-	2.2812	88.2	-	-	-
BEAD	-	3.4765	-135.4	-	2.2282	88.2	-	-	-
TOP2	-	-	-	0.2946	0.5055	-90.0	-	-	-
DISS	-	-	-	-0.2290	1.6920	-1.8	-10.4058	9.7732	121.6
INT	-0.8531	0.3258	-58.4	0.8531	0.3258	121.6	-	-	-
wnln	-3.6535	1.4531	-92.7	3.6535	1.4531	87.3	-	-	-
WLIN	4.7916	4.0514	60.9	-4.7916	4.0514	-119.9	-	-	-
LINS	3.9385	0.8885	112.2	-3.8729	1.6388	-103.4	-4.7916	10.0814	-119.1
nlns	-3.6535	0.8971	-40.0	3.6535	1.5531	82.2	3.6535	3.6159	87.3

TABLE 6a: Budget terms for case #2 with θ_1^*=.12 category 7 composite regimes. The units are the tendencies of the upper and lower level equations (times 1000) in the first six cloumns; the last three columns are the contributions to the w field. Individual terms explained in text, equations also in text.

REGIME TYPE II BEHAVIOR: RIDGE

	φ_1	AMP.	PHASE	ϕ_1	amp.	phase	ω_1	AMP.	PHASE
WAVE	0.1582	0.0498	-110.2	-0.0106	0.0105	-13.0			
ad11	-	0.0810	112.3	-	0.0087	-114.0	0.1424	0.2210	-63.3
ad21	-	0.1234	-74.7	-	0.0756	-100.6	0.2476	1.1965	-38.0
ad12	-	0.3885	-178.9	-	0.2692	-156.1	4.6079	2.6351	-28.9
ad22	-	-	-	-	-	-	2.2954	-	-
sum	-	0.3900	-172.4	-	0.3255	-144.1	7.2933	4.0112	-33.4
AD11	-	6.8985	-20.2	-	0.0972	-103.0	-	-	-
BETA	-	5.3710	159.8	-	1.1320	-103.0	-	-	-
BEAD	-	1.5275	-20.2	-	1.2292	-103.0	-	-	-
TOP2	-	-	-	-1.0372	1.8657	90.0	-	-	-
DISS	-	-	-	0.8454	0.8396	167.0	-10.6925	7.8248	-121.7
INT	-0.8436	0.2608	58.3	0.8436	0.2608	-121.7	-	-	-
wnln	-7.2933	1.6120	146.6	7.2933	1.6120	-33.4	-	-	-
WLIN	8.1614	0.1493	-108.4	-8.1614	0.1493	71.6	-	-	-
LINS	7.3178	1.5878	-16.4	-7.5097	1.4165	146.7	-8.1614	0.3715	71.6
nlns	-7.2933	1.9233	154.2	7.2933	1.5279	-44.9	7.2933	4.0112	-33.4

REGIME TYPE II BEHAVIOR: TROUGH

	φ_1	AMP.	PHASE	ϕ_1	amp.	phase	ω_1	AMP.	PHASE
WAVE	0.1739	0.0811	132.4	0.0040	0.0223	179.1			
ad11	-	0.2124	46.3	-	0.0206	138.8	0.4927	0.0291	-63.7
ad21	-	0.3435	56.8	-	0.0528	35.3	0.7064	2.1130	77.8
ad12	-	0.4362	48.4	-	0.1411	28.4	1.7766	1.7951	108.8
ad22	-	-	-	-	-	-	0.5869	-	-
sum	-	0.9892	50.9	-	0.1880	36.2	3.5625	3.7408	91.8
AD11	-	12.3515	-137.6	-	0.0772	-90.9	6.4109	17.8558	-87.3
BETA	-	8.7473	42.4	-	2.4011	89.1	-	-	-
BEAD	-	3.6043	-137.6	-	2.3239	89.1	-	-	-
TOP2	-	-	-	0.1591	0.6986	-90.0	-	-	-
DISS	-	-	-	-0.3165	1.7809	-0.9	-10.5134	10.1679	118.6
INT	-0.8496	0.3389	-61.4	0.8496	0.3389	118.6	-	-	-
wnln	-3.5625	1.5031	-88.2	3.5625	1.5031	91.8	-	-	-
WLIN	4.1025	3.9258	65.7	-4.1025	3.9258	-114.3	-	-	-
LINS	3.2529	1.2292	136.2	-3.4103	1.6859	-88.5	-4.1025	9.7688	-114.3
nlns	-3.5625	0.9952	-47.6	3.5625	1.6169	86.3	3.5625	3.7403	91.8

TABLE 6b: The same as Table 6a except for periods of Regime type II behavior during a single regime event in case #2 with $\theta_1^* = .12$.

REGIME TYPE II

	TROUGH					RIDGE				
	Theory		Full model			Theory		Full model		
	ad21	ad12	ad11	ad21	ad12	ad21	ad12	ad11	ad21	ad12
φ	.2209	1.4603	.2124	.3435	.4362	.3258	1.1326	.0810	.1234	.3885
A	58.1°	49.1°	46.3°	56.8°	48.4°	-151.0°	-179.0°	112.3°	-74.7°	-178.9°
ϕ	.1345	1.3146	.0206	.0528	.1141	.8770	.9216	.0087	.0756	.2691
α	9.2°	10.7°	138.8°	35.3°	28.4°	-151.0°	-168.0°	-114.0°	-101.0°	-156.0°
ω_1	.5492	1.3115	.4927	.7064	1.7766	.9774	.8811	.1424	.2476	4.6079
ω_φ	.1339	1.2590	.0291	2.1130	1.7951	.3025	.9563	.2210	1.1965	2.6351
ω_α	121.0°	110.0°	-63.7°	77.8°	108.8°	-42.7°	-53.0°	-63.3°	-38.0°	-28.9°

TABLE 7a

CATEGORY 7 COMPOSITE REGIME

	TROUGH					RIDGE				
	Theory		Full model			Theory		Full model		
	ad21	ad12	ad11	ad21	ad12	ad21	ad12	ad11	ad21	ad12
φ	.1917	1.2520	.2873	.3751	.5033	2.0000	2.3373	.4212	.0225	.2099
A	59.4°	50.7°	47.3°	39.9°	57.2°	-150.0°	-152.0°	138.9°	-41.2°	174.1°
ϕ	.0870	1.1925	.0125	.0609	.1174	2.6918	2.7619	.0153	.0292	.0945
α	13.4°	12.5°	47.3°	39.9°	57.2°	-142.0°	-153.0°	156.3°	-99.2°	-144.0°
ω_1	.3848	1.5605	.8666	.9148	1.5059	.6594	1.5973	.9481	.5975	2.6670
ω_φ	.1330	1.2853	.3364	1.8192	1.6961	.3259	1.9210	1.1994	1.7124	1.5825
ω_α	122.0°	110.0°	51.1°	73.7°	108.9°	-42.6°	-39.2°	-83.8°	-54.1°	-31.2°

TABLE 7c

TABLE 7a: Comparison of phase and relative amplitudes of the transport terms from the stability calculation with the full model regime budgets for the tendency equations (7.1) in Chapter 7 in phase and amplitude form. φ = amplitude of upper level wave tendency, A=phase of upper level wave tendency, ϕ= amplitude of lower level wave tendency, α= phase of lower level wave tendency, w_1 = zonal w contribution, w_φ = amplitude of wave w contribution, w_α = phase of wave w contribution. The experiments were conducted for case #2 with θ_1^*=.12 for two periods of regime type II behavior. Amplitudes from stability calculation (theory) are divided by the corresponding terms in the regime budgets (full model). Further explanation of the "theory" amplitude ratios is provided in the text. Table 7c is the same as Table 7a except for the category 7 composite regimes.

REGIME TYPE II

	Theory sum	Full model sum	Theory sum	Full model sum
φ	.53	.989	.49	.390
A	50.3^{o}	50.9^{o}	-176.7^{o}	-172.4^{o}
ϕ	.12	.188	.32	.326
α	9.9^{o}	36.2^{o}	-164.4^{o}	-144.1^{o}
ω_{φ}	1.90	3.74	2.97	4.010
ω_{α}	111.2^{o}	91.8^{o}	-52.3^{o}	-33.4^{o}
	TROUGH		RIDGE	

TABLE 7b

Comparison of the vector sum of the transport components predicted by theory to that observed in the budgets for the periods of trough and ridge regime type II behavior mentioned in Tables 6b and 7a. Amplitudes of the theoretical calculation were obtained by setting $B^2=.75$ in the trough regime and setting $B^2=1.03$ in the ridge regime. Notation otherwise the same as in Table 7a.

CASE #2 REGIME-EQUILIBRIA $\theta_1^* = .12$ (ad22 = 0)

RIDGE BRANCH

	ψ_1	ψ_2	ψ_3	θ_1	θ_2	θ_3
.00	.0644	.0115	-.0520	.0804	-.0109	-.0494
.01	.0677	.0110	-.0494	.0816	-.0107	-.0466
.02	.0693	.0103	-.0461	.0829	-.0105	-.0436
.03	.0711	.0094	-.0426	.0843	-.0102	-.0402
.04	.0732	.0082	-.0387	.0858	-.0099	-.0364
.05	.0756	.0066	-.0342	.0874	-.0095	-.0320
.06	.0783	.0045	-.0290	.0890	-.0090	-.0271
.07	.0811	.0019	-.0232	.0905	-.0084	-.0215
.08	.0838	-.0012	-.0169	.0915	-.0079	-.0155
.09	.0860	-.0046	-.0106	.0919	-.0076	-.0095
.10	.0870	-.0075	-.0056	.0914	-.0075	-.0048
.11	.0869	-.0091	-.0030	.0903	-.0076	-.0024
.12	.0862	-.0099	-.0019	.0891	-.0077	-.0014
.15	.0837	-.0110	-.0007	.0857	-.0081	-.0003
.20	.0802	-.0118	-.0001	.0810	-.0087	.0001
.50	.0695	-.0128	.0011	.0655	-.0105	.0004
1.00	.0628	-.0120	.0022	.0545	-.0124	.0007
1.50	.0587	-.0103	.0029	.0489	-.0138	.0012
2.00	.0547	-.0081	.0035	.0453	-.0148	.0017

TROUGH BRANCH

	ψ_1	ψ_2	ψ_3	θ_1	θ_2	θ_3
.00	.0792	-.0535	.0471	.0740	-.0240	.0461
.01	.0801	-.0520	.0459	.0748	-.0230	.0450
.02	.0810	-.0504	.0447	.0757	-.0220	.0437
.03	.0819	-.0487	.0433	.0766	-.0210	.0423
.04	.0829	-.0468	.0417	.0777	-.0199	.0408
.05	.0839	-.0447	.0400	.0788	-.0187	.0391
.06	.0850	-.0424	.0380	.0801	-.0175	.0371
.07	.0862	-.0397	.0356	.0815	-.0161	.0347
.08	.0876	-.0366	.0326	.0832	-.0146	.0318
.09	.0891	-.0324	.0284	.0853	-.0127	.0277
.10	.0910	-.0241	.0190	.0891	-.0097	.0187

TABLE 8a: List of the regime-equilibria midlevel streamfunction and potential temperature in spectral component form for selected values of the energy ratio for case #2 with $\theta_1^* = .12$. The parameterized effects of ad22 are not included.

CASE #2 REGIME- EQUILIBRIA $\theta_1^* = .12$

RIDGE BRANCH

	ψ_1	ψ_2	ψ_3	θ_1	θ_2	θ_3
.00	.0664	.0115	-.0520	.0804	-.0109	-.0494
.01	.0678	.0111	-.0488	.0815	-.0104	-.0463
.02	.0695	.0106	-.0452	.0827	-.0098	-.0428
.03	.0714	.0097	-.0412	.0839	-.0092	-.0389
.04	.0737	.0085	-.0364	.0853	-.0086	-.0343
.05	.0763	.0066	-.0309	.0867	-.0079	-.0290
.06	.0792	.0039	-.0243	.0881	-.0072	-.0227
.07	.0820	.0003	-.0169	.0891	-.0067	-.0156
.08	.0843	-.0037	-.0095	.0893	-.0065	-.0086
.09	.0850	-.0070	-.0042	.0885	-.0066	-.0036
.10	.0844	-.0084	-.0021	.0872	-.0068	-.0016
.15	.0794	-.0102	-.0002	.0806	-.0076	.0001
.20	.0755	-.0107	.0003	.0757	-.0081	.0003
.50	.0642	-.0112	.0015	.0604	-.0099	.0008
1.00	.0567	-.0096	.0025	.0502	-.0115	.0014
1.50	.0517	-.0073	.0030	.0451	-.0124	.0018
2.00	.0475	-.0053	.0031	.0419	-.0128	.0020

TROUGH BRANCH

	ψ_1	ψ_2	ψ_3	θ_1	θ_2	θ_3
.00	.0792	-.0535	.0471	.0740	-.0240	.0461
.01	.0801	-.0517	.0457	.0748	-.0229	.0448
.02	.0809	-.0499	.0443	.0757	-.0218	.0433
.03	.0819	-.0478	.0426	.0767	-.0206	.0417
.04	.0828	-.0456	.0408	.0777	-.0193	.0398
.05	.0839	-.0430	.0386	.0789	-.0180	.0377
.06	.0850	-.0401	.0361	.0803	-.0165	.0352
.07	.0862	-.0365	.0328	.0819	-.0148	.0320
.08	.0876	-.0317	.0281	.0839	-.0126	.0274
.085	.0884	-.0281	.0243	.0854	-.0112	.0237
.087	.0888	-.0260	.0219	.0862	-.0104	.0214

CATEGORY 7 REGIMES

TROUGH:					
.0882	-.0382	.0284	.0853	-.0171	.0277
RIDGE:					
.0810	.0095	-.0239	.0875	-.0049	-.0226

TABLE 9a: Same as Table 8a except that the parameterized effects of ad22 are included. This table is plotted in Figure 15a. For comparison, we have also included the category 7 full model composite regimes in spectral component form.

CASE #2 REGIME-EQUILIBRIA $\theta_1^* = .15$ (ad22 = 0)

RIDGE BRANCH

	Ψ_1	Ψ_2	Ψ_3	Θ_1	Θ_2	Θ_3	
.00	.0631	-.0023	-.0637	.0867	-.0313	-.0594	(unstable)
.01	Unstable limit cycle						
.02-.07	Stable limit cycles						
.08	.0803	-.0013	-.0378	.0989	-.0196	-.0344	
.09	.0835	-.0023	-.0328	.1004	-.0177	-.0297	
.10	.0866	-.0038	-.0275	.1017	-.0159	-.0247	
.11	.0896	-.0055	-.0220	.1026	-.0142	-.0196	
.12	.0921	-.0074	-.0166	.1030	-.0127	-.0146	
.15	.0955	-.0126	-.0046	.1012	-.0103	-.0035	
.20	.0922	-.0143	-.0013	.0952	-.0102	-.0008	
.50	.0793	-.0153	.0004	.0752	-.0113	-.0003	
1.00	.0720	-.0149	.0015	.0615	-.0130	-.0004	
1.50	.0684	-.0139	.0023	.0545	-.0145	-.0002	
2.00	.0655	-.0124	.0030	.0500	-.0159	.0002	

TROUGH BRANCH

	Ψ_1	Ψ_2	Ψ_3	Θ_1	Θ_2	Θ_3
.00	.0801	-.0719	.0600	.0741	-.0329	.0589
.01	.0808	-.0706	.0591	.0747	-.0320	.0580
.02	.0816	-.0693	.0582	.0754	-.0310	.0571
.03	.0825	-.0680	.0572	.0762	-.0301	.0561
.04	.0834	-.0666	.0562	.0770	-.0291	.0550
.05	.0843	-.0651	.0551	.0778	-.0280	.0540
.06	.0853	-.0635	.0540	.0787	-.0270	.0528
.07	.0863	-.0618	.0528	.0797	-.0259	.0516
.08	.0874	-.0599	.0514	.0807	-.0247	.0502
.09	.0885	-.0580	.0499	.0819	-.0234	.0487
.10	.0898	-.0558	.0483	.0831	-.0223	.0471
.11	.0911	-.0533	.0464	.0845	-.0209	.0452
.12	.0926	-.0505	.0441	.0861	-.0194	.0429
.13	.0943	-.0473	.0413	.0880	-.0177	.0402
.14	.0961	-.0431	.0376	.0904	-.0158	.0365
.15	.0986	-.0366	.0311	.0940	-.0131	.0302

TABLE 8b: Same as Table 8a except for case #2 with $\theta_1^* = .15$. The parameterized effects of ad22 are not included.

CASE #2 REGIME-EQUILIBRIA $\theta_1^* = .15$

RIDGE BRANCH

	ψ_1	ψ_2	ψ_3	θ_1	θ_2	θ_3	
.00	.0631	-.0233	-.0637	.0867	-.0313	-.0594	(unstable)
.01-.06	Stable limit cycles						
.07	.0779	.0010	-.0393	.0955	-.0181	-.0361	
.08	.0811	-.0000	-.0336	.0968	-.0160	-.0308	
.09	.0843	-.0016	-.0275	.0979	-.0139	-.0250	
.10	.0873	-.0037	-.0210	.0986	-.0122	-.0190	
.11	.0898	-.0062	-.0147	.0988	-.0108	-.0131	
.12	.0915	-.0087	-.0092	.0984	-.0099	-.0079	
.13	.0921	-.0106	-.0053	.0975	-.0094	-.0043	
.14	.0917	-.0116	-.0033	.0961	-.0093	-.0025	
.15	.0909	-.0122	-.0023	.0947	-.0093	-.0016	
.20	.0866	-.0133	-.0007	.0884	-.0095	-.0004	
.30	.0802	-.0136	.0001	.0795	-.0100	-.0000	
.50	.0730	-.0137	.0008	.0689	-.0109	.0001	
1.00	.0651	-.0128	.0020	.0562	-.0126	.0004	
1.50	.0606	-.0111	.0029	.0499	-.0140	.0009	
2.00	.0563	-.0088	.0034	.0345	-.0151	.0016	

TROUGH BRANCH

	ψ_1	ψ_2	ψ_3	θ_1	θ_2	θ_3
.00	.0801	-.0719	.0600	.0741	-.0329	.0589
.01	.0808	-.0704	.0590	.0747	-.0319	.0579
.02	.0816	-.0689	.0579	.0754	-.0309	.0568
.03	.0825	-.0674	.0568	.0762	-.0298	.0557
.04	.0833	-.0657	.0556	.0770	-.0287	.0545
.05	.0843	-.0639	.0543	.0778	-.0275	.0532
.06	.0852	-.0620	.0530	.0788	-.0263	.0518
.07	.0863	-.0600	.0515	.0799	-.0251	.0503
.08	.0874	-.0578	.0498	.0809	-.0238	.0486
.09	.0886	-.0553	.0479	.0821	-.0224	.0467
.10	.0899	-.0525	.0457	.0835	-.0208	.0446
.11	.0913	-.0492	.0431	.0851	-.0192	.0419
.12	.0929	-.0453	.0397	.0871	-.0172	.0386
.13	.0948	-.0397	.0345	.0897	-.0147	.0336
.135	.0961	-.0352	.0299	.0918	-.0130	.0291
.136	.0965	-.0337	.0283	.0925	-.0124	.0276
.137	.0969	-.0313	.0257	.0935	-.0116	.0251

TABLE 9b: Same as Table 8b except the parameterized effects of ad22 have been included. This table is plotted in Figure 15b.

STREAM FUNCTION (2.6) a

$$\dot{\Psi}_1 = c_1 h_2 (\theta_3 - \Psi_3) - k(\Psi_1 - \theta_1)$$

$$\dot{\Psi}_2 = \frac{c_1 n^2}{n^2+1}(\Psi_1\Psi_3 + \theta_1\theta_3) + \frac{c_4 n^2}{n^2+1}(\Psi_4\Psi_6 + \theta_4\theta_6) + \frac{\beta n \Psi_3}{n^2+1} - k(\Psi_2 - \theta_2)$$

$$+ \frac{3c_6}{n^2+1}(1-n^2)(\Psi_5\Psi_8 + \theta_5\theta_8 - \Psi_6\Psi_7 - \theta_6\theta_7)$$

$$\dot{\Psi}_3 = \frac{-c_1}{n^2+1}[n^2(\Psi_1\Psi_2 + \theta_1\theta_2) - h_2(\Psi_1 - \theta_1)] - \frac{c_4 n^2}{n^2+1}(\Psi_4\Psi_5 + \theta_4\theta_5) - \frac{\beta n \Psi_2}{n^2+1} - k(\Psi_3 - \theta_3)$$

$$- \frac{3c_6}{n^2+1}(1-n^2)(\Psi_5\Psi_7 + \theta_5\theta_7 + \Psi_6\Psi_8 + \theta_6\theta_8)$$

$$\dot{\Psi}_4 = \frac{c_4}{4}[3(\Psi_3\Psi_5 + \theta_3\theta_5 - \Psi_2\Psi_6 - \theta_2\theta_6) + h_2(\theta_4 - \Psi_6)] + \frac{3c_5}{4}(\Psi_5\Psi_9 + \theta_8\theta_9)$$

$$- \frac{3c_5}{4}(\Psi_7\Psi_{10} - \theta_7\theta_{10}) - k(\Psi_4 - \theta_4)$$

$$\dot{\Psi}_5 = \frac{c_2}{n^2+4}(n^2+3)(\Psi_1\Psi_5 + \theta_1\theta_5) + \frac{c_4}{n^2+4}(n^2-3)(\Psi_3\Psi_4 + \theta_3\theta_4) + \frac{\beta n \Psi_6}{n^2+4} - k(\Psi_5 - \theta_5)$$

$$+ \frac{c_6}{n^2+4}[3n^2(\Psi_2\Psi_8 + \theta_2\theta_8 - \Psi_3\Psi_7 - \theta_3\theta_7) - h_2(\theta_8 - \Psi_8)]$$

$$\dot{\Psi}_6 = \frac{-c_2}{n^2+4}(n^2+3)(\Psi_1\Psi_5 + \theta_1\theta_5) - \frac{c_4}{n^2+4}[(n^2-3)(\Psi_2\Psi_4 + \theta_2\theta_4) + h_2(\theta_4 - \Psi_4)] - \frac{\beta n \Psi_5}{n^2+4} - k(\Psi_6 - \theta_6)$$

$$- \frac{c_6}{n^2+4}[3n^2(\Psi_3\Psi_8 + \theta_3\theta_8 + \Psi_2\Psi_7 + \theta_2\theta_7) - h_2(\theta_7 - \Psi_7)]$$

$$\dot{\Psi}_7 = \frac{4c_3 n^2}{4n^2+1}(\Psi_1\Psi_8 + \theta_1\theta_8) + \frac{4c_6 n^2}{4n^2+1}(\Psi_4\Psi_{10} + \theta_4\theta_{10}) + \frac{2n\beta\Psi_8}{4n^2+1} - k(\Psi_7 - \theta_7)$$

$$+ \frac{c_6}{4n^2+1}[3(\Psi_2\Psi_6 + \theta_2\theta_6 + \Psi_3\Psi_5 + \theta_3\theta_5) - h_2(\theta_6 - \Psi_6)]$$

$$\dot{\Psi}_8 = \frac{-4c_2 n^2}{4n^2+1}(\Psi_1\Psi_7 + \theta_1\theta_7) - \frac{4c_5 n^2}{4n^2+1}(\Psi_4\Psi_9 + \theta_4\theta_9) + \frac{2n\beta\Psi_8}{4n^2+1} - k(\Psi_7 - \theta_7)$$

$$+ \frac{c_6}{4n^2+1}[3(\Psi_3\Psi_6 + \theta_3\theta_6 - \Psi_2\Psi_5 - \theta_2\theta_5) + h_2(\theta_5 - \Psi_5)]$$

$$\dot{\Psi}_9 = \frac{(4n^2+3)}{4n^2+4}c_4(\Psi_1\Psi_{10} + \theta_1\theta_{10}) + \frac{(4n^2+3)}{4n^2+4}c_5(\Psi_4\Psi_8 + \theta_4\theta_8) + \frac{2n\beta\Psi_{10}}{4n^2+4} - k(\Psi_9 - \theta_9)$$

$$\dot{\Psi}_{10} = -\frac{(4n^2+3)}{4n^2+4}c_4(\Psi_1\Psi_9 + \theta_1\theta_9) - \frac{(4n^2+3)}{4n^2+4}c_5(\Psi_4\Psi_7 + \theta_4\theta_7) - \frac{2n\beta\Psi_9}{4n^2+4} - k(\Psi_{10} - \theta_{10})$$

$$(\sigma_0+1)\dot{\theta}_1 = c_1[(\theta_2\psi_3-\psi_2\theta_3)+\sigma_0\tau_2(\psi_3-\theta_3)]+c_2(\theta_5\psi_6-\theta_6\psi_5)+c_3(\theta_7\psi_8-\psi_7\theta_8)$$
$$+c_4(\theta_9\psi_{10}-\theta_{10}\psi_9)+h(\theta_1^*-\theta_1)+k\sigma_0\psi_1-\sigma_0(k+2k')\theta_1$$

$$(\sigma_0+\tfrac{1}{n^2+1})\dot{\theta}_2 = \frac{-c_1}{n^2+1}[(1-\sigma_0n^2)\theta_1\psi_3-(1+\sigma_0n^2)\psi_1\theta_3]-\frac{c_4}{n^2+1}[(1-\sigma_0n^2)\theta_4\psi_6-(1+\sigma_0n^2)\psi_4\theta_6]$$
$$+\frac{c_6}{n^2+1}[(1+3\sigma_0(1-n^2))(\theta_5\psi_8-\theta_6\psi_7)+(3\sigma_0(1-n^2)-1)(\theta_8\psi_5-\theta_7\psi_6)]$$
$$+\frac{\beta n\sigma_0\theta_3}{n^2+1}-\frac{h\theta_2}{n^2+1}+k\sigma_0\psi_2-(k+2k')\sigma_0\theta_2$$

$$(\sigma_0+\tfrac{1}{n^2+1})\dot{\theta}_3 = \frac{c_1}{n^2+1}[(1-\sigma_0n^2)\theta_1\psi_2-(1+\sigma_0n^2)\psi_1\theta_2+\sigma_0\tau_2(\theta_1-\psi_1)]+\frac{c_4}{n^2+1}[(1-\sigma_0n^2)\theta_4\psi_5-(1+\sigma_0n^2)\psi_4\theta_5]$$
$$-\frac{c_6}{n^2+1}[(1+3\sigma_0(1-n^2))(\theta_5\psi_7+\theta_6\psi_8)+(3\sigma_0(1-n^2)-1)(\psi_5\theta_7+\psi_6\theta_8)]$$
$$-\frac{\beta n\sigma_0\theta_2}{n^2+1}-\frac{h\theta_3}{n^2+1}+k\sigma_0\psi_3-(k+2k')\sigma_0\theta_3$$

$$\dot{\theta}_4(\sigma_0+\tfrac{1}{4}) = \frac{c_4}{4}[(1-3\sigma_0)(\theta_2\psi_6-\theta_3\psi_5)-(1+3\sigma_0)(\psi_2\theta_6-\psi_3\theta_5)+\sigma_0\tau_2(\psi_6-\theta_6)]-\frac{h\theta_4}{4}$$
$$+\frac{c_5}{4}[(1-3\sigma_0)(\theta_7\psi_{10}-\theta_8\psi_9)-(1+\sigma_03)(\psi_7\theta_{10}-\psi_8\theta_9)]+k\sigma_0\psi_4-(k+2k')\sigma_0\theta_4$$

$$\dot{\theta}_5(\sigma_0+\tfrac{1}{n^2+4}) = \frac{-c_2}{n^2+4}[(1-\sigma_0(n^2+3))\theta_1\psi_6-(1+\sigma_0(n^2+3))\psi_1\theta_6]+\frac{c_4}{n^2+4}[(1+\sigma_0(n^2-3))\theta_3\psi_4$$
$$+(\sigma_0(n^2-3)-1)\psi_3\theta_4]+\frac{\beta n\sigma_0\theta_6}{n^2+4}-\frac{h\theta_5}{n^2+4}+k\sigma_0\psi_5-(k+2k')\sigma_0\theta_5$$
$$+\frac{c_6}{n^2+4}[(1-3\sigma_0n^2)(\theta_3\psi_7-\theta_2\psi_8)-(1-3\sigma_0n^2)(\psi_3\theta_7-\psi_2\theta_8)-\sigma_0\tau_2(\psi_8-\theta_8)]$$

$$\dot{\theta}_6(\sigma_0+\tfrac{1}{n^2+4}) = \frac{c_2}{n^2+4}[(1-\sigma_0(n^2+3))\theta_1\psi_5-(1+\sigma_0(n^2+3))\psi_1\theta_5]-\frac{c_4}{n^2+4}[(1+\sigma_0(n^2-3)\theta_2\psi_4$$
$$+(\sigma_0(n^2-3)-1)\psi_2\theta_4+\sigma_0\tau_2(\psi_4-\theta_4)]-\frac{\beta n\sigma_0\theta_5}{n^2+4}-\frac{h\theta_6}{n^2+4}+k\sigma_0\psi_6-(k+2k')\sigma_0\theta_6$$
$$+\frac{c_6}{n^2+4}[(1-3\sigma_0n^2)(\theta_2\psi_7+\theta_3\psi_8)-(1+3\sigma_0n^2)(\psi_2\theta_7+\psi_3\theta_8)+\sigma_0\tau_2(\psi_7-\theta_7)]$$

$$\dot{\theta}_7(\sigma_0+\tfrac{1}{4n^2+1}) = \frac{-c_3}{4n^2+1}[(1-4\sigma_0n^2)\theta_1\psi_8-(1+4\sigma_0n^2)\psi_1\theta_8]-\frac{c_5}{4n^2+1}[(1-4\sigma_0n^2)\theta_5\psi_{10}-(1+4\sigma_0n^2)\psi_5\theta_{10}]$$
$$-\frac{c_6}{4n^2+1}[(1-3\sigma_0)(\theta_3\psi_5+\theta_2\psi_6)-(1+3\sigma_0)(\psi_3\theta_5+\psi_2\theta_6)+\sigma_0\tau_2(\psi_6-\theta_6)]+\frac{2n\beta\sigma_0\theta_8}{4n^2+1}-\frac{h\theta_7}{4n^2+1}$$
$$+k\sigma_0\psi_7-(k+2k')\sigma_0\theta_7$$

$$\dot{\theta}_8\left(\sigma_0+\tfrac{1}{4n^2+1}\right) = c_3\left[(1-4\sigma_0 n^2)\,\theta_1\psi_7-(1+4\sigma_0 n^2)\,\psi_1\theta_7\right]+\frac{c_5}{4n^2+1}\left[(1-4\sigma_0 n^2)\,\theta_4\psi_9\right.$$

$$\left.-(1+4\sigma_0 n^2)\,\psi_4\theta_9\right]-\frac{2n\beta\sigma_0\theta_7}{4n^2+1}\;\frac{-h\theta_8}{4n^2+1}+k\sigma_0\psi_8-(k+2k')\,\sigma_0\theta_8$$

$$+\frac{c_6}{4n^2+1}\left[(1-3\sigma_0)(\theta_2\psi_5-\theta_3\psi_6)-(1+3\sigma_0)(\psi_2\theta_5-\psi_3\theta_6)+\sigma_0 t_2(\psi_5-\theta_5)\right]$$

$$\dot{\theta}_9\left(\sigma_0+\tfrac{1}{4n^2+4}\right) = \frac{-c_4}{4n^2+4}\left[(1-\sigma_0(4n^2+3))\,\theta_1\psi_{10}-(1+\sigma_0(4n^2+3))\,\psi_1\theta_{10}\right]+\frac{2n\beta\sigma_0\theta_{10}}{4n^2+4}-\frac{h\theta_9}{4n^2+4}$$

$$\frac{-c_5}{4n^2+4}\left[(1-\sigma_0(4n^2+3))\,\theta_4\psi_8-(1+\sigma_0(4n^2+3))\,\psi_4\theta_8\right]+k\sigma_0\psi_9-(k+2k')\,\sigma_0\theta_9$$

$$\dot{\theta}_{10}\left(\sigma_0+\tfrac{1}{4n^2+4}\right) = \frac{+c_4}{4n^2+4}\left[(1-\sigma_0(4n^2+3))\,\theta_1\psi_9-(1+\sigma_0(4n^2+3))\,\psi_1\theta_9\right]-\frac{2n\beta\sigma_0\theta_9}{4n^2+4}-\frac{h\theta_{10}}{4n^2+4}$$

$$\frac{+c_5}{4n^2+4}\left[(1-\sigma_0(4n^2+3))\,\theta_4\psi_7-(1+\sigma_0(4n^2+3))\,\psi_4\theta_7\right]+k\sigma_0\psi_{10}-(k+2k')\,\sigma_0\theta_{10}$$

	INT	DISS	BETA
$\dot{\varphi}_1 = -\omega_1$	$-k'(\varphi_1-\phi_1)$	0	0
$\dot{\varphi}_2 = -\omega_2/n^2+1$	$-k'(\varphi_2-\phi_2)$	0	$+\beta n \varphi_3/n^2+1$
$\dot{\varphi}_3 = -\omega_3/n^2+1$	$-k'(\varphi_3-\phi_3)$	0	$-\beta n \varphi_2/n^2+1$
$\dot{\phi}_1 = \omega_1$	$+k'(\varphi_1-\phi_1)$	$-2k\phi_1$	0
$\dot{\phi}_2 = \omega_2/n^2+1$	$+k'(\varphi_2-\phi_2)$	$-2k\phi_2$	$+\beta n \phi_3/n^2+1$
$\dot{\phi}_3 = \omega_3/n^2+1$	$+k'(\varphi_3-\phi_3)$	$-2k\phi_3$	$-\beta n \phi_2/n^2+1$
$\dot{\omega}_1 = 0$	0	$-h\theta_1^*/\sigma_0 + h(\varphi_1-\phi_1)/2\sigma_0$	0
$\omega_2 = 0$	0	$+h(\varphi_2-\phi_2)/2\sigma_0$	0
$\omega_3 = 0$	0	$+h(\varphi_3-\phi_3)/2\sigma_0$	0

(7. 1)

TIME MEAN MODE II PROGNOSTIC (BUDGET) EQUATIONS. Variables without primes are time averages. The remaining terms appear on the following pages

	AD11	ad11	ad21
$\dot{\varphi}_1 =$	0	0	0
$\dot{\varphi}_2 =$	$+c_1 n^2 \varphi_1 \varphi_3 / n^2+1$	$+c_1 n^2 \varphi_1' \varphi_3' / n^2+1$	$+c_4 n^2 \varphi_4' \varphi_6' / n^2+1$
$\dot{\varphi}_3 =$	$-c_1 n^2 \varphi_1 \varphi_2 / n^2+1$	$-c_1 n^2 \varphi_1' \varphi_2' / n^2+1$	$-c_4 n^2 \varphi_4' \varphi_5' / n^2+1$
$\dot{\phi}_1 =$	0	0	0
$\dot{\phi}_2 =$	$c_1 n^2 \phi_1 \phi_3 / n^2+1$	$+c_1 n^2 \phi_1' \phi_3' / n^2+1$	$+c_4 n^2 \phi_4' \phi_6' / n^2+1$
$\dot{\phi}_3 =$	$-c_1 n^2 \phi_1 \phi_2 / n^2+1$	$-c_1 n^2 \phi_1' \phi_2' / n^2+1$	$-c_4 n^2 \phi_4' \phi_5' / n^2+1$
$\omega_1 =$	$-c_1(\varphi_2\phi_3 - \varphi_3\phi_2)/2\sigma_0$	$-c_1(\varphi_2'\phi_3' - \varphi_3'\phi_2')/2\sigma_0$	$-c_2(\varphi_5'\phi_6' - \varphi_6'\phi_5')/2\sigma_0$
$\omega_2 =$	$c_1(\varphi_1\phi_3 - \varphi_3\phi_1)/2\sigma_0$	$+c_1(\varphi_1'\phi_3' - \varphi_3'\phi_1')/2\sigma_0$	$+c_4(\varphi_4'\phi_6' - \varphi_6'\phi_4')/2\sigma_0$
$\omega_3 =$	$-c_1(\varphi_1\phi_2 - \varphi_2\phi_1)/2\sigma_0$	$-c_1(\varphi_1'\phi_2' - \varphi_2'\phi_1')/2\sigma_0$	$-c_4(\varphi_4'\phi_5' - \varphi_5'\phi_4')/2\sigma_0$

	ad12	ad22	TCP2
$\dot{\varphi}_1 =$	0	0	0
$\dot{\varphi}_2 =$	$+3(1-n^2)c_6(\varphi_5'\varphi_8' - \varphi_6'\varphi_7')/n^2+1$	0	0
$\dot{\varphi}_3 =$	$-3(1-n^2)c_6(\varphi_5'\varphi_7' - \varphi_6'\varphi_8')/n^2+1$	0	0
$\dot{\phi}_1 =$	0	0	$-c_1 \hbar_2 \phi_3 / n^2+1$
$\dot{\phi}_2 =$	$3(1-n^2)c_6(\phi_5'\phi_8' - \phi_6'\phi_7')/n^2+1$	0	0
$\dot{\phi}_3 =$	$-3(1-n^2)c_6(\phi_5'\phi_7' - \phi_6'\phi_8')/n^2+1$	0	$+c_1 \hbar_2 \phi_1 / n^2+1$
$\omega_1 =$	$-c_3(\varphi_7'\phi_8' - \varphi_8'\phi_7')/2\sigma_0$	$-c_4(\varphi_9'\phi_{10}' - \varphi_{10}'\phi_9')/2\sigma_0$	0
$\omega_2 =$	$+c_6(\varphi_6'\phi_7' - \varphi_7'\phi_6' - \varphi_5'\phi_8' + \varphi_8'\phi_5')/2\sigma_0$	0	0
$\omega_3 =$	$+c_6(\varphi_6'\phi_8' - \varphi_8'\phi_6' + \varphi_5'\phi_7' - \varphi_7'\phi_5')/2\sigma_0$	0	0

$$\dot{\Psi}_1 = c_1 \hbar_2 (\Theta_3 - \Psi_3) - k(\Psi_1 - \epsilon_1)$$

$$\dot{\Psi}_2 = \frac{c_1 n^2}{n^2+1}(\Psi_1\Psi_3 + \epsilon_1\Theta_3) + \frac{\beta n \Psi_3}{n^2+1} - k(\Psi_2 - \Theta_2) + \frac{c_4 n^2}{n^2+1}(\Psi_4\Psi_6 + \Theta_4\Theta_6)$$

$$+ \frac{3c_6(1-n^2)}{n^2+1}(\Psi_5\Psi_8 + \Theta_5\epsilon_8 - \Psi_6\Psi_7 - \Theta_6\Theta_7)$$

$$\dot{\Psi}_3 = \frac{-c_1}{n^2+1}[n^2(\Psi_1\Psi_2 + \epsilon_1\Theta_2) + \hbar_2(\Theta_1 - \Psi_1)] - \frac{\beta n \Psi_2}{n^2+1} - k(\Psi_3 - \Theta_3) - \frac{c_4 n^2}{n^2+1}(\Psi_4\Psi_5 + \Theta_4\Theta_5)$$

$$- \frac{3c_6(1-n^2)}{n^2+1}(\Psi_5\Psi_7 + \Theta_5\Theta_7 + \Psi_6\Psi_8 + \Theta_6\Theta_8)$$

$$\dot{\Theta}_1(\sigma_c+1) = c_1[(\Theta_2\Psi_3 - \Psi_2\Theta_3) + \sigma_0\hbar_2(\Psi_3 - \Theta_3)] + h(\Theta_1^* - \Theta_1) + k\sigma_0\Psi_1 - \sigma_0(k+2k')\Theta_1$$

$$+ c_2(\Theta_5\Psi_6 - \Theta_6\Psi_5) + c_3(\Theta_7\Psi_8 - \Psi_7\Theta_8) + c_4(\Theta_9\Psi_{10} - \Psi_9\Theta_{10})$$

$$\dot{\Theta}_2(\sigma_0 + 1/n^2+1) = \frac{-c_1}{n^2+1}[(1-\sigma_0 n^2)\Theta_1\Psi_3 - (1+\sigma_0 n^2)\Psi_1\Theta_3] + \frac{\beta n \sigma_0 \Theta_3}{n^2+1} - \frac{h\Theta_2}{n^2+1} - (k+2k')\sigma_0\Theta_2$$

$$\frac{-c_4}{n^2+1}[(1-\sigma_0 n^2)\Theta_4\Psi_6 - (1+\sigma_0 n^2)\Psi_4\Theta_6]$$

$$+ \frac{c_6}{n^2+1}[(1+3\sigma_0(1-n^2))(\Theta_5\Psi_8 - \Theta_6\Psi_7) + (3\sigma_0(1-n^2)-1)(\Theta_8\Psi_5 - \Theta_7\Psi_6)]$$

$$\dot{\Theta}_3(\sigma_0 + 1/n^2+1) = \frac{c_1}{n^2+1}[(1-\sigma_0 n^2)\Theta_1\Psi_2 - (1+\sigma_0 n^2)\Psi_1\Theta_2 + \sigma_0\hbar_2(\Theta_1 - \Psi_1)] - \frac{\beta n \sigma_0 \Theta_2}{n^2+1}$$

$$+ \frac{c_4}{n^2+1}[(1-\sigma_0 n^2)\Theta_4\Psi_5 - (1+\sigma_0 n^2)\Psi_4\Theta_5] - \frac{h\Theta_3}{n^2+1} + k\sigma_0\Psi_3 - (k+2k')\sigma_0\Theta_3$$

$$\frac{-c_6}{n^2+1}[(1+3\sigma_0(1-n^2))(\Theta_5\Psi_7 + \Theta_6\Psi_8) + (3\sigma_0(1-n^2)-1)(\Psi_5\Theta_7 + \Psi_6\Theta_8)]$$

MODE II EQUATIONS (10.1)

APPENDIX I

HOW TO WRITE A HIGHLY TRUNCATED SPECTRAL MODEL

Since the nonlinear interaction between externally forced planetary scale waves and travelling baroclinic disturbances appears to be essential for the occurrence of weather regimes, we wish to develop a model which retains its nonlinearity, yet is sufficiently simple to provide understanding of the important mechanisms. The model which best appears to satisfy these criteria is the highly truncated spectral two-layer model, first developed for study of atmospheric phenomena by Lorenz (1960a), and also used by Lorenz (1962,1963), Young (1966), Yau (1977,1980), Charney and DeVore (1979), and Charney and Straus (1980) for further studies. We shall use the approach devised by Lorenz (1960a) to formulate the simplest possible model which contains the necessary physics and degrees of freedom, as postulated by our hypothesis, to establish weather regimes. The model must have zonally inhomogeneous external forcing, be able to represent both the planetary and synoptic scale waves, and be capable of baroclinic instability (which requires some vertical structure). Since weather regimes are primarily large-scale phenomena (planetary and synoptic scale), their dynamics will be approximated by the quasi-geostrophic system of equations which consist of the quasi-geostrophic vorticity equation,

conservation of potential temperature, the hydrostatic approximation, and continuity. For frictionless, adiabatic flow they may be written as:

$$\partial \nabla^2\Psi/\partial t + J(\Psi, \nabla^2\Psi) + \beta\partial\Psi/\partial x + f\nabla^2\chi = 0$$

$$\partial\Theta/\partial t + J(\Psi, \Theta) + \nabla\chi\nabla\Theta + w\,\partial\Theta/\partial p = 0$$

$$\partial\Phi/\partial p = -\alpha = -c_p\,\partial/\partial p(p/p_\infty)^\kappa\Theta$$

$$\partial w/\partial p + \nabla^2\chi = 0$$

where Ψ is the geostrophic streamfunction gz/f, χ is the velocity potential, Φ is the geopotential or gz, Θ is the potential temperature, p_∞ a reference pressure (usually 1000 mb.), κ the ratio $R/c_p = 2/7$, w the change of pressure following the motion (dp/dt), c_p the heat capacity at constant pressure, α the specific volume, f the coriolis parameter $2\Omega\sin\phi_o$, where ϕ_o is some specified latitude, β the gradient of f, $1/a_o(df/d\phi)$ where 'a_o' is the radius of the earth, and J(M,N) is the jacobian $\partial M/\partial x\,\partial N/\partial y - \partial M/\partial y\,\partial N/\partial x$. The quantities $\nabla^2\Psi$ and $\nabla^2\chi$ are the vorticity and divergence, respectively, thus $\nabla\Psi$ and $\nabla\chi$ are proportional to the magnitude of the nondivergent and irrotational winds. The quantity $\nabla^2\chi\nabla\theta + w\,\partial\Theta/\partial p$ is the three dimensional advection of Θ by the irrotational wind.

The simplest possible model which is capable of baroclinic instability is the two-layer model. The two-layer approximation is made by representing the atmosphere as two vertically stacked homogeneous fluids of different density of equal depth with lighter fluid on top, or equivalently, a

three dimensional fluid with constant vertical shear. The two layer equations are obtained by writing the vorticity and thermodynamic equations for each layer where one assumes a linear vertical profile of the dependent variables Ψ, Θ, and χ. The surface will be designated by a subscript 4, the middle of the lower layer by subscript 3, the interface between the layers (or halfway through the depth of the model) by subscript 2, the middle of the upper layer by subscript 1, and the top by 0. The corresponding pressure levels are somewhat arbitrary depending upon whether the top of the model is chosen to be at 0 mb. or 200 mb. The surface is usually chosen to be 1000 mb. With the above conventions, the frictionless, adiabatic, two-layer quasi-geostrophic system of equations become:

$$\partial \nabla^2 \Psi_3 / \partial t + J(\Psi_3, \nabla^2 \Psi_3) + \beta \partial \Psi_3 / \partial x + f \nabla^2 \chi_3 = 0$$

$$\partial \nabla^2 \Psi_1 / \partial t + J(\Psi_1, \nabla^2 \Psi_1) + \beta \partial \Psi_1 / \partial x + f \nabla^2 \chi_1 = 0$$

$$\partial \Theta_3 / \partial t + J(\Psi_3, \Theta_3) + \nabla(\Theta_3 \nabla \chi_3) = 0$$

$$\partial \Theta_1 / \partial t + J(\Psi_1, \Theta_1) + \nabla(\Theta_1 \nabla \chi_1) = 0$$

where the three dimensional advection by the irrotational wind $\nabla\chi\nabla\theta + w\,\partial\theta/\partial p$ has been written as $\nabla(\Theta\nabla\chi)$ via continuity where ∇ is the horizontal del operator and ∇ is the three dimensional del operator.

It is essential for this study to include heating, topography (or some other source of zonal inhomogenity), frictional dissipation, and heat transfer. These processes

will be added to the frictionless, adiabatic equations through the following parameterizations: Frictional dissipation will be modelled by Ekman pumping, thus the drag on the lower layer will be proportional to the vorticity of the lower layer and the vorticity difference between the layers. The constants of proportionality at the surface and between the layers are not, however, assumed to be the same. The heat transfer will be approximated by Newtonian cooling, a simple proportionality constant times the temperature difference between the layers as well as the temperature difference between the lower layer and a prescribed surface temperature. Again, the proportionality constants will not be assumed to be the same. The effects of topography will be to induce a vertical motion proportional to the magnitude of the surface (lower layer) velocity times the slope of the terrain which acts to stretch or compress vortex tubes, and thus will be incorporated in the Jacobian. The driving mechanism (or heating) for the model is taken into account by fixing the surface radiative equilibrium temperature profile, which will simulate the earth's radiative equilibrium equator to pole temperature gradient. The additional terms representing the parameterized effects of external forcing are:

$$\partial\theta_3/\partial t = -2h''\theta_3 + 2h''\theta_3^* + h'''(\theta_1-\theta_3)$$

$$\partial\theta_1/\partial t = -h'''(\theta_1-\theta_3)$$

$$\partial\nabla^2\psi_3/\partial t = -J(\psi_3, f\hbar_0/H) - 2k''\nabla^2\psi_3 + k'''\nabla^2(\psi_1-\psi_3)$$

$$\partial\nabla^2\psi_1/\partial t = -k'''\nabla^2(\psi_1-\psi_3)$$

where 2h'' is the coefficient of heat transfer between the lower layer and the surface, h''' is the coefficient of heat transfer between the lower layer and the upper layer, 2k'' is the coefficient of frictional dissipation between the lower layer and the surface, k''' is the coefficient of frictional dissipation between the lower layer and the upper layer, θ_3^* is the prescribed radiative equilibrium surface temperature, h_0 is the topographic height profile, $h_0 = h_0(x,y)$, and H is the depth of each layer. The Jacobian $J(\psi_3, f h_0/H)$ is accurate only if $h_0/H \ll 1$. The actual nonlinear expression $J(\psi_3, f h_0/(H-h_0))$ has been linearized with the assumption that the height of the topography is small.

It is convenient to rearrange the dependent variables ψ_3, ψ_1, θ_3, and θ_1 into variables representing

mean vorticity $\nabla^2\psi = \nabla^2(\psi_1 + \psi_3)/2$

vertical shear $\nabla^2\tau = \nabla^2(\psi_1 - \psi_3)/2$

mean potential temperature $\theta = (\theta_1 + \theta_3)/2$

static stability $\sigma = (\theta_1 - \theta_3)/2$

mean divergence = 0; $\chi_1 = -\chi_3$.

The system can be closed by relating τ and θ via the geostrophic thermal wind relation for a two layer model and a perfect gas. This transformation produces the system of equations used by Lorenz (1963) with the addition of the beta-effect and topography. The system is as follows:

$$\partial\theta/\partial t + J(\psi,\theta) + J(\tau,\sigma) - \nabla(\sigma\nabla\chi) = h''(\theta^{*}-\theta)$$

$$\partial\sigma/\partial t + J(\psi,\sigma) + J(\tau,\theta) - \nabla(\theta\nabla\chi) = -h''(\theta^{*}-\theta) - 2h'''\sigma$$

$$\partial\nabla^2\psi/\partial t + J(\psi,\nabla^2\psi) + J(\tau,\nabla^2\tau) + \beta\partial\psi/\partial x = -.5\,J(\psi, f\hbar_0/H) + .5\,J(\tau, f\hbar_0/H) + k''\nabla^2(\tau-\psi)$$

$$\partial\nabla^2\tau/\partial t + J(\psi,\nabla^2\tau) + J(\tau,\nabla^2\psi) + \beta\partial\tau/\partial x - f\nabla^2\chi = .5\,J(\psi, f\hbar_0/H) - .5\,J(\tau, f\hbar_0/H) - k''\nabla^2\psi - 2k'''\nabla^2\tau$$

$$\nabla^2\tau = -(c_p b^{*}/2f)\nabla^2\theta \quad \text{(thermal wind)}$$

where $b^{*}=(p_1/p_{00})^{\kappa} - (p_3/p_{00})^{\kappa}$ which then depends upon the specified pressure of the model top.

We shall simplify the system by approximating the static stability as a constant. The primary reason for doing such is mathematical simplicity. Fixing the static stability does not allow for the occurrence of static stabilization through the release of baroclinicity, Lorenz (1960b). Assuming σ to be constant, the system simplifies to:

$$\partial\theta/\partial t + J(\psi,\theta) - \sigma\nabla^2\chi = h''(\theta^{*}-\theta)$$

$$\partial\nabla^2\psi/\partial t + J(\psi,\nabla^2\psi) + J(\tau,\nabla^2\tau) + \beta\partial\psi/\partial x = -.5\,J(\psi, f\hbar_0/H) + .5\,J(\tau, f\hbar_0/H) + k''\nabla^2(\tau-\psi)$$

$$\partial\nabla^2\tau/\partial t + J(\psi,\nabla^2\tau) + J(\tau,\nabla^2\psi) + \beta\partial\tau/\partial x - f\nabla^2\chi = .5\,J(\psi, f\hbar_0/H) - .5\,J(\tau, f\hbar_0/H) - k''\nabla^2\psi - 2k'''\nabla^2\tau$$

$$\nabla^2\tau = -(c_p b^{*}/2f)\nabla^2\theta$$

(Note that when the static stability is assumed constant, the heat transfer coefficient between layers drops out).

The Spectral Equations

The variables η_0, Ψ, Θ, γ, and $\nabla^2\chi$ are non-dimensionalized and expanded in an appropriate set of orthogonal functions F_i, given by (2.3). These series are substituted back into the original equations. The major mathematical difficulty aries in the nonlinear terms where one obtains products of eignefunctions. However, these products can also be further expressed in a series of identical eigenfunctions:

$$L^2 J(F_j, F_k) = \sum_i c_{ijk} F_i$$

$$\text{where} \quad c_{ijk} = L^2/2\pi^2 \iint F_i J(F_j, F_k)\, dx\, dy.$$

The quantities c_{ijk} are referred to as interaction coefficients which are calculated in Appendix II.

Likewise for the beta term:

$$L\,\partial F_i/\partial x = \sum_j b_{ij} F_j$$

$$\text{where} \quad b_{ij} = L/2\pi \iint F_i\, \partial F_j/\partial x\, dx\, dy.$$

With the above definitions, the general system of equations are then given by (2.4). The equations can be further simplified by eliminating w_i between the two Θ_i equations. The system of equations becomes:

$$\dot{\Theta}_i(\sigma_0 + 1/a_i^2) = \sum_j \sum_{j>k} c_{ijk}[(1 + \sigma_0(a_j^2 - a_k^2))\Theta_j\Psi_k +$$
$$((a_j^2 - a_k^2)\sigma_0 - 1)\Psi_j\Theta_k + \sigma_0\pi_j(\Psi_k - \Theta_k) + \sigma_0\pi_k(\Theta_j - \Psi_j)]/a_i^2 +$$
$$\beta\sigma_0/a_i^2 \sum_j b_{ij}\Theta_j + h/a_i^2(\Theta_i^* - \Theta_i) + k\sigma_0\Psi_i - \sigma_0(k + 2k')\Theta_i$$

$$\dot{\Psi}_i = \sum_j \sum_{j>k} c_{ijk}[(a_j^2 - a_k^2)(\Psi_j\Psi_k + \Theta_j\Theta_k) - \pi_j(\Psi_k - \Theta_k) - \pi_k(\Theta_j - \Psi_k)]/a_i^2$$
$$+ \beta/a_i^2 \sum_j b_{ij}\Psi_j - k(\Psi_i - \Theta_i)$$

The actual form of the eigenfunctions depends upon the geometry of the model and the boundary conditions. If there is a boundary, we require that there be no flow across the boundary (no flow through the walls) or, defining s as the boundary,

$$\partial F_i / \partial s = 0 \quad \text{at boundary.}$$

We also require that there be no net torque or momentum drag on the boundary,

$$\int \partial F_i / \partial s \, ds = 0 \quad \text{along boundary.}$$

Ideally, one should choose a spherical domain for the model, but we shall approximate the earth's sphericity using the beta-plane approximation and choose as our domain a periodic channel whose north and south walls are separated by a distance πL or π non-dimensionally. The eastward coordinate will be in the x-direction and the northward coordinate in the

y-direction. The eigenfunctions for such a rectangular geometry are the simple two- dimensional harmonic functions.

The boundary conditions of no flow through the walls and no net torque along the wall determine which of the complete set of harmonic eigenfunctions can be used. What has yet to be determined is the level of truncation.

In order to test the hypothesis, a sufficient number of degrees of freedom must be retained so that the planetary and synoptic-scale waves are represented and can interact directly with each other. These minimum requirements will be met if the model is truncated at two waves in both the meridional direction (y) and the latitudinal direction (x). The relationship between the meridional and latitudinal scales will be determined by the parameter n, whose scaling is discussed in Chapter 3. The eigenfunctions which will be retained are given by (2.5).

Zonally inhomogeneous topographic forcing will be applied only in the largest possible scale (F_2), as discussed in Chapter 2, while all other forms of zonally inhomogeneous forcing, such as heat sources and sinks, will not be considered. Driving wil be accomplished by fixing a zonally homogeneous radiative equilibrium temperature profile from the south to north wall.

Programming the Model

The following is the basic FORTRAN program for the model used in this study:

```
C
C  Set parameters
C
      DELT=.135  (time step)
      FK= .04    (surface friction)
      FK1=.005   (internal friction; between layers)
      BETA=.22   (beta parameter)
      TOP2=.15   (half the topographic parameter)
      H=.045     (heat transfer coefficient)
      SIG=.15    (static stability)
     *T1F=.12    (equator to pole radiative equilibrium temperature)
      RN=1.22    ("zonal" wavenumber)
C
C  Interaction coefficients
C
      C1=-8.*(2.**.5)*RN/(3.*3.141592654)
      C2=C1*4./5.
      C3=C1*2.
      C4=C2*2.
      C5=C4*2.
      C6=RN*3./2.
C
C  Eigenvalues
C
      E1=1./(RN*RN+1.)
```

* TF(I) where I=1,2,...,10 are used to represent θ_I^*. In all cases TF(1) = T1F ≠ 0 and TF(I) for I = 2,...,10 = 0.

```
      E2=1./(RN*RN+4.)
      E3=1./(4.*RN*RN+1.)
      E4=1./(4.*RN*RN+4.)
      E5=-RN*RN
      E6=3.*E5+3.
      E7=E5-3.
      E8=-E5-3.
      E9=3.*E5
      E10=4.*E5
      E11=E10-3.
      E12=SIG*E5
      E13=SIG*E6
      E14=SIG*E7
      E15=SIG*E8
      E16=SIG*E9
      E17=SIG*E10
      E18=SIG*E11
C
C  Topography, frictional, and SIG combinations that occur
 frequently
C  in equations and can therefore be preset to save computing
 time
C
      TOS2=SIG*TOP2
      TOS7=SIG*TOP7
      F1=SIG*(FK+2.*FK1)
```

```
      F2=SIG*FK
      SIG0=1./(SIG+1.)
      SIG1=1./(SIG+E1)
      SIG2=1./(SIG+E2)
      SIG3=1./(SIG+E3)
      SIG4=1./(SIG+E4)
      R0=E1*C6
      R1=E2*C6
      R2=3.*SIG+1.
      R3=3.*SIG-1.
C
C  Time stepping (Lorenz N-cycle scheme where N=4)
C  Y(I) contains variables
C
      DDELT=DELT*4.
      RD=1./DELT
      RDD=1./DDELT
      DO 30 K=1,ISTEP
              WRITE(9,200)K1,(Y(I),I=1,20)
200           FORMAT(1X,I7,1X,10(F7.4,1X),/,9X,10(F7.4,1X)/)
              A1=0.
              B1=RD
              DO 35 J=1,4

C
C  SYSTM subroutine contains model eqautions
```

```
C
                        CALL SYSTM
                        DO 36 I=IL,IM
                                Z(I)=A1*Z(I)
                                Z(I+10)=A1*Z(I+10)
                                Z(I)=(Z(I)+F(I))/B1
                                Z(I+10)=(Z(I+10)+F(I+10))/B1
                                Y(I)=Y(I)+Z(I)
36                              Y(I+10)=Y(I+10)+Z(I+10)
                        B1=B1-RDD
35                      A1=A1-RDD
30              CONTINUE
      END
**
      SUBROUTINE SYSTM
      S1=Y(1)   = Ψ1
      S2=Y(2)   = Ψ2
      S3=Y(3)   = Ψ3
      S4=Y(4)   = Ψ4
      S5=Y(5)   = Ψ5
      S6=Y(6)   = Ψ6
      S7=Y(7)   = Ψ7
      S8=Y(8)   = Ψ8
      S9=Y(9)   = Ψ9
      S10=Y(10)  = Ψ10
      T1=Y(11)   = Θ1
```

```
      T2=Y(12)  = Θ2
      T3=Y(13)  = Θ3
      T4=Y(14)  = Θ4
      T5=Y(15)  = Θ5
      T6=Y(16)  = Θ6
      T7=Y(17)  = Θ7
      T8=Y(18)  = Θ8
      T9=Y(19)  = Θ9
      T10=Y(20)  = Θ10
C
C  Model Wave 1
C
      B=BETA*E1*RN
      F(1)=C1*TOP2*(T3-S3)-FK*(S1-T1)
      F(2)=-E1*C1*E5*(S1*S3+T1*T3)+B*S3-FK*(S2-T2)
      F(3)=E1*C1*(E5*(S1*S2+T1*T2)+TOP2*(S1-T1))-B*S2-FK*(S3-T3)
      F(11)=C1*(T2*S3-S2*T3+TOS2*(S3-T3))+H*(TF(1)-T1)+F2*S1-F1*T1
      F(11)=F(11)*SIG0
      F(12)=(E1*(-C1*(T1*S3*(E12+1.)+S1*T3*(E12-1.))+H*(TF(2)-T2))+S
     1IG*B*T3+F2*S2-F1*T2)*SIG1
      F(13)=(E1*(C1*(T1*S2*(E12+1.)+S1*T2*(E12-1.)+TOS2*(T1-S1))+H*T
     1TF(3)-T3))-B*SIG*T2+F2*S3-F1*T3)*SIG1
      IF(MM.EQ.1) GO TO 100
C
C  Mode 2  Wave 1
C
```

```
      B=BETA*RN*E2
      F(2)=F(2)-E1*C4*E5*(S4*S6+T4*T6)
      F(3)=F(3)+E1*C4*E5*(S4*S5+T4*T5)
      F(4)=.25*C4*(3.*(S3*S5+T3*T5-S2*S6-T2*T6)+TOP2*(T6-S6))-
     1FK*(S4-T4)
      F(5)=E2*(C4*E8*(S3*S4+T3*T4)-C2*E7*(S1*S6+T1*T6))+B*S6-FK*(S5-
     1T5)
      F(6)=E2*(C2*E7*(S1*S5+T1*T5)-C4*(E8*(S2*S4+T2*T4)+TOP2*(T4-S4)
     1))-B*S5-FK*(S6-T6)
      F(11)=F(11)+C2*(T5*S6-S5*T6)*SIG0
      F(12)=F(12)-E1*C4*(T4*S6*(E12+1.)+S4*T6*(E12-1.))*SIG1
      F(13)=F(13)+E1*C4*(T4*S5*(E12+1.)+S4*T5*(E12-1.))*SIG1
      F(14)=(.25*(C4*(R2*(S3*T5-S2*T6)+R3*(T3*S5-T2*S6)+TOS2*(S6-T6
     1))+H*(TF(4)-T4))+F2*S4-F1*T4)/(SIG+.25)
      F(15)=(E2*(C4*(T3*S4*(E15+1.)+S3*T4*(E15-1.))-C2*(T1*S6*(E14+1
     1.)+S1*T6*(E14-1.))+H*(TF(5)-T5))+B*SIG*T6+F2*S5-F1*T5)*SIG2
      F(16)=(E2*(C2*(T1*S5*(E14+1.)+S1*T5*(E14-1.))-C4*(T2*S4*(E15+.
     1.)+S2*T4*(E15-1.)+TOS2*(S4-T4))+H*(TF(6)-T6))-B*SIG*T5+F2*S6-
     F1*
     2T6)*SIG2
      IF(MM.EQ.2) GO TO 100
C
C  Mode 1  Wave 2
C
```

```
      B=BETA*E3*2.*RN
      F(1)=F(1)+C3*TOP7*(T8-S8)
      F(2)=F(2)+RO*(E6*(S5*S8+T5*T8-S6*S7-T6*T7)-TOP7*(S6-T6))
      F(3)=F(3)-RO*(E6*(S5*S7+T5*T7+S6*S8+T6*T8)+TOP7*(S5-T5))
      F(5)=F(5)+R1*(E9*(S3*S7+T3*T7-S2*S8-T2*T8)-TOP2*(T8-S8)+TO
     1P7*(S3-T3))
      F(6)=F(6)+R1*(E9*(S3*S8+T3*T8+S2*S7+T2*T7)+TOP2*(T7-S7)+TO
     1P7*(S2-T2))
      F(7)=E3*(C6*(3.*(S2*S6+T2*T6+S3*S5+T3*T5)-TOP2*(T6-S6))-C3*E1
     10*(S1*S8+T1*T8))+B*S8-FK*(S7-T7)
      F(8)=E3*(C6*(3.*(S3*S6+T3*T6-S2*S5-T2*T5)+TOP2*(T5-S5))+C3*(E1
     10*(S1*S7+T1*T7)+TOP7*(S1-T1)))-B*S7-FK*(S8-T8)
      F(11)=F(11)+C3*(S8*T7-S7*T8+TOS7*(S8-T8))*SIG0
      F(12)=F(12)+RO*((E13+1.)*(T5*S8-T6*S7)+(E13-1.)*(S5*T8-S6*T7)-
     1TOS7*(T6-S6))*SIG1
      F(13)=F(13)-RO*((E13+1.)*(T5*S7+T6*S8)+(E13-1.)*(S5*T7+S6*T8)-
     1TOS7*(T5-S5))*SIG1
      F(15)=F(15)+R1*((E16+1.)*(T3*S7-T2*S8)+(E16-1.)*(S3*T7-S2*T8)-
     1TOS2*(S8-T8)+TOS7*(T3-S3))*SIG2
      F(16)=F(16)+R1*((E16+1.)*(T2*S7+T3*S8)+(E16-1.)*(S2*T7+S3*T8)+
     1TOS2*(S7-T7)+TOS7*(T2-S2))*SIG2
      F(17)=(E3*(C6*(R2*(S3*T5+S2*T6)+R3*(T3*S5+T2*S6)-TOS2*(S6-T6))

 1-C3*(T1*S8*(E17+1.)+S1*T8*(E17-1.))+H*(TF(7)-T7))+B*SIG*T8+F2
*S7-F
     21*T7)*SIG3
```

```
      F(18)=(E3*(C6*(R2*(S3*T6-S2*T5)+R3*(T3*S6-T2*S5)+TOS2*(S5-T5))

 1+C3*(T1*S7*(E17+1.)+S1*T7*(E17-1.)+TOS7*(T1-S1))+H*(TF(8)-T8)
)-B
     2*SIG*T7+F2*S8-F1*T8)*SIG3
      IF(MM.EQ.3) GO TO 100
C
C  Mode 2  Wave 2
C
      B=BETA*E4*RN*2.
      F(4)=F(4)+.25*C5*(3.*(S8*S9+T8*T9-S7*S10-T7*T10)+TOP7*(T10-S1)
     1))
      F(7)=F(7)-C5*E3*E10*(S4*S10+T4*T10)
      F(8)=F(8)+C5*E3*E10*(S4*S9+T4*T9)
      F(9)=-E4*E11*(C4*(S1*S10+T1*T10)+C5*(S4*S8+T4*T8))+B*S10-
     1FK*(S9-T9)
      F(10)=E4*(C4*(S1*S9+T1*T9)*E11+(TOP7*(S4-T4)+E11*(S4*S7+T4*T7)
     1)*C5)-B*S9-FK*(S10-T10)
      F(11)=F(11)+C4*(S10*T9-S9*T10)*SIG0
      F(14)=F(14)+.25*(C5*(R2*(S8*T9-S7*T10)+R3*(T8*S9-T7*S10)+TOS7*
     1(S10-T10)))/(SIG+.25)
      F(17)=F(17)-E3*C5*((E17+1.)*T4*S10+(E17-1.)*S4*T10)*SIG3
      F(18)=F(18)+E3*C5*((E17+1.)*T4*S9+(E17-1.)*S4*T9)*SIG3
      F(19)=(-E4*(C4*((E18+1.)*T1*S10+(E18-1.)*S1*T10)+C5*((E18+1.)*
     1T4
```

```
 1*S8+(E18-1.)*S4*T8)-H*(TF(9)-T9))+B*SIG*T10+F2*S9-F1*T9)*SIG4
      F(20)=(E4*(C4*((E18+1.)*T1*S9+(E18-1.)*S1*T9)+C5*((E18+1.)*T4*
     1S7
 1+(E18-1.)*S4*T7+TOS7*(T4-S4))+H*(TF(10)-T10))-B*SIG*T9+F2*S10
-
     2F1*T10)*SIG4
100   RETURN
      END
```

Have fun and kiss many guinea pigs. Especially cute black ones like Gÿannea piggy.

APPENDIX II

CALCULATION OF THE INTERACTION COEFFICIENTS

The interaction coefficient c_{ijk} is defined as

$$1/2\pi^2 \int_0^{\pi}\int_0^{2\pi} F_i \left(\partial F_j / \partial x \;\; \partial F_k / \partial y - \partial F_j / \partial y \;\; \partial F_k / \partial x \right)$$

where $c_{ijk} = -c_{jik} = c_{kij}$ etc. If we first consider wave-wave interactions only, F_i, F_j, and F_k take the following possible forms:

$$F_i = 2 \begin{matrix} \text{sinmy} \\ \text{sindx} \end{matrix} \begin{matrix} [\text{cosdx}] \\ [\text{sindx}] \end{matrix}$$

$$F_j = 2 \begin{matrix} \text{sinay} \\ \text{sinex} \end{matrix} \begin{matrix} [\text{cosex}] \\ [\text{sinex}] \end{matrix}$$

$$F_k = 2 \begin{matrix} \text{sinby} \\ \text{sinfx} \end{matrix} \begin{matrix} [\text{cosfx}] \\ [\text{sinfx}] \end{matrix}$$

where m, a, b = 1 or 2 and d, e, f = n or 2n. This gives four possible Jacobians

$$J\left(2 \begin{matrix} \text{sinay} \\ \text{sinex} \end{matrix} \begin{matrix} [\text{cosex}] \\ [\text{sinex}] \end{matrix}, \; 2 \begin{matrix} \text{sinby} \\ \text{sinfx} \end{matrix} \begin{matrix} [\text{cosfx}] \\ [\text{sinfx}] \end{matrix} \right)$$

which can be expanded into the following forms:

1 J(2 sinay cosex, 2 sinby cosfx) =

4(-be sinay cosby sinex cosfx + af cosay sinby cosex sinfx)

2 J(2 sinay cosex, 2 sinby sinfx) =

4(-be sinay cosby sinex sinfx - af cosay sinby cosex cosfx)

3 J(2 sinay sinex, 2 sinby cosfx) =

4(be sinay cosby cosex cosfx + af cosay sinby sinex sinfx)

4 J(2 sinay sinex, 2 sinby sinfx) =

4(be sinay cosby cosex sinfx - af cosay sinby sinex cosfx)

The interaction coefficients are given by c_{ijk} =

$$1/2\pi^2 \int_0^{\pi} \int_0^{2\pi} 8 \ (\text{sinmy sindx}) \times \begin{matrix} \text{cosdx} \\ \text{cosex sinfx} \\ -\text{cosex cosfx} \\ -\text{sinex cosfx} \end{matrix} \left(\text{af cosay sinby sinex sinfx} + \text{be sinay cosby cosex cosfx} \right) \begin{matrix} -\text{sinex cosfx} \\ -\text{sinex sinfx} \\ \text{cosex sinfx} \end{matrix}$$

Only three possible integrals over x are non zero in the limit from 0 to 2π and likewise for integrals over y from 0 to π when m, a, b are 1 or 2 and d, e, f are n or 2n.

$$1)\quad \int_0^{2\pi} \cos nx \cos nx \cos 2nx\, dx = \pi/2$$

$$\int_0^{\pi} \cos y \cos y \cos 2y\, dy = \pi/4$$

$$2)\quad \int_0^{2\pi} \cos nx \sin nx \cos 2nx\, dx = \pi/2$$

$$\int_0^{\pi} \cos y \sin y \sin 2y\, dy = \pi/4$$

$$3)\quad \int_0^{2\pi} \sin nx \sin nx \cos 2nx\, dx = -\pi/2$$

$$\int_0^{\pi} \sin y \sin y \cos 2y\, dy = -\pi/4$$

We consider only those combinations which are non zero over the x integration first. From the #1 Jacobian, we have

$$\iint (1/2\pi^2)\, 2 \sin my \begin{matrix}\cos dx \\ \sin dx\end{matrix} J(2 \sin ay \cos ex,\ 2 \sin by \cos fx)$$

which gives:

$$\#1\quad 8/2\pi^2 \int_0^{\pi}\int_0^{2\pi} [af \sin my \cos ay \sin by \begin{matrix}\cos dx \\ (\sin dx \cos ex \sin fx) -\end{matrix}$$

$$be \sin my \sin ay \cos by \begin{matrix}\cos dx \\ (\sin dx \sin ex \cos fx)]\end{matrix}$$

where d, e, f are determined from the eigenfunctions F_i, F_j, F_k. (Care must be taken to remember that the Jacobian takes derivatives of the eigenfunctions F_i, F_j, F_k when seeking non-zero combinations of i, j, k). Since all permutations change only the sign of the interaction coefficient and non-zero combinations are such that two of d, e, f are equal while the remaining constant is double, we will choose d=e=n and f=2n. Then there is no combination of eigenfunctions

whose x-dependent part for i, j, k corresponds to cos-cos-cos2, respectively, that leads to non-zero interactions, but sin-cos-cos2 combinations do. They are:

3 5 7 3 5 9 6 2 7 6 2 9.

In Jacobian #2, we have

$$\iint (1/2\pi^2)\, 2\ \text{sinmy}\ \overset{\text{cosdx}}{\text{sindx}}\ J(\ 2\ \text{sinay cosex},\ 2\ \text{sinby sinfx})$$

which gives

$$\#2\quad 8/2\pi^2 \int_0^{\pi}\int_0^{2\pi} [-\text{be sinmy sinay cosby}\ \overset{\text{cosdx}}{(\text{sindx sinex sinfx})} -$$

$$\overset{\text{cosdx}}{\text{af sinmy cosay sinby}}\ (\text{sindx cosex cosfx})].$$

Cos-cos-sin2 gives:

2 5 8 and 2 5 10

Sin-cos-sin2 gives no non-zero combinations.

In Jacobian #3, we have:

$$\iint (1/2\pi)\, 2\ \text{sinmy}\ \overset{\text{cosdx}}{\text{sindx}}\ J(\ 2\ \text{sinay sinex},\ 2\ \text{sinby cosfx})$$

which gives

$$\#3\quad 8/2\pi^2 \int_0^{\pi}\int_0^{2\pi} [\text{be sinmy sinay cosby}\ \overset{\text{cosdx}}{(\text{sindx cosex cosfx})} +$$

$$\overset{\text{cosdx}}{\text{af sinmy cosay sinby}}\ (\text{sindx sinex sinfx})].$$

Cos-sin-cos2 gives:

2 6 7 2 6 9 5 3 7 5 3 9

Sin-sin-cos2 gives no non-zero combinations.

In Jacobian #4, we have:

$$\iint (1/2\pi^2)\, 2\ \text{sinmy}\ \overset{\text{cosdx}}{\text{sindx}}\ J(\ 2\ \text{sinay sinex},\ 2\ \text{sinby sinfx})$$

which gives

$$\#4\quad 8/2\pi^2 \int_0^{\pi}\int_0^{2\pi} [\text{be sinmy sinay cosby}\ \overset{\text{cosdx}}{(\text{sindx cosex sinfx})} -$$

$$\text{af sinmy cosay sinby}\ \overset{\text{cosdx}}{(\text{sindx sinex cosfx})}]$$

Cos-sin-sin2 gives no non-zero combinations. Sin-sin-sin2 gives:

3 6 8 3 6 10.

The final set of non-zero i, j, k for the 4 possible interaction integrals are:

#1) 3 5 7 3 5 9 6 2 7 6 2 9

#2) 2 5 8 2 5 10

#3) 2 6 7 2 6 9 5 3 7 5 3 9

#4) 3 6 8 3 6 10

We can then use the corresponding integrals to calculate the interactions. For all cases, integrating over x we obtain (where e=n and f=2n)

$$\#1 \quad 8/2\pi^2 \int_0^{\pi} [af \sin my \cos ay \sin by\ (\pi/2)$$
$$- be \sin my \sin ay \cos by\ (-\pi/2)]\ dy$$

$$\#2 \quad -8/2\pi^2 \int_0^{\pi} [be \sin my \sin ay \cos by\ (\pi/2)$$
$$+ af \sin my \cos ay \sin by\ (\ /2)]\ dy$$

$$\#3 \quad 8/2\pi^2 \int_0^{\pi} [be \sin my \sin ay \cos by\ (\pi/2)$$
$$+ af \sin my \cos ay \sin by\ (\pi/2)]\ dy$$

$$\#4 \quad 8/2\pi^2 \int_0^{\pi} [be \sin my \sin ay \cos by\ (\pi/2)$$
$$- af \sin my \cos ay \sin by\ (-\pi/2)]\ dy.$$

Now we integrate over y from 0 to π for the values of m, a, b given by the sets of i, j, k that survive the x-integration done above. This eliminates several other combinations. Since m, a, b comes in only sin-sin-cos or sin-cos-sin only i, j, k that give m, a, b of the form 1 1 2 1 2 1 and 2 1 1 will be non-zero.

#1 3 5 7 3 5 9 6 2 7 6 2 9 gives

1 2 1 1 2 2 2 1 1 2 1 2

thus only 3 5 7 and 6 2 7 survive.

#2 2 5 8 2 5 10 gives

1 2 1 1 2 2

thus only 2 5 8 survives.

#3 2 6 7 2 6 9 5 3 7 5 3 9 gives

1 2 1 1 2 2 2 1 1 2 1 2

thus only 2 6 7 and 5 3 7 survive.

#4 3 6 8 3 6 10 gives 1 2 1 1 2 2

thus only 3 6 8 survives.

The integration over y gives:

#1) 3 5 7 = $8/2\pi^2$ [4n $(-\pi/4)$ $(\pi/2)$ - n $(\pi/4)$ $(-\pi/2)$] =

-3n/2

6 2 7 = $8/2\pi^2$ [2n $(\pi/4)$ $(\pi/2)$ - n $(\pi/4)$ $(-\pi/2)$] = 3n/2

#2) 2 5 8 = $8/2\pi^2$ [-n $(\pi/4)$ $(\pi/2)$ - 4n $(-\pi/4)$ $(\pi/2)$] =

3n/2

#3) 2 6 7 = $8/2\pi^2$ [n $(\pi/4)$ $(\pi/2)$ + 4n $(-\pi/4)$ $(\pi/2)$] =

-3n/2

5 3 7 = $8/2\pi^2$ [n $(\pi/4)$ $(\pi/2)$ + 2n $(\pi/4)$ $(\pi/2)$] = 3n/2

#4) 3 6 8 = $8/2\pi^2$ [n $(\pi/4)$ $(\pi/2)$ - 4n $(-\pi/4)$ $(-\pi/2)$] =

-3n/2

Thus 2 5 8 = - 2 6 7 = - 3 5 7 = - 3 6 8 = 3n/2. (Note that #3 simply duplicates #1).

The interaction coefficients that involve zonal flows are considerably simpler since the integral only involves double

products in the x-dependent components. The general form for these integrals are:

$$1/2\pi^2 \int_0^{\pi}\int_0^{2\pi} \sqrt{2}\ \text{cosmy}\ J(\ 2\ \text{sinay}\ \begin{matrix}\text{cosex}\\ \text{sinex}\end{matrix},\ 2\ \text{sinby}\ \begin{matrix}\text{cosfx}\\ \text{sinfx}\end{matrix}).$$

(All integrals with two zonal components are zero since the Jacobian involves x derivatives). The expanded form of the integral is

$$\sqrt{2}\quad 4/2\pi^2 \int_0^{\pi}\int_0^{2\pi} \text{cosmy}\ \times$$

$$\begin{matrix}\text{cosex sinfx} & & \text{-sinex cosfx}\\ \text{-cosex cosfx} & & \text{-sinex sinfx}\end{matrix}$$
$$(\text{af cosay sinby}\ \begin{matrix}\text{sinex sinfx}\\ \text{-sinex cosfx}\end{matrix}\ +\text{be sinay cosby}\ \begin{matrix}\text{cosex cosfx}\\ \text{cosex sinfy}\end{matrix})$$

Non-zero values in the x-integration occur only for the squared functions

$\int_0^{2\pi} \text{sinx sinx dx} = \pi$ and $\int_0^{2\pi} \text{cosx cosx dx} = \pi$, which states that e must equal

f. This eliminates two of the four possible integrals above. The two remaining integrals are then identical except for sign. The j, k eigenfunctions which lead to the sin sin cos cos in the above integral have sin, cos x-structure, respectively. Combinations i, j, k which satisfy this requirement are:

1 2 3, 1 5 6, 1 7 8, 1 9 10, 4 2 3,

4 5 6, 4 7 8, 4 9 10 where a=b

and

1 2 6, 1 5 3, 1 7 10, 1 9 8, 4 2 6,

4 5 3, 4 7 10, 4 9 8 where a=b.

Performing the x-integration gives:

$$2\sqrt{2}/\pi \int_0^{\pi} e(a \cos my \cos ay \sin by + b \cos my \sin ay \cos by)\, dy$$

Non-zero combinations of the cos-cos-sin integrals where a equals b are:

$$\int_0^{\pi} \cos y \cos y \sin y\, dy = 2/3$$

$$\int_0^{\pi} \cos y \cos 2y \sin 2y\, dy = 4/15$$

Therefore 4 2 3, 4 5 6, 4 7 8, and 4 9 10 are zero.

Non-zero combinations of the triple integral for a not equal to b are:

$$\int_0^{\pi} \cos 2y \cos y \sin 2y\, dy = 4/15 \quad \text{(same as above)}$$

$$\int_0^{\pi} \cos 2y \sin y \cos 2y\, dy = 14/15.$$

The final set of non-zero zonal-wave interaction coefficients are:

$1\ 2\ 3 = -8\sqrt{2}\ n/3\pi$	$4\ 2\ 6 = -64\sqrt{2}\ n/15\pi$
$1\ 5\ 6 = -32\sqrt{2}\ n/15\pi$	$4\ 5\ 3 = -64\sqrt{2}\ n/15\pi$
$1\ 7\ 8 = -16\sqrt{2}\ n/3\pi$	$4\ 7\ 10 = -128\sqrt{2}\ n/15\pi$
$1\ 9\ 10 = -64\sqrt{2}\ n/15\pi$	$4\ 9\ 8 = -128\sqrt{2}\ n/15\pi$

The final set of wave-wave interaction coefficients are:

2 5 8 = 3n/2

2 6 7 = -3n/2

3 5 7 = -3n/2

3 6 8 = -3n/2

APPENDIX III

OBTAINING THE MODE 11 EQUILIBRIA

The Mode 11 equations given by (4.1) of part I are as follows:

$$0=c\bar{n}_2(\Theta_3-\Psi_3)-k(\Psi_1-\Theta_1) \tag{a3.1}$$

$$0=cn^2(\Psi_1\Psi_3+\Theta_1\Theta_3)+\beta n\Psi_3-k(n^2+1)(\Psi_2-\Theta_2) \tag{a3.2}$$

$$0=-cn^2(\Psi_1\Psi_2+\Theta_1\Theta_2)-\beta n\Psi_2-k(n^2+1)(\Psi_3-\Theta_3)+c\bar{n}_2(\Psi_1-\Theta_1) \tag{a3.3}$$

$$0=c(\Theta_2\Psi_3-\Psi_2\Theta_3)+c\sigma_0\bar{n}_2(\Psi_3-\Theta_3)+h(\Theta_1^*-\Theta_1)+k\sigma_0\Psi_1-(k+2k')\Theta_1\sigma_0 \tag{a3.4}$$

$$0=-c[(1-\sigma_0 n^2)\Theta_1\Psi_3-(1+\sigma_0 n^2)\Psi_1\Theta_3]+\beta\sigma_0 n\Theta_3-h\Theta_2+k\sigma_0(n^2+1)\Psi_2-(n^2+1)\sigma_0(k+2k')\Theta_2 \tag{a3.5}$$

$$0=c[(1-\sigma_0 n^2)\Theta_1\Psi_2-(1+\sigma_0 n^2)\Psi_1\Theta_2]-\beta\sigma_0 n\Theta_2-h\Theta_3+k\sigma_0(n^2+1)\Psi_3-(n^2+1)\sigma_0(k+2k')\Theta_3+c\bar{n}_2\sigma_0(\Theta_1-\Psi_1) \tag{a3.6}$$

where $c=-8(2)^{\frac{1}{2}}\,n/3\pi$.

If the values of the variables Ψ_1 and Θ_1 are prescribed or taken as known constants, the system defined by (a3.2), (a3.3), (a3.5), and (a3.6) constitute a linear system in the wave variables Ψ_2, Ψ_3, Θ_2, and Θ_3. Using (a3.1) to eliminate the term $(\Psi_1-\Theta_1)$, we obtain a homogeneous system in the wave variables which is given by the following:

$$-K\Psi_2 + A\Psi_3 + K\Theta_2 + B\Theta_1\Theta_3 = 0$$

$$-A\Psi_2 - T\Psi_3 - B\Theta_1\Theta_2 + T\Theta_3 = 0$$

$$L\Psi_2 + C\Theta_1\Psi_3 - M\Theta_2 + D\Theta_3 = 0$$

$$-C\Theta_1\Psi_2 + S\Psi_3 - D\Theta_2 - P\Theta_3 = 0$$

where

$A = n^2 c\Psi_1 + \beta n$ $\quad C = -c(1 - \sigma_0 n^2)$ $\quad T = k(n^2+1) + (c\bar{n}_2)^2/k$

$B = n^2 c$ $\quad D = c(1 + \sigma_0 n^2)\Psi_1 + \beta\sigma_0 n$ $\quad P = M + \sigma_0(c\bar{n}_2)^2/k$

$K = k(n^2+1)$ $\quad M = h + \sigma_0(n^2+1)(k+2k')$ $\quad S = \sigma_0 T$

$L = \sigma_0 k(n^2+1)$ $\quad R = k/(c\bar{n}_2)$.

In order to have a solution with nonzero wave variables (a non-trivial solution), the determinant of the coefficients must then be zero, which places a condition on the variables Ψ_1 and Θ_1.

Setting the determinant of the coefficients to zero gives a fourth degree equation in Θ_1 given by the following:

$$B^2C^2\Theta_1^4 + (BCMT + C^2KT + B^2LS + BCKP - 2ABCD)\Theta_1^2$$
$$+ (ACMT + BDLT + 2CDKT + ABMS + BDKS + ABLP + ACKP)\Theta_1$$
$$+ (KLST - KMST + KMPT - KLPT + ADLT + D^2KT + ADKS + A^2MP + A^2D^2)$$

or

$$A1\,\Theta_1^4 + B1\,\Theta_1^2 + C1\,\Theta_1 + D1 = 0$$

which has an analytic solution. By solving the quartic equation, we can get $\Theta_1 = f(\Psi_1)$. Thus to obtain all the equilibria, we select a value of Ψ_1 and solve for the four possible roots Θ_1. The only useful roots are Θ_1 both

positive and real. For each of these values of Θ_1, we then compute the corresponding wave variables by using (a3.1) with any three of (a3.2), (a3.3), (a3.5), and (a3.6). Using (a3.1), (a3.2), (a3.3), and (a3.5), we obtain

$$\Psi_2 = -X(B^2 C\Theta_1^3 + BMT\Theta_1 + CKT\Theta_1 - ABD\Theta_1 + AMT + DKT)/V$$

$$\Theta_3 = -X(B^2 CK\Theta_1^2 + ABL\Theta_1 + ACK\Theta_1 + KMT - KLT + A^2 M)/V$$

$$\Theta_2 = X(ABC\Theta_1^2 - BLT\Theta_1 - CKT\Theta_1 - ALT - DKT - A^2 D)/V$$

$$\Psi_3 = X + \Theta_3$$

where $V = (B\Theta_1 + A)(BL\Theta_1 + CK\Theta_1 + AM + DK)$ and $X = R(\Psi_1 - \Theta_1)$. We then have to satisfy

$$c(\Theta_2\Psi_3 - \Psi_2\Theta_3) + h(\Theta_1^* - \Theta_1) - 2k'\sigma_b\Theta_1 = g(\Psi_1)$$

such that $g(\Psi_1)$ becomes zero. These values of Ψ_1 are found numerically by using the binomial chop.

We select a value of Ψ_1 and an increment $\Delta\Psi_1$ and compare $g(\Psi_1)$ to $g(\Psi_1+\Delta\Psi_1)$ to see if the value of g has changed sign (crossed zero). We then converge on the equilibrium value of Ψ_1 that makes g identically zero by halving the interval $\Delta\Psi_1$ and performing a similar check on g, shown

symbolically below:

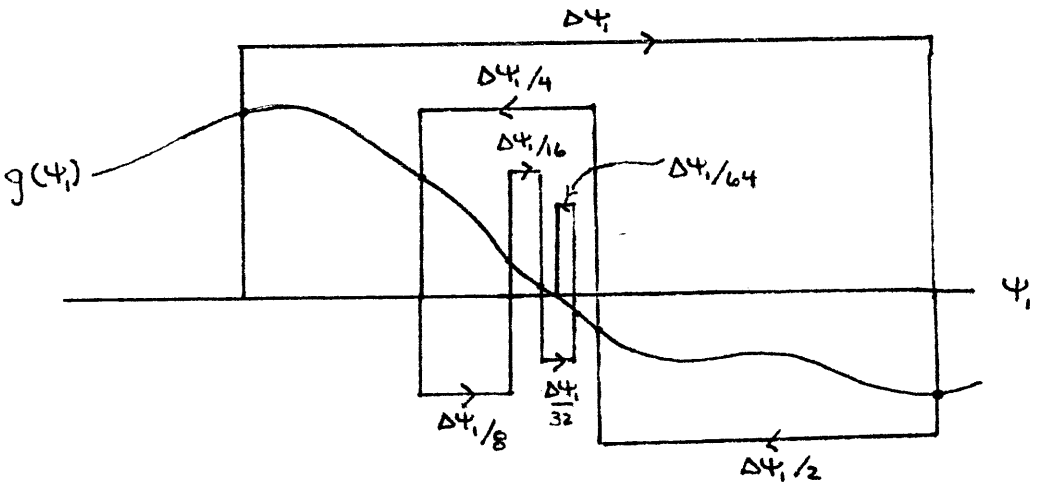

We can then obtain all the equilibria provided we choose $\Delta\Psi_1$ small enough and cover a sufficiently large range of values of Ψ_1.

APPENDIX IV

STABILITY CALCULATION

The stability of the various equilibria are calculated by the standard process of introducing a perturbation about the equilibrium state and solving an eigenvalue problem for the growth rate of this perturbation. The first step in such an analysis involves writing the dependent variables Ψ_i and Θ_i as $\Psi_i = \bar{\Psi}_i + \Psi_i'$ and $\Theta_i = \bar{\Theta}_i + \Theta_i'$ where $\bar{\Psi}_i$ and $\bar{\Theta}_i$ are the equilibrium values. We substitute this form of the dependent variables into the system of equations and linearize about the equilibrium values $\bar{\Psi}_i$ and $\bar{\Theta}_i$, e.g., we neglect terms involving products of perturbations, $\Psi_i'\Theta_j'$. We then look for solutions of the linearized system of equations by assuming the perturbations have the form $\Psi_i' = \text{Real } \hat{\Psi}_i e^{\gamma t}$ where both $\hat{\Psi}_i$ and γ may be complex.

If we do this calculation for our model equations, we obtain a system of 20 homogeneous simultaneous equations with 20 unknowns, $\hat{\Psi}_i$ and $\hat{\Theta}_i$, where $i = 1,2,\ldots, 10$. The only nontrivial solution ($\hat{\Psi}_i$, $\hat{\Theta}_i \neq 0$) occurs when the determinant of the coefficients are zero, which gives us a condition on the values of γ. Since there are 20 independent equations, there will be, in general, 20 different values of γ (eigenvalues) which are roots of the system. Fortunately,

since the equilibria possess only Mode 11 structure, the perturbation matrix obtained from the 20 linearized model equations breaks down into three submatices as discussed in the text. The solution of the eigenvalue and eigenvector problem can then be obtained by solving each of the three submatrices independently. The actual solutions were obtained by using the EIGRF routines of the Goddard NASA Space Flight Institute in Maryland. The three perturbation matrices are as follows:

$$\begin{pmatrix} a_{11} & a_{12} & a_{13} & \cdots & a_{16} \\ a_{21} & a_{22} & & & \\ a_{31} & & & & \\ \vdots & & & & \\ a_{61} & & & & a_{66} \end{pmatrix}$$

MODE 11

$$\begin{pmatrix} b_{11} & b_{12} & b_{13} & \cdots & b_{110} \\ b_{21} & b_{22} & & & \\ b_{31} & & & & \\ \vdots & & & & \\ b_{101} & & & & b_{1010} \end{pmatrix}$$

MODE 21 + MODE 12

$$\begin{pmatrix} c_{11} & c_{12} & c_{13} & c_{14} \\ c_{21} & c_{22} & & \\ c_{31} & & & \\ c_{41} & & & c_{44} \end{pmatrix}$$

MODE 22

MODE II

$a_{11} = -k$

$a_{12} = 0$

$a_{21} = c_1 n^2 \Psi_3 / n^2+1$

$a_{22} = -k$

$a_{31} = -c_1 (n^2 \Psi_2 - h_2) / n^2+1$

$a_{32} = -[c_1 n^2 \Psi_1 + \beta n] / n^2+1$

$a_{41} = k\sigma_0 / \sigma_0+1$

$a_{42} = -c_1 \Theta_3 / \sigma_0+1$

$a_{51} = c_1 (1+\sigma_0 n^2) \Theta_3 / (1+\sigma_0(n^2+1))$

$a_{52} = k\sigma_0 / (\sigma_0 + 1/n^2+1)$

$a_{61} = -c_1 [(1+\sigma_0 n^2)\Theta_2 + \sigma_0 h_2] / (1+\sigma_0(n^2+1))$

$a_{62} = c_1 (1-\sigma_0 n^2)\Theta_1 / (1+\sigma_0(n^2+1))$

$a_{13} = -c_1 h_2$

$a_{14} = k$

$a_{23} = (c_1 n^2 \Psi_1 + \beta n) / n^2+1$

$a_{24} = c_1 n^2 \Theta_3 / n^2+1$

$a_{33} = -k$

$a_{34} = -c_1 (n^2 \Theta_2 + h_2) / n^2+1$

$a_{43} = c_1 (\Theta_2 + \sigma_0 h_2) / \sigma_0+1$

$a_{44} = -(h + \sigma_0 (k+2k')) / \sigma_0+1$

$a_{53} = -c_1 (1-\sigma_0 n^2)\Theta_1 / (1+\sigma_0(n^2+1))$

$a_{54} = -c_1 (1-\sigma_0 n^2)\Psi_3 / (1+\sigma_0(n^2+1))$

$a_{63} = k\sigma_0 / (\sigma_0 + 1/n^2+1)$

$a_{64} = c_1 [(1-\sigma_0 n^2)\Psi_2 + \sigma_0 h_2] / (1+\sigma_0(n^2+1))$

$a_{15} = 0$

$a_{16} = c_1 h_2$

$a_{25} = k$

$a_{26} = c_1 n^2 \Theta_1 / n^2+1$

$a_{35} = -c_1 n^2 \Theta_1 / n^2+1$

$a_{36} = k$

$a_{45} = -c_1 \Psi_3 / \sigma_0+1$

$a_{46} = -c_1 (\Psi_2 + \sigma_0 h_2) / \sigma_0+1$

$a_{55} = -(h + \sigma_0 (k+2k')(n^2+1)) / (1+\sigma_0(n^2+1))$

$a_{56} = [c_1 (1+\sigma_0 n^2)\Psi_1 + \beta n \sigma_0] / (1+\sigma_0(n^2+1))$

$a_{65} = -[c_1 (1+\sigma_0 n^2)\Psi_1 + \beta n \sigma_0] / (1+\sigma_0(n^2+1))$

$a_{66} = -(h + \sigma_0 (k+2k')(n^2+1)) / (1+\sigma_0(n^2+1))$

MODE 21 and MODE 12

$b_{11} = -k$

$b_{21} = c_4(n^2-3)\Psi_3/n^2+4$

$b_{31} = -c_4((n^2-3)\Psi_2-h_2)/n^2+4$

$b_{41} = k\sigma_0/(\sigma_0+1/4)$

$b_{51} = c_4(1+\sigma_0(n^2-3))\Theta_3/(\sigma_0(n^2+4)+1)$

$b_{61} = -c_4[(1+\sigma_0(n^2-3))\Theta_2+\sigma_0 h_2]/(\sigma_0(n^2+4)+1)$

$b_{71} = 0$

$b_{81} = 0$

$b_{91} = 0$

$b_{01} = 0$

$b_{12} = 3c_4\Psi_3$

$b_{22} = -k$

$b_{32} = (-c_2(n^2+3)\Psi_1-\beta n)/(n^2+4)$

$b_{42} = -c_4(1-3\sigma_0)\Theta_3/(4\sigma_0+1)$

$b_{52} = k\sigma_0/(\sigma_0+1/n^2+4)$

$b_{62} = c_2(1-\sigma_0(n^2+3))\Theta_1/(\sigma_0(n^2+4)+1)$

$b_{72} = 3c_6\Psi_2/(4n^2+1)$

$b_{82} = -c_6(3\Psi_2+h_2)/(4n^2+1)$

$b_{92} = -c_6(1-3\sigma_0)\Theta_2/(\sigma_0(4n^2+1)+1)$

$b_{02} = c_6[(1-3\sigma_0)\Theta_2+\sigma_0 h_2]/(\sigma_0(4n^2+1)+1)$

$b_{13} = -(3c_4\Psi_2+h_2c_4)/4$

$b_{23} = (c_2(n^2+3)\Psi_1+\beta n)/(n^2+4)$

$b_{33} = -k$

$b_{43} = c_4[(1-3\sigma_0)\Theta_2+\sigma_0 h_2]/(4\sigma_0+1)$

$b_{53} = -c_2(1-\sigma_0(n^2+3))\Theta_1/(1+\sigma_0(n^2+4))$

$b_{63} = k\sigma_0/(\sigma_0+1/n^2+4)$

$b_{73} = c_6(3\Psi_2+h_2)/(4n^2+1)$

$b_{83} = 3c_6\Psi_3/4n^2+1$

$b_{93} = -c_6[(1-3\sigma_0)\Theta_2+\sigma_0 h_2]/(1+\sigma_0(4n^2+1))$

$b_{03} = -c_6(1-3\sigma_0)\Theta_3/(1+\sigma_0(4n^2+1))$

$b_{14} = k$

$b_{24} = c_4(n^2-3)\Theta_3/n^2+4$

$b_{34} = -c_4[(n^2-3)\Theta_2+h_2]/n^2+4$

$b_{44} = -(h+\sigma_0(k+2k')4)/4\sigma_0+1$

$b_{54} = c_4(\sigma_0(n^2-3)-1)\Psi_3/(\sigma_0(n^2+4)+1)$

$b_{64} = -c_4[(\sigma_0(n^2-3)-1)\Psi_2-\sigma_0 h_2]/(1+\sigma_0(n^2+4)+1)$

$b_{74} = 0$

$b_{84} = 0$

$b_{94} = 0$

$b_{04} = 0$

$b_{15} = 3c_4\Theta_3/4$

$b_{25} = k$

$b_{35} = -c_2(n^2+3)\Theta_1/n^2+4$

$b_{45} = c_4(1+3\sigma_0)\Psi_2/4\sigma_0+1$

$b_{55} = -(h+(k+2k')\sigma_0(n^2+4))/(1+\sigma_0(n^2+4))$

$b_{65} = [-c_2(1+\sigma_0(n^2+3))\Psi_1-\beta n\sigma_0]/(1+\sigma_0(n^2+4))$

$b_{75} = 3c_6\Theta_3/4n^2+1$

$b_{85} = -c_6(3\Theta_2-h_2)/4n^2+1$

$b_{95} = c_6(1+3\sigma_0)\Psi_3/(1+\sigma_0(4n^2+1))$

$b_{05} = -c_6[(1+3\sigma_0)\Psi_2+\sigma_0 h_2]/(1+\sigma_0(4n^2+1))$

$b_{16} = (-3c_4\Theta_2+h_2)/4$

$b_{26} = c_2(n^2+3)\Theta_1/n^2+4$

$b_{36} = k$

$b_{46} = -c_4[(1+3\sigma_0)\Psi_2+\sigma_0 h_2]/4\sigma_0+1$

$b_{56} = [c_2(1+\sigma_0(n^2+3))\Psi_1+\beta n\sigma_0]/(1+\sigma_0(n^2+4))$

$b_{66} = -(h+\sigma_0(k+2k')(n^2+4))/(1+\sigma_0(n^2+4))$

$b_{76} = c_6(3\Theta_2-h_2)/4n^2+1$

$b_{86} = 3c_6\Theta_3/4n^2+1$

$b_{96} = c_6[(1+3\sigma_0)\Psi_2+\sigma_0 h_2]/(1+\sigma_0(4n^2+1))$

$b_{06} = c_6(1+3\sigma_0)\Psi_3/(1+\sigma_0(4n^2+1))$

MODE 21 and MODE 12 cont.

$b_{17} = 0$

$b_{27} = -3c_6 n^2 \Psi_3 / n^2+4$

$b_{37} = -c_6(3n^2\Psi_2 + h_2)/n^2+4$

$b_{47} = 0$

$b_{57} = -c_6(3n^2\sigma_0 - 1)\Theta_3 / (1+\sigma_0(n^2+4)$

$b_{67} = c_6[(1-3\sigma_0 n^2)\Theta_2 + \sigma_0 h_2] / (1+\sigma_0(n^2+4))$

$b_{77} = -k$

$b_{87} = -(4c_3 n^2 \Psi_1 + 2n\beta)/4n^2+1$

$b_{97} = k\sigma_0 / (\sigma_0 + 1/4n^2+1)$

$b_{07} = c_3(1-4\sigma_0 n^2)\Theta_1 / (1+\sigma_0(4n^2+1))$

$b_{18} = 0$

$b_{28} = c_4(3n^2\Psi_2 + h_2)/n^2+4$

$b_{38} = -c_6 3n^2 \Psi_3 / n^2+4$

$b_{48} = 0$

$b_{58} = -c_6[(1-3\sigma_0 n^2)\Theta_2 + \sigma_0 h_2] / (1+\sigma_0(n^2+4))$

$b_{68} = c_6(1-3\sigma_0 n^2)\Theta_3 / (1+\sigma_0(n^2+4))$

$b_{78} = (c_3 4n^2 \Psi_1 + 2n\beta)/4n^2+1$

$b_{88} = -k$

$b_{98} = -c_3(1-4\sigma_0 n^2)\Theta_1 / (1+\sigma_0(4n^2+1))$

$b_{08} = k\sigma_0 / (\sigma_0 + 1/4n^2+1)$

$b_{19} = 0$

$b_{29} = -3c_6 n^2 \Theta_3 / n^2+4$

$b_{39} = -c_6(3n^2\Theta_2 - h_2)/n^2+4$

$b_{49} = 0$

$b_{59} = -c_6(1+3\sigma_0 n^2)\Psi_3 / (1+\sigma_0(n^2+4))$

$b_{69} = -c_6[(1+3\sigma_0 n^2)\Psi_2 + \sigma_0 h_2] / (1+\sigma_0(n^2+4))$

$b_{79} = k$

$b_{89} = -c_3 4n^2 \Theta_1 / 4n^2+1$

$b_{99} = -(h+\sigma_0(k+2k')(4n^2+1)) / (1+\sigma_0(4n^2+1))$

$b_{09} = -[c_3(1+4\sigma_0 n^2)\Psi_1 + 2n\beta\sigma_0] / (\sigma_0(4n^2+1)+1)$

$b_{10} = 0$

$b_{20} = c_6(3n^2\Theta_2 - h_2)/n^2+4$

$b_{30} = -3c_6 n^2 \Theta_3 / n^2+4$

$b_{40} = 0$

$b_{50} = c_6[(1+3\sigma_0 n^2)\Psi_2 + \sigma_0 h_2] / (1+\sigma_0(4\sigma_0 n^2))$

$b_{60} = -c_6(1+3\sigma_0 n^2)\Psi_3 / (1+\sigma_0(n^2+4))$

$b_{70} = 4c_3 n^2 \Theta_1 / 4n^2+1$

$b_{80} = k$

$b_{90} = [c_3(1+4\sigma_0 n^2)\Psi_1 + 2n\beta\sigma_0] / (1+\sigma_0(4n^2+1))$

$b_{00} = -(h+\sigma_0(k+2k')(4n^2+1)) / (1+\sigma_0(4n^2+1))$

$$c_{11} = -k$$

$$c_{21} = -\left[c_4(4n^2+3)\Psi_1 + 2n\beta\right]/4n^2+4$$

$$c_{31} = k\sigma_0/(\sigma_0 + 1/4n^2+4)$$

$$c_{41} = c_4\left[(1-\sigma_0(4n^2+3))\Theta_1\right]/(\sigma_0(4n^2+4)+1)$$

$$c_{12} = (c_4(4n^2+3)\Psi_1 + 2n\beta)/4n^2+4$$

$$c_{22} = -k$$

$$c_{32} = -c_4(1-\sigma_0(4n^2+3))\Theta_1/(\sigma_0(4n^2+4)+1)$$

$$c_{42} = k\sigma_0/(\sigma_0 + 1/4n^2+4)$$

$$c_{13} = k$$

$$c_{23} = -c_4(4n^2+3)\Theta_1/4n^2+4$$

$$c_{32} = -\left(h + \sigma_0(k+2k')(4n^2+4)\right)/(1+\sigma_0(4n^2+4))$$

$$c_{43} = -\left(c_4((4n^2+3)\sigma_0+1)\Psi_1 + 2n\beta\sigma_0\right)/(1+\sigma_0(4n^2+4))$$

$$c_{14} = c_4(4n^2+3)\Theta_1/4n^2+4$$

$$c_{24} = k$$

$$c_{34} = (c_4(1+\sigma_0(4n^2+3))\Psi_1 + 2n\beta\sigma_0)/(1+\sigma_0(4n^2+4))$$

$$c_{14} = -(h + \sigma_0(4n^2+4)(k+2k'))/(1+\sigma_0(4n^2+4))$$

APPENDIX V

THE BREAKDOWN OF TRANSPORTS BY STABILITY THEORY

The differences between the transports obtained diagnostically from the full model and those obtained theoretically from the stability analysis appear to be a consequence of the finite amplitude Mode 22 wave. We were able to ascertain this result by conducting a few simple experiments.

We integrated the full model as usual (initializing the Mode 21 and Mode 12 variables with the real part of the most unstable eigenmode), except that we held the time mean Mode 11 variables fixed. In this manner we hoped to investigate the series of events which led to the breakdown of the linear theory, eliminating the effects of the time variability of the large-scale terms themselves. After certain intervals of time had elapsed, we calculated the budgets of this "fixed" model diagnostically for comparison with those predicted theoretically by the linear analysis.

As expected, the agreements were at first exact since we were still in the linear domain (the Mode 21 and Mode 12 variables were still small). The agreements continued to be exact until the Mode 22 wave grew (suddenly) to finite

amplitude. After this time, the differences between the budgets calculated from the "fixed" model and that predicted by linear theory had the same qualitative characteristics as the differences between the full model regime budgets and that predicted by linear theory. Though the breakdown of the prediction of the ad21 and ad22 components in the "fixed" model by the linear theory appears to be associated with the sudden amplification of the Mode 22 wave, we do not know whether it is a result of nonlinear processes or secondary instabilities, however, we are confident that the appearance of the finite amplitude Mode 22 wave is a major factor in the descrepancies between the full model ad21 and ad22 observed budgets and that predicted by stability theory.